



UNIVERSITÄT
BAYREUTH

Jenseits von Cisplatin: Aufklärung der intrazellulären
Lokalisation und antitumoralen Wirkungen neuer target-
spezifischer Platinkomplexe mit N-heterozyklischen
Carbenliganden

Dissertation

zur Erlangung des akademischen Grades eines

Doktors der Naturwissenschaften (*Dr. rer. nat.*)

an der Fakultät für Biologie, Chemie und Geowissenschaften

der Universität Bayreuth

Vorgelegt von

Matthias Franz-Josef Hans Rothemund

aus München

Bayreuth, 2020

Die vorliegende Arbeit wurde im Zeitraum von September 2015 bis Mai 2019 in Bayreuth am Lehrstuhl für Organische Chemie I (OC I) unter Betreuung von Herrn Prof. Dr. Rainer Schobert angefertigt.

Vollständiger Abdruck der von der Fakultät für Biologie, Chemie und Geowissenschaften der Universität Bayreuth genehmigten Dissertation zur Erlangung des akademischen Grades eines Doktors der Naturwissenschaften (*Dr. rer. Nat.*).

Dissertation eingereicht am:	22.07.2020
Zulassung durch die Promotionskommission:	29.07.2020
Wissenschaftliches Kolloquium:	19.11.2020

Amtierender Dekan: Prof. Dr. Matthias Breuning

Prüfungsausschuss:

Prof. Dr. Rainer Schobert	(Gutachter)
Prof. Dr. Birgit Weber	(Gutachterin)
Prof. Dr. Carlo Unverzagt	(Vorsitz)
Prof. Dr. Birte Höcker	

Meinem Vater

Inhaltsverzeichnis

Abkürzungsverzeichnis	iii
Zusammenfassung.....	- 1 -
Summary.....	- 4 -
1 Einleitung.....	- 7 -
1.1 World Cancer Burden	- 7 -
1.2 Tumorentstehung und -progression.....	- 8 -
1.3 Die klassische Platin-Tumorthherapie	- 12 -
1.3.1 Peyrone's Chlorid – Die Wiederentdeckung.....	- 12 -
1.3.2 (Klassischer) Wirkmechanismus von Platinverbindungen.....	- 14 -
1.4 Zelluläre Reaktion auf DNA-Schäden	- 16 -
1.5 Apoptose – Der programmierte Zelltod	- 18 -
1.6 Entwicklung neuartiger Metallkomplexe für die Tumorthherapie.....	- 21 -
1.6.1 Steuerung der biologischen Aktivität durch Ligandenvariation	- 22 -
1.6.2 Alternative Ziele	- 23 -
1.6.3 Prodrugs – Der nächste Schritt.....	- 25 -
1.7 Targetfindung über Azid-Alkin Cycloaddition	- 26 -
2 Zielsetzung	- 29 -
3 Synopsis.....	- 30 -
3.1 Vorstellung der Teilprojekte	- 30 -
3.2 Untersuchungen zur biologischen Aktivität neuer (un)symmetrischer <i>N,N</i> - Dibenzylimidazol Pt ^{II} -Komplexe	- 32 -
3.2.1 Toxizität und DNA-Interaktionsstudien (un)symmetrischer Komplexe des Typs <i>cis-[Pt^{II}Cl(L)(NHC)^l(NHC)²]</i>	- 32 -
3.2.2 Auswirkung der Ladung und Lipophilie auf den Wirkort und -mechanismus von Komplexen des Typs <i>cis-[Pt^{II}Cl(L)(NHC)^l(NHC)²]</i>	- 35 -
3.3 Biologische Wirkung und DNA-Interaktionsstudien unymmetrischer <i>N,N</i> - Dialkylbenzimidazol-2-yliden-Platin(II) Komplexe	- 39 -
3.4 Zytotoxische Wirkung und DNA-Interaktion von symmetrischen Platin(IV) Komplexen und ihrer Platin(II) Analoga	- 43 -
4 Literaturverzeichnis.....	- 46 -
5 Publikationen.....	- 53 -

5.1	Darstellung des Eigenanteils	- 53 -
5.1.1	<i>Eigenanteil an Publikation I</i>	- 54 -
5.1.2	<i>Eigenanteil an Publikation II</i>	- 55 -
5.1.3	<i>Eigenanteil an Publikation III</i>	- 56 -
5.1.4	<i>Eigenanteil an Publikation IV</i>	- 57 -
5.2	Publikation I	- 58 -
5.3	Publikation II	- 90 -
5.4	Publikation III.....	- 108 -
5.5	Publikation IV	- 151 -
6	Aufstellung weiterer Publikationen.....	- 185 -
7	Posterbeiträge und Konferenzen	- 188 -
8	Danksagung	- 189 -
9	Eidesstattliche Versicherung und Erklärung des Verfassers.....	- 190 -

Abkürzungsverzeichnis

518A2	Melanomzellen
A	Adenin
AIF	<i>Apoptosis-inducing factor</i>
Apaf1	<i>Apoptotic Protease Activating Factor 1</i>
ATM	<i>Ataxia Tangiectasia Mutated</i>
ATP	Adenosintriphosphat
ATR	<i>Ataxia Relangiectasia and Rad3 Related</i>
Bak	<i>Bcl-2-antagonist/killer 1</i>
Bax	<i>Bcl-2 activated protein X</i>
Bcl-2	<i>B-cell lymphoma 2</i>
BCRP	<i>Breast Cancer Resistance Protein</i>
Bcl-X _L	<i>Bcl-2 extra large</i>
Bid	<i>BH interacting-domain death agonist</i>
C	Cytosin
CA-4	Combretastatin A-4
Cas	Caspase
Ccc	<i>covalently closed circular</i>
CDDP	<i>Cis-Diammindichloridoplatin(II)</i>
CDK	<i>Cyclin Dependent Kinase</i>
ct-DNA	<i>calf thymus DNA</i>
CTR1	<i>Copper Transporter 1</i>
CuAAC	Kupfer katalysierte Azid-Alkin Cycloaddition
Cyt-c	Cytochrom-c
CZE	Tschechische Republik
Destatis	Deutsches Statistisches Bundesamt
DISC	<i>Death Inducing Signaling Complex</i>
DLC	<i>Delocalized Lipophilic Cations</i>
DLD-1	<i>Duke's type C, kolorektales Adenokarzinom</i>
DMF	Dimethylformamid
DMSO	Dimethylsulfoxid
DNA	<i>Desoxyribonucleic acid</i>
DNA-Pk	<i>DNA-dependent Protein kinase</i>

Ea.Hy926	Endothelhybridzellen
<i>E. coli</i>	<i>Escherichia coli</i>
EGF	<i>Endothelial Growth Factor</i>
EMSA	<i>Electrophoretic Mobility Shift Assay</i>
EndoG	Endonuclease G
EtdBr	Ethidiumbromid
FAAS	<i>Flame atom absorption spectrometry</i>
FADD	<i>Fas-Associated protein with a Death Domain</i>
FasL	Fas-Ligand
FasR	Fas-Rezeptor
FDA	<i>Food and Drug Administration</i>
G	Guanin
G-Phase	<i>Gap-Phase</i>
GSH	Glutathion
HDFa	<i>Human Dermal Fibroblasts adult</i>
HT-29	Kolorektale Adenokarzinomzellen
HCT116	Kolorektale Karzinomzellen
IAP	<i>Inhibitor of Apoptosis Protein</i>
IARC	<i>International Agency for Research on Cancer</i>
IC ₅₀	<i>Half maximal inhibitory concentration</i>
ICR	<i>Institute of Cancer Research</i>
Kb-V1	Zervixkarzinomzellen
LICQ	<i>Li's colocalization quotient</i>
MCF-7	Mammakarzinomzellen
<i>mdr</i>	<i>multi drug resistant</i>
Mio.	Millionen
NHC	<i>N-Heterozyklisches Carben</i>
oc	<i>open circular</i>
Panc-1	Pankreaskarzinomzellen
PC	<i>Pearson's colocalization coefficient</i>
P-gp	P-Glykoprotein
Puma	<i>P53 upregulated modulator of apoptosis</i>
ROS	<i>Reactive Oxygen Species</i>
smac	<i>second mitochondrial activator of caspases</i>

Abkürzungsverzeichnis

S-Phase	Synthese-Phase
tBid	<i>trunkated Bid</i>
TF	Transkriptionsfaktor
TNF	Tumornekrosefaktor
Topo	Topotecan
TrxR	Thioredoxinreductase
U87	<i>Likely</i> Glioblastomzellen
Vbl	Vinblastin
VEGF	<i>Vascular endothelial growth factor</i>
vgl	Vergleiche
Vpm	Verapamil
WHO	<i>World Health Organization</i>
wt	Wildtyp

Zusammenfassung

Der anhaltende Anstieg neoplastischer Neuerkrankungen und damit verbundener Todesfälle, wiederkehrende Resistenzentwicklungen gegen aktuelle Chemotherapeutika und ihre starken Nebenwirkungen stellen die Wissenschaft auch nach mehreren Jahrzehnten erfolgreicher Tumorbekämpfung vor die Aufgaben bessere, selektivere Wirkstoffe für die Tumorthapie zu finden. Aufgrund ihrer hohen Stabilität und Variabilität haben sich *N*-heterozyklische Carbenkomplexe (NHC) in den letzten Jahren als vielversprechende Kandidaten für die Entwicklung neuer antitumoraler Wirkstoffe hervorgetan. Die im Rahmen dieser Arbeit vorgestellten Pt^{II} und Pt^{IV} NHC Komplexe mit verschiedenen *N,N*-dibenzylimidazol-2-yliden und *N,N*-dialkylbenzimidazol-2-yliden Liganden (vgl. Abbildung 1), wurden *in vitro* auf ihre allgemeine antitumorale Aktivität mit Fokus auf ihre DNA-Interaktionsfähigkeit, intrazelluläre Lokalisation und damit verbundene Auswirkungen auf zelluläre Prozesse untersucht.

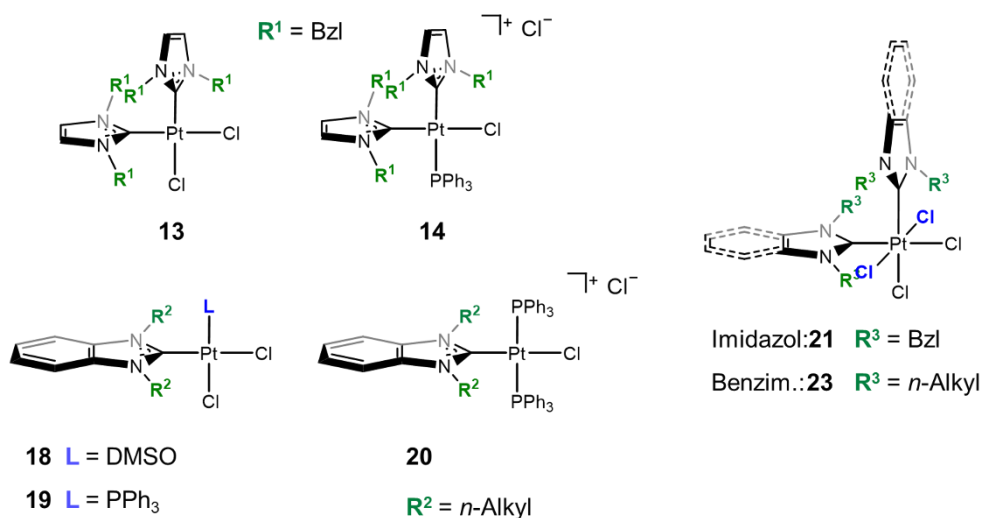


Abbildung 1. Zusammenstellung der verschiedenen Komplextypen, die in dieser Arbeit behandelt wurden.

Der erste Teil dieser Arbeit beschäftigt sich mit der Aufklärung des Wirkmechanismus neuer (un)symmetrischer, (un)geladener Komplexe **13** und **14** des Typs *cis*-[Pt^{II}Cl(L)(NHC)¹(NHC)²] mit *N,N*-dibenzylimidazol-2-yliden (NHC) und Cl/PPh₃ (L) Liganden. Wie schon ähnliche Pt^{II} Komplexe zuvor zeigten Komplexe mit Eigenschaften von delokalisierten lipophilen Kationen (dlc) eine aufnahmeabhängige, erhöhte Toxizität. Ebenso nahmen die sekundären Liganden und das Einführen einer positiven Gesamtladung Einfluss auf die Interaktion mit DNA, welche in ihrer Intensität die von Cisplatin weit überstieg. Die Lokalisation von

fluoreszenzmarkierten Derivaten dieser Serie zeigte sowohl die ungeladenen als auch die geladenen Komplexe hauptsächlich an den Mitochondrien, was untypisch für Platinkomplexe ist. Einhergehend mit diesem Wirkort wurden negative Auswirkungen auf die Redoxhomöostase und der Zusammenbruch des Mitochondrienmembranpotentials $\Delta\Psi$ in Tumorzellen nach Behandlung mit Komplexen dieser Serie festgestellt. Damit unterscheiden sie sich deutlich von Cisplatin, welches seinen Hauptwirkort an der DNA findet. Weitere Unterschiede zwischen der Wirkung von Cisplatin und den untersuchten Platinkomplexen zeigten sich in ihrem Einfluss auf den Zellzyklus, das Zytoskelett und die Aktivierung der Apoptose. Einhergehend mit oxidativem Stress lösen die kationischen Komplexe **14** einen G₁-Arrest und nicht wie Cisplatin einen S-Phasenarrest, und eine starke Ausbildung von *stress fibers* im Aktinzytoskelett aus. Letztendlich konnte für die geladenen Komplexe **14** die Aktivierung der apoptosevermittelnden Caspasen nachgewiesen werden. Die geringere Aktivität der ungeladenen Komplexe **13** beschränkte sich nicht auf ihre Auswirkungen auf die Menge an toxischer reaktiver Sauerstoffspezies. So verursachten sie keinen Zellzyklusarrest und waren auch nicht in der Lage Caspasen zu aktivieren. Der, von dem von Cisplatin verschiedene, Wirkmechanismus der *cis*-[Pt^{II}Cl(L)(NHC)¹(NHC)²] Komplexe dieser Generation bietet die Möglichkeit gemilderter Nebenwirkungen, da gesunde Körperzellen eine höhere Toleranz für oxidativen Stress besitzen als Tumorzellen und DNA-Reparaturmechanismen nicht in dem Ausmaß aktiviert werden, wie es bei einer Cisplatin-Therapie geschieht.

Der zweite Teil dieser Arbeit beschäftigt sich mit der Untersuchung des Einflusses der sekundären Liganden und der Gesamtladung der Komplexe auf ihre antitumorale Aktivität und die Art, sowie die Stärke ihrer DNA-Interaktion. Untersucht wurde dies an einer Serie von (un)geladenen [(1,3-Dialkylbenzimidazol-2-yliden)-(L)Cl]platin(II) Komplexen (**18-20**). Wie schon die zuvor untersuchten Komplexe zeigten die Komplexe dieser Serie eine zelluläre Aufnahme, die stark abhängig von der Art der sekundären Liganden war. Komplexe, die Eigenschaften delokalisierter lipophiler Kationen zeigen, wurden am stärksten in Zellen aufgenommen und zeigten die höchste Toxizität. Insbesondere bei Komplexen mit einem PPh₃ Liganden hatte auch die Länge der Alkylkette deutlichen Einfluss auf die Aufnahme. Im Gegensatz zu den Komplexen **13** und **14** standen Aufnahmeraten der Komplexe jedoch in keinem Zusammenhang mit den Cytotoxizitäten, die sich in dieser Serie sprunghaft verhielten.

Detaillierte DNA-Interaktionsstudien der Komplexe zeigten, dass die ungeladenen Komplexe **18-19** direkt koordinativ an Guaninbasen der DNA binden und die geladenen Komplexe **20** erst eine rasche elektrostatische Interaktion mit dem negativ geladenen Phosphatrückgrat eingehen und anschließend eine koordinative Bindung. Alle getesteten Komplexe bilden monofunktionelle DNA-Addukte aus, und destabilisieren, verdrehen und entwinden die DNA in geringerem Ausmaß als Cisplatin. Derartige Schäden der DNA könnten unerkannt bleiben und Reparaturmechanismen der Tumorzellen umgehen.

Die starken Nebenwirkungen, die eine Chemotherapie oft mit sich bringt, regt zu gezielteren Ansätzen der Chemotherapie an. Inaktive *prodrugs*, Metallkomplexe höherer Oxidationsstufen, die durch die Reduktion in der veränderten Tumorumgebung aktiviert werden, stellen eine Möglichkeit dar, ungewollte Nebeneffekte zu reduzieren. Der dritte Teil dieser Arbeit handelt von der antitumoralen Aktivität von *cis*- und *trans*-[Pt^{IV}Cl₄(NHC)₂]-Komplexen wie **21** oder **23** und ihrer Pt^{II} Analoga. Die Pt^{IV} Komplexe dieser Serie zeigten größtenteils eine ähnliche antitumorale Aktivität wie ihre Pt^{II} Analoga. Die Geometrie der Pt^{IV} Komplexe verhindert eine *in vitro* DNA-Interaktion, und macht sie somit zu potenziellen *Prodrugs* für die Tumorthherapie. Vergebliche Versuche einer *in situ* Reduktion stimmen mit Forschungsergebnissen überein, dass kleinere Moleküle nicht für die Reduktion der Pt^{IV} Komplexe verantwortlich sind, sondern diese durch größere Moleküle, wie Proteine oder Enzyme reduziert werden.^[130] Die dennoch im Vergleich zu den Pt^{II} Komplexen gleich gute Aktivität der Pt^{IV} Komplexe weist auf eine intrazelluläre Reduktion zu ihren Pt^{II} Analoga hin. Eine durch die *Prodrug*-Eigenschaften ermöglichte nebenwirkungsärmere Therapie muss jedoch noch durch Untersuchungen im Maus-Xenograft Model bestätigt werden.

NHC-Platinkomplexe stellen aufgrund ihrer physikochemischen Eigenschaften vielversprechende Kandidaten für die Tumorthherapie dar, da über Ligandenvariation nicht nur die Lipophilie, die Stabilität und andere Komplexeigenschaften eingestellt werden können, sondern eine gezielte Tumorthherapie mit Vermeidung von aufkommender Resistenzen und Nebenwirkungen möglich werden.

Summary

The increasing number of neoplastic diseases and resulting deaths, the reoccurring development of resistances against current chemotherapeutics and their strong side effects challenge researchers, despite decades of successful fight against cancer, to search for better, more selective agents for tumor therapy. In recent years, due to their high stability and variability, *N*-heterocyclic carbene complexes have proven to be promising candidates for the development of new anti-tumor agents. The Pt^{II} and Pt^{IV} NHC complexes with varying *N,N*-dibenzylimidazole-2-ylidene and *N,N*-dialkylbenzimidazole-2-ylidene ligands (*cf.* Figure 1) presented in this work, have been tested *in vitro* for their overall anti-tumoral activity, with focus on their DNA interaction, intracellular localization and associated effects on cellular processes.

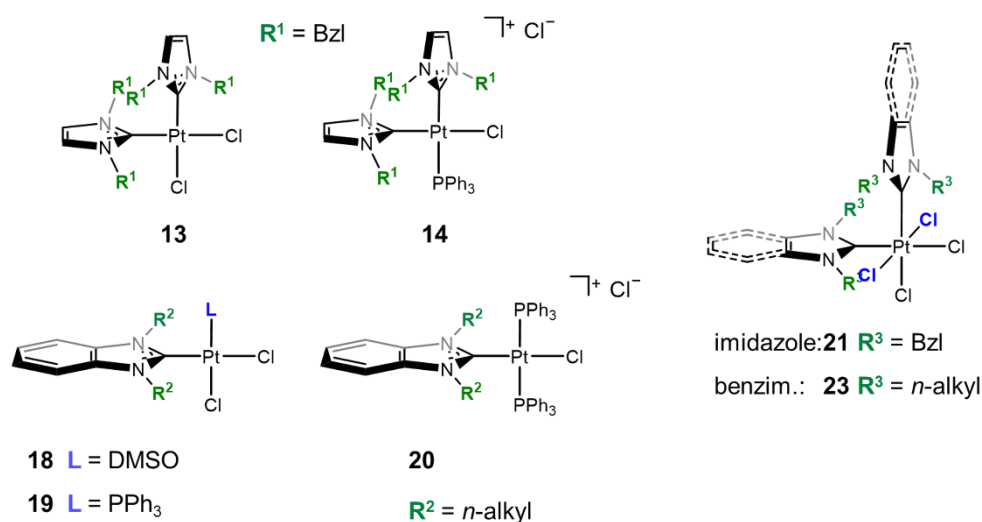


Figure 1. Compilation of the different types of complexes, that were covered by this work.

The first part of this work elucidates the mode of action of new (un)symmetrical (un)charged complexes **13** and **14** of the type *cis*-[Pt^{II}Cl(L)(NHC)¹(NHC)²], bearing *N,N*-dibenzylimidazole-2-ylidene (NHC) and Cl/PPh₃ (L) ligands. As similar Pt^{II} complexes previously, complexes with characteristics of delocalized lipophilic cations (dlc) showed an uptake-dependent, heightened toxicity. Similarly, the secondary ligands and the introduction of a positive charge strongly influenced the DNA interaction, which surpassed the intensity of that of cisplatin by far. The localization of fluorescence-tagged derivatives of this series showed that the uncharged as well as the charged complexes accumulate at the mitochondria, which is untypically for platinum complexes. Motivated by this target location, negative effects on the redox homeostasis and the collapse of the mitochondria membrane potential $\Delta\Psi$ in tumor cells was observed after treatment with complexes of this series. This distinguishes

them from cisplatin, whose main target is the DNA. Further differences between the effects of cisplatin and the here investigated platinum complexes are visible in their influence on the cell cycle progression, the cytoskeleton, and the activation of apoptosis. Connected with oxidative stress the cationic complexes **14** cause a G₁-arrest and not a S-phase arrest, like cisplatin, and a strong formation of stress fibers in the actin cytoskeleton. Finally, the activation of apoptosis mediating caspases was proven for the charged complexes. The reduced activity of the neutral complexes was not limited to the generation of toxic reactive oxygen species. The neutral complexes did not cause a cell cycle arrest and were not able to activate caspases. The from that of cisplatin different mode of action of the *cis*-[Pt^{II}Cl(L)(NHC)¹(NHC)²] complexes of this generation affords the possibility of mitigated side effects, as healthy cells possess a higher tolerance for oxidative stress than tumor cells and DNA repair mechanisms are not activated to the extent caused by cisplatin therapy.

The second part of this work investigates the influence of the secondary ligands and the overall charge of NHC complexes on their antitumoral activity, with focus on the character and intensity of the DNA interaction. This was investigated using a series of (un)charged *N,N*-dialkylbenzimidazol-2-ylidene platinum(II) complexes (**18-20**) with doubling length of the alkyl chains (methyl - *n*-octyl) and either DMSO, or up to two PPh₃ ligands. As the previously tested complexes **13-14**, complexes of this series showed a cellular uptake that strongly depended on the identity of the secondary ligands. Complexes with dlc characteristics were quickly taken up into the cells. For complexes with one PPh₃ ligand the length of the alkyl chain had the most prominent influence on the uptake. In contrast to complexes **13-14**, the uptake rate of these complexes stood in no relation to their cytotoxicities, which were erratic in this series. Detailed DNA interaction studies of complexes **18-20** revealed that the uncharged complexes form coordinative bonds with guanine bases of the DNA and kationic complexes **20** first form electrostatic interactions with the negatively charged phosphate backbone and subsequently coordinative interactions. All complexes were found to form monofunctional DNA-adducts, and thus to destabilize, distort, and unwind the DNA less than Cisplatin. These leasons could remain unrecognized and circumvent repair mechanisms of the tumor cells.

The third part of this work challenges the strong side effects that chemotherapy often entails, which motivate for a more targeted approach of tumor therapy. Inactive

prodrugs, metal complexes of higher oxidation states that are activated through reduction in the altered tumor environment, present an opportunity to reduce unwanted side effects. A series of *cis*- and *trans*-[Pt^{IV}Cl₄(NHC)₂] complexes as **21** or **23** showed mostly the same antitumoral activity as their Pt^{II} analogs. The geometry of the Pt^{IV}-complexes impairs *in vitro* DNA interaction, making them potential prodrugs for cancer therapy. Failed *in situ* reduction experiments correspond to recent research that small molecules are not responsible for reduction of the Pt^{IV} complexes, but large molecules such as proteins or enzymes.^[130] The to the Pt^{II} complexes similar activity of the Pt^{IV} complexes indicates an intracellular reduction to the Pt^{II} analogs. A side effect reduced therapy, made possible through these prodrug characteristics, still needs to be confirmed in xenograft mouse models.

NHC-platinum complexes present, due to their physicochemical characteristics, promising candidates for tumor therapy. Via finetuning of the lipophilicity, stability and other characteristics, a targeted tumor therapy with alternative modes of action, thus bypassing emerging resistances and side effects could be possible.

1 Einleitung

1.1 World Cancer Burden

Seit den 1980ern veröffentlicht die *World Health Organisation* (WHO) regelmäßig Berichte und Prognosen über die weltweite Verteilung maligner neoplastischer Neuerkrankungen, also bösartiger Tumorerkrankungen, und den daraus resultierenden Todesfällen.^[1–3] Von Beginn dieser statistischen Erfassung an, ist eine Zunahme in beiden Fällen zu verzeichnen. 2008 prognostizierte die WHO für die kommenden Jahre einen drastischen Anstieg an Krebsneuerkrankungen und damit verbundener Todesfälle.^[2] In ihrem *World Cancer Report* von 2014 schätzte die WHO basierend auf Daten des GLOBOCAN Projekts der IARC für 2012 die Anzahl der Krebsneuerkrankungen auf 14 Mio. und die Anzahl damit verbundener Todesfälle auf 8 Mio..^[3] 2018 veröffentlichte die IARC eine neue Schätzung von weltweit 18.1 Mio. Krebsneuerkrankungen und damit verbundene Todesfälle von 9.6 Mio., ein noch stärkerer Anstieg als ursprünglich prognostiziert.^[4] Häufig wird ein Zusammenhang zwischen diesem drastischen Anstieg an Krebsneuerkrankungen und der zunehmend veränderten Lebensweise der Menschen in Bezug auf Ernährung, Alkoholkonsum, Rauchen und anderer menschengemachter Umwelteinflüsse geknüpft.^[5–8] 2018 waren, dem statistischen Bundesamt (Destatis, Stand Juni, 2020) nach, in Deutschland maligne Neoplasien nach Erkrankungen des Herz-/Kreislaufsystems zur, die zweithäu-

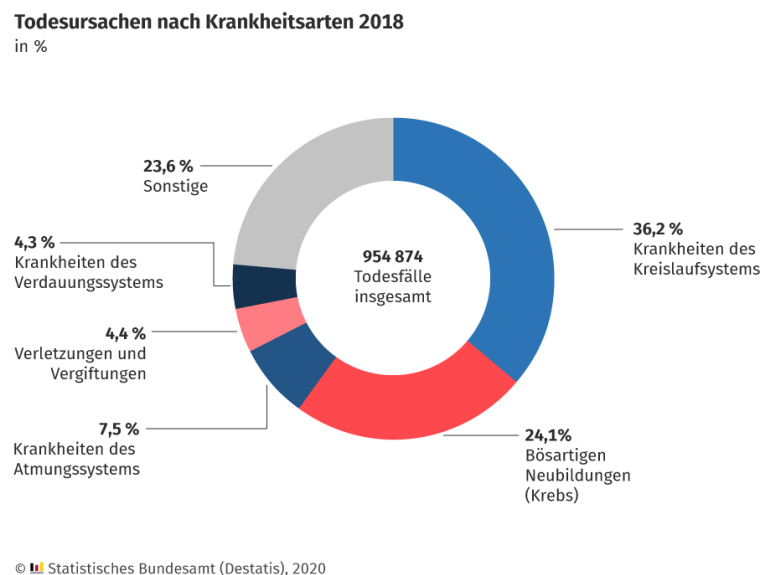


Abbildung 2. Grafische Darstellung der Todesursachen nach Krankheitsarten 2018 in Deutschland. Krebs stellt nach Erkrankungen des Herz-Kreislaufsystems die zweithäufigste Krankheitsursache der Todesfälle in Deutschland dar (Destatis, 22.06.2020).^[9]

figste Ursache krankheitsbedingter Todesfälle (vgl. Abbildung 2).^[9,10] Circa 24% aller Todesfälle 2018 ließen sich auf maligne Neoplasien zurückführen. Zu den fünf häufigsten Tumorarten, die zum Tod führten, gehörten Lungen- und Bronchial-, Mamma-, Pankreas-, Kolon-, und Prostatakarzinome.^[10] Obwohl in den letzten Jahren große Fortschritte in der Aufklärung der Ursachen und molekularen Vorgänge der Tumorbildung und der präventiven und intervenierenden Medizin gemacht wurden, stellt Krebs nach wie vor eine ernstzunehmende Belastung für die Bevölkerung dar. Diese anhaltende Problematik und die im Verlauf dieser Arbeit beschriebenen Probleme der aktuellen Tumorbehandlung stellen die Wissenschaft und Medizin weiterhin vor die Aufgabe neue Therapieansätze und -strategien gegen Tumorerkrankungen zu finden.

1.2 Tumorentstehung und -progression

Der Fortschritt der Wissenschaft ermöglichte in den letzten Jahrzehnten die Aufdeckung molekularer Vorgänge, die während der Tumorentstehung und -progression ablaufen. HANAHAN und WEINBERG definierten 2000 die sogenannten *Hallmarks of Cancer* und fügten diesen 2011 einige neu entdeckte *hallmarks* hinzu (vgl. Abbildung 3).^[11,12] Diese *hallmarks* beschreiben Eigenschaften, die sich Zellen während der Transformation zur Tumorzelle aneignen und welchen Einfluss das darum liegende Gewebe, von HANAHAN und WEINBERG erstmals als Tumorumgebung definiert, auf Tumorwachstum und -progression hat. Zu diesen Eigenschaften zählen

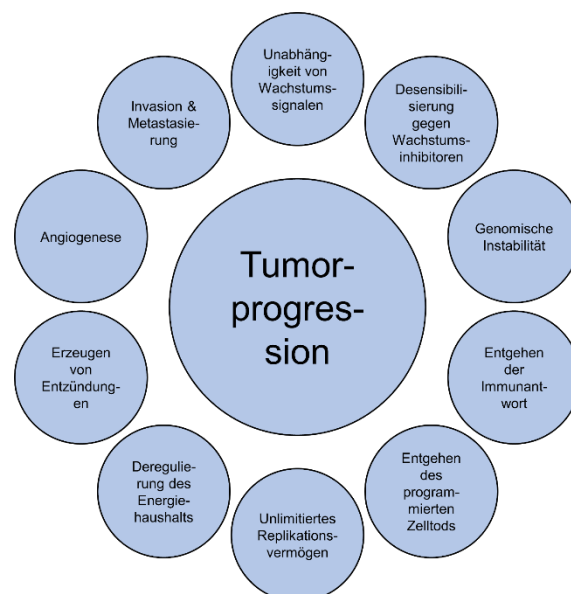


Abbildung 3. *Hallmarks of Cancer*, von HANAHAN & WEINBERG definierte Eigenschaften, die Tumorzellen bzw. Tumore bei ihrer Entstehung und ihrem Wachstum erlangen.^[11,12]

die (1) Unabhängigkeit von Wachstumssignalen, (2) Desensibilisierung gegenüber Wachstumsinhibitoren, (3) genomische Instabilität, (4) das Entkommen vor der körpereigenen Immunantwort und (5) des programmierten Zelltods, (6) ein unlimitiertes Replikationsvermögen, (7) die Deregulierung des zellulären Energiehaushaltes, (8) das Erzeugen tumorfördernder Entzündungsreaktionen, (9) die Aktivierung von Angiogenese, und (10) der Invasion und Metastasierung.^[12] Die Proliferation einer Zelle ist stark abhängig vom Gleichgewicht zwischen externen und internen, wachstumsfördernden und -inhibierenden Signalen. In der Regel üben vor allem die umliegenden Zellen durch Sezernieren derartiger Signale einen starken Einfluss auf das Wachstumsverhalten einer Zelle aus. Veränderte Expressionslevel der Signalproteine oder Mutationen der Rezeptoren führen zur Unabhängigkeit dieser Wachstumssignale (1 & 2). Dies hat zur Folge, dass die transformierenden Zellen unter chronisch erhöhter Proliferation stehen und das umliegende Gewebe durch wachstumsinhibierende Signale keinen Einfluss mehr auf die Proliferation der Tumorzelle nehmen kann.^[13] Diese verstärkte Proliferationsrate kann weitere *hallmarks* nach sich ziehen. Durch das Umgehen sogenannter Zellzyklus *checkpoints* (vgl. Abbildung 4), Kontrollpunkte, die die intra- und extrazellulären Bedingungen für den Verlauf des Zellzyklus prüfen, kommt es z.B. zu einer erhöhten Instabilität des Genoms (3).^[14] Diese *checkpoints* können den Zellzyklus an den Phasenübergängen anhalten, wenn z.B. die DNA-Synthese nicht korrekt verlief, die Mitose oder die Zellteilung nicht vollständig beendet wurde. Auch der allgemeine Zustand der Zelle

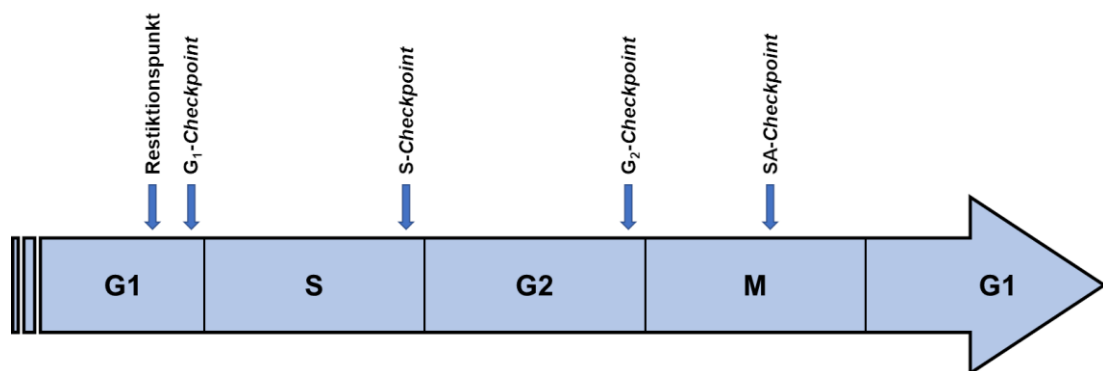


Abbildung 4. Zellzyklus *checkpoints* kontrollieren den korrekten Ablauf des Zellzyklus. Der Restriktionspunkt überprüft externe und interne Bedingungen der Zelle für Eintritt in den Zellzyklus, der G₁-, S- und G₂ Checkpoint stoppen den Zellzyklus bei DNA Schäden (G₁, S, G₂), Störungen an der Replikationsgabel (S) oder unvollständig replizierter DNA (G₂). Der *spindle assembly checkpoint* (SA) stoppt den Zellzyklus in der Mitose (M), wenn die Chromosomen nicht vollständig an die mitotische Spindel gebunden sind.

bzw. negative Umwelteinflüsse können zu Zellzyklusarretierungen führen.^[14] Durch das Ausschalten dieser *checkpoints* erhöht sich die Mutationsrate der Zellen da Fehler, die normalerweise korrigiert worden wären einfach übergangen und an die Tochterzellen weitergegeben werden.^[15–17] Weiterhin hat die erhöhte Proliferationsrate einen starken Stoffwechselanstieg und einen veränderten Energiehaushalt der entarteten Zellen zur Folge (7). Dies äußert sich unter anderem in veränderten Expressionslevel von Enzymen und Proteinen, die das intrazelluläre Redoxmilieu aufrechterhalten (z.B. TrxR, GSH) und in einer erhöhten Menge sogenannter ROS, ein Resultat erhöhter mitochondrialer Aktivität.^[18,19] Der erhöhte Stoffwechsel der Tumorzellen verursacht in der Tumorumgebung eine konstante Hypoxie und ein reduktives Milieu. Dieser hypoxische Zustand und der erhöhte Nährstoffverbrauch aktivieren Strategien der Tumorzellen, die bei weiterem Verlauf schwerwiegende Folgen für den Patienten haben können. Tumorzellen rekrutieren ab einer Tumorgröße weniger Millimeter das umliegende Gewebe dazu, Blutgefäße zum Wachstum anzuregen (Angiogenese)(9).^[20–22] Sekretierte VEGF's stimulieren Endothelzellen der nahegelegenen Blutgefäße zur Teilung und zur Ausweitung des Gefäßsystems in Richtung Tumor. Das tumorale Blutgefäßsystem versorgt den Tumor mit den nötigen Nährstoffen und ermöglicht es dem Tumorgewebe sich weiter auszubreiten. Im Gegensatz zu gesunden Blutgefäßen ist das tumorale Blutgefäßsystem aufgrund seines unregulierten Wachstums ungleichmäßig, fehlerhaft und oft löchrig.^[21,22] Einige Tumorzellen können sich vom Primärtumor ablösen, in das umliegende Gewebe (Invasion) und die Blutgefäße eindringen (Intravasation), über die Blut- und Lymphbahnen in entfernte Teile des Körpers wandern, dort wieder aus den Blutgefäßen heraustreten (Extravasation), und neue Tumorkolonien bilden (Metastasierung)(vgl. Abbildung 5).^[23,24] In den meisten Fällen sind es diese neuen Tumorherde und die negativen Auswirkungen auf die dort liegende Umgebung (z.B. , die letztendlich zum Tod führen.^[25] Die fehlerhafte Ausbildung der Blutgefäße begünstigt dies und erschwert eine Behandlung des Tumors, da Chemotherapeutika eher im Gewebe versickern als ihr Ziel zu erreichen.^[21,22] Es ist nicht zwingend, dass sich ein Tumor alle diese Eigenschaften aneignet, und auch die Reihenfolge ist nicht festgelegt.^[11,12]

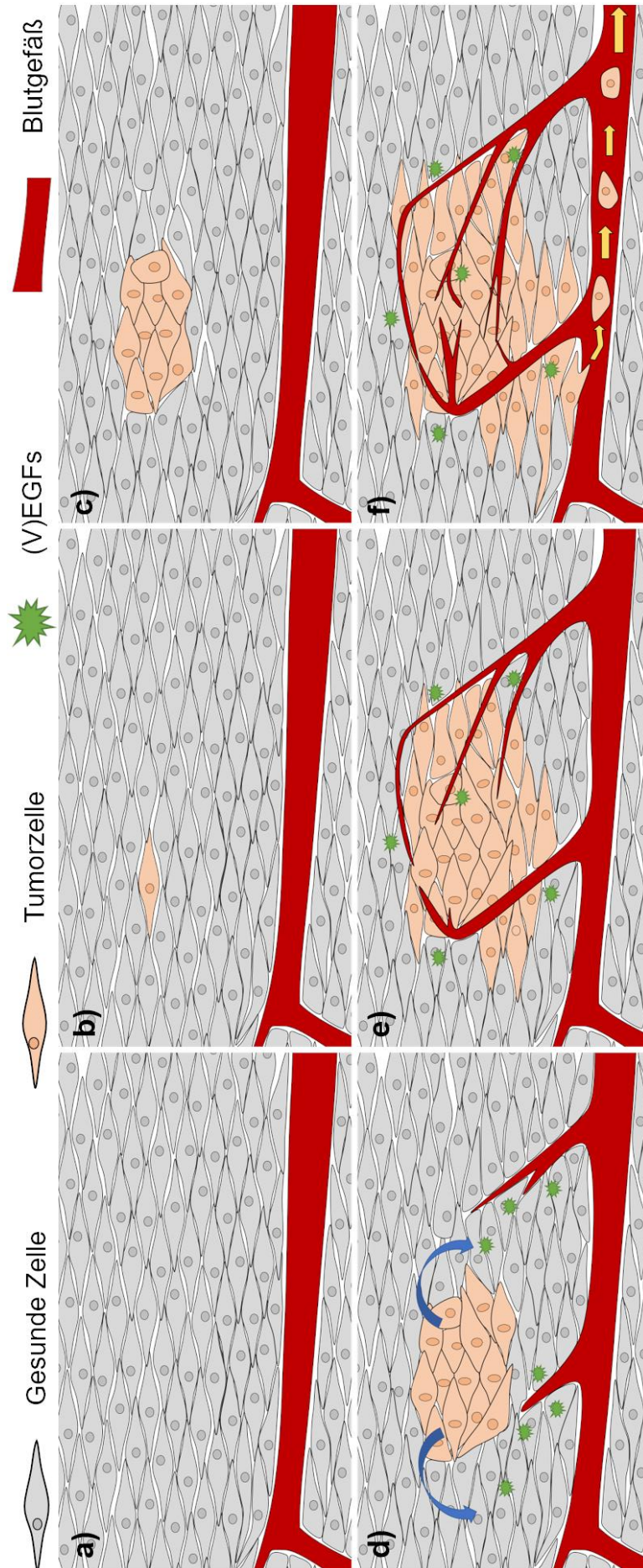


Abbildung 5. Tumorentstehung und -progression durch Transformation einer gesunden Zelle (a, b). Die Tumorzelle vermehrt sich und verdrängt umliegende gesunde Zellen (c). Ab einer Größe von ca. 2 mm reichen die durch das Gewebe diffundierten Nährstoffe und der Sauerstoff nicht mehr aus, um die Tumorzellen zu versorgen. Die Tumorzellen regen durch Sekretion von (V)EGFs Blutgefäße im umliegenden Gewebe zur Sprossung an (d). Die Endothelzellen der Blutgefäße teilen sich in Richtung Tumor und es bildet sich ein tumorales Blutgefäßsystem (d, e). Einzelne Zellen können dem Tumorverband entkommen (f), durch das Gewebe wandern (Migration), in die Blutbahn eindringen (Intravasation), in entfernte Körperteile gelangen, dort wieder in das Gewebe eindringen (Extravasation) und sekundäre Tumorherde bilden (Metastasierung).^[11,12,24]

1.3 Die klassische Platin-Tumorthherapie

Die Kenntnis von den molekularen Vorgängen während der Transformation und dem Tumorwachstum bietet die Chance gezielt auf den Tumor und die Tumorumgebung einwirken zu können. Einige der *hallmarks* bieten ideale *targets* für die Tumorthherapie. So wurde die Suche nach immer besseren, spezifischeren Wirkstoffen, die eine erhöhte Aktivität und gleichzeitig geringere Nebenwirkungen als bisher verwendete Wirkstoffe aufweisen zu einem wichtigen Forschungsbereich der pharmazeutischen Wissenschaft. Wirkstoffe die gezielt bestimmte *targets* ansprechen rückten in den Fokus der Forschung. Zu diesen *targets* gehören u.a. die DNA, die Mitochondrien, das Zytoskelett und essenzielle zelluläre Prozesse, die über das Wachstum und Überleben einer Tumorzelle entscheiden können, sowie das tumorale Blutgefäßsystem. Die klassische Tumorthherapie zielt auf die nucleare DNA ab. Die Schädigung der DNA und damit verbundener Prozesse kann je nach Ausmaß der Störung schwerwiegende Folgen für eine Zelle haben. Die Geschichte der Platin-Tumorthherapie geht viele Jahre auf BARNETT ROSENBERG und dessen zufällige Entdeckung der biologischen Wirkung von Cisplatin, die Aufklärung des genauen Wirkmechanismus und die Entwicklung zu den heute eingesetzten Tumorwirkstoffen zurück.^[26,27]

1.3.1 Peyrone's Chlorid – Die Wiederentdeckung

Als B. ROSENBERG *et al.* 1965 bei ihrer Untersuchung der Auswirkungen elektromagnetischer Felder auf das Wachstumsverhalten von *E. coli* zufällig die biologische Aktivität von dem damals als Peyrone's Chlorid (1844 M. PEYRONE) bekannten Cisplatin entdeckten, ahnten sie nicht, dass sie mit ihrer Entdeckung und der darauffolgenden Forschung eine neue Ära der Tumorthherapie, die einige Jahrzehnte andauern sollte, einläuteten.^[28,29] Während ihrer Untersuchungen beobachteten die Wissenschaftler nach Anlegen einer elektrischen Spannung eine Verlängerung der Bakterienzellen um das ca. 300 fache der Ursprünglichen Größe. Dieser Effekt blieb auch nach Abschalten des Stroms erhalten, was ROSENBERG *et al.* zu dem Schluss brachte, dass diese Verlängerung der Bakterien nicht ein Effekt der elektrischen Felder, sondern auf neugebildete Verbindungen im Bakterienmedium zurückzuführen war.^[29] Bei der Durchführung ihrer Experimente reagierte von der Platinelektrode abgelöstes Platin, das aufgrund seiner chemischen Inertheit häufig verwendet wurde, mit dem Ammoniumchlorid im Medium zu dem heute als Cisplatin bekannten *cis-*

$[\text{Pt}^{\text{II}}\text{Cl}_2(\text{NH}_3)_2]$ (**1**) und seinem Platin(IV) Analog $\text{cis-}[\text{Pt}^{\text{IV}}\text{Cl}_4(\text{NH}_3)_2]$ (**2**) (vgl. Abbildung 6).^[29]

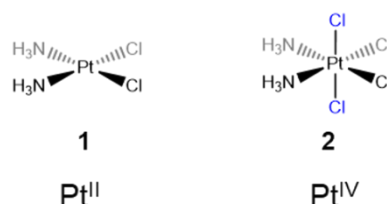


Abbildung 6. Strukturen des von M. PEYRONE 1844 erstmals synthetisierten und von B. ROSENBERG et al. 1965 wiederentdeckten $\text{cis-}[\text{Pt}^{\text{II}}\text{Cl}_2(\text{NH}_3)_2]$ (1**) und seines Pt^{IV}-Analog $\text{cis-}[\text{Pt}^{\text{IV}}\text{Cl}_4(\text{NH}_3)_2]$ (**2**).**^[29,30]

In den nächsten Jahren konnten ROSENBERG *et al.* zeigen, dass Cisplatin nicht nur das Wachstum verschiedener Gram-negativer Bakterien inhibiert, sondern auch zum Wachstumsstopp und zur Regression von Sarkoma 180-Tumoren und Leukämie L1210 führte, die in *ICR* Mäuse gepflanzt wurden.^[30,31] 1978 wurde Cisplatin schließlich von der FDA zur Behandlung von Hodenkrebs zugelassen. Basierend auf der erfolgreichen klinischen Anwendung von Cisplatin wurde in den nächsten Jahren eine Vielzahl verschiedener Platin- und anderer Metallverbindungen auf ihre antitumorale Wirkung hin untersucht, mit dem Ziel die dosislimitierenden Nebenwirkungen von Cisplatin, wie Nephro-, Neuro-, und Ototoxizität, Anämie, sowie Übelkeit, und Erbrechen, zu senken und die Bioverfügbarkeit und die Tumorspezifität zu erhöhen.^[32–36] Auf diese Weise wurde eine zweite und dritte Generation von Cisplatin-Analoga entwickelt, welche zwar eine reduzierte Nephrotoxizität und einen Rückgang anderer Nebenwirkungen verzeichnen ließen, jedoch andere Nachteile wie z.B. geringere Effektivität mit sich brachten (vgl. Abbildung 7).^[26,37,38]

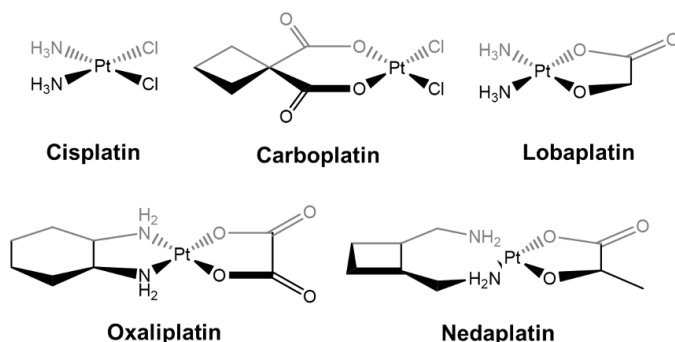


Abbildung 7. Strukturen der ersten, zweiten und dritten Generation von Cisplatin-Wirkstoffen, die heute weltweit oder nur in bestimmten Ländern zur Tumorbehandlung zugelassen sind: Cisplatin, Carboplatin, Lobaplatin, Oxaliplatin und Nedaplatin.

Trotz ihrer gemilderten, jedoch weiterhin bestehenden Nebenwirkungen gehören diese Platinverbindungen auch heute noch zu den Standardbehandlungen von Tumorerkrankungen und werden bei soliden Krebserkrankungen der Hoden, Eierstöcke, der Blase, verschiedener Arten von Lungenkrebs, Melanome, Lymphome

und Myelome bevorzugt eingesetzt.^[39,40] Während Cisplatin, Oxaliplatin und Carboplatin weltweit für die klinische Anwendung zugelassen sind, werden Nedaplatin (Japan), Lobaplatin (China) nur in bestimmten Ländern verwendet.^[36]

1.3.2 (Klassischer) Wirkmechanismus von Platinverbindungen

Cisplatin und seine Analoga folgen dem gleichen Wirkmechanismus und binden an Purinbasen der DNA. Während der Chemotherapie werden die Cisplatin-Verbindungen in einer mit Mannitol versetzten Saline gelöst parenteral verabreicht.^[41,42] Die Zugabe von Mannitol lindert die Nephrotoxizität, eine der Nebenwirkungen der Platin-Chemotherapie, die Chlorid-haltige Saline (154 mM) verhindert einen vorzeitigen Austausch der Chlorliganden gegen Wasser. Im Blut verhindert dies der natürliche Chloridionengehalt.^[42,43] Gelangt das Platinsalz aus dem Blutstrom über Diffusion oder aktive Transporter wie den Kupfertransporter CTR1 in die Zelle, kommt es aufgrund des Konzentrationsabfalls an Chloridionen von ca. 100 mM im extrazellulären Raum auf ca. 4 mM im Cytosol zum Austausch eines oder beider Chloridliganden gegen Wasser und zur Bildung des aktiven *cis*-Diamminodiaquaplatin(II) (vgl. Abbildung 8).^[41,44,45] Durch den Ligandenaustausch liegt der Komplex nun positiv geladen vor und kann nicht mehr durch die Zellmembran diffundieren.^[41] In einigen Tumorentitäten sind Transporter wie CTR1 entscheidend bei der Resistenzbildung gegen Platintherapeutika. So wird die CTR1-Expression stark reduziert sobald bestimmte Tumorentitäten mit Cisplatin oder

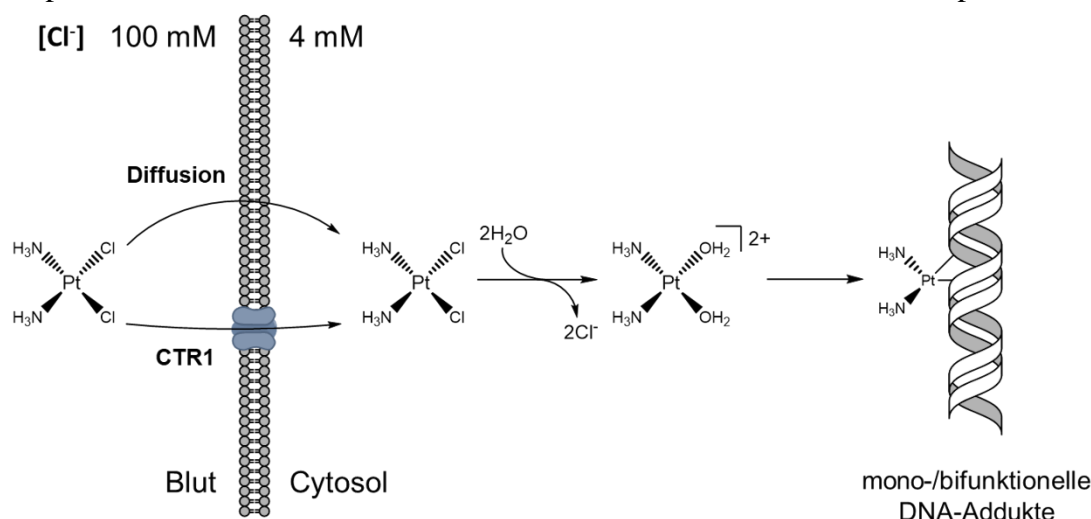


Abbildung 8. Schema der Aufnahme, Aktivierung und Adduktbildung von Cisplatin mit DNA. Die Aufnahme des neutralen Cisplatin erfolgt durch Diffusion oder aktive Transporter (z.B. CTR1) aus dem Blut in die Zelle. Der Austausch der Chlor-Liganden gegen Wasser findet aufgrund des Konzentrationsunterschieds der Chloridionen im Blutstrom und im Cytosol statt. Die Bildung von mono- oder bifunktionellen DNA-Addukten erfolgt bevorzugt mit Guanin und Adenin. Abbildung frei nach ALERDEN *et al.*.^[41]

Kupferverbindungen behandelt werden. Der Verlust von CTR1 hat einen starken Anstieg der Cisplatin-Resistenz zur Folge.^[26,41,46,47]

Erreicht der aktive, aquierte Platinkomplex die DNA im Zellkern so bildet er mono- oder bifunktionelle Addukte mit Nucleobasen in der großen Furche der DNA.^[26,27,41] Dabei wird das Pt-Atom spezifisch vom N⁷ von Guaninbasen (vgl. Abbildung 9) koordiniert, in wenigen Fällen auch von Adeninbasen.^[27] Die übrigen Stickstoffatome der Purinbasen stehen aufgrund von sterischen Einschränkungen in der Doppelhelix für die Komplexbildung nicht zur Verfügung. Der Austausch des zweiten Aqualiganden

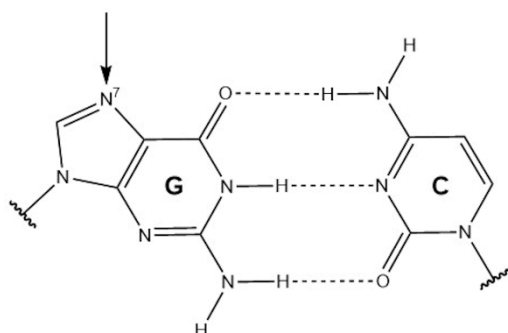


Abbildung 9. Angriffspunkt von Cisplatin und seinen Analoga in der GC-Basenpaarung. Cisplatin bindet bevorzugt am N⁷ der Guaninbasen. Aufgrund von sterischen Hinderungen stehen die anderen Stickstoffe als Reaktionspartner in der Doppelhelix nicht zu Verfügung.

ermöglicht die Verknüpfung zweier direkt benachbarter Nucleobasen im gleichen Strang, was die Paarungen *cis*-GG (1,2-intrastrang, ca. 65% der Fälle) oder *cis*-AG (1,2-intrastrang, ca. 25 % der Fälle) ermöglicht.^[27,47] Seltener sind bifunktionelle Addukte mit Guaninbasen, zwischen denen eine weitere Nucleobase (N) liegt (GNG 1,3-intrastrang). Ebenso selten sind monofunktionelle Addukte an Guanin

oder bifunktionelle Addukte mit zwei Guaninbasen an verschiedenen DNA-Strängen (*cis*-GG-interstrang).^[27,47,48] Die Ausbildung einer 1,2-intrastrang Verknüpfung über zwei benachbarte Guaninbasen führt zum Abknicken der DNA um ca. 40°-70° in Richtung der großen Furche und einer Entwindung der Doppelhelix um 10°-23° (vgl. Abbildung 10).^[27,50-52] Die Verdrehung der DNA verhindert das korrekte Binden von DNA-assoziierten Proteinen, bzw. das Ablesen der genetischen Information und essenzielle zelluläre Prozesse werden angehalten. In einer derartig geschädigten Tumorzelle werden über Sensoren (ATM, ATR) die DNA Schäden erkennen eine Reihe zellulärer Signalwege, die zu Überlebensstrategien bei DNA-Schädigungen gehören aktiviert und versucht diese rückgängig zu machen bzw. die Apoptose auslöst.^[53-55]

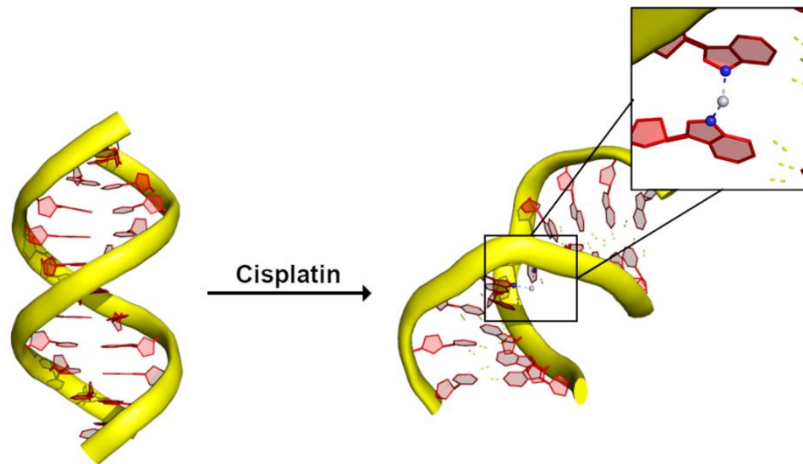


Abbildung 10. Morphologische Veränderung einer B-DNA Doppelhelix (links) nach Aus-bildung einer 1,2-Intrastrang-verknüpfung mit Cisplatin (rechts). Die Verknüpfung zweier benachbarter Guaninbasen führt zum Abknicken der DNA in Richtung der *major groove*, und folglich zur Aktivierung von zellulären *pathways*, die mit DNA-Reparatur und *cell survival* assoziiert sind, und letztendlich zur Aktivierung von Apoptose.^[49,51]

1.4 Zelluläre Reaktion auf DNA-Schäden

TP53 gehört zu einigen wenigen Genen, welche als „Wächter“ die Transformation einer gesunden Zelle zu einer Krebszelle verhindern und stellt einen der wichtigsten Regulatoren der Zellzyklus-*checkpoints* dar. *TP53* trägt in ca. 50 % aller Tumorerkrankungen eine Mutation, die das Expressionsprodukt inaktiviert oder vollständig löscht.^[56] Das Tumorsuppressorgen codiert für den Transkriptionsfaktor p53, welcher aufgrund von genotoxischen und anderen zellulären Stresssignalen aktiviert wird und verschiedene Überlebensstrategien der Zelle aktivieren kann.^[57] Das Protein wird in jeder Zelle konstant produziert, unterliegt jedoch einer natürlichen Instabilität und kommt daher in gesunden Zellen fast nicht vor.^[58–60] Zu den Stresssignalen, welche p53 aktivieren gehören DNA-Schäden, Hypoxie, Hyperoxie, die Aktivierung von Oncogenen wie *myc* oder *Ras*, durch einen erhöhten zellulären Metabolismus verursachter Nährstoffmangel und einige mehr (vgl. Abbildung 11).^[58–59] Die Aktivierung von p53 löst je nach Ursache des Stresssignals verschiedene Zellantworten aus. Eines der primären Signale, die zu einer p53-Aktivierung führen ist die Beeinträchtigung der DNA z.B. durch Strahlung, genotoxische Verbindungen oder oxidative Schäden.^[61] In den letzten Jahren wurde p53 mit zunehmend mehr Stressreaktionen der Zelle in Verbindung gebracht und gilt heute als Dreh- und Angelpunkt für die Vermittlung der verschiedensten Stressreaktionen. Zu den wichtigsten Folgen, die die p53 Aktivierung mit sich bringt, gehören der

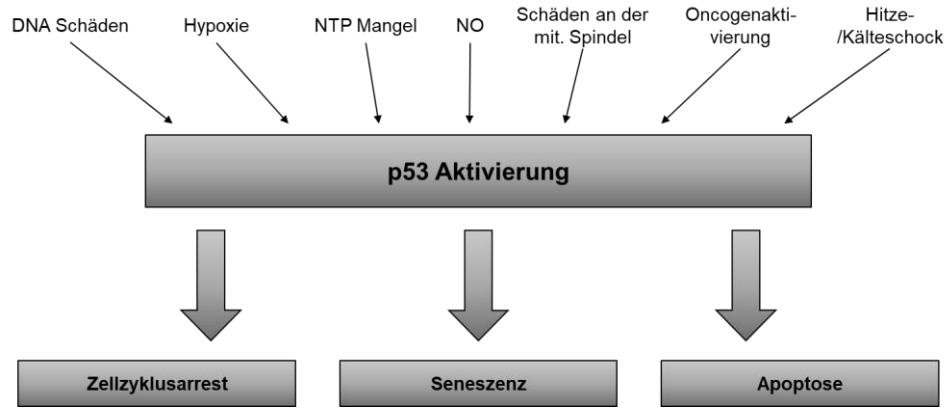


Abbildung 11. Aktivierung von p53 durch Stresssignale wie DNA-Schäden, Hypoxie, NTP-Mangel, Stickstoffmonoxidlevel, Schäden der mitotischen Spindel, Aktivierung von Oncogenen oder Hitze-/Kälteschock der Zelle, resultierend in Zellzyklusarrest, Seneszenz oder Apoptose. ^[58,59]

Zellzyklusarrest, Seneszenz der Zelle oder der programmierte Zelltod, die Apoptose.^[57] Der Arrest am Kontrollpunkt einer Phase des Zellzyklus gibt der Zelle Zeit entsprechend auf die Stressursache zu reagieren und z.B. DNA-Reparaturmechanismen zu aktivieren. Die Aktivierung von p53 erfolgt durch posttranslationale Modifikationen des Proteins wie Phosphorylierungen durch ATM, ATR oder DNA-PK.^[53–55] Diese drei Kinasen erkennen Schäden an der DNA und geben dieses Signal an p53 weiter. Das sonst instabile Protein wird dadurch stabilisiert und akkumuliert in der Zelle. p53 fördert als Transkriptionsfaktor die Expression verschiedener Proteine und Enzyme, die Teil von DNA-Reparaturmechanismen sind, das Fortschreiten im Zellzyklus beeinträchtigen oder das Schicksal der Zelle durch Einleiten von Seneszenz oder Apoptose entscheiden können. Wird die DNA beeinträchtigt fördert die erhöhte p53 Konzentration die Expression von p21.^[62–65] Dieses bindet und inhibiert cyclin/CDK-Komplexe, welche für das Fortschreiten im Zellzyklus von der G₁-Phase in die S-Phase kontrollieren, d.h. die Zelle arretiert am Kontrollpunkt in der G₁-Phase des Zellzyklus (vgl. Abbildung 12).^[66,67] AP-1, bzw. Sp1 können, aktiviert durch eine toxische ROS Konzentration, die p21-Expression direkt aktivieren und verhindert einen oxidativen Schaden der DNA bzw. deren Replikation.^[69–72] Der Charakter des Stresssignals bestimmt die Art der p53 Aktivierung und folglich eine entsprechende Stressantwort. So kann p53 auch einen Zellzyklusarrest während der S-Phase und am G₂/M Kontrollpunkt auslösen.^[73] Durch Auslösen bestimmter Stresssituationen und dadurch das Aktivieren von p53 vermittelten Signalwegen lassen sich Tumorzellen gezielt bekämpfen.

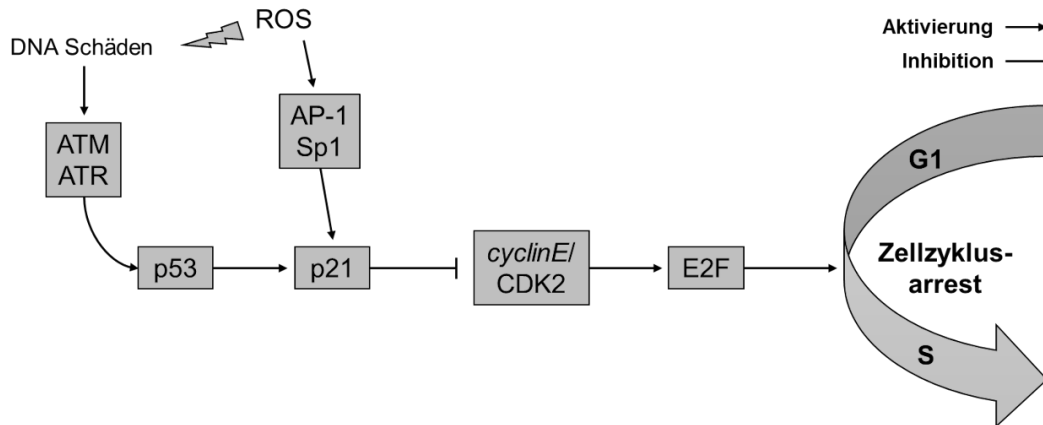


Abbildung 12. Signalweg des Zellzyklusarrests am G₁/S Checkpoint. DNA Schäden werden von ATM/ATR erkannt, schädliche Konzentrationen von ROS durch AP-1/SP1. ATM/ATR stabilisiert p53, welches als Transkriptionsfaktor die Expression von p21 vermittelt. AP-1/SP1 aktivieren ebenfalls die Expression von p21. Dieses bindet an cyclin/CDK Proteinkomplexe und inhibiert deren Aktivität. E2F, nötig für den Übergang von der G₁-Phase in die S-Phase, wird nicht mehr phosphoryliert und bleibt inaktiv. Es kommt zum G₁-Arrest der Zelle.^[53–55,61,66,68]

1.5 Apoptose – Der programmierte Zelltod

Bei irreversiblen Schäden der DNA, toxischen ROS-Mengen, oder anderer irreparablen Zellschäden wird u.a. der programmierte Zelltod, die Apoptose ausgelöst.^[74,75] Diese läuft, im Gegensatz zum Zelltod durch Nekrose, streng reguliert und „sauber“ ab.^[76] Eine Zelle erfährt während der Apoptose charakteristische morphologische Veränderungen: Die Zelle schrumpft und rundet sich ab. Komponenten des Zytoskeletts depolymerisieren, und die Kernlamina wird abgebaut, die DNA kondensiert und fragmentiert.^[74] Die abgebauten Zellbestandteile werden in sogenannten apoptotischen Körperchen verpackt (*blebbing*) und von Phagocyten oder benachbarten Zellen absorbiert, bevor sie ihren Inhalt in das Gewebe entlassen (vgl. Abbildung 13). Während der Nekrose schwillt die Zelle an, bis sie platzt und ihren gesamten Zellinhalt in das Gewebe frei gibt.^[74,76] Dies ruft Entzündungsreaktionen des Gewebes hervor und kann benachbarte Zellen schädigen.^[77] Die Regulation der Apoptose unterliegt einem verschränkten Netz von zellulären pro- und anti-apoptotischen Signalketten. Verschiebt sich das Gleichgewicht dieser Signale in

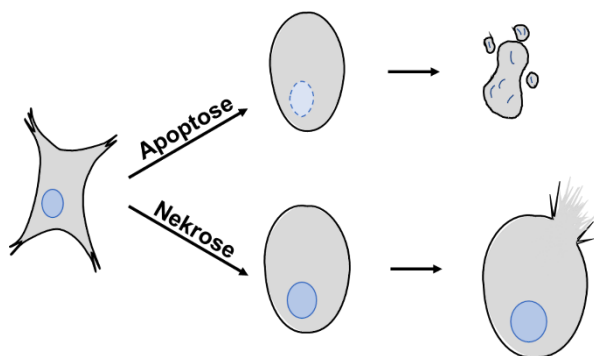


Abbildung 13. Morphologische Veränderungen einer apoptotischen und einer nekrotischen Zelle. Die apoptotische Zelle schrumpft, rundet sich ab. Nach Abbau von Proteinen und DNA werden Zellbestandteile in apoptotischen Körperchen verpackt und durch benachbarte Zellen phagocytiiert. Die nekrotische Zelle schwillt an bis ihre Plasmamembran reißt und der Zellinhalt in das Gewebe freigegeben wird. Blau – Nucleus.^[74]

Richtung pro-apoptotisch wird eine Kaskade von Protease-Aktivierungen ausgelöst, die sich nicht nur selbst verstärkt, sondern auch nicht mehr aufzuhalten ist.^[75,78]

Im Folgenden sollen vereinfacht die zellulären Mechanismen und insbesondere die Rolle der Caspasen während der Apoptose-Induktion, Signalweitergabe und Ausführung genauer erläutert werden.

Apoptose kann in einer Zelle über verschiedene Signalwege, u.a. den extrinsischen und den intrinsischen und einen von diesen unabhängigen Weg ausgelöst werden.^[75,79,80] Der extrinsische Signalweg (vgl. Abbildung 14) wird über *TNF*-Todesrezeptoren (z.B. *FasR*) durch binden extrazellulärer Signale (z.B. *FasL*) aktiviert.^[79,81] Über ihre intrazelluläre Todesdomäne rekrutieren sie Proteine (*FADD*, *Procaspasen-8/-10*), die den sogenannten DISC bilden. Durch die räumliche Nähe der Procaspasen im DISC aktivieren sich diese autokatalytisch. Die aktiven Caspasen fungieren als Initiatorcaspasen der Effektorcaspasen -3, -6 und -7, welche letztendlich den Abbau der Zelle vermitteln.^[82,83] Oft reichen die Signale des extrinsischen Signalweges nicht aus, um den *point of no return* zu überschreiten, weshalb der extrinsische auch den intrinsischen Apoptoseweg rekrutiert und aktiviert.^[75,79,84,85]

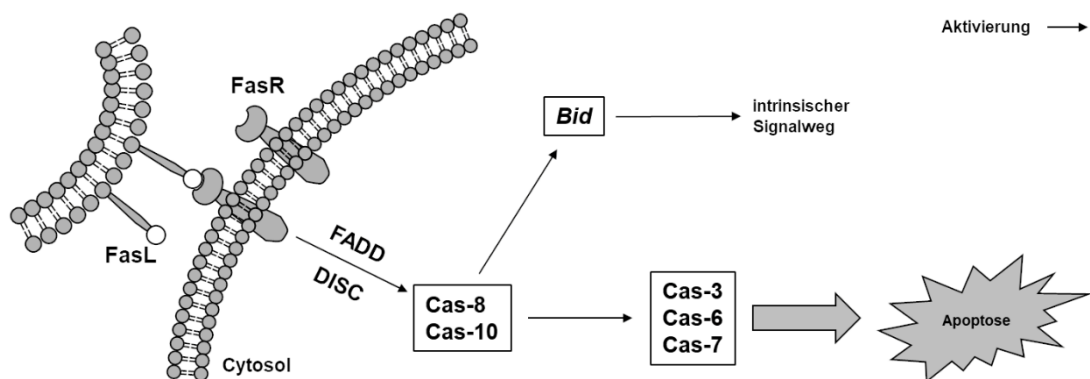


Abbildung 14 Aktivierung des extrinsischen Signalweges durch Binden des TNF Liganden FasL an die Todesrezeptoren FasR. Das Signal wird durch Rekrutierung von FADD und Bilden des DISC in das Zellinnere weitergegeben. Im DISC werden die Initiatorcaspasen-8 und -10 autokatalytisch aktiviert, die ihrerseits das Signal an die Effektorcaspasen-3, -6 und -7 weitergeben. Bid verbindet den extrinsischen und intrinsischen Signalweg.^[75,82–85]

Der intrinsische Signalweg wird durch Schäden an der DNA, chemotoxische Substanzen, starke Veränderungen von zellulären Signalwegen, exzessive Aktivierung der Zellprogression und anderen proapoptotischen Signalen ausgelöst (vgl. Abbildung 15).^[79] Pro- und antiapoptotische Mitglieder der Bcl-2 Familie regulieren den intrinsischen Signalweg durch gegenseitige Interaktion und Inhibition.^[86] Kommt es z.B. zur irreversiblen Schädigung der DNA leitet der Transkriptionsfaktor p53, die Expression von proapoptotischen Proteinen (*Puma*, *Noxa*) ein, welche ihrerseits

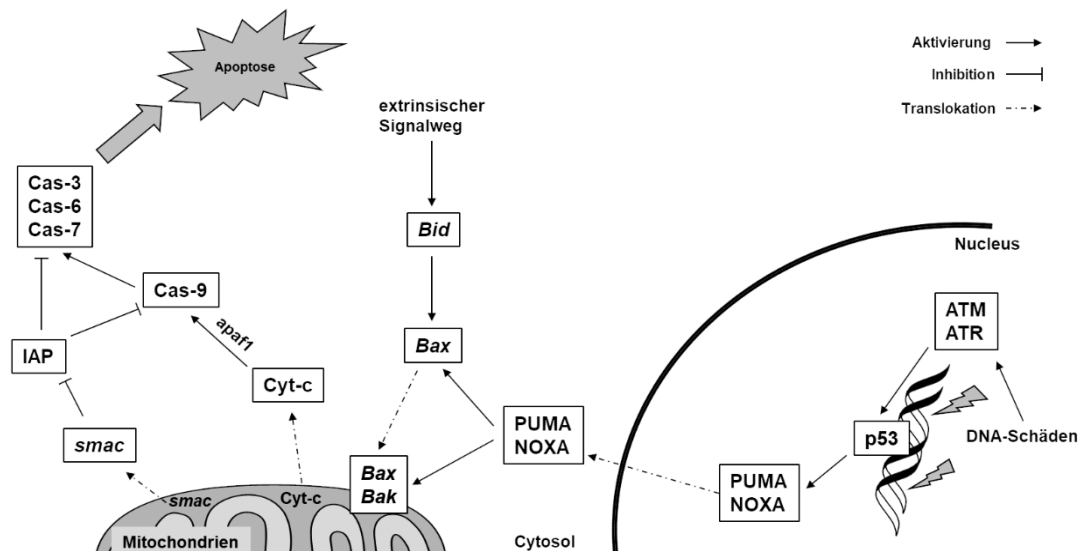


Abbildung 15. Aktivierung des intrinsischen Signalwegs durch Schädigung der DNA. Kontrollproteine wie ATM oder ATR erkennen irreparable Schäden an der DNA und stabilisieren p53. Dieses fungiert als TF für PUMA und NOXA. Diese aktivieren proapoptotische Mitglieder der Bcl-2 Familie (z.B. Bax, Bak), welche in der Mitochondrienmembran integriert Poren bilden und Proteine wie Cytochrom-c oder smac in das Cytosol freisetzen. Cytochrom-c bildet gemeinsam mit apaf1 und der Procaspase-9 das Apoptosom. Die Initiatorcaspase-9 aktiviert sich autokatalytisch und gibt das Signal an die Effektorcaspasen-3,-6,-7 weiter. Smac inhibiert die Caspaseinhibitoren IAP. Bax kann ebenfalls über den extrinsischen Signalweg durch Bid (tBid) aktiviert werden.^[66,88,90,92–94]

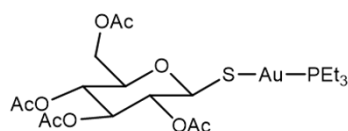
Apoptosevermittler (*Bax*, *Bak*) aktivieren.^[87–89] Aktiviert bilden *Bax* und *Bak* Membranporen und Faktoren wie Cytochrom-c oder *smac* entkommen aus dem Intermembranraum der Mitochondrien ins Cytosol. Cytochrom-c, das normalerweise als Elektronentransporter in der mitochondrialen Atmungskette fungiert, übt nun im Cytosol eine sekundäre, apoptose vermittelnde Funktion aus und aktiviert im Apoptosom (*apaf1*) die Initiatorprocaspase-9.^[79,90,91] Caspase-9, welche sich wie die Initiator Caspasen des extrinsischen Weges, durch ihre räumliche Nähe im Apoptosom erst selbst und anschließend wiederum die Caspasen-3, -6 und -7 aktivieren.^[93,94] Das Bcl-2 Protein *Bid* verknüpft diese zwei Signalwege (extrinsisch und intrinsisch) indem es von Caspase-8 gespalten wird und als *tBid* *Bax* aktiviert.^[92] Um eine zufällige Aktivierung der Apoptosewege zu verhindern wird das Signal der autokatalytisch aktiven Caspasen durch IAPs gedämpft. Diese Inhibitoren interagieren entweder mit dem aktiven Zentrum oder markieren die Caspasen durch Ubiquitinierung für den Abbau.^[95] Aus den Mitochondrien freigesetzte Regulatoren wie *smac* inhibieren die Aktivität der IAPs und verstärken das apoptotische Signal.^[96] Die aktiven Effektor-Caspasen aktivieren Enzyme, wie Proteasen, Kinasen und DNAsen, oder bauen selbst Kompartimente der Zellen ab.^[79, 97-100]

Die Mitochondrien vermitteln nicht nur indirekt die Apoptose, sondern können auch direkt als *target* der Tumorthherapie angesprochen werden. Die direkte Deregulierung

der Redoxhomöostase durch das gezielte Erzeugen von ROS oder die Inhibition von Enzymen, die das Redoxmilieu aufrecht erhalten (z.B. TrxR), bricht das Mitochondrienmembranpotential ($\text{MMP } \Delta\Psi$) zusammen, wodurch Apoptose-Vermittler wie Cytochrom-c aus dem Intermembranraum freigesetzt werden und die apoptotische Kaskade aktivieren.^[79,101] Neben der Caspase-vermittelten Apoptose kann der Verlust des MMPs auch eine Caspase-unabhängige Form der Apoptose auslösen. Hierbei wird der Zelltod direkt durch Faktoren (z.B. AIF, EndoG) des Mitochondrienintermembranraumes vermittelt, ohne dass die Caspasen aktiviert werden.^[79,102,103] EndoG, eine mitochondriale DNase, fragmentiert die DNA im Zellkern, AIF löst die Chromatinkondensation und den Abbau der nuclearen DNA aus.^[104,105]

1.6 Entwicklung neuartiger Metallkomplexe für die Tumorthherapie

Lange bevor ihre Wirkmechanismen bekannt waren, wurden bereits Metalle in der Medizin eingesetzt. Dabei hatten die Menschen früh die Wirkung verschiedener Metalle gegen unterschiedliche Krankheiten erkannt. So nutzten schon die Chinesen ca. 2000 v. Chr. Metalle in der Medizin. Gold wurde gegen Arthritis, Bismuth gegen Magengeschwüre, und Silber bei bakteriellen Infektionen eingesetzt.^[106] Die ersten Behandlungen von Leukämie mit Metallverbindungen lassen sich auf das 16. Jahrhundert zurückführen.^[107]



Auranofin

Abbildung 16. Struktur des antirheumatischen Auranofins.

Auranofin (vgl. Abbildung 16), eine Goldverbindung, ist seit 1985 zur Behandlung von rheumatischer Arthritis zugelassen.^[108] Neben seiner anti-arthritischen Wirkung zeigte sich Auranofin auch gegenüber anderen Krankheiten als wirkungsvoll, darunter auch Krebs.^[109]

Seitdem wurde eine Vielzahl verschiedener Liganden, die selbst eine biologische Aktivität aufweisen mit biologisch aktiven Metallen wie Gold, Silber, Ruthenium, Osmium und natürlich Platin kombiniert, um eine Wirkungssteigerung aus Liganden und Metall zu erreichen.^[106,110] Die Variation der Liganden kann, neben der biologischen Wirkung, Einfluss auf verschiedene physikochemische Eigenschaften, wie Komplexstabilität, -ladung, und -löslichkeit nehmen und dadurch z.B. die Bioverfügbarkeit am Tumor, die Aufnahme der Komplexe in die Zelle oder die zellulären *targets* bestimmen.

1.6.1 Steuerung der biologischen Aktivität durch Ligandenvariation

Beispiele für den Einfluss, den Liganden auf die biologische Wirkung von Pt^{II}-Komplexen haben können stellen die Komplexe einer Serie von NHC Platinkomplexen mit (1,3-Dibenzyl)imidazol-2-yliden Liganden und verschiedenen, *cis*- und *trans*-ständigen Sekundärliganden von MUENZNER *et al.* dar (vgl. Abbildung 17).^[111]

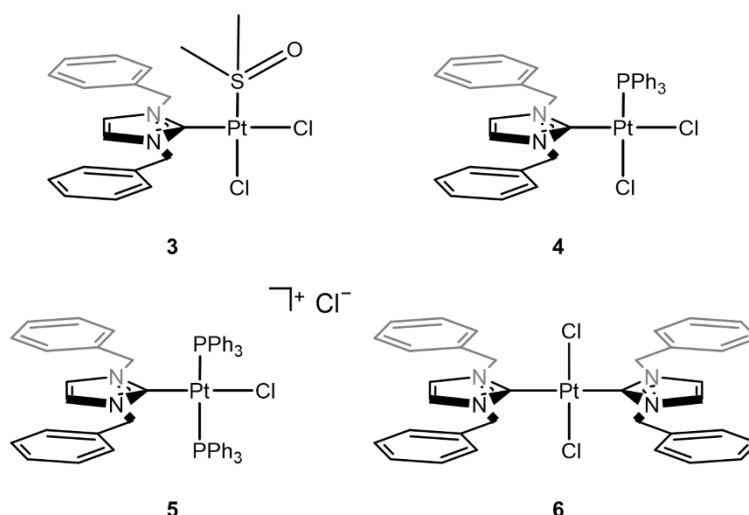
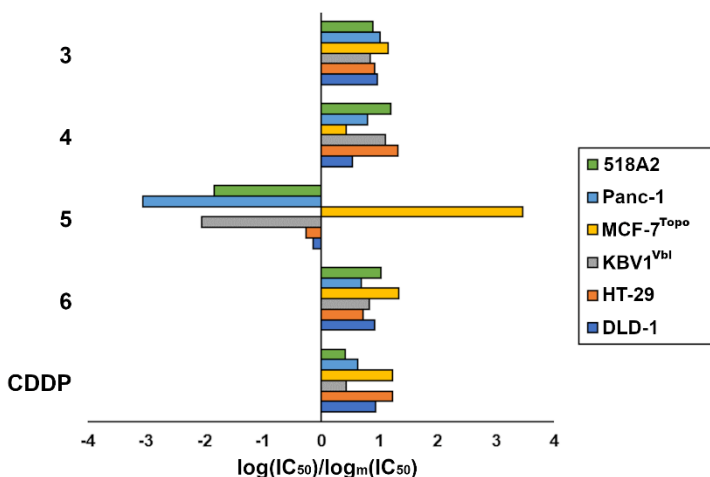


Abbildung 17. NHC-Pt^{II} Komplexe 3-6 mit variierenden sekundären Liganden, verschiedener Größe, Lipophilie, bzw. positiver Gesamtladung.^[111]

Von diesen zeigten die Komplexe **3-6** relevante Aktivitäten und bemerkenswerte Aktivitätsmuster (vgl. Abbildung 18). Mit steigender Anzahl an PPh₃ Substitutionen und dem Einführen einer positiven Ladung am Platinzentrum erhöhte sich die Toxizität der Verbindungen (**6** < **3** < **4** < **5**). Dies steht im Zusammenhang mit der gleichzeitig ansteigenden Lipophilie.^[111] Der geladene Komplex **5** wies gegenüber den getesteten Tumorzelllinien sogar eine antitumorale Aktivität mit IC₅₀-Werten im

Abbildung 18. Überblick (log(IC₅₀)/log_m(IC₅₀)) über die Toxizität der Komplexe 3-6 im Vergleich mit Cisplatin (CDDP). Die Werte sind im Verhältnis zur mittleren Aktivität (log_m(IC₅₀)) aller Komplexe angezeigt. Für IC₅₀ Werte > 50 oder > 100 µM wurden zur Berechnung des Logarithmus genau 50 oder 100 µM angenommen. Negative bzw. positive Balken zeigen im Vergleich zum Mittelwert bessere bzw. schlechtere Aktivitäten an.^[111]



nanomolaren Konzentrationsbereich auf, darunter auch Cisplatin-resistente Zelllinien.

DNA-Interaktionsstudien zeigten, dass sich die Art und Intensität der Interaktion der Komplexe mit dem Austausch des DMSO Liganden durch ein oder zwei PPh₃ und dadurch der Einführung einer positiven Ladung beeinflussen liess. Während der DMSO Komplex **3** vor allem kovalent an die DNA bindet und dies in zu Cisplatin ähnlicher Menge, verschiebt sich die Interaktionsart mit zunehmender Abschirmung der Chlorliganden durch PPh₃ immer weiter zu einer nicht-kovalenten, elektrostatischen Interaktion. Komplex **5** zeigt letztlich eine fast ausschließlich elektrostatische Interaktion mit der DNA und löst vor allem die Kondensation und Aggregation der DNA aus. *trans*-Komplex **6** interagiert trotz annehmbarer toxischer Aktivität gar nicht mit der DNA.^[111]

Neben den Unterschieden der Art und Intensität der DNA-Interaktion zwischen **3-5** und Cisplatin, zeigten sich diese auch bei der Messung der Zellzyklusprogression behandelter Tumorzellen. **3** verursachte wie Cisplatin einen G₂/M Arrest, **4** dagegen tötete die Zellen, ohne einen Arrest zu verursachen und **5** löste in den Zellen einen G₁ Arrest aus.^[111]

1.6.2 Alternative Ziele

Die Schädigung anderer *targets* kann ebenfalls zum Zellzyklusarrest bzw. dem Absterben der Zelle führen. Die Mitochondrien stellen für jede Zelle überlebenswichtige Organelle dar. Der Endosymbiontentheorie nach entwickelten sich Mitochondrien als eigenständige Lebensformen und wurden im Laufe der Evolution von Einzellern aufgenommen und lebten in Symbiose mit ihren Wirtszellen.^[112] Heute sind diese aufgenommenen Lebensformen weitestgehend zurückentwickelt und sind gemeinhin als „Kraftwerke der Zelle“ bekannt. Neben ihrer Hauptfunktion zur Produktion von Energieträgern wie ATP durch die in der Mitochondrienmembran integrierte Atmungskette, tragen die Mitochondrien zu vielen weiteren zellulären Prozessen und Signalgebungen bei. Als Nebenprodukt der Atmungskette entstehen sogenannte reaktive Sauerstoffspezies (ROS) wie Peroxide (H₂O₂) oder Superoxide (O₂⁻). Diese sind hochreaktive Verbindungen, die in der Zelle durch Oxidation von Proteinen, Lipiden und auch der DNA schwere Schäden hervorrufen können.^[70,72] In geringen Konzentrationen tragen ROS dagegen zur zellulären Signalgebung bei.^[18] Die natürlich vorkommende Menge intrazellulärer ROS wird streng kontrolliert, da sie einen für das Zellschicksal entscheidenden Einfluss nehmen können. In Tumorzellen

ist der Grundausschuss von ROS durch die verstärkte Mitochondrienaktivität erhöht, wodurch weiterer oxidativer Stress schädlicher für Tumorzellen ist als für Gesunde. Gezieltes Eingreifen in die Redox-Homöostase oder gezielte Schädigung der Mitochondrien bzw. ihrer Funktion oder der Funktion dort lokalisierter Enzyme kann in Tumorzellen die Proliferation stoppen und im Idealfall den kontrollierten Zelltod auslösen. Der Einfluss der Liganden oder auch die Art des Metalls auf die biologische Wirkung haben beschränkt sich nicht nur auf die direkte Interaktion der Komplexe mit ihren *targets* (z.B. DNA), sondern kann auch den zellulären Wirkort bestimmen. Ausnutzen lassen sich dabei sowohl physikochemische Eigenschaften der Komplexe als auch die Eigenschaften der Zellkompartimente. Mitochondrien besitzen wegen ihrer Funktion als Energielieferant der Zelle, einen chemischen und elektrischen Gradienten über die Mitochondrienmembran.^[113] Durch die negative Ladung auf der Membrannenseite ist es möglich, dass sogenannte delokalisierte, lipophile Kationen (DLCs) die Membran passieren und in den Mitochondrien akkumulieren. In Tumorzellen ist dieser Gradient aufgrund der mitochondrialen Aktivität erhöht.^[113] Dies bietet eine Selektivität der DLCs für Tumorzell-Mitochondrien, da sie hier stärker akkumulieren als in denen gesunder Zellen. Während für Pt^{II} Komplexe grundsätzlich die DNA als primärer Wirkort angenommen wird, können über eine positive Ladung bzw. erhöhte Lipophilie auch andere *targets* angesteuert werden. Beispiele für Pt^{II}-Komplexe, die aufgrund ihrer Lipophilie oder Ladung in den Mitochondrien akkumulieren sind in Abbildung 19 dargestellt.

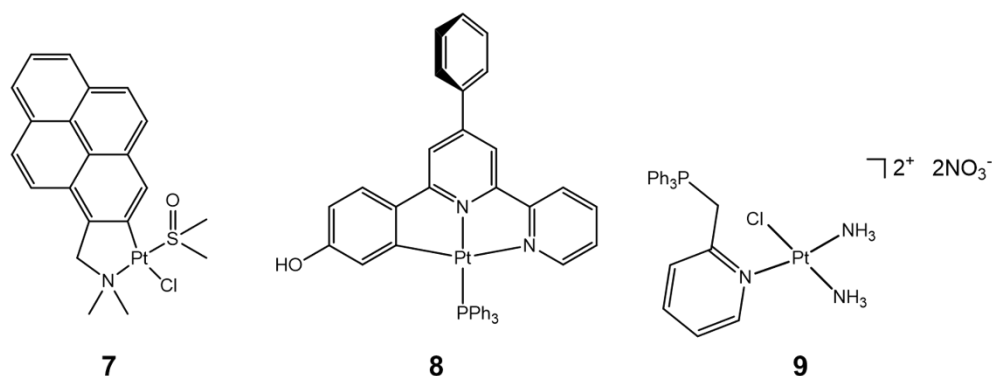


Abbildung 19. Strukturen von drei Pt^{II}-Komplexen von Ruiz *et al.* 7, JINGLING *et al.* 8 und ZHU *et al.* 9, die aufgrund ihrer Lipophilie und Ladung nicht an der nuclearen DNA, sondern in den Mitochondrien akkumulieren.^[114–116]

1.6.3 *Prodrugs – Der nächste Schritt*

Trotz der Milderung der Nebenwirkungen von Cisplatin, durch Anwendung der zweiten Generation an Platinkomplexen, konnten diese nicht komplett beseitigt werden. In den letzten Jahren wurde das Augenmerk der Forschung von aktiven Metallverbindungen, auf Metallverbindungen höherer Oxidationsstufen (z.B. Pt^{IV} , Ru^{III}) gerichtet. Diese gelten als unreaktiver und biologisch inaktiver als ihre niedrigeren Oxidationsstufen (Pt^{II} , Ru^{II}).^[117] Die Aktivierung der Platin-*Prodrugs* findet erst in der hypoxischen Tumorzelle statt. Dort werden die inaktiven Vorstufen zu ihren aktiven Komplexen reduziert. Einige Beispiele von ersten Pt^{IV} -*Prodrugs* (Tetraplatin, Iproplatin, Satraplatin, LA-12),^[118–121] die bereits klinische Studien durchlaufen haben, sind in Abbildung 20 dargestellt. Die Verbindungen scheiterten, trotz vielversprechender Aktivität in verschiedenen Phasen der klinischen Studien. Die Studien von LA-12 und Tetraplatin wurden bereits nach Phase I beendet.^[119,122]

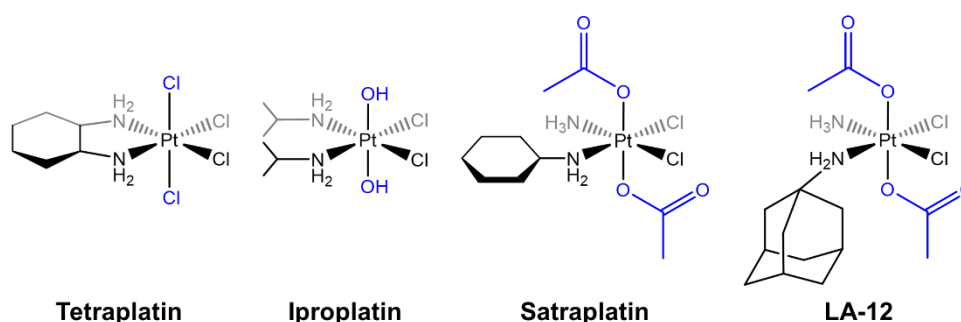


Abbildung 20. Strukturen der Pt^{IV} -*Prodrugs* Tetraplatin, Iproplatin, Satraplatin, und LA12, die jeweils klinische Studien durchliefen, jedoch nicht die erhofften Effekte zeigten und daher in unterschiedlichen Phasen zurückgezogen wurden.^[119,121]

Auch Iproplatin konnte sich in klinischen Studien nicht als ein, bezüglich seiner (Neben-)Wirkung, besseres Antitumormedikament erweisen.^[119] Als vielversprechend wurde vor allem Satraplatin gehandelt. Diese Verbindung kann, aufgrund ihrer geringen Reaktivität und guten Löslichkeitseigenschaften im Gegensatz zu anderen Platin-Chemotherapeutika statt parenteral, oral verabreicht werden. Ähnlich wie die bereits verwendeten Chemotherapeutika wirkt Satraplatin, reduziert zum entsprechenden Pt^{II} -Komplex, im Zellkern durch Inter- und Intrastrangverknüpfung der DNA. Im Gegensatz zu Cisplatin und seinen Analoga werden DNA-Addukte, die durch Satraplatin gebildet wurden, nicht von allen DNA-Reparaturmechanismen der Zelle erkannt.^[118,123] Auf diese Weise können Resistenzen gegenüber Cisplatin umgangen werden und selbst Tumorerkrankungen behandelt werden, bei denen eine normale Platintumorthherapie nicht wirken würde. Satraplatin wurde jedoch ebenfalls

nach anfänglich vielversprechenden Ergebnissen erster klinischer Studien nach Phase III aufgrund eines mangelnden Nachweises, dass es die Überlebenschance der Patienten erhöht zurückgezogen.^[119,124–128] Trotz der mangelnden Aktivität der Pt^{IV}-Komplexe in den klinischen Studien zeigen derartige Komplexe ein hohes Potential. Die beiden axialen Liganden, die als Abgangsliganden gelten, bieten durch entsprechende Modifikationen die Möglichkeit weitere biologisch aktive Verbindungen mit in die Zelle einzuschleusen, die durch Reduktion des Komplexes erst im Tumor selbst freigesetzt werden. Dies ermöglicht einen dualen Wirkmechanismus, den des freigesetzten aktiven Metallkomplexes und den der Abgangsliganden. Aufkommende Studien zur Reduktion und Aktivierung von Pt^{IV}-*Prodrugs* konnten zeigen, dass die Komplexe nicht durch das veränderte Redoxmilieu in der Tumorzelle, sondern durch membrangebundene Proteine oder Enzyme reduziert werden.^[117,129,130]

1.7 Targetfindung über Azid-Alkin Cycloaddition

Trotz der guten Wirkung *in vitro* oder auch *in vivo* stellt sich häufig die Frage ob Verbindungen, wie die in 1.6. vorgestellten, letztendlich in der Zelle auch an ihren bestimmten Wirkort gelangen. Komplexe **7-9** sind gute Vertreter von Platinkomplexen, die nicht wie Cisplatin an der DNA im Kern wirken, sondern ein alternatives *target*, die Mitochondrien, haben. Biochemische und molekularbiologische Methoden bieten die Möglichkeit den Wirkort von Wirkstoffen in der Zelle ausfindig zu machen. Die Azid-Alkin Cycloaddition nach Huisgen eignet sich auf mehrerlei Weise gut für die intrazelluläre Lokalisation, bzw. *target*-Findung neuer Wirkstoffe. Basierend auf der Forschung von HUISGEN *et al.*^[131] zur 1,3-dipolaren Cycloaddition wurde von MELDAL *et al.*^[132] und SHARPLESS *et al.*^[133] 2002 eine kupferkatalysierte Variante der Reaktion (CuAAC) vorgestellt. In dieser Variante reagiert ein terminal ständiges Alkin und ein Azid selektiv zu einem 1,4-disubstituierten 1,2,3-Triazol.^[134,135] Durch die einfachen Reaktionsbedingungen und Bioortogonalität der Reaktanden kann diese Kopplungsreaktion in der Zelle gut für die Verknüpfung von entsprechenden Alkinderivaten von Wirkstoffen und z.B. Azid-Fluorophoren zur Visualisierung oder Azid-*Beads* für *pull down* Experimente für eine spätere *Target*-Identifikation eingesetzt werden.^[136] Der Vorteil der nachträglichen, intrazellulären Fluoreszenzmarkierung ist, dass eine Alkinsubstitution am Wirkstoff wegen ihrer geringen Größe und Orthogonalität kaum Auswirkungen auf die

Substanzeigenschaften, insbesondere auf die Wirkung hat. Im Gegensatz dazu würde die Synthese eines Wirkstoffes mit einem großen Fluorophor wie z.B. Anthracen die Eigenschaften des Wirkstoffs verändern und eine Vergleichbarkeit des markierten und nicht markierten Derivats erschweren. Ein in der Zelle fixierter, nachträglich über CuAAC mit einem Fluorophor wie z.B. 3-Azido-7-hydroxycumarin markierter Wirkstoff lässt sich über (konfokale) Fluoreszenzmikroskopie in der Zelle aufspüren und durch entsprechende Cofärbungen z.B. an einem Zellorganell lokalisieren. Fluoreszenzfarbstoffe wie 3-Azido-7-hydroxycumarin eignen sich besonders für die Fluoreszenzmarkierung, da sie erst nach der Additionsreaktion fluoreszieren und somit nur das resultierende Konjugat sichtbar ist. (vgl. Abbildung 21).^[137]

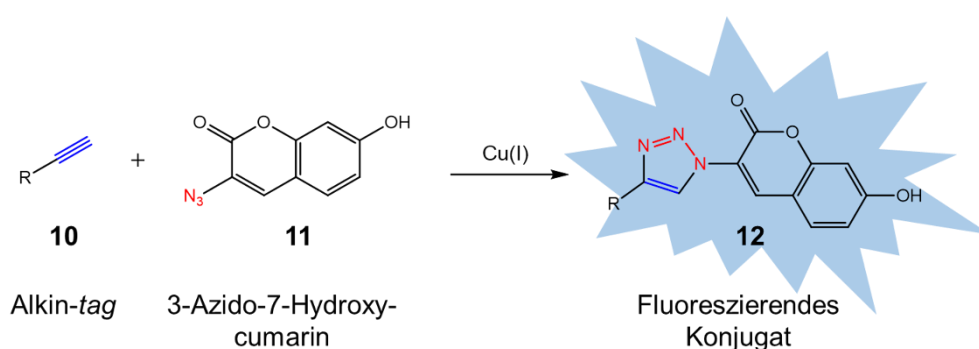


Abbildung 21. Cu(I)-katalysierte Azid-Alkin Cycloaddition eines terminalen Alkins **10** mit dem nicht fluoreszierenden 3-Azido-7-Hydroxycumarin **11** zum fluoreszenten 1,4 disubstituierten 1,2,3 Triazol **12**.

2 Zielsetzung

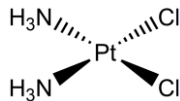
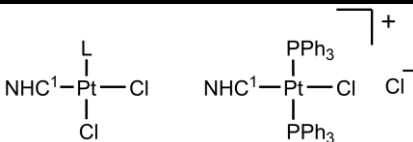
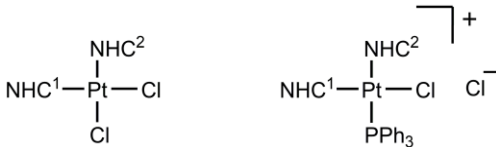
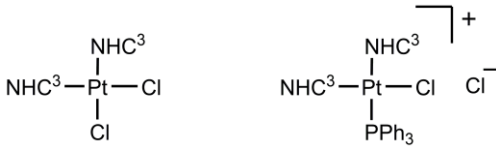
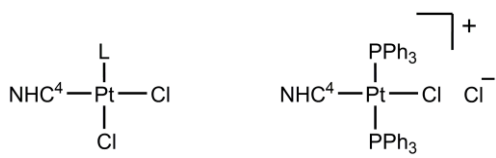
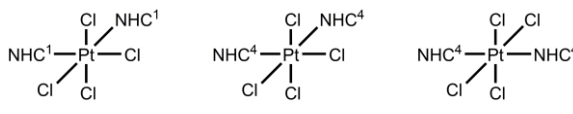
Cisplatin und dessen Derivate, wie Carboplatin oder Oxaliplatin gehören heute weltweit zu den Standardtherapeutika neoplastischer Neuerkrankungen. Immer häufiger auftretende Resistenzbildungen gegenüber diesen Tumorwirkstoffen und die schweren Nebenwirkungen die eine solche Therapie mit sich bringt, macht die stete Suche nach aktiveren, spezifischeren Wirkstoffen, mit verringerten Nebenwirkungen als die bisher Verfügbaren weiterhin unabdingbar.^[33-35] Weiterentwicklungen dieser Verbindungen konnten bisher in den klinischen Studien nicht überzeugen. Die gezielte Kombination aus Metallen und bioaktiven Liganden birgt ein großes Potential um Tumorzellen gezielt ansprechen zu können. Die Modifikationsmöglichkeiten *N*-heterozyklischer Carbene und die Stabilität ihrer Komplexe machen sie zu idealen Liganden bioaktiver Metallverbindungen. In präklinischen Studien sollte die antitumorale Wirkung neuer (un)symmetrischer NHC-Platin(II) und -Platin(IV) Komplexe untersucht und bewertet werden. Drei Generationen von *N,N*-Dibenzylimidazol-Pt^{II}, *N,N*-Dialkylbenzimidazol-Pt^{II} Komplexen und Pt^{IV} Analoga einzelner Vertreter dieser Komplextypen wurden, basierend auf vorangegangenen Untersuchungen von NHC-Pt^{II} Komplexen^[111], am Lehrstuhl für Organische Chemie der Universität Bayreuth synthetisiert. Zur Evaluation der antitumoralen Aktivität und Aufklärung ihres Wirkmechanismus sollten verschiedene biochemische und molekularbiologische Methoden *in vitro* unter anderem an etablierten humanen Tumorzelllinien verschiedener Entitäten angewandt werden. Neben der Feststellung der Selektivität und Effektivität gegenüber Tumorzellen sollte nicht nur der Wirkmechanismus, sondern auch der intrazelluläre Wirkort dieser Komplexe aufgeklärt werden. Die Ergebnisse aus diesen präklinischen Studien zu Selektivität, Wirkmechanismus und Wirkort sollen eine Grundlage für die weitere Entwicklung neuer selektiverer Platin-basierter Wirkstoffe für die Tumorthherapie dienen.

3 Synopsis

3.1 Vorstellung der Teilprojekte

Im Rahmen der vorliegenden kumulativen Dissertationsschrift wurden drei neue Generationen von (un)symmetrischen *cis*- und *trans*-NHC Pt^{II} und Pt^{IV} Komplexen hinsichtlich der Auswirkungen struktureller Modifikationen auf ihre antitumorale Aktivität untersucht. Die Entwicklung der neuen Komplexe erfolgte aufgrund vorangegangener Arbeiten der Arbeitsgruppe mit NHC-Metallkomplexen (z.B. Generation I). Eine Übersicht über die verschiedenen Generationen der Platinkomplexe ist in Abbildung 22 dargestellt. Die erste im Rahmen dieser Arbeit untersuchte Serie von *cis*-Dibenzylimidazol-Pt^{II} Komplexen (Generation II) beinhaltet sowohl symmetrische als auch unsymmetrische Komplexe, die auf ihre Toxizität und DNA Interaktion getestet wurden (Publikation I). Zur weiteren Aufklärung ihres Wirkmechanismus wurden fortführende Untersuchungen mit aktiven Vertretern dieser Serie durchgeführt. Zur Feststellung des intrazellulären Wirkorts dieser Komplexe wurden alkinylierte Derivate über intrazelluläre Klickreaktion fluoreszenzmarkiert. (Publikation II). Die Weiterentwicklung dieser Komplexe führte zum Austausch der *N,N*-Dibenzylimidazol-Liganden gegen *N,N*-Dialkylbenzimidazole verschiedener Alkylkettenlängen (Generation III). Die Untersuchungen dieser Serie beschäftigt sich mit den Auswirkungen der Alkylkettenlänge, bzw. denen der weiteren Liganden und damit auch der Ladung auf die Toxizität, Zellaufnahme, Zellzyklusprogression und den Charakter der DNA-Interaktion (Publikation III). Die letzte hier vorgestellte Serie (Generation IV) von Platinkomplexen beschreibt den Vergleich der antitumoralen Effekte, d.h. der Toxizität und DNA-Interaktion, von *cis*-Pt^{II} Komplexen mit Liganden aus Generation II und III und ihren Pt^{IV} Analoga (Publikation IV).

Die in dieser Arbeit in vier Publikationen vorgestellten Verbindungen wurden am Lehrstuhl für Organische Chemie I der Universität Bayreuth von Dr. Tobias Rehm synthetisiert. Ein Teil der Untersuchung zur strukturellen oder weiterführenden Aufklärung der Wirkmechanismen wurde in Kooperation mit dem Lehrstuhl für anorganische Chemie II der Universität Bayreuth oder dem Institut für Biophysik an der *Academy of Science of the Czech Republic* in Brunn (CZE) durchgeführt.

Cisplatin		Generation I ^[111]	
			
Generation II		Publikation I & II	
		Novel <i>cis</i> -[(NHC) ¹ (NHC) ² (L)Cl]platinum (II) complexes – synthesis, structures, and anticancer activities <i>Dalton Trans.</i> 2016	
		Antitumoral effects of mitochondria-targeting neutral and cationic <i>cis</i> -[bis(1,3-dibenzylimidazol-2-ylidene)(L)Cl]Pt(II) complexes <i>Dalton Trans.</i> 2020	
Generation III		Publikation III	
		<i>N,N</i> -Dialkylbenzimidazol-2-ylidene platinum complexes – effects of alkyl residues and ancillary <i>cis</i> -ligands on anticancer activity <i>Dalton Trans.</i> 2018	
Generation IV		Publikation IV	
		Synthesis, structures and cytotoxic effects in vitro of <i>cis</i> and <i>trans</i> -[Pt ^{IV} Cl ₄ (NHC) ₂] complexes and their Pt ^{II} precursors <i>Dalton Trans.</i> 2019	

L: DMSO/PPh₃; NHC¹/NHC²: *N,N*-Dialkylimidazol-2-yliden, *N,N*-Dibenzylimidazol-2-yliden; NHC³: *N,N*-Di(*p*-ethinylbenzyl)imidazol-2-yliden; NHC⁴: *N,N*-Dialkylbenzimidazol-2-yliden.

Abbildung 22. Übersicht über die in dieser Arbeit behandelten Generationen an Platin(II) und Platin(IV) NHC Komplexen. Basierend auf den Strukturen von Cisplatin und vorangegangenen Arbeiten von MUENZNER *ET AL.*^[111] (erster Abschnitt) wurden im Rahmen dieser Arbeit drei Generationen (Generation II – Generation IV) (un)symmetrischer NHC *cis*- und *trans*-Pt^{II} und -Pt^{IV} Komplexe mit substituierten (Benz-)Imidazoliganden hinsichtlich ihrer antitumoralen Wirkung untersucht.

3.2 Untersuchungen zur biologischen Aktivität neuer (un)symmetrischer *N,N*-Dibenzylimidazol Pt^{II} -Komplexe

3.2.1 Toxizität und DNA-Interaktionsstudien (un)symmetrischer Komplexe des Typs $\text{cis-}[\text{Pt}^{\text{II}}\text{Cl}(\text{L})(\text{NHC})^1(\text{NHC})^2]$

Diese Publikation stellt ein neues Konzept zur Synthese und erste biologische Untersuchungen der antitumoralen Aktivität einer zweiten Generation von (un)symmetrischen Platinkomplexen des Typs $\text{cis-}[\text{Pt}^{\text{II}}\text{Cl}(\text{L})(\text{NHC})^1(\text{NHC})^2]$ vor.^[138] Die Synthese einer vorangegangenen ersten Generation ähnlicher Platinkomplexe, und Untersuchungen zu deren biologischen Aktivität wurden 2015 von MUENZNER *et al.*^[111] vorgestellt und sind Abschnitt 1.6.1. der Einleitung zusammengefasst.

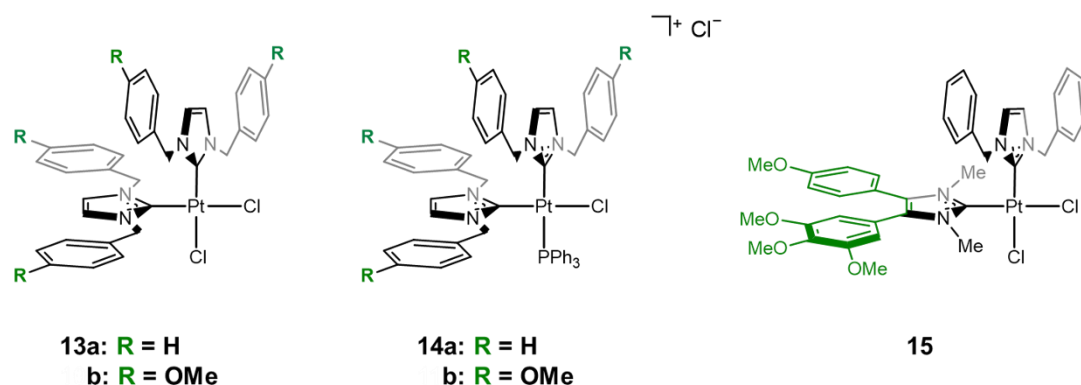
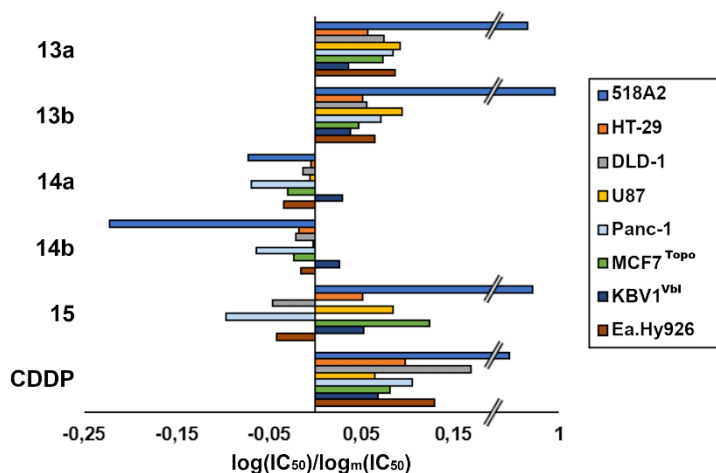


Abbildung 23. Strukturen der aktivsten Vertreter der Pt^{II} -Komplexe des Typs $\text{cis-}[\text{Pt}^{\text{II}}\text{Cl}(\text{L})(\text{NHC})^1(\text{NHC})^2]$ die symmetrischen, ungeladenen Pt^{II} -Komplexe **13, ihre kationischen Analoga **14** und der unsymmetrische, ungeladene Komplex **15** mit dem Strukturmotiv von CA-4.**

Die in dieser Publikation vorgestellten Komplexe variieren in den Benzylsubstitutionen der Imidazol-2-ylidenliganden, bzw. durch Austausch eines Chlorliganden durch Triphenylphosphan, in ihrer Gesamtladung. Die Strukturen der aktivsten Vertreter (**13**, **14**) dieser Serie sind in Abbildung 23 abgebildet. Ebenfalls aufgeführt wurde der ungeladene, unsymmetrische Komplex **15**, der wegen des Strukturmotivs des vaskular-disruptiven Naturstoffes Combretastatin A-4 (CA-4) an einem der Liganden und seiner selektiven Wirkung gegenüber CA-4 sensitiven Zelllinien ebenfalls aus den übrigen Verbindungen heraussticht. Die Komplexe wurden mittels MTT-basierter Antiproliferationsassays auf ihre antitumorale Wirkung gegenüber humanen Krebszelllinien verschiedener Entitäten und mittels EMSA auf ihr DNA-Interaktionsvermögen hin untersucht. Abbildung 24 gibt einen Überblick über die antitumorale Aktivität von **13-15**.

Abbildung 24. Überblick ($\log(\text{IC}_{50})/\log_m(\text{IC}_{50})$) über die Toxizität der Komplexe 13a,b, 14a,b und 15 im Vergleich mit Cisplatin (CDDP). Die Werte sind im Verhältnis zur mittleren Aktivität ($\log_m(\text{IC}_{50})$) aller Komplexe angezeigt. Für IC_{50} Werte > 50 oder $> 100 \mu\text{M}$ wurden zur Berechnung des Logarithmus genau 50 oder 100 μM angenommen. Negative bzw. positive Balken zeigen im Vergleich zum Mittelwert bessere bzw. schlechtere Aktivitäten an.^[138]



Während die IC_{50} Werte der ungeladenen Komplexe **13** im niedrigen mikromolaren Bereich liegen, zeigten sich die, durch den Austausch eines Chlorliganden durch Triphenylphosphan, positiv geladenen Komplexe **14** mit IC_{50} Werten im nanomolaren Konzentrationsbereich als wesentlich aktiver. Komplex **15** zeigte eine hohe Selektivität für Zelllinien, die sich sensitiv gegenüber dem Naturstoff CA-4 erwiesen hatten (DLD-1, Panc-1, Ea.Hy926) und gibt mit nanomolaren IC_{50} Werten einen ersten Hinweis auf einen Synergismus der antitumoralen Wirkung durch den Platinkomplex und dem CA-4 Motiv des Liganden.^[138] Ein derartiger Synergismus konnte bei anderen Komplexen mit CA-4 Motiven am NHC Liganden nicht beobachtet werden.^[112]

Die Untersuchungen der DNA Interaktion (vgl. Abbildung 25) des ungeladenen Komplexes **13b** und des geladenen Komplexes **14b** bestätigen die Ergebnisse der vorangegangenen Untersuchungen mit **3-6**.^[111] Der ungeladene Komplex **13b**

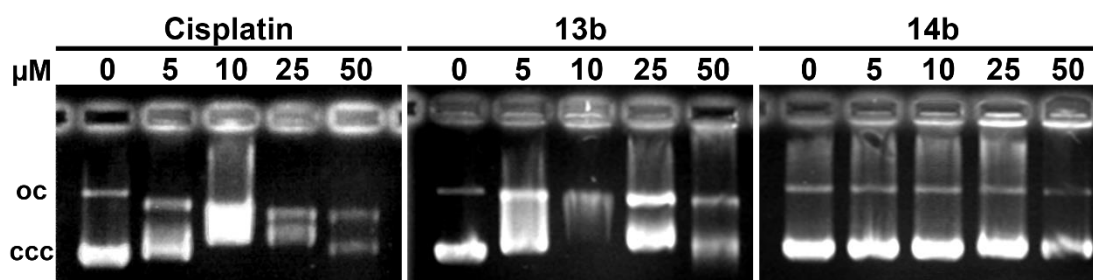


Abbildung 25. EMSA von Cisplatin, der Komplexe *cis*-[Pt^{II}(NHC)₂Cl₂] **13b und *cis*-[Pt^{II}Cl(NHC)₂(PPh₃)]⁺Cl⁻ **14b** mit zirkulärer pBR322 Plasmid DNA nach 24 h Inkubation. Die Interaktion mit der Plasmid-DNA zwingt diese aus der kompakten ccc-Form in die sperrigere oc-Form mit geringerer Elektromobilität. Cisplatin und **13b** zeigen eine typische Bandenretardation mit aufeinander zulaufender oc und ccc Form, wobei der Effekt von **13b** auf die oc-Form geringer ausfällt. **14** dagegen zeigt keine Bandenretardation, sondern aggregiert DNA in den Taschen des Agarosegels. [Adapted from T. Rehm, M. Rothemund *et al.*, *Dalton Trans.* 2016, 45, 15390; DOI: 10.1039/c6dt02350a - with permission from the Royal Society of Chemistry]**

verursachte im EMSA eine konzentrations-abhängige Bandenretardation, ähnlich zu der von Cisplatin. Dieser Effekt ist typisch für eine koordinative Bindung der DNA-Basen an die Platinzentren der Komplexe. Der geladene Komplex **14b** führte nicht zu einer Bandenretardation, sondern zu DNA-Aggregaten, die während der Elektrophorese nicht mehr aus den Geltaschen wandern, was auf elektrostatische Wechselwirkungen zwischen dem kationischen Komplex und dem negativ geladenen Phosphatrückgrat hinweist.

Details in: Novel *cis*-[(NHC)¹(NHC)²(L)Cl]platinum(II) complexes – synthesis, structures and anticancer activities

Tobias Rehm, Matthias Rothemund, Julianne K. Muenzner, Awal Noor, Rhett Kempe, and Rainer Schobert

Dalton Trans. **2016**, 45, 15390.

3.2.2 Auswirkung der Ladung und Lipophilie auf den Wirkort und -mechanismus von Komplexen des Typs $cis-[Pt^{II}Cl(L)(NHC)^1(NHC)^2]$

In dieser Publikation sind die Ergebnisse weiterführender Untersuchungen des Wirkmechanismus von **13a** und **14a** als Vertreter für die ungeladenen und geladenen Komplexe der *cis*-[Bis(1,3-dibenzylimidazol-2-yliden)]platin(II) Serie beschrieben.^[139] Zur intrazellulären Lokalisation der Komplexe wurden die Alkin-Derivate **16** und **17** synthetisiert (Abbildung 26).

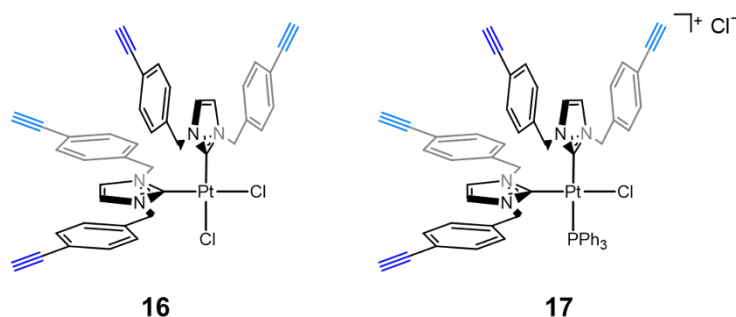
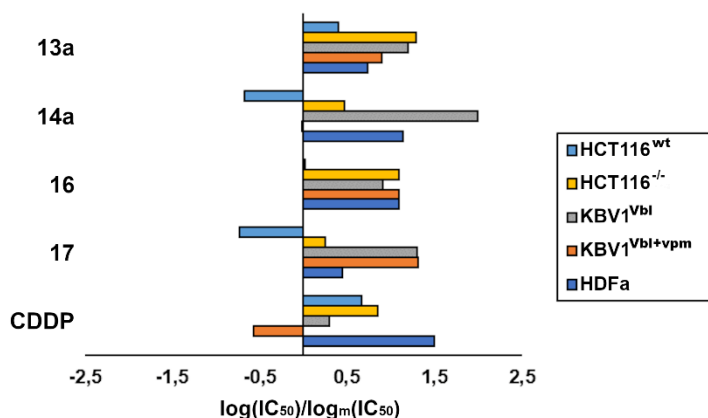


Abbildung 26. Strukturen der Alkin-derivate 16 und 17, die zur Aufklärung des zellulären Wirkorts über intrazelluläre Azid-Alkin-Cycloaddition mit 3-Azido-7-hydroxycumarin fluoreszenzmarkiert werden.

Zusätzliche Untersuchungen zu den zuvor durchgeführten Antiproliferationsassays an der p53 *knock-out* mutanten Zelllinie HCT116^{-/-} zeigten, dass die Aktivität der Komplexe stark von der Funktionalität des Tumorsuppressors p53 abhängt (Abbildung 27). Durch die Zugabe von Verapamil, eines kompetitiven Inhibitors des Effluxtransporters Pg-p1, der in der *mdr* Zelllinie KbV1^{Vbl} überexprimiert wird, konnte die Aktivität der Komplexe **13a** und **14a** wiederhergestellt werden. Im Vergleich zu den gesunden Hautfibroblasten HDFa zeigten sich die Komplexe **13a**, **16** und **17** selektiv für Tumorzellen, **16** sogar gänzlich inaktiv gegenüber den Fibroblasten.

Abbildung 27. Überblick ($\log(IC_{50})/\log_m(IC_{50})$) über die Toxizität der Komplexe 13a, 14a, 16 und 17 im Vergleich mit Cisplatin (CDDP). Die Werte sind im Verhältnis zur mittleren Aktivität ($\log_m(IC_{50})$) aller Komplexe angezeigt. Für IC_{50} Werte > 50 oder > 100 μ M wurden zur Berechnung des Logarithmus genau 50 oder 100 μ M angenommen. Negative bzw. positive Balken zeigen im Vergleich zum Mittelwert bessere bzw. schlechtere Aktivitäten an.^[139]

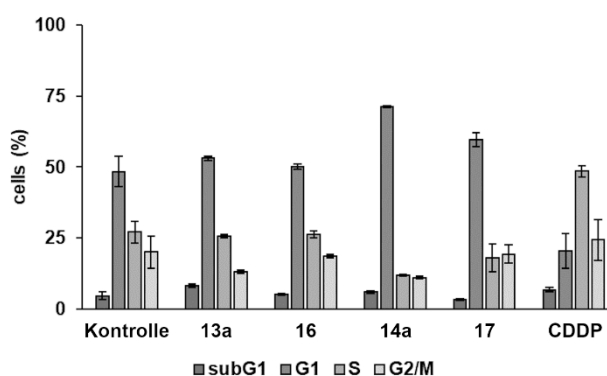


Über ICP-MS Messungen des Platingehalts von 518A2 Melanomzellen konnte eine Abhängigkeit der erhöhten Aktivität des geladenen Komplexes **14a** von einer vermutlich durch die positive Ladung verstärkten Aufnahme festgestellt werden.

In EtdBr-Sättigungsassays verhinderten sowohl der geladene als auch der ungeladene Komplex durch Interaktion mit linearer Lachsspermien-DNA die Interkalation von EtdBr in gleichem Ausmaß, und übertrafen den Effekt von Cisplatin bei weitem. Dies steht im Kontrast zum oben beschriebenen EMSA mit zirkulärer Plasmid-DNA, in dem sich deutliche Unterschiede zwischen **13b** und **14b** zeigten.

Die Messung des Zellzyklus behandelter Melanomzellen ergab starke Unterschiede zwischen den Komplexen **13a**, **14a** und Cisplatin (Abbildung 28). Während Cisplatin einen deutlichen Arrest der Zellen in der S-Phase auslöst, verursachte **13a** keinen und **14a** einen G₁-Phasenarrest. Dies deutet auf von Cisplatin verschiedene oder zusätzliche Wirkmechanismen der getesteten Komplexe hin.

Abbildung 28. Zellzyklusanalysen von 518A2 Melanomzellen nach 24 h Behandlung mit 13a, 14a, 16, 17 und Cisplatin (CDDP). Während **13a** und **16** keinen Arrest auslösen, verursachen **14a** und **17** im Gegensatz zu Cisplatin einen G₁-Arrest. Cisplatin arretiert die Zellen in der S-Phase. [Adapted from T. Rehm, M. Rothemund *et al.*, *Dalton Trans.* 2020; DOI: 10.1039/d0dt01664k - with permission from the Royal Society of Chemistry]



Die weitestgehend identischen Eigenschaften, wie Zytotoxizität und Zellzyklusinterferenz, der Alkinkomplexe **16** und **17** und der von **13a** und **14a** macht Erstere zu geeigneten Vertretern für die Lokalisation der ungeladenen und geladenen Komplexe dieser Serie. Durch intrazelluläre Cu^I-katalysierte Azid-Alkin Cycloaddition der Komplexe **16** bzw. **17** mit 3-Azido-7-hydroxycumarin (siehe Kapitel 1.7) und anschließender konfokaler Fluoreszenzmikroskopie wurde sowohl der geladene als auch der ungeladene Komplex an den Mitochondrien von 518A2 Melanomzellen lokalisiert. Die Berechnung der Colokalisationsfaktoren PC und LICQ, deren Werte bei vollständiger Colokalisation 1 bzw. 0.5 annehmen, aus den Fluoreszenzsignalen der markierten Komplexe und der eines *Mitotracker*TM bestätigte dies sowohl für **16** (PC 0.89; LICQ 0.46) als auch für **17** (PC 0.90; LICQ 0.47) quantitativ (vgl. Abbildung 29).

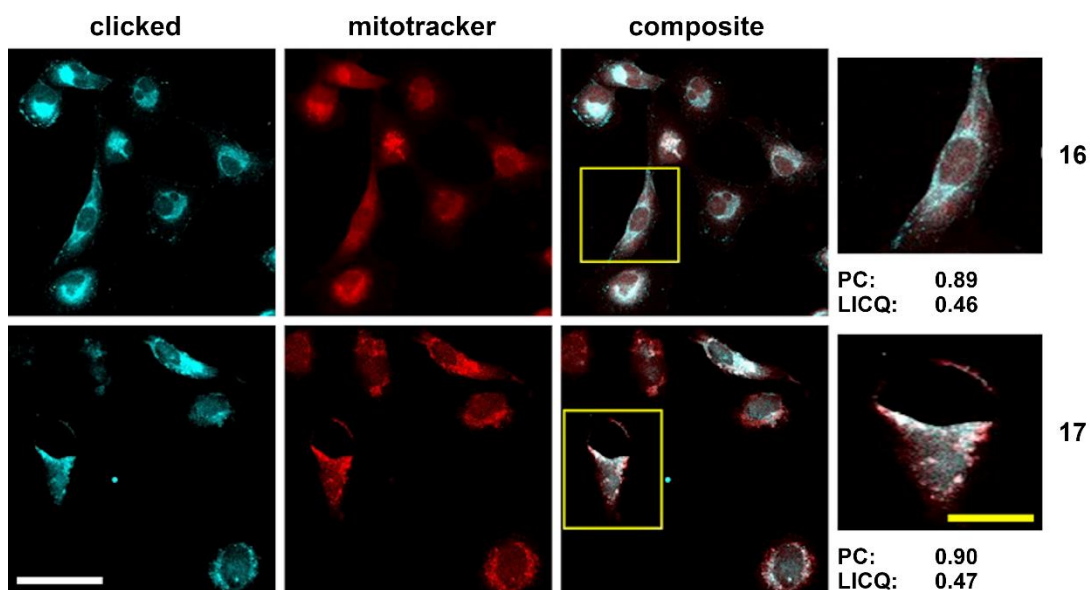


Abbildung 29. Konfokale Fluoreszenzaufnahmen der fluoreszenzmarkierten Komplexe 16 und 17 in 518A2 Melanomzellen. PC und LICQ sind ein Maß für die Überlagerung der Fluoreszenzsignale der Komplexe (türkis) und des *Mitotracker*TM (rot). Maßstab weiß: 50 µm, gelb: 25 µm. [Adapted from T. Rehm, M. Rothemund *et al.*, *Dalton Trans.* 2020; DOI: 10.1039/d0dt01664k - with permission from the Royal Society of Chemistry]

Untersuchungen des Mitochondrienmembranpotentials $\Delta\Psi$ und der intrazellulären ROS Konzentrationen bestätigten, dass die Komplexe einen negativen Einfluss auf die Mitochondrienfunktionalität ausüben. Beide Komplextypen **13a/16** und **14a/17** verringerten das mitochondriale Membranpotential $\Delta\Psi$ und erhöhten gleichzeitig die Menge intrazellulärer Sauerstoffspezies (Abbildung 30). Den stärkeren Anstieg an ROS verursachten die geladenen Komplexe **14a/17**. Dies fügt sich in das bereits beobachtete Aktivitätsmuster. Die Menge an ROS, die durch die ungeladenen Komplexe **13a/16** erzeugt wird reicht nicht aus, um einen Zellzyklus-arrest

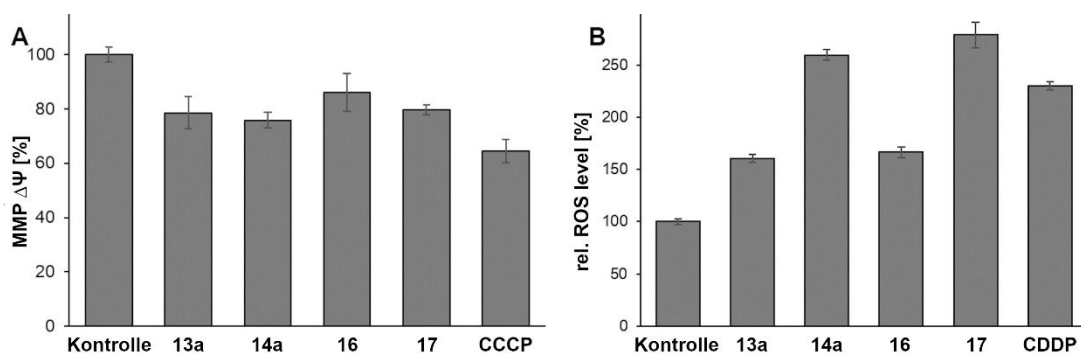


Abbildung 30. A) Untersuchung des Mitochondrienmembranpotentials $\Delta\Psi$ (MMP) mittels TMRM-Färbung von behandelten 518A2-Melanomzellen. B) Untersuchung der intrazellulären ROS-Menge behandelter 518A2-Melanomzellen mittels DCFH-DA-Färbung. Die Komplexe **13a/16** und **14a/17** verringern das MMP bei gleichzeitiger Erhöhung der Konzentration reaktiver Sauerstoffspezies. [Adapted from M. Rothemund, S. I. Bär *et al.*, *Dalton Trans.* 2020; DOI: 10.1039/d0dt01664k - with permission from the Royal Society of Chemistry]

auszulösen. Ebenfalls konnte eine starke *stress fiber* Bildung des *f*-Aktins als Reaktion auf den erhöhten oxidativen Stress in den Melanomzellen nachgewiesen werden. Letztendlich löst Komplex **14a** die Caspase-3/-7 vermittelte Apoptose in den Melanomzellen aus. Für Komplex **13a** wird ein Caspase-unabhängiger Zelltod vermutet, da dieser nicht in der Lage war die Caspasen-3 und -7 zu aktivieren, jedoch eine Reduktion des $\Delta\Psi$ bei gleichzeitigem Anstieg der ROS verursachte. Dieser war jedoch nicht ausreichend, um die Caspase-vermittelte Apoptose auszulösen.

Details in: Antitumoral effects of mitochondria-targeting neutral and cationic *cis*-[bis(1,3-dibenzylimidazol-2-ylidene)(L)Cl]Pt(II) complexes

Matthias Rothemund, Sofia I. Bär, Tobias Rehm, H. Kostrhunova, V. Brabec and Rainer Schobert

Dalton Trans. **2020**, 49, 8901.

3.3 Biologische Wirkung und DNA-Interaktionsstudien unymmetrischer *N,N*-Dialkylbenzimidazol-2-yliden-Platin(II) Komplexe

Die in dieser Publikation vorgestellten Verbindungen stellen eine dritte Generation von *cis*-NHC-Pt^{II} Komplexen, basierend auf den vorhergegangenen Arbeiten zu *cis*-[Bis(1,3-dibenzylimidazol-2-yliden)(L)Cl]platin(II) Komplexen dar (vgl. Abbildung 31).^[140] Statt eines Imidazolliganden wurde ein Benzimidazolligand eingeführt. Dieser

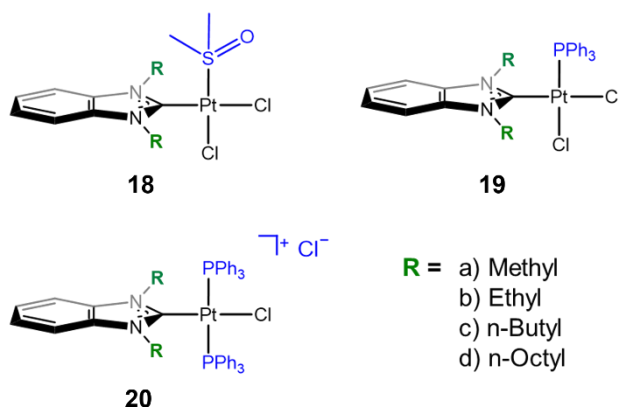


Abbildung 31 Strukturen der *N,N*-Dialkylbenzimidazol-2-yliden Pt^{II} Komplexe mit variierender Alkylkettenlänge und sekundären Liganden **18-20**. Über die Kettenlänge (a-d: methyl-, ethyl-, n-butyl-, n-octyl-) und Austausch des DMSO (**18**), durch PPh₃ (**19**) und dem Einführen einer positiven Ladung durch Austausch eines weiteren Liganden gegen PPh₃ (**20**) lassen sich gezielt die Bioaktivität, bzw. DNA-Interaktion steuern.

trägt *N*-Alkylsubstitutionen variierender Längen (a) methyl-, b) ethyl-, c) butyl- und d) octyl-) und verschiedene sekundäre Liganden (**18** DMSO, **19** PPh₃, **20** (PPh₃)₂⁺), bzw. eine positive Gesamtladung. Die Auswirkung der strukturellen Modifikationen auf die antitumorale Wirkung wurde über ihre Toxizität, den Charakter der DNA-Interaktion und den Effekt auf die Zellzyklusprogression untersucht.

Die Komplexe zeigen, hinsichtlich des Austausches der sekundären Liganden DMSO (**18**) durch PPh₃ (**19**) und eines weiteren Chlorliganden durch PPh₃ und der damit einhergehenden positiven Ladung (**20**) einen ähnlichen Trend bezüglich der Aufnahme

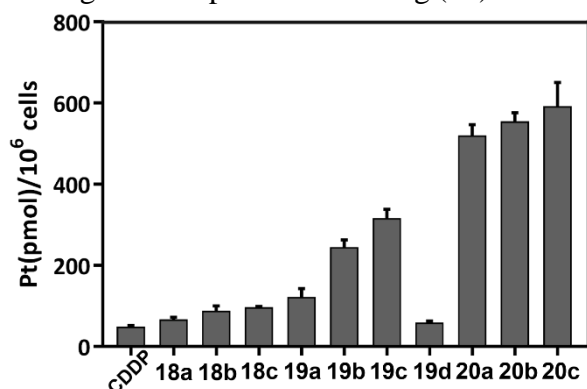


Abbildung 32. Platingehalt von HCT116^{wt} Kolonkarzinomzellen nach Behandlung mit **18a-c**, **19a-d**, **20a-c** oder Cisplatin (CDDP) via ICP-MS. [Adapted from T. Rehm, M. Rothemund *et al.*, Dalton Trans. 2018, 47, 17367; DOI: 10.1039/d8dt03360a - with permission from the Royal Society of Chemistry]

und Toxizitätssteigerung wie NHC-Pt^{II} Komplexe der ersten und zweiten Generation.^[111,138,139] Die kationischen Komplexe **20** werden stärker in Kolonkarzinomzellen aufgenommen, als die ungeladenen Derivate **18** und **19**. Dies spiegelt auch die Zunahme der Toxizität wider (DMSO < PPh₃ < (PPh₃)₂⁺) (vgl. Abbildung 32). Die Länge der

Alkylketten nimmt bei den ungeladenen Komplexen **19** einen deutlichen Einfluss (octyl- < methyl- < ethyl- < butyl-) auf die Aufnahme in die Zellen. Bei den kationischen Komplexen **20** übersteigt der Effekt der Ladung den der Alkylketten. Eine Auswirkung der Alkylkettenlänge ist nicht in den Toxizitäten der Komplexe wiederzufinden, die über die gesamte Serie eher sprunghaft ist (vgl. Abbildung 33). Interessanterweise sticht der ethylsubstituierte, ungeladene Komplex **19b** als besonders selektiv für langsam wachsende Kolonkarzinomzellen mit IC_{50} Werten nahe derer der kationischen Komplexe **20** hervor. Mit einer reduzierten Toxizität der Komplexe in den HCT116^{-/-} im Vergleich zum Wildtyp, sind die Verbindungen stark abhängig vom Zustand des Tumorsuppressors p53. Während die Komplexe die Resistenz der *mdr* MCF-7^{Topo} Zellen, die das Effluxprotein BCRP überexprimieren, zu umgehen scheinen, ist ihre Toxizität in den *mdr* KbV1^{Vbl} Zervixkarzinomzellen, die den Effluxtransporter P-gp1 überexprimieren, stark reduziert, kann jedoch durch die Zugabe eines kompetitiven Inhibitors für P-gp1, wie Verapamil, wieder hergestellt wellt werden.

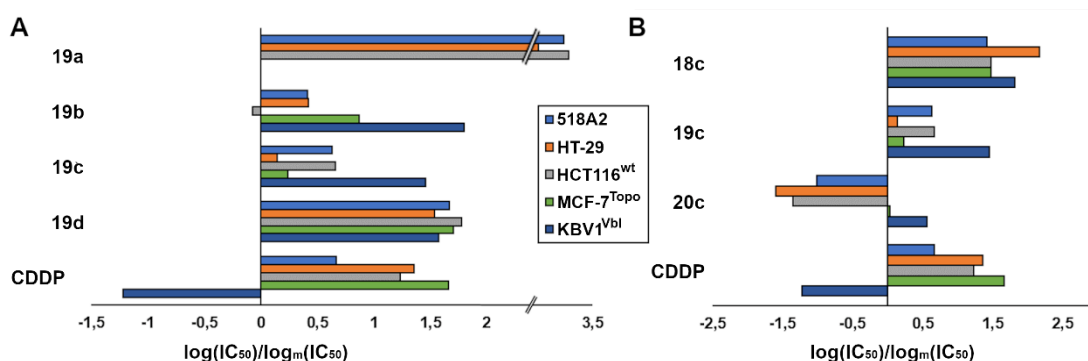


Abbildung 33. Überblick ($\log(IC_{50})/\log_m(IC_{50})$) über die Toxizität der Komplexe 18c, 19a-d und 20c im Vergleich mit Cisplatin. Die Werte sind im Verhältnis zur mittleren Aktivität ($\log_m(IC_{50})$) aller Komplexe angezeigt. Für IC_{50} Werte >50 oder >100 μ M wurden zur Berechnung des Logarithmus genau 50 oder 100 μ M angenommen. Negative bzw. positive Balken zeigen im Vergleich zum Mittelwert bessere bzw. schlechtere Aktivitäten an. **A** Auswirkung der Länge der Alkylsubstitution, **B** der sekundären Liganden, bzw. Gesamtladung bei gleichbleibender Kettenlänge der Alkylsubstitution (*n*-Butyl), auf die Aktivität.^[140]

In vitro Studien der Interaktion der Komplexe mit verschiedenen DNA-Typen gab Aufschluss über die Kinetik und den Charakter der Interaktion mit DNA und darüber wie stark diese durch die Komplexe beeinträchtigt wird. Erste *in vitro* Untersuchungen (EMSA) der DNA-Interaktionsfähigkeit der Komplexe zeigten, dass sich der bei den *cis*-[Bis(1,3-benzylimidazol-2-yliden)]platin(II) Komplexen beobachtete Trend, der Entwindung bzw. Aggregation zirkulärer Plasmid-DNA auch hier fortsetzt. In EtdBr-Sättigungsassays verursachen vor allem die geladenen Komplexe **20** eine starke

Reduktion der EtdBr-Fluoreszenz (vgl. Abbildung 34 A). Ebenfalls stark stechen die ungeladenen Komplexe **18d** und **19d** heraus. Detaillierte *in vitro* Studien zur DNA-Interaktion ergaben, dass sich die morphologischen Veränderungen der DNA, die die Komplexe verursachen, stark von denen von Cisplatin unterscheiden. Die ungeladenen Komplexe **18** und **19** binden direkt koordinativ an Guaninbasen der DNA, die geladenen Komplexe dagegen gehen zunächst eine elektrostatische Interaktion mit dem negativ geladenen Phosphatrückgrat der DNA ein und binden erst anschließend koordinativ an die Basen (vgl. Abbildung 34 B).

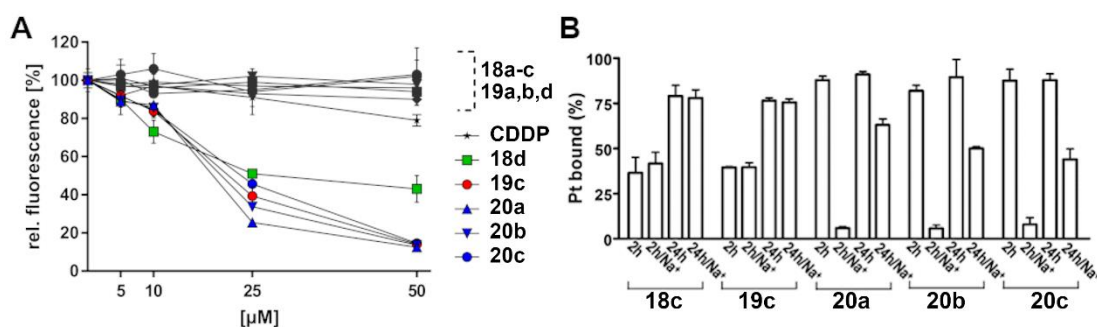


Abbildung 34. DNA-Interaktion der N,N-Dialkylbenzimidazol-2-yliden Platin(II) Komplexe. **A** EtdBr-Sättigungsassay der Komplexe **18**, **19**, **20** und Cisplatin mit Lachsspermien-DNA. Die Interaktion mit der DNA verhindert die Interkalation von EtdBr zwischen die Basenpaare und reduziert folglich die gemessene Fluoreszenz. **B** FAAS-Analyse des Platingehalts an ct-DNA nach Dialyse gegen Wasser oder einen *high salt* Puffer (0.1 M NaCl). Der Salzpuffer neutralisiert die negative Ladung des Phosphatrückgrats der DNA und eliminiert die elektrostatische Wechselwirkung zwischen der DNA und den Platinkomplexen, sodass nur kovalent gebundene Komplexe verbleiben. [Adapted from T. Rehm, M. Rothemund *et al.*, *Dalton Trans.* 2018, 47, 17367; DOI: 10.1039/d8dt03360a - with permission from the Royal Society of Chemistry]

Die Addukte, die die Komplexe mit der DNA bilden sind, im Gegensatz zu denen von Cisplatin, vor allem monofunktionell und dadurch ist auch die negative Auswirkung auf die DNA-Integrität weniger prominent. Die Komplexe verursachen eine geringere Entwindung der DNA (ca. 6°) als Cisplatin (ca. 13°) und knicken sie in geringerem Maße ab.

Unterschiede zwischen der Wirkung der Komplexe und Cisplatin zeigen sich nicht nur an der DNA-Interaktion, sondern auch in ihrer Auswirkung auf zelluläre Prozesse wie den Zellzyklusablauf. Während Cisplatin in mikromolaren Konzentrationen einen S-Phasenarrest von Kolonkarzinomzellen auslöst, verursachen die butyl-substituierten Komplexe **19c** (PPh_3) und **20c** ($(\text{PPh}_3)_2$) einen G1-Arrest der Zellen, ungeachtet der p53-Funktionalität (vgl. Abbildung 34), bereits im nanomolaren Konzentrationsbereich. Komplex **18c** verursachte dagegen gar keinen Zellzyklusarrest.

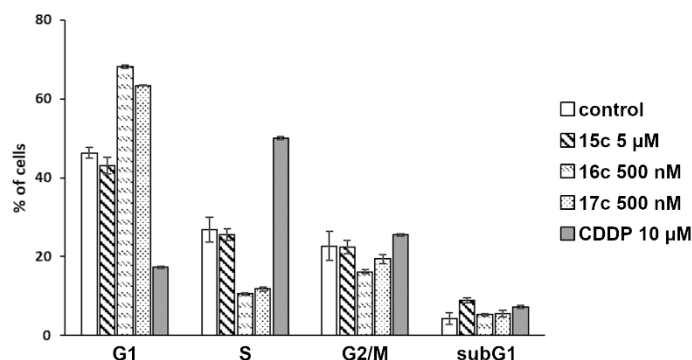


Abbildung 35. Zellzyklusanalyse von HCT116^{wt} Kolonkarzinomzellen nach 24 h Inkubation mit 18c, 19c, 20c, Cisplatin (CDDP) oder DMSO als Negativkontrolle. Im Gegensatz zu Cisplatin (S-Phasenarrest) verursachen Komplexe **18c** keinen, **19c** und **20c** einen G₁-Arrest der Kolonkarzinomzellen. Dies weist auf einen von Cisplatin verschiedenen Wirkmechanismus hin. [Adapted from T. Rehm, M. Rothmund *et al.*, *Dalton Trans.* 2018, 47, 17367; DOI: 10.1039/d8dt03360a - with permission from the Royal Society of Chemistry]

Details in: ***N,N*-Dialkylbenzimidazol-2-ylidene platinum complexes – effects of alkyl residues and acillary *cis*-ligands on anticancer activity**

Tobias Rehm, Matthias Rothmund, Alexander Bär, Thomas Dietl, Rhett Kempe, Hara Kostrhunova, Viktor Brabec, Jana Kasparkova, and Rainer Schobert

Dalton Trans. **2018**, 47, 17367.

3.4 Zytotoxische Wirkung und DNA-Interaktion von symmetrischen Platin(IV) Komplexen und ihrer Platin(II) Analoga

Wie schon zuvor beschrieben, verursachen gängige Platinwirkstoffe auf Grund ihrer Unspezifität starke Nebenwirkungen und anhaltende Organschädigungen. In den letzten Jahren zeigten Pt^{IV} Komplexe großes Potential als Alternative zu den aktuell verwendeten Pt^{II} Komplexen. Diese Publikation beschreibt die Oxidation von Pt^{II} Komplexen des Typs *cis*-/*trans*- $[\text{Pt}^{\text{II}}\text{Cl}_2(\text{NHC})_2]$ zu ihren entsprechenden Pt^{IV} Komplexen *cis*-/*trans*- $[\text{Pt}^{\text{IV}}\text{Cl}_4(\text{NHC})_2]$, erste Untersuchungen der zytotoxischen Wirkung, und die Auswirkungen der Oxidation auf die DNA-Interaktionsfähigkeit, wobei die NHC Liganden entweder *N,N*-Dibenzylimidazol-2-ylidene oder *N,N*-Dialkylbenzimidazol-2-ylidene mit variierender Länge der Alkylsubstitution sind (vgl. Abbildung 36).^[141]

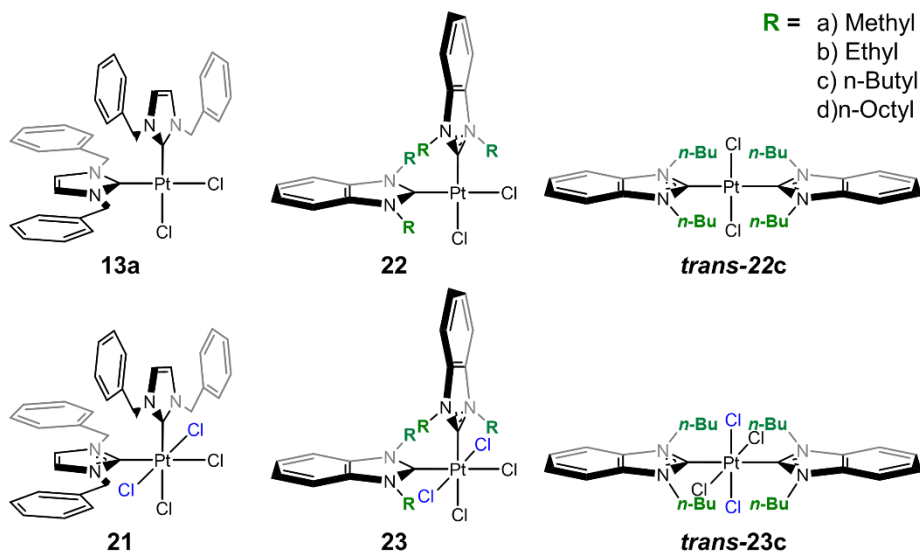


Abbildung 36. Strukturen der *cis*-/*trans*- Pt^{IV} Komplexe 21, 23, trans-23c und ihrer Pt^{II} Analoga 13a, 22 und trans-22c.

In Antiproliferationsstudien zeigten die $\text{Pt}^{\text{II}}/\text{Pt}^{\text{IV}}$ Paare **13a/21**, **22c/23c** und **trans-22c/trans-23c** gegenüber den getesteten Zelllinien vergleichbar gute bis moderate antitumorale Aktivität im niederen mikromolaren Konzentrationsbereich (vgl. Abbildung 37). Dies steht im Einklang mit der Annahme, dass Pt^{IV} Komplexe als biologisch inaktivere, stabilere *Prodrugs* für ihre Pt^{II} Analoga gelten und in den Tumorzellen durch Hypoxie oder größere Zellbestandteile wie Proteine oder Enzyme zu den aktiven Pt^{II} Komplexen reduziert werden.^[130] Die meisten Verbindungen zeigten dabei eine höhere Aktivität gegenüber der p53 *knock-out* Zelllinie HCT116^{-/-}

als der des Wildtyps. Lediglich der Pt^{IV} Komplex **21** wies gegenüber der Mutante eine geringere Toxizität als bei den Wildtypzellen auf.

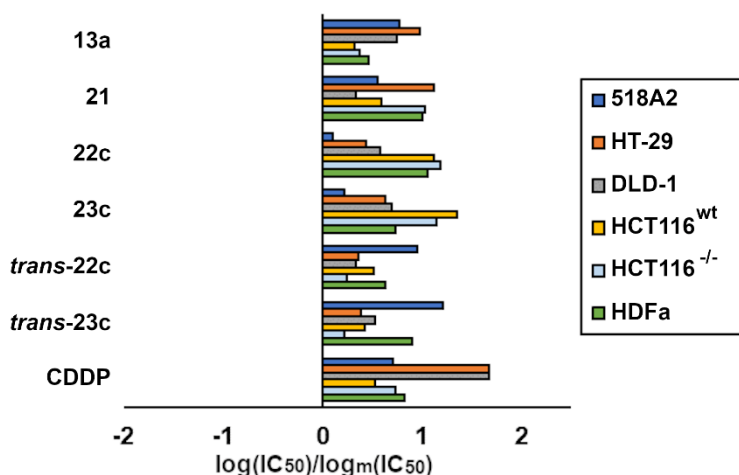


Abbildung 37. Überblick ($\log(\text{IC}_{50})/\log_m(\text{IC}_{50})$) über die Toxizität der Komplexe 13a, 21, 22c, 23c, *trans*-22c und *trans*-23c im Vergleich mit Cisplatin (CDDP). Die Werte sind im Verhältnis zur mittleren Aktivität ($\log_m(\text{IC}_{50})$) aller Komplexe angezeigt. Für IC_{50} Werte > 50 oder $> 100 \mu\text{M}$ wurden zur Berechnung des Logarithmus genau 50 oder $100 \mu\text{M}$ angenommen. Negative bzw. positive Balken zeigen im Vergleich zum Mittelwert bessere bzw. schlechtere Aktivitäten an.^[141]

Die biologische Inertheit von Pt^{IV} Komplexen zeigte sich bei ersten *in vitro* Untersuchungen zum DNA-Interaktionsvermögen der Komplexe **13a** und **21** (vgl. Abbildung 38). Während der Pt^{II} Komplex **13a** eine starke konzentrationsabhängige Reduktion der Ethidiumbromidfluoreszenz verursachte, die auch die von Cisplatin weit übertraf, hatte der Pt^{IV} Komplex **21** nur geringfügige Auswirkungen. Eine *in situ* Reduktion von **21** zu **13a** mittels Ascorbinsäure schlug fehl, was in Übereinstimmung mit Untersuchungen steht, nach denen Pt^{IV} Komplexe in Tumorzellen eher durch *large molecules* (z.B. Membranproteine) und nicht durch *small molecules* wie Ascorbinsäure oder Glutathion reduziert werden.^[130]

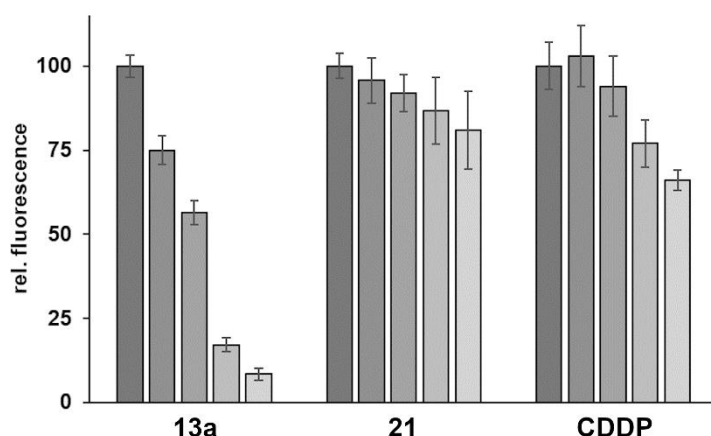


Abbildung 38. Relative EtdBr-Fluoreszenz nach Interkalation in lineare Lachsspermien-DNA, die mit **13a**, **21** oder **Cisplatin (CDDP)** behandelt wurde. Die Werte sind in Relation zur EtdBr-Fluoreszenz in unbehandelter DNA berechnet. [Adapted from T. Rehm, M. Rothmund *et al.*, *Dalton Trans.* 2019, 48, 16358; DOI: 10.1039/c9dt02438g - with permission from the Royal Society of Chemistry]

Details in: Synthesis, structures and cytotoxic effects *in vitro* of *cis*- and *trans*-
[Pt^{IV}Cl₄(NHC)₂] complexes and their Pt^{II} precursors

Tobias Rehm, Matthias Rothemund, Thomas Dietl, Rhett Kempe, and Rainer Schobert

Dalton Trans. **2019**, 48, 16358.

4 Literaturverzeichnis

- [1] B. W. Stewart, P. Kleihues, *World cancer report*, IARC Press, Lyon **2003**.
- [2] P. Boyle, B. Levin, *World cancer report: 2008*, IARC Press, Lyon **2008**.
- [3] B. W. Stewart (Ed.), *World Cancer Report 2014*, IARC Press, Lyon **2014**.
- [4] F. Bray, J. Ferlay, I. Soerjomataram, A. Jemal, *et al.*, *CA-Cancer J. Clin.* **2018**, 68, 394.
- [5] S. Wu, S. Powers, W. Zhou, Y. A. Hannun, *Nature* **2015**, 529, 43.
- [6] N. Khan, F. Afaq, H. Mukhtar, *Cancer lett.* **2010**, 293, 133.
- [7] V. A. Katzke, R. Kaaks, T. Kühn, *Cancer J.* **2015**, 21, 104.
- [8] S. C. Larsson, J. Permert, N. Håkansson, A. Wolk, *et al.*, *Br. J. Canc.* **2005**, 93, 1310.
- [9] Statistisches Bundesamt (Destatis), *Todesursachen nach Krankheitsarten*, Stand **2020** https://www.destatis.de/DE/Themen/Gesellschaft-Umwelt/Gesundheit/_Grafik/_Statisch/todesursache-krankheitsarten.png?__blob=poster (abgerufen 22.06.2020, 08:43 Uhr)
- [10] Statistisches Bundesamt (Destatis), *Tabelle Sterbefälle durch Krebs insgesamt 2018*, Stand 19.05.2020, Abrufdatum 22.06.2020, Datenlizenz by-2-0.
- [11] D. Hanahan, R. A. Weinberg, *Cell* **2000**, 100, 57.
- [12] D. Hanahan, R. A. Weinberg, *Cell* **2011**, 144, 646.
- [13] M. A. Feitelson, A. Arzumanyan, R. J. Kulathinal, S. Newsheer, *et al.*, *Semin. Cancer Biol.* **2015**, 35 Suppl., S25.
- [14] L. Hartwell, T. Weinert, *Science* **1989**, 246, 629.
- [15] A. G. Paulovich, D. P. Toczyski, L. H. Hartwell, *Cell* **1997**, 88, 315.
- [16] L. H. Hartwell, M. B. Kastan, *Science* **1994**, 266, 1821.
- [17] L. Sandell, *Cell* **1993**, 75, 729.
- [18] V. Aggarwal, H. S. Tuli, A. Varol, G. Sethi, *et al.*, *Biomolecules* **2019**, 9, 735.
- [19] D. Mustacich, G. Powis, *Biochem. J.* **2000**, 346, 1.
- [20] N. Nishida, H. Yano, T. Nishida, M. Kojiro, *et al.*, *Vasc. Health Risk Manag.* **2006**, 2, 213.
- [21] M. Rajabi, S. A. Mousa, *Biomedicines* **2017**, 5, 34.
- [22] D. W. Siemann, *Cancer Treat. Rev.* **2011**, 37, 63.

- [23] T. N. Seyfried, L. C. Huysentruyt, *Crit. Rev. Oncog.* **2013**, 18, 43.
- [24] K. W. Hunter, N. P. S. Crawford, J. Alsarraj, *Breast Cancer Res.* **2008**, 10 Suppl. 1, S2.
- [25] H. Dillekås, M. S. Rogers, O. Straume, *Cancer Med.* **2019**, 8, 5574.
- [26] L. Kelland, *Nat. Rev. Cancer* **2007**, 7, 573.
- [27] E. R. Jamieson, S. J. Lippard, *Chem. Rev.* **1999**, 99, 2467.
- [28] M. Peyrone, *Ann. Chem. Pharm.* **1844**, 51, 1.
- [29] B. Rosenberg, L. van Camp, T. Krigas, *Nature* **1965**, 205, 698.
- [30] B. Rosenberg, L. van Camp, J. E. Trosko, V. H. Mansour, *Nature* **1969**, 222, 385.
- [31] B. Rosenberg, L. VanCamp, *Cancer Res.* **1970**, 30, 1799.
- [32] R. C. DeConti, B. R. Toftness, R. C. Lange, W. A. Creasey, *Cancer Res.* **1973**, 33, 1310.
- [33] Z. Livshits, R. B. Rao, S. W. Smith, *Emerg. Med. Clin. N. Am.* **2014**, 32, 167.
- [34] J. Hildebrand, *Curr. Opin. Oncol.* **2006**, 18, 321.
- [35] T. Karasawa, P. S. Steyger, *Toxicol. Lett.* **2015**, 237, 219.
- [36] R. Oun, Y. E. Moussa, N. J. Wheate, *Dalton Trans.* **2018**, 47, 6645.
- [37] T. B. de Castria, E. M. K. da Silva, A. F. T. Gois, R. Riera, *Cochrane Database Syst. Rev.* **2013**, CD009256.
- [38] R. J. Knox, F. Friedlos, D. A. Lydall, J. J. Roberts, *Cancer Res.* **1986**, 46, 1972.
- [39] N. J. Wheate, S. Walker, G. E. Craig, R. Oun, *Dalton Trans.* **2010**, 39, 8113.
- [40] M. G. Apps, E. H. Y. Choi, N. J. Wheate, *Endocr.-Rel. Cancer* **2015**, 22, R219.
- [41] R. A. Alderden, M. D. Hall, T. W. Hambley, *J. Chem. Educ.* **2006**, 83, 728.
- [42] M. D. Hall, K. A. Telma, K.-E. Chang, M. M. Gottesman, *et al.*, *Cancer Res.* **2014**, 74, 3913.
- [43] R. P. Williams, B. W. Ferlas, P. C. Morales, A. J. Kurtzweil, *J. Oncol. Pharm. Pract.* **2017**, 23, 422.
- [44] D. P. Gately, S. B. Howell, *Br. J. Cancer* **1993**, 67, 1171.
- [45] S. Ishida, J. Lee, D. J. Thiele, I. Herskowitz, *Proc. Natl. Acad. Sci. USA* **2002**, 99, 14298.
- [46] A. K. Holzer, G. H. Manorek, S. B. Howell, *Mol. Pharmacol.* **2006**, 70, 1390.

- [47] A. Eastman, *Biochemistry* **1986**, 25, 3912.
- [48] A. M. Fichtinger-Schepman, J. L. van der Veer, J. H. den Hartog, J. Reedijk, *et al.*, *Biochemistry* **1985**, 24, 707.
- [49] L. G. Marzilli, J. S. Saad, Z. Kuklenyik, Y. Xu, *et al.*, *J. Am. Chem. Soc.* **2002**, 123, 2764.
- [50] B. Feng, M. P. Stone, *Chem. Res. Toxicol.* **1995**, 8, 821.
- [51] J. H. den Hartog, C. Altona, J. H. van Boom, J. Reedijk, *et al.*, *J. Biomol. Struct. Dyn.* **1985**, 2, 1137.
- [52] J. Reedijk, *Chem. Commun.* **1996**, 7, 801.
- [53] R. S. Tibbetts, K. M. Brumbaugh, J. M. Williams, R. T. Abraham, *et al.*, *Gen. Dev.* **1999**, 13, 152.
- [54] N. D. Lakin, B. C. Hann, S. P. Jackson, *Oncogene* **1999**, 18, 3989.
- [55] R. A. Woo, K. G. McLure, S. P. Lees-Miller, P. W. Lee, *et al.*, *Nature* **1998**, 394, 700.
- [56] F. Perri, S. Pisconti, G. D. V. Scarpatti, *Ann. Transl. Med.* **2016**, 4, 522.
- [57] S. Bates, K. H. Vousden, *Curr. Opin. Genet. Dev.* **1996**, 6, 12.
- [58] S. L. Harris, A. J. Levine, *Oncogene* **2005**, 24, 2899.
- [59] W. R. Taylor, S. E. DePrimo, A. Agarwal, M. G. R. Stark, *et al.*, *Mol. Biol. Cell* **1999**, 10, 3607.
- [60] A. K. Hock, A. M. Vigneron, S. Carter, K. H. Vousden, *et al.*, *EMBO J.* **2011**, 30, 4921.
- [61] S.-Y. Hyun, Y.-J. Jang, *Oncotarget* **2014**, 6, 4804.
- [62] T. Waldman, K. W. Kinzler, B. Vogelstein, *Cancer Res.* **1995**, 55, 5187.
- [63] W. S. el-Deiry, T. Tokino, V. E. Velculescu, B. Vogelstein, *et al.*, *Cell* **1993**, 75, 817.
- [64] J. W. Harper, G. R. Adami, N. Wei, S. J. Elledge, *et al.*, *Cell* **1993**, 75, 805.
- [65] M. L. Agarwal, A. Agarwal, W. R. Taylor, G. R. Stark, *Proc. Natl. Acad. Sci. USA* **1995**, 92, 8493.
- [66] J. W. Harper, S. J. Elledge, K. Keyomarsi, E. Swindell, *et al.*, *Mol. Biol. Cell* **1995**, 6, 387.
- [67] C. Bertoli, J. M. Skotheim, R. A. M. de Bruin, *Nat. Rev. Mol. Cell Bio.* **2013**, 14, 518.
- [68] A. Maréchal, L. Zou, *CSH. Perspect. Biol.* **2013**, 5, a012716.

- [69] C.-M. Aliouat-Denis, N. Dendouga, I. van den Wyngaert, J. E. Vialard, *et al.*, *Mol. Cancer Res.* **2005**, 3, 627.
- [70] F. Esposito, L. Russo, G. Chirico, F. Cimino, *et al.*, *IUBMB life* **2001**, 52, 67.
- [71] J. Boonstra, J. A. Post, *Gene* **2004**, 337, 1.
- [72] A. L. Fitzgerald, A. A. Osman, T.-X. Xie, J. N. Myers, *et al.*, *Cell Death Dis.* **2015**, 6, e1678.
- [73] M. L. Agarwal, A. Agarwal, W. R. Taylor, G. R. Stark, *Proc. Natl. Acad. Sci. USA* **1998**, 95, 14775.
- [74] J. C. Reed, *Am. J. Pathol.* **2000**, 157, 1415.
- [75] S. G. Solano-Gálvez, J. Abadi-Chiriti, L. Gutiérrez-Velez, R. Vázquez-López, *et al.*, *Med. Sci.* **2018**, 6, 54.
- [76] P. Golstein, G. Kroemer, *Trends Biochem. Sci.* **2007**, 32, 37.
- [77] K. L. Rock, H. Kono, *Annu. Rev. Pathol.* **2008**, 3, 99.
- [78] D. R. Green, G. P. Amarante-Mendes, *Results Probl. Cell. Differ.* **1998**, 24, 45.
- [79] S. Elmore, *Toxicol. Pathol.* **2007**, 35, 495.
- [80] J. Chai, Y. Shi, *Nat. Sci. Rev.* **2014**, 1, 101.
- [81] R. M. Locksley, N. Killeen, M. J. Lenardo, *Cell* **2001**, 104, 487.
- [82] F. C. Kischkel, S. Hellbardt, I. Behrmann, M. E. Peter, *EMBO J.* **1995**, 14, 5579.
- [83] H. Wajant, *Science* **2002**, 296, 1635.
- [84] J. H. Russell, T. J. Ley, *Annu. Rev. Immunol.* **2002**, 20, 323.
- [85] M. Barry, R. C. Bleackley, *Nat. Rev. Immunol.* **2002**, 2, 401.
- [86] Y. Tsujimoto, *Genes Cells* **1998**, 3, 697.
- [87] L.-N. Zhang, J.-Y. Li, W. Xu, *Cancer Gene Ther.* **2013**, 20, 1.
- [88] Y. Zhang, D. Xing, L. Liu, *Mol. Biol. Cell* **2009**, 20, 3077.
- [89] D. Westphal, G. Dewson, P. E. Czabotar, R. M. Kluck, *Biochim. Biophys. Acta* **2011**, 1813, 521.
- [90] M. Zhang, J. Zheng, R. Nussinov, B. Ma, *Sci. Rep.* **2017**, 7, 2635.
- [91] X. Saelens, N. Festjens, L. Vande Walle, P. Vandenabeele, *et al.* *Oncogene* **2004**, 23, 2861.
- [92] H. Li, H. Zhu, C. J. Xu, J. Yuan, *Cell* **1998**, 94, 491.
- [93] P. Fuentes-Prior, G. S. Salvesen, *Biochem. J.* **2004**, 384, 201.

- [94] S. B. Bratton, G. S. Salvesen, *J. Cell Sci.* **2010**, *123*, 3209.
- [95] J. Silke, P. Meier, *CSH Perspect. Biol.* **2013**, *5*, a008730
- [96] C. Adrain, E. M. Creagh, S. J. Martin, *EMBO J.* **2001**, *20*, 6627.
- [97] M. M. Compton, *Cancer Metastasis Rev.* **1992**, *11*, 105.
- [98] A. H. Wyllie, *Nature* **1980**, *284*, 555.
- [99] A. H. Wyllie, R. G. Morris, A. L. Smith, D. Dunlop, *J. Pathol.* **1984**, *142*, 67.
- [100] M. Enari, H. Sakahira, H. Yokoyama, S. Nagata, *et al.*, *Nature* **1998**, *391*, 43.
- [101] T. C. Karlenius, K. F. Tonissen, *Cancers* **2010**, *2*, 209.
- [102] M. Donovan, T. G. Cotter, *Biochim. Biophys. Acta* **2004**, *1644*, 133.
- [103] S. W. G. Tait, D. R. Green, *Oncogene* **2008**, *27*, 6452.
- [104] L. Y. Li, X. Luo, X. Wang, *Nature* **2001**, *412*, 95.
- [105] S. A. Susin, H. K. Lorenzo, N. Zamzami, G. Kroemer, *et al.* *Nature* **1999**, *397*, 441.
- [106] B. Desoize, *Anticancer Res.* **2004**, *24*, 1529.
- [107] P. Köpf-Maier, *Eur. J. Clin. Pharmacol.* **1994**, *47*, 1.
- [108] G. C. Bernhard, *J. Lab. Clin. Med.* **1982**, *100*, 167.
- [109] T. Onodera, I. Momose, M. Kawada, *Chem. Pharm. Bull.* **2019**, *67*, 186.
- [110] G. N. Kaluđerović, S. Gómez-Ruiz, D. Maksimović-Ivanić, S. Mijatović, *et al.*, *Bioionorg. Chem. Appl.* **2012**, *2012*, 705907.
- [111] J. K. Muenzner, T. Rehm, B. Biersack, R. Schobert, *et al.*, *J. Med. Chem.* **2015**, *58*, 6283.
- [112] L. Sagan, *J. Theor. Biol.* **1967**, *14*, 255.
- [113] J. S. Modica-Napolitano, J. R. Aprille, *Adv. Drug. Deliv. Rev.* **2001**, *49*, 63.
- [114] A. Zamora, S. A. Pérez, M. Rothmund, J. Ruiz, *et al.*, *Chemistry* **2017**, *23*, 5614.
- [115] Z. Zhu, Z. Wang, C. Zhang, X. Wang, *et al.*, *Chem. Sci.* **2019**, *10*, 3089.
- [116] J. Li, X. He, Y. Zou, C. Chen, *et al.*, *Metallomics* **2017**, *9*, 726.
- [117] Y. Shi, S.-A. Liu, D. J. Kerwood, J. C. Dabrowiak, *et al.*, *J. Inorg. Biochem.* **2012**, *107*, 6.
- [118] A. Bhargava, U. N. Vaishampayan, *Exp. Opin. Investig. Drugs* **2009**, *18*, 1787.

- [119] A. Casini, A. K. Gorle, E. J. Peterson, R. K.O. Sigel, *et al.*, *Metallodrugs: Development and Action of Anticancer Agents, Physics, Chemistry, Materials Sc, Geosc* **2017**, De Gruyter. Berlin, Boston.
- [120] E. Fokkema, H. J.M. Groen, M. N. Helder, C. Meijer, *et al.*, *Biochem. Pharmacol.* **2002**, 63, 1989.
- [121] P. Zhang, P. J. Sadler, *Eur. J. Inorg. Chem.* **2017**, 2017, 1541.
- [122] T. J. O'Rourke, G. R. Weiss, P. New, G. M. Clark, *et al.*, *Anti-Cancer Drugs* **1994**, 5, 520.
- [123] S. Chatterjee, S. Kundu, A. Bhattacharyya, P. J. Dyson, *et al.*, *J. Biol. Inorg. Chem.* **2008**, 13, 1149.
- [124] L. R. Kelland, B. A. Murrer, G. Abel, K. R. Harrap, *et al.*, *Cancer Res.* **1992**, 52, 822.
- [125] N. Graf, S. J. Lippard, *Adv. Drug Deliv. Rev.* **2012**, 64, 993.
- [126] A. O. Sartor, D. P. Petrylak, J. A. Witjes, C. N. Sternberg, *et al.*, *J. Clin. Oncol.* **2008**, 26, 5003.
- [127] N. Shah, D. S. Dizon, *Future Oncol.* **2009**, 5, 33.
- [128] H. Choy, C. Park, M. Yao, *Clin. Cancer Res.* **2008**, 14, 1633.
- [129] C. K. J. Chen, P. Kappen, T. W. Hambley, *Metallomics* **2019**, 11, 686.
- [130] D. Gibson, *Dalton Trans.* **2016**, 45, 12983.
- [131] R. Huisgen, *Proc. Chem. Soc.* **1961**, 357.
- [132] C. W. Tornøe, C. Christensen, M. Meldal, *J. Org. Chem.* **2002**, 67, 3057.
- [133] V. V. Rostovtsev, L. G. Green, V. V. Fokin, K. B. Sharpless, *Angew. Chem. Int. Ed. Engl.* **2002**, 41, 2596.
- [134] Meldal, Sharpless, E. Haldón, M. C. Nicasio, P. J. Pérez, *Org. Biomol. Chem.* **2012**, 13, 9528.
- [135] L. Zhou, C. J. Brassard, X. Zahng, R. J. Clark, *et al.*, *Chem. Rec.* **2016**, 16, 1501.
- [136] M. H. Wright, S. A. Sieber, *Nat. Prod. Rep.* **2016**, 33, 681.
- [137] K. Sivakumar, F. Xie, B. M. Cash, Q. Wang, *et al.*, *Org. Lett.* **2004**, 6, 4603.
- [138] T. Rehm, M. Rothmund, J. K. Muenzner, R. Schobert, *et al.*, *Dalton Trans.* **2016**, 45, 15390.
- [139] M. Rothmund, S. I. Bär, T. Rehm, R. Schobert, *et al.*, *Dalton Trans.* **2020**, 49, 8901.

- [140] T. Rehm, M. Rothmund, A. Bär, R. Schobert, *et al.*, *Dalton Trans.* **2018**, 47, 17367.
- [141] T. Rehm, M. Rothmund, T. Dietel, R. Schobert, *et al.*, *Dalton Trans.* **2019**, 48, 16358.

5 Publikationen

5.1 Darstellung des Eigenanteils

Die in dieser Arbeit abgebildeten Veröffentlichungen erwuchsen aus Kooperationen mit anderen Arbeitsgruppen. Zu diesen Arbeitsgruppen gehören der Lehrstuhl für Anorganische Chemie II der Universität Bayreuth und das Institut für Biophysik an der Akademie der Wissenschaft der Tschechischen Republik in Brünn (CZE). Die Publikationen wurden mit der Genehmigung des Journals abgedruckt.

Es folgt eine Erklärung des Eigenanteils an den jeweiligen Publikationen.

5.1.1 Eigenanteil an Publikation I

Ergebnisse zu diesem Thema wurden 2016 in *Dalton Transactions* unter dem Titel

“Novel cis-[(NHC)¹(NHC)²(L)Cl]platinum(II) complexes – synthesis, structures, and anticancer activities”

von den Autoren

*Tobias Rehm, Matthias Rothmund, Julienne K. Muenzner, Awal Noor, Rhett Kempe
und Rainer Schobert*

veröffentlicht.

Die Arbeit wurde in Kooperation mit dem Lehrstuhl für Anorganische Chemie II der Universität Bayreuth durchgeführt.

Eigenanteil:

Die Konzeption, Durchführung und Auswertung der biologischen Untersuchungen der Verbindungen, d.h. die Bestimmung der IC₅₀ Werte der untersuchten Komplexe und die Untersuchungen zur DNA-Interaktion wurden von mir vorgenommen. Entsprechende Abschnitte und Abbildungen in der Publikation wurden von mir verfasst, bzw. erstellt. Planung, Synthese und Analytik der Verbindungen stammten von Tobias Rehm, bzw. Mitgliedern des Lehrstuhls für Anorganische Chemie II (Universität Bayreuth). Von Julienne K. Muenzner stammten die in dieser Publikation aufgeführten IC₅₀ Werte von Cisplatin. Die Arbeit wurde zusammen mit Tobias Rehm und Prof. Rainer Schobert verfasst.

5.1.2 Eigenanteil an Publikation II

Ergebnisse zu diesem Thema wurden 2020 bei *Dalton Transactions* unter dem Titel

“Antitumoral effects of mitochondria-targeting neutral and cationic *cis*-
[bis(1,3-dibenzylimidazol-2-ylidene)(L)Cl]Pt(II) complexes”

von den Autoren

*Matthias Rothmund, Sofia I. Bär, Tobias Rehm, Hanah Kostrhunova, Viktor
Brabec, und Rainer Schobert*

veröffentlicht.

Die Arbeit wurde in Kooperation mit Mitarbeitern des Instituts für Biophysik an der Akademie der Wissenschaft der Tschechischen Republik durchgeführt.

Eigenanteil:

Die Konzeption und Planung der biologischen Untersuchungen stammen von mir. Experimente zur Toxizität (MTT-Tests), die Zellzyklusanalysen, Experimente zur Lokalisation und Caspaseaktivierung und deren Auswertung wurden von mir durchgeführt. Von Sofia Bär stammen weitere MTT-Tests, die Experimente zu reaktiven Sauerstoffspezies und dem Mitochondrienmembranpotential, sowie die Zytoskelettfärbungen. Entsprechende Abbildungen und Textabschnitte wurden jeweils von mir oder Sofia Bär verfasst. Die Planung und Durchführung der Synthese der in dieser Arbeit untersuchten Verbindungen und deren Analytik wurde von Tobias Rehm durchgeführt. Entsprechende Textabschnitte und Abbildungen stammen von ihm. Hana Kostrhunova und Viktor Brabec haben die ICP-MS Messungen der Aufnahme der Komplexe gemessen und ausgewertet. Das Manuskript wurde von Sofia Bär und mir, in Zusammenarbeit mit Rainer Schobert verfasst.

5.1.3 Eigenanteil an Publikation III

Ergebnisse zu diesem Thema wurden 2018 in *Dalton Transactions* unter dem Titel

“N,N-Dialkylbenzimidazol-2-ylidene platinum complexes - effects of alkyl residues and ancillary cis-ligands on anticancer activity”

von den Autoren

Tobias Rehm, Matthias Rothmund, Alexander Bär, Thomas Dietel, Rhett Kempe, Hana Kostrhunova, Viktor Brabec, Jana Kasparkova, und Rainer Schobert

veröffentlicht.

Die Arbeit wurde in Kooperation mit dem Lehrstuhl für Anorganische Chemie II der Universität Bayreuth und dem Institut für Biophysik an der Akademie der Wissenschaft der Tschechischen Republik in Brünn (CZE) durchgeführt.

Eigenanteil:

Während Tobias Rehm die Planung und Durchführung der Synthese und Analytik der Verbindungen vornahm, und Alexander Bär nötige Verbindungen nachsynthetisierte, führten die Angehörigen des Lehrstuhls der anorganischen Chemie II die Strukturaufklärung durch Röntgenkristallografie und Elementaranalyse durch. Die Untersuchung der biologischen Aktivität, d.h. Bestimmung der Toxizitäten (IC₅₀-Werte), die Abhängigkeit vom p53-Status, sowie grundlegende DNA-Interaktionsuntersuchungen und Zellzyklusanalysen wurden von mir durchgeführt. Die Aufnahme der Verbindungen in die Zellen und weiterführende DNA-Interaktionsstudien wurden von den Mitarbeitern von Prof. Brabec am Institut für Biophysik (Brünn) vorgenommen. Die Arbeit wurde von Tobias Rehm und mir in Zusammenarbeit mit Prof. Rainer Schobert zu gleichen Teilen verfasst. Die Arbeiten von Prof. Brabec *et al.* wurden von mir in das Manuskript eingepflegt.

5.1.4 Eigenanteil an Publikation IV

Ergebnisse zu diesem Thema wurden 2019 in *Dalton Transactions* unter dem Titel

“Synthesis, structures and cytotoxic effects in vitro of *cis*- and *trans*-
[Pt^{IV}Cl₄(NHC)₂] complexes and their Pt^{II} precursors”

von den Autoren

*Tobias Rehm, Matthias Rothmund, Thomas Dietel, Rhett Kempe, und Rainer
Schobert*

veröffentlicht

Die Arbeit wurde in Kooperation mit dem Lehrstuhl für Anorganische Chemie II der Universität Bayreuth durchgeführt.

Eigenanteil:

Planung und Synthese der Verbindungen wurden von Tobias Rehm durchgeführt. Die Charakterisierung der Verbindungen wurden von Tobias Rehm und Thomas Dietl durchgeführt. Die Planung und Durchführung der biologischen Studien, d.h. die Untersuchung der Toxizität und der DNA-Interaktion *in vitro*, sowie die Stabilitätsuntersuchungen per UV-Vis Spektrometrie wurden von mir vorgenommen und ausgewertet. Entsprechende Abbildungen und Textabschnitte stammen von mir. Die Arbeit wurde zusammen mit Tobias Rehm und Prof. Rainer Schobert verfasst.

5.2 Publikation I

Novel *cis*-[(NHC)¹(NHC)²(L)Cl]platinum(II) complexes – synthesis, structures, and anticancer activities

*Tobias Rehm,^a Matthias Rothmund,^a Julienne K. Muenzner,^a Awal Noor,^b Rhett Kempe^b und Rainer Schobert^{*a}*

^aOrganic Chemistry Laboratory, University of Bayreuth, Universitätsstr. 30, 95440 Bayreuth

^bLehrstuhl fuer Anorganische Chemie II (Catalyst Design), University Bayreuth, Universitaetstr. 30, 95440 Bayreuth

*e-mail: Rainer.Schobert@uni-bayreuth.de

Dalton Trans. 2016, 45, 15390 – 15398.



Cite this: *Dalton Trans.*, 2016, **45**, 15390

Novel *cis*-[(NHC)¹(NHC)²(L)Cl]platinum(II) complexes – synthesis, structures, and anticancer activities†

Tobias Rehm,^a Matthias Rothemund,^a Julienne K. Muenzner,^a Awal Noor,^b Rhett Kempe^b and Rainer Schober^{*a}

A general synthesis of novel platinum(II) complexes bearing two different, *cis*-oriented, N-heterocyclic carbene (NHC) ligands is presented. Easily accessible *cis*-[Pt^{II}(NHC)(DMSO)] precursor complexes were converted to either *cis*-[Pt^{II}(NHC)₂Cl₂] complexes such as **5a** and **5b**, or to novel mixed *cis*-[Pt^{II}(NHC)¹(NHC)²Cl₂] complexes such as **5c–h** by successive introduction of the individual carbene ligands. The 'symmetric' complexes **5a** and **5b** were also converted to cationic *cis*-[Pt^{II}(NHC)₂(PPh₃)Cl]⁺Cl[−] complexes **8a** and **8b**. The structures of the ten new complexes, comprising benzylated and alkylated imidazol-2-ylidene ligands, were analysed by ¹H, ¹³C and ¹⁹⁵Pt NMR spectroscopy and also by X-ray diffraction for **5a**, **5d**, **5h**, and **8a**. The neutral complexes **5** were cytotoxic against a panel of seven human cancer cell lines with IC₅₀ values in the low micromolar range, while the cationic complexes **8** reached even nanomolar IC₅₀ values. Complex **5h** carrying the substitution pattern of the natural anti-tumoral agent Combretastatin A-4 showed a conspicuous specificity for cancer cell lines sensitive to this drug. In electrophoretic mobility shift assays, the *cis*-biscarbene complexes **5b** and **8b** led to an unwinding or aggregation of plasmid DNA, while the *trans*-biscarbene complex **1b** showed no such effect.

Received 13th June 2016,
Accepted 28th August 2016
DOI: 10.1039/c6dt02350a
www.rsc.org/dalton

Introduction

Metal complexes of N-heterocyclic carbenes (NHCs) were reported as early as 1968 by Wanzlick *et al.* and others.^{1,2} But it was not until the isolation of a crystalline carbene by Arduengo *et al.*³ in 1991 that NHCs turned from mere curiosities into applicable chemical reagents. Nowadays, they are routinely used as organocatalysts for a wide range of established reactions.⁴ NHC metal complexes are among the most efficient catalysts for reactions such as olefin metathesis⁵ and Pd-catalysed coupling reactions.^{6,7} More recently, their medicinal aspects came to the fore.^{8,9} With the successful history of anticancer active platinum compounds¹⁰ in mind, bioactive NHC complexes were devised of metals such as Pd,¹¹ Ag,¹² Cu,¹³ Ru,¹⁴ Au,¹⁵ and Pt.¹⁶ Meanwhile, a general picture of structure–activity correlations for such complexes is

unfolding, allowing a prediction of the influence of the central metal, the NHC substituents, the charge, the lipophilicity, and the sterical encumbrance around the metal centre on their biological properties. We recently studied the influence of the latter factor, sterical congestion, in a series of platinum complexes.¹⁷

Unlike complexes *trans*-[Pt^{II}(NHC)₂Cl₂] **1**, featuring a poor NHC leaving group, the complexes *cis*-[Pt^{II}(DMSO)(NHC)Cl₂] **2** which bear a well accessible chlorido leaving ligand, had bound to DNA as expected. Substitution of DMSO for PPh₃ gave complex **3** which still, though to a lesser extent, bound coordinatively to DNA but also initiated some DNA aggregation. The cationic complex *trans*-[Pt^{II}(PPh₃)₂(NHC)Cl]⁺Cl[−] **4**, featuring a sterically shielded chlorido ligand, exclusively induced DNA aggregation (Fig. 1).

For a more nuanced assessment of such steric effects we now developed an access to platinum(II) complexes with two different, *cis*-positioned NHC ligands (Scheme 1). Complexes *cis*-[Pt^{II}(NHC)₂L₂] with two identical NHC ligands had been synthesised before by Röschenhaler *et al.*,¹⁸ and Nolan *et al.*^{19,20} using *cis*-[Pt(DMSO)₂Cl₂], [Pt(cod)Cl₂], or [Pt(cod)Me₂] as precursors. Displacement of the leaving ligands DMSO or cod, respectively, by two equivalents of the free or masked NHC led to the desired *cis*-biscarbene complexes. However, these protocols do not allow the synthesis of mixed *cis*-[Pt^{II}(NHC)¹(NHC)²L₂] complexes.

^aOrganic Chemistry Laboratory, University Bayreuth, Universitätsstrasse 30, 95440 Bayreuth, Germany. E-mail: Rainer.Schober@uni-bayreuth.de

^bLehrstuhl fuer Anorganische Chemie II (Catalyst Design), University Bayreuth, Universitätsstrasse 30, 95440 Bayreuth, Germany

†Electronic supplementary information (ESI) available: NMR spectra of **5a–h** and **5a,b**; synthesis of **1b**; ligand synthesis. CCDC 1481378–1481381. For ESI and crystallographic data in CIF or other electronic format see DOI: 10.1039/c6dt02350a

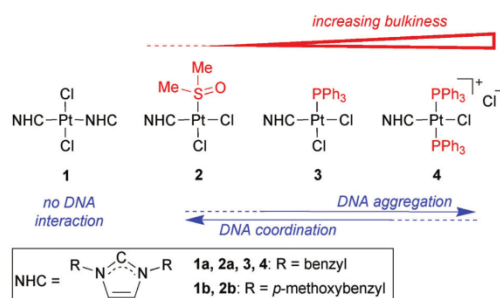
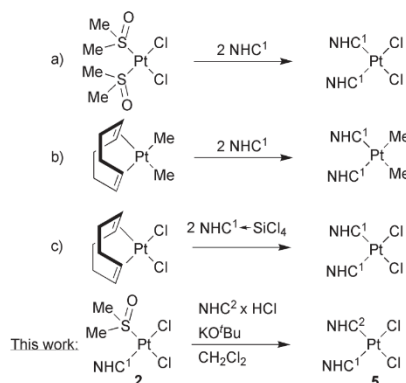


Fig. 1 NHC-platinum(II) complexes with spectator ligands of increasing bulkiness and their modes of DNA interaction.¹⁷



Scheme 1 Syntheses of *cis*-bis(NHC) complexes of platinum(II) by (a) Nolan *et al.*,¹⁹ (b) Nolan *et al.*,²⁰ (c) Röschenzhaler *et al.*,¹⁸ and a new access to complexes *cis*-[Pt^{II}(NHC)¹(NHC)²Cl₂] 5.

Results and discussion

Synthesis and characterisation

The key intermediates for our new synthesis are *cis*-[Pt^{II}(NHC)(DMSO)Cl₂] complexes such as 2, first synthesised by Rourke *et al.* in 2007.²¹ This group found that using DMSO instead of CH₂Cl₂ as the solvent for the carbene transfer from silver NHC complexes to suitable sources of the desired metal, *e.g.* K₂PtCl₄, led to the formation of monocarbene complexes of type 2 rather than to the formation of *trans*-biscarbene complexes of type 1. The DMSO ligand can then be substituted by a more electron-rich ligand such as a phosphane,^{17,21} or, as detailed in this work, a second NHC ligand.

We prepared eight new *cis*-[Pt^{II}(NHC)¹(NHC)²Cl₂] complexes 5 with six different NHCs as ligands *via* DMSO precursor complexes 2. Since the two NHC ligands are introduced one at a time, complexes with two different NHCs can be synthesised starting from two different imidazolium salts 6 (ImH¹) and 7 (ImH²)^{22–26} (Scheme 2). We employed imidazolium chlorides that were 1,3-benzylated, or -alkylated. For the synthesis of

cis-[Pt^{II}(NHC)¹(NHC)²Cl₂] complexes 5 the respective complex *cis*-[Pt^{II}(DMSO)(NHC)¹Cl₂] 2 was treated with ImH²Cl 7 and KO^tBu to generate (NHC)². The resulting mixture was stirred in dry CH₂Cl₂ for 16 hours by which time the DMSO had been completely substituted by (NHC)² and the pure product complexes 5 were obtained by precipitation in yields of up to 93%. Replacing the base KO^tBu by K₂CO₃, NaOMe or CaH₂ had little influence on the yields as had the use of acetonitrile as a solvent.

The *cis* configuration of complexes 5 was confirmed by ¹H and ¹³C NMR spectroscopy. In line with a previous study¹⁷ of the complexes 2a and 3, the ¹H NMR spectra of complexes 5 showed an inequivalency of the two geminal protons of each benzylic CH₂ group (one facing the neighbouring chlorine, the other the second NHC) and their splitting up into two doublets. These corresponding signals are 0.44 to 1.13 ppm apart and couple with ²J_{AB} = 14.34 to 14.95 Hz. This corroborates the *cis* configuration of the NHC ligands as well as the perpendicular orientation of the imidazole ring relative to the plane spanned by the PtCl₂ fragment (Fig. 2).

Further evidence is provided by the ¹³C NMR shifts of the carbene carbon signals ranging from 147.8 to 149.9 ppm, typical of carbon atoms in a *cis*-NHC-L-PtCl₂ environment.^{17,21,27} While the symmetric complexes 5a and 5b showed only one carbene carbon signal, the mixed complexes gave rise to two inequivalent signals for the different NHC ligands.

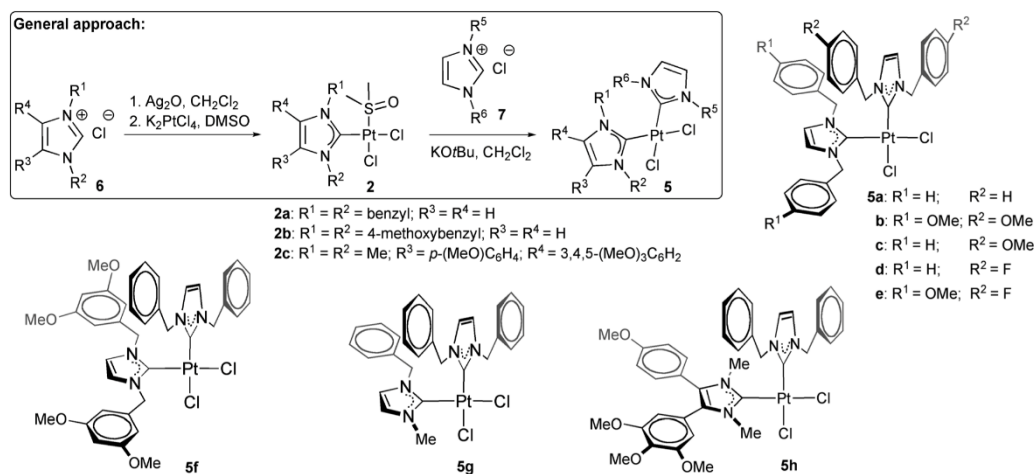
Complexes 5g and 5h showed distinct ¹H NMR spectra with coupling constants ²J_{AB} = 15.11 to 15.26 Hz and overall more complex spectra as each CH₂ proton has a different surrounding and thus a distinctive shift. In the ¹³C NMR spectrum of 5g the carbene carbon of the *N*-methylated NHC ligand peaks at 146.6 ppm.

We also prepared cationic complexes 8 from the symmetric complexes 5a and 5b by substitution of a chlorido for a triphenylphosphane ligand (Scheme 3).

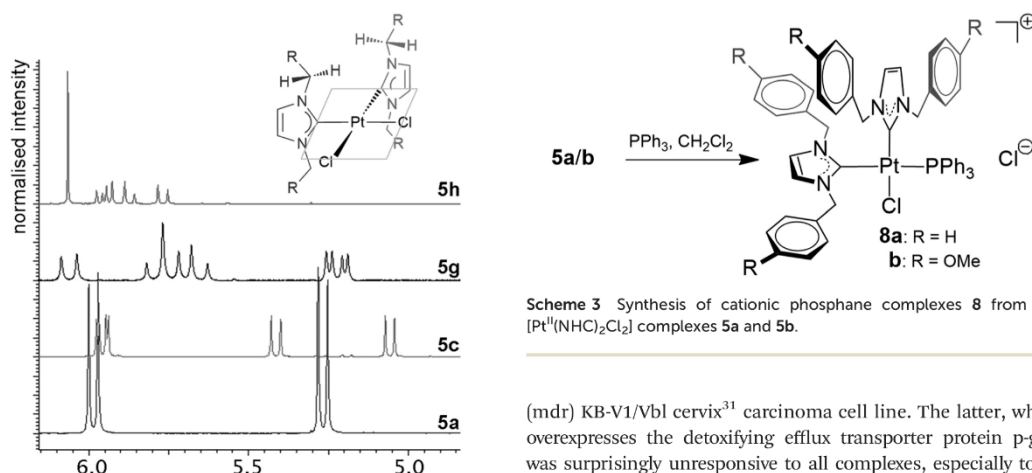
Their ¹H NMR spectra showed more complex CH₂ signals due to the additional asymmetry. Their carbene carbon signals in the ¹³C NMR spectra appeared as doublets with ²J_{CP} = 10 Hz (*cis* to PPh₃) and 151 Hz (*trans* to PPh₃), respectively. The ³¹P–¹⁹⁵Pt coupling of ¹J_{PtP} = 2366 Hz (8a) and 2361 Hz (8b) was visible as were the phosphane signals at 13.09 (8a) and 13.34 ppm (8b) in the ³¹P NMR spectra.

X-ray crystallography

Crystals suitable for X-ray diffraction analyses were grown by slow infusion of hexane into saturated solutions of 5a, 5d, 5h, or 8a in CH₂Cl₂ kept at 4 °C. Fig. 3 shows their molecular structures. The characteristic bond lengths and angles were similar for all four complexes. The distances between the platinum and the carbene carbon atoms were in the range of 1.97–1.99 Å, only in the phosphane complex 8a the distances were slightly longer with 2.02 Å and 2.07 Å. The Pt–Cl distances lay between 2.35 and 2.36 Å, while the Pt–P bond of 8a was 2.31 Å long. The C–Pt–C angles ranged from 93.7° (8a) to 96.4° (5d) for those complexes that bore 1,3-dibenzylimidazol-2-



Scheme 2 General synthesis and structures of complexes 5a–h.

Fig. 2 Relevant ¹H NMR signals of inequivalent benzylic CH₂ protons of complexes 5 proving the *cis* configuration.

ylidene ligands. In the case of **5h** the C–Pt–C angle was reduced to 90.4°.

Anticancer activity

Complexes **5** and **8** were investigated for their cytotoxicity against a panel of seven human cancer cell lines of six entities and an endothelial cell line using the MTT-based viability assay.^{28,29} Table 1 summarises the resulting IC₅₀ (72 h) values. All complexes **5a–h** showed remarkable efficacies with low micromolar IC₅₀ values against all cell lines, save for the cisplatin resistant HT-29 colon³⁰ and the multidrug-resistant

(mdr) KB-V1/Vbl cervix³¹ carcinoma cell line. The latter, which overexpresses the detoxifying efflux transporter protein p-gp1, was surprisingly unresponsive to all complexes, especially to **5h** that bears the structural motif of the natural anticancer drug combretastatin A-4 (CA-4). Complex **5h** was also less active than most other test compounds against the mdr MCF7/Topo³² mamma carcinoma cell line which overexpresses the efflux transporter BCRP34 (breast cancer resistance protein). This is an indication for **5h** being a substrate of these drug efflux pumps.

Against CA-4 sensitive cancer cell lines such as DLD-1 colon carcinoma and Panc-1 pancreatic cancer, and also against the hybrid endothelial Ea.Hy926 cells, complex **5h** retained the activity of the natural lead compound CA-4, showing IC₅₀ concentrations in the low nanomolar range.

As we have already shown in previous work, exchange of one chlorido for a phosphane ligand can enhance the cytotoxicity significantly, probably due to an increase in lipophilicity, solubility and thus of cellular uptake.¹⁷ This was observed here as well when going from the neutral dichlorido

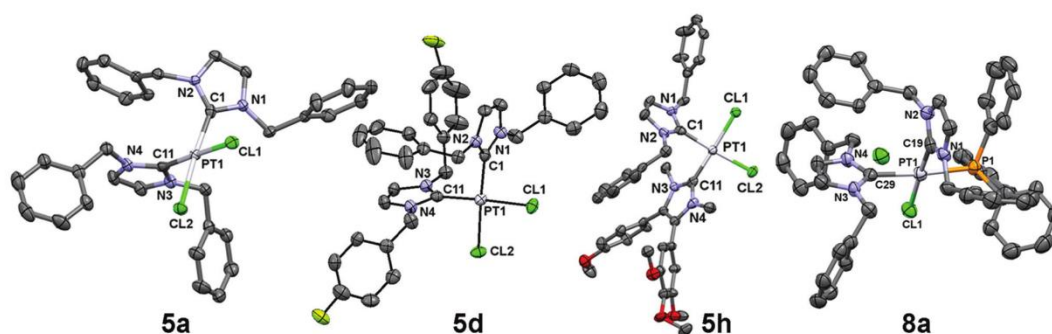


Fig. 3 Molecular structures of complexes **5a**, **5d**, **5h**, and **8a** as thermal ellipsoid representations at 50% probability level (H atoms omitted). Selected bond lengths [Å] and angles [°]: **5a**: Pt1–Cl1 2.362(3), Pt1–Cl2 2.350(2), Pt1–C1 1.969(3), Pt1–C11 1.967(3), Cl1–Pt1–Cl2 90.5(7), Cl1–Pt1–C1 88.5(6), Cl1–Pt1–C11 176.5(1), Cl2–Pt1–C1 175.8(6), Cl2–Pt1–C11 86.2(9), C1–Pt1–C11 94.6(8); **5d**: Pt1–Cl1 2.355(6), Pt1–Cl2 2.355(6), Pt1–C1 1.971(4), Pt1–C11 1.971(4), Cl1–Pt1–Cl2 92.1(7), Cl1–Pt1–C1 85.7(6), Cl1–Pt1–C11 176.9(4), Cl2–Pt1–C1 176.9(4), Cl2–Pt1–C11 85.7(6), C1–Pt1–C11 96.4(0); **5h**: Pt1–Cl1 2.359(2), Pt1–Cl2 2.361(8), Pt1–C1 1.984(4), Pt1–C11 1.991(2), Cl2–Pt1–C1 89.5(3), Cl2–Pt1–C11 92.6(2), Cl2–Pt1–C1 176.9(2), Cl1–Pt1–C11 176.2(8), Cl1–Pt1–C1 87.4(0), C1–Pt1–C11 90.4(6); **8a**: Pt1–Cl1 1.348(7), Pt1–P1 2.312(7), Pt1–C29 2.072(7), Pt1–C29 2.016(4), Cl1–Pt1–P1 92.0(5), Cl1–Pt1–C29 87.0(9), Cl1–Pt1–C19 176.2(7), P1–Pt1–C29 172.6(1), P1–Pt1–C19 87.5(7), C19–Pt1–C29 93.7(5).

Table 1 Means \pm SD of IC₅₀ (72 h) values [μ M] of complexes **5**, **8**, and cisplatin (CDDP) in MTT assays against human cancer cell lines and an endothelial hybrid cell line as calculated from four independent measurements

Cell line	IC ₅₀ (72 h) [μ M]									
	5a	5b	5c	5d	5e	5f	5g	5h	8a	8b
518A2	6.2 \pm 0.4	7.9 \pm 0.4	5.6 \pm 0.2	6.1 \pm 0.5	5.2 \pm 0.3	7.1 \pm 0.5	39.0 \pm 1.0	6.5 \pm 0.2	0.86 \pm 0.05	0.60 \pm 0.15
HT-29	14.6 \pm 1.4	11.1 \pm 2.0	13.9 \pm 1.4	21.6 \pm 1.5	4.1 \pm 0.4	6.6 \pm 0.5	39.7 \pm 2.0	11.1 \pm 0.7	0.82 \pm 0.06	0.45 \pm 0.03
DLD-1	4.7 \pm 1.4	3.2 \pm 0.1	5.1 \pm 0.6	4.0 \pm 0.2	5.7 \pm 1.4	11.1 \pm 0.9	30.2 \pm 5.2	0.39 \pm 0.07	0.77 \pm 0.04	0.66 \pm 0.02
U87	7.2 \pm 0.2	7.7 \pm 0.5	9.0 \pm 1.1	5.0 \pm 0.3	4.5 \pm 0.4	7.3 \pm 0.3	>50	6.1 \pm 2.1	0.89 \pm 0.19	0.95 \pm 0.21
Panc-1	3.5 \pm 0.7	2.9 \pm 0.0	3.0 \pm 0.1	4.2 \pm 0.4	6.7 \pm 1.3	6.0 \pm 0.1	38.8 \pm 3.7	0.24 \pm 0.05	0.36 \pm 0.00	0.39 \pm 0.03
MCF7/Topo	8.6 \pm 2.0	4.0 \pm 0.2	11.1 \pm 5.6	7.6 \pm 0.9	3.2 \pm 0.5	13.7 \pm 0.9	42.1 \pm 2.7	37.1 \pm 5.6	0.43 \pm 0.01	0.52 \pm 0.03
Kb-V1/Vbl	11.7 \pm 0.8	13.9 \pm 1.1	16.1 \pm 0.8	18.1 \pm 2.6	43.5 \pm 2.1	21.0 \pm 1.0	>50	35.5 \pm 1.3	7.3 \pm 1.2	6.0 \pm 0.3
Ea.Hy926	6.8 \pm 1.6	4.2 \pm 0.4	5.6 \pm 1.9	7.6 \pm 0.2	3.2 \pm 0.5	13.4 \pm 0.5	45.3 \pm 1.2	0.4 \pm 0.08	0.48 \pm 0.01	0.72 \pm 0.03

518A2 – human melanoma, HT-29 – human colon adenocarcinoma, DLD-1 – Dukes type C colorectal adenocarcinoma, U87 – human glioblastoma, Panc-1 – human pancreatic carcinoma, MCF7/Topo – human breast cancer, Kb-V1/Vbl – human cervix carcinoma, Ea.Hy926 – endothelial hybrid cells.

complexes **5a–b** to the phosphane complexes **8a–b** which are typical ‘delocalised lipophilic cations’ (DLCs). They were efficacious with submicromolar IC₅₀ values against most of the cell lines. Again, the KbV1/Vbl cells were least responsive requiring single-digit micromolar IC₅₀ concentrations (**8a**: 7 μ M; **8b**: 6 μ M).

In vitro DNA interaction

We investigated the DNA interaction of *trans*-[Pt^{II}(NHC)₂Cl₂] complex **1b**, the isomeric *cis*-complex **5b**, and its cationic analogue *cis*-[Pt^{II}(NHC)₂(PPh₃Cl)]⁺Cl[−] **8b** by means of an electrophoretic mobility shift assay (EMSA) with circular pBR322 plasmid DNA (Fig. 4). The *trans* configured complex **1b** did not alter the DNA morphology, *i.e.* the ratio of open circular (oc) and covalently closed circular (ccc) forms. In contrast, its *cis* isomer **5b** led to a distinct unwinding of the plasmid DNA in a

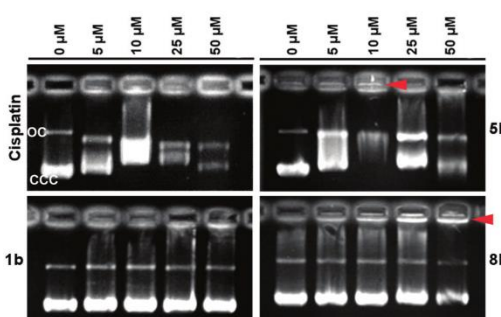


Fig. 4 Modification of gel electrophoretic mobility of pBR322 plasmid DNA when incubated for 24 h with different concentrations of cisplatin, **1b**, **5b**, and **8b** (oc = open circular, ccc = covalently closed circular DNA form; the red arrows mark DNA aggregates).

concentration-dependent manner, as is also typical of cisplatin, apparent from a pronounced band shift with a maximum at a concentration of 10 μM of **5b**. At this concentration the DNA also seems to aggregate to adducts that remain in the gel pocket during electrophoresis, not able to permeate the pores of the gel. The same phenomenon was observed for **8b**, yet to a greater extent. It initiated immediate aggregation of the plasmid DNA without any conversion of its topological *oc* and *ccc* isomers. Such effects had previously been observed¹⁷ and corroborated by light scattering experiments and studies of the DNA binding kinetics for complexes **3** and **4**. They suggest that the mode of DNA interaction is mainly governed by the sterical shielding of the chlorido leaving ligand or the metal centre.

Conclusions

We have developed a new synthetic protocol that gives access to *cis*-[Pt^{II}(NHC)¹(NHC)²L¹L²] complexes with two different NHC ligands. Ten complexes were prepared, structurally elucidated, and screened for antiproliferative activity against human tumour cells. Their activity was surprisingly high on average, with a considerable degree of structure-dependent cell line specificity. For some complexes we observed a breach of the cisplatin and multidrug resistance of certain cancer cell lines. Mechanistically, DNA seems to be a major target of these new platinum complexes, albeit in a more differentiated way when compared to cisplatin. In EMSA experiments with circular plasmid DNA, the neutral *cis*-biscarbene complex **5b** bound coordinatively to it leading to its unwinding. Apparently, complex **5b** also initiated the aggregation of this form of DNA to some extent. This needs to be confirmed by further experiments. The cationic *cis*-biscarbene complex **8b** seems to have led exclusively to DNA aggregation. The *trans*-biscarbene complex **1b** showed no such effects. Obviously, the mode of DNA interaction is correlated to the replaceability and sterical accessibility of the leaving ligand, and the overall charge of the complex.

Another interesting aspect is the retention of intrinsic ligand bioactivity in the complexes, *e.g.* for the CA-4 derived complex **5h**. This should allow a high degree of liberty in devising new pleiotropic anticancer complexes with various combinations of NHC ligands, spectator ligands, and leaving groups that contribute their inherent activity and so influence the overall pharmacological properties. Likewise, our new access to *cis*-biscarbene complexes, which is very likely not restricted to platinum, will be of interest to catalysis chemists as it offers a way to fine-tune the stereoelectronic properties of NHC complex catalysts more minutely than before.

Experimental

Materials and methods

All chemicals and reagents were purchased from Sigma Aldrich, Alfa Aesar, or ABCR and were used without further

purification. Melting points are uncorrected; NMR spectra were run on a 500 MHz spectrometer; chemical shifts are given in ppm (δ) and referenced relative to the internal solvent signal; ¹⁹⁵Pt NMR shifts are quoted relative to $\Xi(^{195}\text{Pt}) = 21.496784$ MHz, K₂PtCl₄ was used as external standard ($\delta = -1612.81$); mass spectra: direct inlet, EI, 70 eV; elemental analyses: Vario EL III and HEKAtech EA 3000 elemental analysers; X-ray diffractometers: STOE-IPDS II and STOE-STADIVARI. All biotested compounds were >95% pure by elemental analysis. *N*-Methyl- and *N*-benzylimidazolium salts were prepared according to literature procedures (*cf.* ESI[†]),^{22–25} as were 1,3-dimethyl-4-(3',4',5'-trimethoxyphenyl)-5-(4''-methoxyphenyl)imidazolium iodide²⁶ and complex **2a**.¹⁷ Complex **1b** was prepared analogously to **1a**¹⁷ and is described in the ESI[†].

Syntheses and characterisation

***cis*-[Dichlorido-(1,3-di(4-methoxybenzyl)imidazol-2-ylidene)(dimethylsufoxide)]platinum(II) (2b)**. A mixture of 1,3-di(4-methoxybenzyl)imidazolium chloride (177 mg, 513 μmol) and CH₂Cl₂ (10 mL) was treated with silver(I) oxide (59 mg, 257 μmol) and stirred for 24 h at room temperature. Solids were filtered off and the silver NHC complex was precipitated by addition of hexane. After decanting and drying *in vacuo* this intermediate complex (200 mg, 443 μmol) was dissolved in DMSO (7.5 mL), treated with K₂PtCl₄ (184 mg, 443 μmol), and the mixture was stirred at 60 °C for 24 h. CH₂Cl₂ was added, the reaction mixture was filtered, and the filtrate was washed with water and dried over Na₂SO₄. The volatiles were removed *in vacuo* and the remainder was recrystallised from CH₂Cl₂/hexane to yield 225 mg (78%) of white crystals of m.p. 206 °C. ¹H NMR (CDCl₃, 500 MHz): δ 3.26 (s, 6H, CH₃, DMSO), 3.81 (s, 6H, OCH₃), 5.60 (virt. t, *J* = 15.3 Hz, 4H, CH₂), 6.78 (s, 2H, CH, imidazole), 6.92 (d, *J* = 8.5 Hz, 4H, Ar), 7.33 (d, *J* = 8.5 Hz, 4H, Ar); ¹³C NMR (CDCl₃, 126 MHz): δ 45.6 (DMSO), 53.9 (CH₂), 55.3 (OCH₃), 114.3 (Ar), 121.0 (CH, imidazole), 126.9 (Ar), 129.7 (Ar), 143.8 (NCN), 159.7 (Ar); EI-MS: *m/z* 502 (5%, -Cl₂, -DMSO), 416 (9), 401 (7), 308 (10), 241 (8), 188 (10), 121 (100), 78 (12).

***cis*-[Dichlorido-(1,3-dimethyl-4-(3',4',5'-trimethoxyphenyl)-5-(4''-methoxyphenyl)imidazol-2-ylidene)(dimethylsufoxide)]platinum(II) (2c)**. Analogously to **2b**, complex **2c** (155 mg, 78%) was obtained from 1,3-dimethyl-4-(3',4',5'-trimethoxyphenyl)-5-(4''-methoxyphenyl)imidazolium iodide (143 mg, 287 μmol), silver(I) oxide (33 mg, 144 μmol), K₂PtCl₄ (119 mg, 287 μmol), and DMSO (6 mL) as white crystals of m.p. 143 °C. ¹H NMR (CDCl₃, 500 MHz): δ 3.59 (s, 6H, CH₃, DMSO), 3.71 (s, 6H, 3', 5'-OCH₃), 3.79 (s, 3H, 4''-OCH₃), 3.83 (s, 3H, 4'-OCH₃), 3.90 (s, 3H, NCH₃), 3.94 (s, 3H, NCH₃), 6.33 (s, 2H, Ar), 6.86 (d, *J* = 8.4 Hz, 2H, Ar), 7.10 (d, *J* = 8.8 Hz, 2H, Ar); ¹³C NMR (CDCl₃, 126 MHz): δ 36.2 (N-CH₃), 46.3 (DMSO), 55.3 (4''-OCH₃), 56.2 (3', 5'-OCH₃), 60.9 (4'-OCH₃), 107.8 (Ar, C-2', -6'), 114.3 (C-2'', -6''), 119.5 (Ar, C-1'), 122.7 (Ar, C-1'), 131.5 (C-4, -5, imidazole), 131.8 (Ar, C-3'', -5''), 138.6 (Ar, C-4'), 142.5 (NCN), 153.3 (Ar, C-3', -5'), 160.2 (Ar, C-4''); EI-MS: *m/z* 712 (M⁺, 1%),

635 (2, -DMSO), 562 (2, -Cl₂, -DMSO), 415 (6), 369 (11), 355 (67), 340 (34), 78 (56), 63 (56), 50 (100), 36 (98).

General procedure for the preparation of *cis*-[Pt^{II}(NHC)¹(NHC)²Cl₂] complexes 5

Complex 2 (1 equiv.) and the respective imidazolium chloride 7 (1 equiv.) were dissolved in dry CH₂Cl₂ (60 mL mmol⁻¹) and treated with KO^tBu (1.2 equiv.) under an atmosphere of dry argon. After stirring at room temperature for 16 h solids were filtered off and the pure product 5 was precipitated by adding diethyl ether at 4 °C.

***cis*-[Dichlorido-bis(1,3-dibenzylimidazol-2-ylidene)] platinum(II) (5a).** Complex 5a (60 mg, 93%) was obtained from 2a (50 mg, 84.4 μmol), 1,3-dibenzylimidazolium chloride (24 mg, 84.4 μmol), and KO^tBu (11 mg, 101 μmol) yield 60 mg (93%) as white crystals of m.p. 287 °C. Elemental analysis (%): calc. for C₃₄H₃₂N₄PtCl₂ (762.63): C, 53.55; H, 4.23; N, 7.35. Found: C, 53.04; H, 4.48; N, 7.39. ¹H NMR (CDCl₃, 500 MHz): δ 5.27 (d, *J* = 14.6 Hz, 4H, CH₂), 5.99 (d, *J* = 14.6 Hz, 4H, CH₂), 6.52 (s, 4H, imidazole CH), 7.12–7.19 (m, 8H, Ar), 7.27–7.33 (m, 12H, Ar); ¹³C NMR (CDCl₃, 126 MHz): δ 54.1 (CH₂), 120.5 (imidazole CH), 128.2 (Ar), 128.9 (Ar), 134.9 (Ar), 149.0 (NCN); ¹⁹⁵Pt NMR (CDCl₃): δ -3605.3; EI-MS: *m/z* 762 (M⁺, 7%), 726 (11, -Cl), 689 (24, -Cl₂), 441 (18), 247 (51), 157 (29), 91 (100). *Crystal data*: C₃₄H₃₂N₄PtCl₂, *M* = 762.62, monoclinic, space group *P*2(1)/*c*, *a* = 7.5380(3), *b* = 33.6480(12), *c* = 12.1810(5) Å, α = γ = 90°, β = 95.951(3)°, *V* = 3072.9(2) Å³, *Z* = 4, λ = 0.71069 Å, μ = 4.77 mm⁻¹, *T* = 133 K; 12 924 reflections measured, 6540 unique; final refinement to convergence on *R*² gave *R* = 0.0276 and *R*_w = 0.0601, GOF = 0.766. CCDC 1481381.

***cis*-[Dichlorido-bis(1,3-di(4-methoxybenzyl)imidazol-2-ylidene)] platinum(II) (5b).** Complex 2b (88 mg, 135 μmol), 1,3-di(4-methoxybenzyl)imidazolium chloride (47 mg, 135 μmol), and KO^tBu (18 mg, 162 μmol) yielded 74 mg (62%) of 5b as white crystals of m.p. 211 °C. Elemental analysis (%): calc. for C₃₆H₄₀O₄N₄PtCl₂ (882.74): C, 51.70; H, 4.57; N, 6.35. Found: C, 51.75; H, 4.46; N, 6.39. ¹H NMR (CDCl₃, 500 MHz): δ 3.77 (s, 12H, OCH₃), 5.19 (d, *J* = 14.3 Hz, 4H, CH₂), 5.93 (d, *J* = 14.3 Hz, 4H, CH₂), 6.53 (s, 4H, imidazole CH), 6.77–6.83 (d, *J* = 8.5 Hz, 8H, Ar), 7.08–7.16 (d, *J* = 8.5 Hz, 8H, Ar); ¹³C NMR (CDCl₃, 126 MHz): δ 53.7 (CH₂), 55.3 (OCH₃), 114.3 (Ar), 120.3 (imidazole CH), 126.9 (Ar), 129.9 (Ar), 148.2 (NCN), 159.6 (Ar); ¹⁹⁵Pt NMR (CDCl₃): δ -3601.0; EI-MS: *m/z* 882 (M⁺, 2%), 845 (4, -Cl), 809 (18, -Cl₂), 502 (16), 379 (9), 307 (11), 187 (11), 121 (100).

***cis*-[Dichlorido-(1,3-dibenzylimidazol-2-ylidene)(1,3-di(4-methoxybenzyl)imidazol-2-ylidene)]platinum(II) (5c).** Complex 2a (104 mg, 176 μmol), 1,3-di(4-methoxybenzyl)imidazolium chloride (61 mg, 176 μmol), and KO^tBu (24 mg, 211 μmol) gave 78 mg (54%) of 5c as white crystals of m.p. 243 °C. Elemental analysis (%): calc. for C₃₆H₃₆O₂N₄PtCl₂ (822.69): C, 52.56; H, 4.41; N, 6.81. Found: C, 52.18; H, 4.81; N, 6.98; ¹H NMR (CDCl₃, 500 MHz): δ 3.77 (s, 6H, OCH₃), 5.06 (d, *J* = 14.3 Hz, 2H, CH₂), 5.41 (d, *J* = 14.3 Hz, 2H, CH₂), 5.96 (2 × d, *J* = 14.3 Hz, 4H, CH₂), 6.45 (s, 2H, imidazole CH), 6.59 (s, 2H, imidazole CH), 6.80 (d, *J* = 8.5 Hz, 4H, Ar), 7.12 (d, *J* = 8.5 Hz, 4H,

Ar), 7.16 (m, 4H, Ar), 7.29 (m, 6H, Ar); ¹³C NMR (CDCl₃, 126 MHz): δ 53.6 (CH₂), 54.1 (CH₂), 55.3 (OCH₃), 114.3 (Ar), 120.2 (imidazole CH), 120.6 (imidazole CH), 126.8 (Ar), 128.2 (Ar), 128.4 (Ar), 128.9 (Ar), 129.9 (Ar), 134.9 (Ar), 147.9 (NCN), 149.3 (NCN), 159.6 (Ar); ¹⁹⁵Pt NMR (CDCl₃): δ -3603.0; EI-MS: *m/z* 822 (M⁺, 6%), 786 (8, -Cl), 749 (27, -Cl₂), 502 (9), 441 (22), 307 (11), 247 (38), 157 (30), 121 (100), 91 (79).

***cis*-[Dichlorido-(1,3-dibenzylimidazol-2-ylidene)(1,3-di(4-fluorobenzyl)imidazol-2-ylidene)]platinum(II) (5d).** Complex 2a (80 mg, 135 μmol), 1,3-di(4-fluorobenzyl)imidazolium chloride (43 mg, 135 μmol), and KO^tBu (18 mg, 162 μmol) afforded 57 mg (53%) of 5d as white crystals of m.p. 241 °C. Elemental analysis (%): calc. for C₃₄H₃₀N₄F₂PtCl₂ (798.62): C, 51.13; H, 3.79; N, 7.02. Found: C, 50.61; H, 3.66; N, 7.04; ¹H NMR (CDCl₃, 126 MHz): δ 4.96 (d, *J* = 14.3 Hz, 2H, CH₂), 5.48 (d, *J* = 15.0 Hz, 2H, CH₂), 5.92 (d, *J* = 15.0 Hz, 2H, CH₂), 6.08 (d, *J* = 14.3 Hz, 2H, CH₂), 6.45 (s, 2H, imidazole CH), 6.63 (s, 2H, imidazole CH), 6.98 (t, *J* = 8.7 Hz, 4H, Ar), 7.13–7.18 (m, 4H, Ar), 7.21 (dd, *J* = 8.7, 5.2 Hz, 4H, Ar), 7.28–7.34 (m, 6H, Ar); ¹³C NMR (CDCl₃, 126 MHz): δ 53.4 (CH₂), 54.1 (CH₂), 115.9 (d, ²*J*_{CF} = 21.8 Hz, Ar), 120.4 (imidazole CH), 120.8 (imidazole CH), 127.9 (Ar), 128.4 (Ar), 129.0 (Ar), 130.3 (d, ³*J*_{CF} = 8.2 Hz, Ar), 130.6 (Ar), 134.8 (Ar), 149.0 (NCN), 149.1 (NCN), 162.7 (d, ¹*J*_{CF} = 248 Hz, Ar); ¹⁹⁵Pt NMR (CDCl₃): δ -3605.2; EI-MS: *m/z* 798 (M⁺, 8%), 761 (28, -Cl), 725 (100, -Cl₂), 477 (24), 441 (33), 283 (45), 247 (81), 109 (60), 91 (44). *Crystal data*: C₃₄H₂₈N₄F₂PtCl₂, *M* = 796.59, monoclinic, space group *C*2/*c*, *a* = 15.6790(6), *b* = 14.1220(6), *c* = 15.1390(8) Å, α = γ = 90°, β = 113.895(5)°, *V* = 3064.8(3) Å³, *Z* = 4, λ = 0.71069 Å, μ = 4.80 mm⁻¹, *T* = 133 K; 19 249 reflections measured, 3070 unique; final refinement to convergence on *R*² gave *R* = 0.0267 and *R*_w = 0.0639, GOF = 0.984. CCDC 1481378.

***cis*-[Dichlorido-(1,3-di(4-fluorobenzyl)imidazol-2-ylidene)(1,3-di(4-methoxybenzyl)imidazol-2-ylidene)]platinum(II) (5e).** Complex 5e (13 mg, 11%) was obtained from 2b (88 mg, 135 μmol), 1,3-di(4-fluorobenzyl)imidazolium chloride (43 mg, 135 μmol), and KO^tBu (18 mg, 162 μmol) as white crystals of m.p. 223 °C. Elemental analysis (%): calc. for C₃₆H₃₄N₄O₂F₂PtCl₂ (858.67): C, 50.36; H, 3.99; N, 6.52. Found: C, 49.91; H, 4.13; N, 6.32; ¹H NMR (CDCl₃, 500 MHz): δ 3.77 (s, 6H, OCH₃), 5.13 (d, *J* = 14.6 Hz, 2H, CH₂), 5.22 (d, *J* = 14.3 Hz, 2H, CH₂), 5.88 (d, *J* = 14.3 Hz, 2H, CH₂), 6.04 (d, *J* = 14.6 Hz, 2H, CH₂), 6.54 (s, 2H, imidazole CH), 6.56 (s, 2H, imidazole CH), 6.80 (d, *J* = 8.5 Hz, 4H, Ar), 6.97 (t, *J* = 8.7 Hz, 4H, Ar), 7.12 (d, *J* = 8.5 Hz, 4H, Ar), 7.21 (dd, *J* = 8.7, 5.2 Hz, 4H, Ar); ¹³C NMR (CDCl₃, 126 MHz): δ 53.4 (CH₂), 53.6 (CH₂), 55.3 (OCH₃), 114.3 (Ar), 115.9 (d, ²*J*_{CF} = 21.8 Hz, Ar), 120.5 (imidazole CH), 120.5 (imidazole CH), 126.7 (Ar), 129.7 (Ar), 130.3 (d, ³*J*_{CF} = 8.2 Hz, Ar), 130.6 (d, ¹*J*_{CF} = 2.7 Hz, Ar), 147.8 (NCN), 149.0 (NCN), 159.7 (Ar), 162.7 (d, ¹*J*_{CF} = 249 Hz, Ar); ¹⁹⁵Pt NMR (CDCl₃): δ -3601.7; EI-MS: *m/z* 858 (M⁺, 6%), 822 (10, -Cl), 786 (39, -Cl₂), 663 (8), 502 (12), 477 (27), 283 (31), 175 (25), 121 (100), 109 (98).

***cis*-[Dichlorido-(1,3-dibenzylimidazol-2-ylidene)(1,3-bis(3,5-dimethoxybenzyl)imidazol-2-ylidene)]platinum(II) (5f).** Complex 5f (35 mg, 26%) was obtained from 2a (90 mg,

153 μmol), 1,3-bis(3,5-dimethoxybenzyl)imidazolium chloride (62 mg, 153 μmol), and KO^tBu (21 mg, 184 μmol) as white crystals of m.p. 237 °C. Elemental analysis (%): calc. for $\text{C}_{38}\text{H}_{40}\text{O}_4\text{N}_4\text{PtCl}_2$ (882.74): C, 51.70; H, 4.57; N, 6.35. Found: C, 51.41; H, 5.18; N, 6.43; ^1H NMR (CDCl_3 , 500 MHz): δ 3.73 (s, 12H, OCH_3), 5.05 (d, J = 14.3 Hz, 2H, CH_2), 5.32 (d, J = 15.0 Hz, 2H, CH_2), 5.97 (dd, J = 14.6, 1.8 Hz, 4H, CH_2), 6.35 (t, J = 2.4 Hz, 2H, Ar), 6.42 (d, J = 2.4 Hz, 4H, Ar), 6.52 (s, 2H, imidazole CH), 6.60 (s, 2H, imidazole CH), 7.17 (m, 4H, Ar), 7.28–7.33 (m, 6H, Ar); ^{13}C NMR (CDCl_3 , 126 MHz): δ 54.1 (CH_2), 54.1 (CH_2), 55.6 (OCH_3), 100.3 (Ar), 106.3 (Ar), 120.6 (imidazole CH), 120.8 (imidazole CH), 128.2 (Ar), 128.4 (Ar), 129.0 (Ar), 135.0 (Ar), 137.3 (Ar), 148.9 (NCN), 148.9 (NCN), 161.2 (Ar); ^{195}Pt NMR (CDCl_3): δ –3604.0; EI-MS: m/z 882 (M^+ , 4%), 846 (14, –Cl), 809 (17, –Cl₂), 689 (17), 561 (13), 442 (16), 367 (37), 247 (100), 157 (22), 91 (74).

cis-[Dichlorido-(1,3-dibenzylimidazol-2-ylidene)(1-benzyl-3-methylimidazol-2-ylidene)]platinum(II) (5g). Complex **5g** (29 mg, 50%) was obtained from **2a** (50 mg, 84.4 μmol), 1-benzyl-3-methylimidazolium chloride (18 mg, 84.4 μmol), and KO^tBu (15 mg, 127 μmol) as white crystals of m.p. 243 °C. Elemental analysis (%): calc. for $\text{C}_{28}\text{H}_{28}\text{N}_4\text{PtCl}_2$ (686.54): C, 48.98; H, 4.11; N, 8.16. Found: C, 48.55; H, 3.80; N, 7.83; ^1H NMR (CDCl_3 , 500 MHz): δ 3.92 (s, 3H, CH_3), 5.23 (m, 2H, CH_2), 5.61–5.71 (d, J = 15.1 Hz, 1H, CH_2), 5.71–5.83 (2 \times d, J = 15.1 Hz, 2H, CH_2), 6.08 (d, J = 14.5 Hz, 1H, CH_2), 6.50 (d, J = 1.4 Hz, 1H, imidazole CH), 6.52 (d, J = 1.4 Hz, 1H, imidazole CH), 6.64 (d, J = 1.4 Hz, 1H, imidazole CH), 6.67 (d, J = 1.4 Hz, 1H, imidazole CH), 7.02–7.09 (m, 2H), 7.11–7.19 (m, 4H), 7.25–7.34 (m, 9H); ^{13}C NMR (CDCl_3 , 126 MHz): δ 37.9 (CH_3), 53.8 (CH_2), 54.0 (CH_2), 54.1 (CH_2), 120.0 (imidazole CH), 120.4 (imidazole CH), 120.9 (imidazole CH), 122.4 (imidazole CH), 127.7 (Ar), 127.8 (Ar), 128.3 (Ar), 128.9 (Ar), 128.9 (Ar), 129.0 (Ar), 134.8 (Ar), 135.0 (Ar), 148.1 (NCN), 149.0 (NCN); ^{195}Pt NMR (CDCl_3): δ –3610.7; EI-MS: m/z 686 (M^+ , 3%), 650 (9, –Cl), 613 (21, –Cl₂), 441 (8), 365 (18), 284 (7), 247 (43), 171 (80), 158 (16), 91 (100).

cis-[Dichlorido-(1,3-dibenzylimidazol-2-ylidene)(1,3-dimethyl-4(3',4',5'-trimethoxyphenyl)-5(4"-methoxyphenyl)imidazol-2-ylidene)]platinum(II) (5h). Complex **5h** (19 mg, 73%) was obtained from **2c** (21 mg, 30 μmol), 1,3-dibenzylimidazolium chloride (9 mg, 30 μmol), and KO^tBu (4 mg, 35 μmol) as white crystals of m.p. 266 °C. Elemental analysis (%): calc. for $\text{C}_{38}\text{H}_{40}\text{N}_4\text{O}_4\text{PtCl}_2$ (882.74): C, 51.70; H, 4.57; N, 6.35. Found: C, 51.51; H, 4.69; N, 6.26; ^1H NMR (CDCl_3 , 500 MHz): δ 3.66 (s, 6H, OCH_3), 3.73 (s, 3H, NCH_3), 3.79 (s, 3H, OCH_3), 3.81 (s, 3H, NCH_3), 3.82 (s, 3H, OCH_3), 5.77 (d, J = 15.3 Hz, 1H, CH_2), 5.87 (d, J = 15.3 Hz, 1H, CH_2), 5.95 (2 \times d, J = 15.6 Hz, 2H, CH_2), 6.07 (s, 2H, Ar), 6.71 (d, J = 2.1 Hz, 1H, imidazole CH), 6.73 (d, J = 2.1 Hz, 1H, imidazole CH), 6.82 (m, 4H, Ar), 7.11 (dd, J = 8.0, 1.8 Hz, 2H, Ar), 7.21 (dd, J = 8.0, 1.8 Hz, 2H, Ar), 7.29–7.37 (m, 6H, Ar); ^{13}C NMR (CDCl_3 , 126 MHz): δ 36.2 (NCH_3), 36.3 (NCH_3), 54.2 (CH_2), 54.3 (CH_2), 55.3 (OCH_3), 56.2 (OCH_3), 60.9 (OCH_3), 107.7 (Ar), 114.1 (Ar), 119.8 (Ar), 120.7 (imidazole CH), 120.9 (imidazole CH), 123.0 (Ar), 127.6 (Ar), 127.9 (Ar), 128.3 (Ar), 129.0 (Ar), 131.1 (Ar), 131.5 (Ar), 135.2 (Ar), 138.5 (Ar),

146.6 (NCN), 149.3 (NCN), 153.1 (Ar), 160.0 (Ar); ^{195}Pt NMR (CDCl_3): δ –3616.9; EI-MS: m/z 882 (M^+ , 1%), 847 (8, –Cl), 819 (39, –Cl₂), 690 (5), 561 (4), 369 (12), 247 (100), 157 (7), 91 (47). **Crystal data:** $\text{C}_{38}\text{H}_{40}\text{N}_4\text{O}_4\text{PtCl}_2 \cdot \text{CH}_2\text{Cl}_2$, M = 967.65, monoclinic, space group $P2(1)/c$, a = 11.1330(4), b = 29.7780(14), c = 12.1160(4) Å, α = γ = 90°, β = 101.539(3)°, V = 3935.5(3) Å³, Z = 4, λ = 0.71069 Å, μ = 3.88 mm^{–1}, T = 133 K; 23 066 reflections measured, 7701 unique; final refinement to convergence on F^2 gave R = 0.058 and R_w = 0.1494, GOF = 0.934. CCDC 1481379.

General procedure for the preparation of cis-[Pt^{II}(NHC)₂(PPh₃)Cl]⁺Cl[–] complexes 8

A solution of triphenylphosphane (5 equiv.) and complex **5** (1 equiv.) in CH_2Cl_2 (100 mL mmol^{–1}) was stirred at room temperature for 16 h. The solvent was removed *in vacuo*, and the residue was recrystallised from CH_2Cl_2 /hexane.

cis-[Chlorido-bis(1,3-dibenzylimidazol-2-ylidene)(triphenylphosphane)]platinum(II) chloride (8a). Complex **8a** (32 mg, 95%) was obtained from **5a** (25 mg, 32.8 μmol) and triphenylphosphane (43 mg, 164 μmol) as colourless crystals of m.p. 173 °C. Elemental analysis (%): calc. for $\text{C}_{52}\text{H}_{47}\text{N}_4\text{PPTCl}_2$ (1024.92): C, 60.94; H, 4.62; N, 5.47. Found: C, 60.74; H, 4.58; N, 5.37; ^1H NMR (CDCl_3 , 500 MHz): δ 4.68 (d, J = 14.6 Hz, 2H, CH_2), 4.96 (d, J = 14.0 Hz, 2H, CH_2), 5.69 (d, J = 14.6 Hz, 2H, CH_2), 5.92 (d, J = 14.0 Hz, 2H, CH_2), 6.68 (s, 2H, imidazole CH), 7.02 (d, J = 7.6 Hz, 4H, Ar), 7.12 (t, J = 7.6 Hz, 4H, Ar), 7.19–7.25 (m, 4H, imidazole CH, Ar), 7.25–7.29 (m, 5H, Ar), 7.31–7.42 (m, 17H, Ar, PPh₃), 7.47–7.53 (m, 3H, PPh₃); ^{13}C NMR (CDCl_3 , 126 MHz): δ 54.0 (CH_2), 54.3 (CH_2), 121.8 (imidazole CH), 123.2 (imidazole CH), 128.1 (Ar), 128.7 (Ar), 128.8 (Ar), 129.0 (d, $^1J_{\text{CP}}$ = 55 Hz, PPh₃), 129.0 (d, $^3J_{\text{CP}}$ = 11 Hz, PPh₃), 129.1 (Ar), 131.4 (d, $^4J_{\text{CP}}$ = 2.7 Hz, PPh₃), 134.2 (d, $^2J_{\text{CP}}$ = 11 Hz, PPh₃), 134.3 (Ar), 144.9 (d, $^2J_{\text{CP-cis}}$ = 10 Hz, NCN), 162.8 (d, $^2J_{\text{CP-trans}}$ = 151 Hz, NCN); ^{31}P NMR (CDCl_3 , 202 MHz): δ 13.1 ($^1J_{\text{PtP}}$ = 2366 Hz); ^{195}Pt NMR (CDCl_3): δ –4098.7/–4120.8 (d, J_{PtP} = 2377 Hz); EI-MS: m/z 762 (11%, –PPh₃), 726 (14, –Cl, –PPh₃), 689 (42, –Cl₂, –PPh₃), 597 (9), 441 (33), 350 (11), 262 (99), 247 (100), 183 (52), 157 (34), 91 (95). **Crystal data:** $\text{C}_{52}\text{H}_{47}\text{N}_4\text{PPTCl}_2 \cdot \text{CH}_2\text{Cl}_2 \cdot 2\text{H}_2\text{O}$, M = 1145.84, triclinic, space group $P\bar{1}$, a = 11.4460(4), b = 11.7520(4), c = 19.7120(8) Å, α = 75.959(3)°, β = 74.604(3)°, γ = 73.708(3)°, V = 2412.88(16) Å³, Z = 2, λ = 0.71069 Å, μ = 3.21 mm^{–1}, T = 133 K; 34 049 reflections measured, 9655 unique; final refinement to convergence on F^2 gave R = 0.0582 and R_w = 0.1538, GOF = 0.994. CCDC 1481380.

cis-[Chlorido-bis(1,3-di(4-methoxybenzyl)imidazol-2-ylidene)(triphenylphosphane)]platinum(II) chloride (8b). Complex **8b** (23 mg, 88%) was obtained from **5b** (20 mg, 22.7 μmol) and triphenylphosphane (30 mg, 114 μmol) as colourless crystals of m.p. 138 °C. Elemental analysis (%): calc. for $\text{C}_{56}\text{H}_{55}\text{N}_4\text{O}_4\text{PPTCl}_2$ (1145.02): C, 58.74; H, 4.84; N, 4.89. Found: C, 58.39; H, 4.98; N, 4.93; ^1H NMR (CDCl_3 , 500 MHz): δ 3.71 (s, 6H, OCH_3), 3.79 (s, 6H, OCH_3), 4.55 (d, J = 14.3 Hz, 2H, CH_2), 5.00 (d, J = 14.3 Hz, 2H, CH_2), 5.52 (d, J = 14.3 Hz, 2H, CH_2), 5.84 (d, J = 14.3 Hz, 2H, CH_2), 6.56–6.64 (d, J = 8.5 Hz, 4H, Ar),

6.71 (s, 2H, imidazole CH), 6.84–6.90 (d, $J = 8.5$ Hz, 4H, Ar), 6.90–6.96 (d, $J = 8.5$ Hz, 4H, Ar), 7.12 (s, 2H, imidazole CH), 7.22–7.26 (d, $J = 8.5$ Hz, 4H, Ar), 7.29–7.41 (m, 12H, PPh₃), 7.47–7.52 (m, 3H, PPh₃); ¹³C NMR (CDCl₃, 126 MHz): δ 53.6 (CH₂), 53.9 (CH₂), 55.3 (OCH₃), 55.3 (OCH₃), 114.4 (Ar), 114.5 (Ar), 121.6 (imidazole CH), 122.7 (imidazole CH), 125.4 (Ar), 126.3 (Ar), 129.0 (d, $J_{CP} = 10$ Hz, PPh₃), 129.1 (d, $J_{CP} = 55$ Hz, PPh₃), 129.9 (Ar), 130.1 (Ar), 131.3 (d, $J_{CP} = 2.7$ Hz, PPh₃), 134.2 (d, $J_{CP} = 10$ Hz, PPh₃), 144.0 (d, $J_{CP-cis} = 10$ Hz, NCN), 162.6 (d, $J_{CP-trans} = 151$ Hz, NCN); ³¹P NMR (CDCl₃, 202 MHz): δ 13.3 ($J_{PPt} = 2360$ Hz); ¹⁹³Pt NMR (CDCl₃): δ -4097.4/-4119.3 (d, $J_{PtP} = 2361$ Hz); EI-MS: m/z 848 (6%, -Cl, -PPh₃), 809 (21, -Cl₂, -PPh₃), 687 (6), 501 (19), 379 (10), 307 (14), 262 (86), 183 (97), 121 (100).

X-ray data collection and structural determination

Data collection and cell refinement by X-Area-TOE. The single crystal samples were irradiated with Mo-K α at 133 K. The structures were solved by direct methods using SIR 97 and refined by full matrix least-squares on F^2 for all data using SHELXL 2014. All hydrogen atoms were added at calculated positions and refined using a riding model. Anisotropic thermal displacement parameters were used for all non-hydrogen atoms. For **5d**, the two fluorine atoms on the phenyl rings were disordered and the corresponding hydrogens could not be located, yet detected in the ¹H NMR spectrum. For further details cf. ESI.† The crystallographic data were deposited with The Cambridge Crystallographic Data Centre CCDC under no. 1481381 (**5a**), 1481378 (**5d**), 1481379 (**5h**), 1481380 (**8a**).

Growth inhibition assay (MTT assay)

The antiproliferative effect of the complexes **5a–h**, **8a**, and **8b** on cells of 518A2 melanoma, different human colon carcinomas (HT-29, DLD-1), U87 glioblastoma, Panc-1 pancreatic cancer, mdr MCF-7/Topo breast cancer, and KbV1/Vbl cervix carcinoma, and on endothelial hybrid cells Ea.Hy926 was assessed. Cells were seeded in flat-bottom 96-well microtiter plates at a density of $0.05 \times 10^6 \text{ mL}^{-1}$ ($0.1 \times 10^6 \text{ mL}^{-1}$ for U87 and Ea.Hy926) in culture medium and incubated until the cells nearly reached confluency at 37 °C. Test compound solutions were diluted from freshly made 10 mM stock solutions in DMF (5 mM in DMSO for **5g**, 10 mM in DMSO for CDDP) with water, and added to each well of the microtiter plates with working concentrations ranging from 100 μM to 25 nM. DMF or DMSO was used as a negative control. Treatment of the cells with **5a–h** and **8a–b** lasted for 72 h at 37 °C. The culture medium was replaced with a solution of MTT [3-(4,5-dimethylthiazol-2-yl)-2,5-diphenyltetrazoliumbromide] (0.05% in PBS) and the cells were incubated for another 2 h. The MTT solution was discarded and the water-insoluble formazan crystals, formed by metabolically viable cells, were dissolved in SDS/DMSO. The absorbance of the formazan solution was measured at 630 nm, the background absorbance at 570 nm. Means \pm SDs were calculated from four independent values.

Electrophoretic mobility shift assay (EMSA assay)

The complexes **1b**, **5b**, and **8b** were tested for their interaction with circular pBR322 plasmid DNA in electrophoretic mobility shift assays according to a general method by Huq *et al.*³³ Briefly, 1.5 μg pBR322 plasmid DNA in freshly sterile-filtrated TE buffer (10 mM Tris/HCl, 1 mM EDTA, pH 8.0) were incubated with 0 μM (TE buffer with plasmid DNA), 5 μM , 10 μM , 25 μM and 50 μM of the complexes or cisplatin as a positive control for 24 h at 37 °C. Agarose gel electrophoresis (1%) was conducted at 66 V for 4 h. DNA bands were visualised *via* staining with 10 $\mu\text{g mL}^{-1}$ ethidium bromide in 0.5 \times TBE buffer (900 mM Tris/HCl, 900 mM boric acid, 25 mM EDTA, pH 8.3) for 30 min at room temperature. The stained DNA was documented by UV excitation. EMSA assays were performed at least twice for each of the tested complexes.

Acknowledgements

We thank the Deutsche Forschungsgemeinschaft (grant Scho402/12), the COST Action CM1105 'Functional metal complexes that bind to biomolecules', and the University Bayreuth Graduate School for financial support.

Notes and references

- 1 H.-W. Wanzlick and H.-J. Schönherr, *Angew. Chem., Int. Ed.*, 1968, **7**, 141–142.
- 2 K. Öfele, *J. Organomet. Chem.*, 1968, **12**, P42–P43.
- 3 A. Arduengo, R. Harlow and M. Kline, *J. Am. Chem. Soc.*, 1991, **113**, 361–363.
- 4 (a) N. Marion, S. Díez-González and S. Nolan, *Angew. Chem., Int. Ed.*, 2007, **46**, 2988–3000; (b) D. M. Flanagan, F. Romanov-Michailidis, N. A. White and T. Rovis, *Chem. Rev.*, 2015, **115**, 9307–9387; (c) A. Grossmann and D. Enders, *Angew. Chem., Int. Ed.*, 2012, **51**, 314–325.
- 5 M. Scholl, S. Ding, C. Lee and R. Grubbs, *Org. Lett.*, 1999, **1**, 953–956.
- 6 C. Zhang, J. Huang, M. Trudell and S. Nolan, *J. Org. Chem.*, 1999, **64**, 3804–3805.
- 7 W. Herrmann, M. Elison, J. Fischer, C. Kocher and G. Artus, *Angew. Chem., Int. Ed.*, 1995, **34**, 2371–2374.
- 8 L. Oehninger, R. Rubbiani and I. Ott, *Dalton Trans.*, 2013, **42**, 3269–3284.
- 9 A. Gautier and F. Cisnetti, *Metallomics*, 2012, **4**, 23–32.
- 10 L. Kelland, *Nat. Rev. Cancer*, 2007, **7**, 573–584.
- 11 S. Ray, R. Mohan, J. K. Singh, M. K. Samantaray, M. Shaikh, D. Panda and P. Ghosh, *J. Am. Chem. Soc.*, 2007, **129**, 15042–15053.
- 12 L. Eloy, A.-S. Jarrousse, M.-L. Teyssot, A. Gautier, L. Morel, C. Jolival, T. Cresteil and S. Roland, *ChemMedChem*, 2012, **7**, 805–814.
- 13 M.-L. Teyssot, A.-S. Jarrousse, A. Chevy, A. De Haze, C. Beaudoin, M. Manin, S. Nolan, S. Díez-González, L. Morel and A. Gautier, *Chem. – Eur. J.*, 2009, **15**, 314–318.

- 14 L. Oehninger, M. Stefanopoulou, H. Alborzinia, J. Schur, S. Ludewig, K. Namikawa, A. Muñoz-Castro, R. Köster, K. Baumann, S. Wölfl, W. Sheldrick and I. Ott, *Dalton Trans.*, 2013, **42**, 1657–1666.
- 15 (a) J. Weaver, S. Gaillard, C. Toye, S. Macpherson, S. Nolan and A. Riches, *Chem. – Eur. J.*, 2011, **17**, 6620–6624; (b) P. Barnard, M. Baker, S. Berners-Price and D. Day, *J. Inorg. Biochem.*, 2004, **98**, 1642–1647.
- 16 M. Skander, P. Retailleau, B. Bourrié, L. Schio, P. Maillet and A. Marinetti, *J. Med. Chem.*, 2010, **53**, 2146–2154.
- 17 J. K. Muenzner, T. Rehm, B. Biersack, A. Casini, I. de Graaf, P. Worawutputtapong, A. Noor, R. Kempe, V. Brabec, J. Kasparkova and R. Schobert, *J. Med. Chem.*, 2015, **58**, 6283–6292.
- 18 L. C. Lewis-Alleyne, B. S. Bassil, T. Böttcher and G.-V. Röschenthaler, *Dalton Trans.*, 2014, **43**, 15700–15703.
- 19 S. Fantasia, A. Pasini and S. Nolan, *Dalton Trans.*, 2009, **38**, 8107–8110.
- 20 G. Fortman, A. Slawin and S. Nolan, *Dalton Trans.*, 2010, **39**, 3923–3930.
- 21 C. Newman, R. Deeth, G. Clarkson and J. Rourke, *Organometallics*, 2007, **26**, 6225–6233.
- 22 M. Bouhrara, E. Jeanneau, L. Veyre, C. Copere and C. Thieuleux, *Dalton Trans.*, 2011, **40**, 2995–2999.
- 23 L. Naya, D. Vazquez-García, A. Fernandez, M. Lopez-Torres, I. Marcos, O. Lenis, M. Pereira, J. Vila and J. Fernandez, *J. Organomet. Chem.*, 2014, **772–773**, 192–201.
- 24 K. Fujita, K. Inoue, J. Sato, T. Tsuchimoto and H. Yasuda, *Tetrahedron*, 2016, **72**, 1205–1212.
- 25 H. Shiota, H. Matsuzaki, S. Ramati and J. Wishart, *J. Phys. Chem. B*, 2015, **119**, 9173–9187.
- 26 L. Kaps, B. Biersack, H. Müller-Bunz, K. Mahal, J. Münzner, M. Tacke, T. Mueller and R. Schobert, *J. Inorg. Biochem.*, 2012, **106**, 52–58.
- 27 S. Fantasia, J. Petersen, H. Jacobsen, L. Cavallo and S. Nolan, *Organometallics*, 2007, **26**, 5880–5889.
- 28 T. Mosmann, *J. Immunol. Methods*, 1983, **65**, 55–63.
- 29 A. Kazuo and M. Norio, *Neurosci. Res.*, 2000, **38**, 325–329.
- 30 C. Sergeant, N. Franco, C. Chapusot, S. Lizard-Nacol, N. Isambert, M. Correia and B. Chauffert, *Cancer Chemother. Pharmacol.*, 2002, **49**, 445–452.
- 31 D.-W. Shen, C. Cardarelli, J. Hwang, M. Cornwell, N. Richert, S. Ishii, I. Pastan and M. M. Gottesman, *J. Biol. Chem.*, 1986, **261**, 7762–7770.
- 32 M. Kühnle, M. Egger, C. Müller, A. Mahringer, G. Bernhardt, G. Fricker, B. König and A. Buschauer, *J. Med. Chem.*, 2009, **52**, 1190–1197.
- 33 M. A. Chowdhury, F. Huq, A. Abdullah, P. Bearle and K. Fisher, *J. Inorg. Biochem.*, 2005, **99**, 1098–1112.

Electronic Supplementary Material (ESI) for Dalton Transactions.
This journal is © The Royal Society of Chemistry 2016

Electronic Supporting Information

Novel cis-[(NHC)¹(NHC)²(L)Cl]platinum(II) complexes – synthesis, structures, and anticancer activities

Tobias Rehm,^a Matthias Rothemund,^a Julienne K. Muenzner,^a Awal Noor,^b Rhett Kempe,^b and Rainer Schobert^a

^a*Organic Chemistry Laboratory, University Bayreuth, Universitaetsstrasse 30, 95440 Bayreuth.*

E-mail: Rainer.Schobert@uni-bayreuth.de

^b*Lehrstuhl fuer Anorganische Chemie II (Catalyst Design), University Bayreuth, Universitaetsstrasse 30, 95440 Bayreuth.*

Table of content:

General information	S1
Synthesis and characterization of imidazolium chlorides and complex 1b	S2
X-ray structural analysis data of complexes 5a , 5d , 5h and 8a (Table S1)	S3
NMR spectra of complexes 2b-c , 5a-h and 8a-b (Fig. S1-S36)	S4
References	S22

General information

All chemicals and reagents were purchased from Sigma Aldrich, Alfa Aesar or ABCR and were used without further purification. Melting points are uncorrected; NMR spectra were run on a 500 MHz spectrometer; chemical shifts are given in ppm (δ) and referenced relative to the internal solvent signal; ¹⁹⁵Pt NMR shifts are quoted relative to $\Xi(^{195}\text{Pt}) = 21.496784$ MHz, K₂PtCl₄ was used as external standard ($\delta ^{195}\text{Pt} = -1612.81$); mass spectra: direct inlet, EI, 70 eV; X-Ray diffractometers: STOE-IPDS II and STOE-STADIVARI. *N*-methyl- and *N*-benzylimidazolium salts were prepared based on literature procedures¹⁻⁴ and complex **1b** was prepared analogously to **1a**⁵ as described herein.

S1

Synthesis and characterization of imidazolium chlorides and complex 1b

General procedure:

Imidazole (1eq) and the respective benzyl chloride (2.1 eq) in acetonitrile (10 mL/mmol) were treated with K_2CO_3 (1.2 eq) and the resulting mixture was heated to 70 °C for 3-5 days. After filtration the solvent was evaporated in vacuo and the residue was washed several times with Et_2O .

Synthesis of 1,3-dibenzylimidazolium chloride:¹

Imidazole (100 mg, 1.47 mmol), benzyl chloride (355 μ L) and K_2CO_3 (244 mg) in acetonitrile (15 mL) for 72 h gave 333 mg (80%) of a colorless oil. 1H NMR ($CDCl_3$, 500 MHz): δ 5.43 (4 H, s), 7.17 - 7.24 (6 H, m), 7.33 - 7.42 (6 H, m), 10.85 (1 H, s).

Synthesis of 1,3-di(4-methoxybenzyl)imidazolium chloride:

Imidazole (100 mg, 1.47 mmol), 4-methoxybenzyl chloride (417 μ L) and K_2CO_3 (244 mg) in acetonitrile (15 mL) for 72 h gave 500 mg (99%) of a pale yellow gum. 1H NMR ($CDCl_3$, 500 MHz): δ 3.74 (6 H, s), 5.43 (4 H, s), 6.84 (4 H, d, $J=8.9$ Hz), 7.22 (2 H, s), 7.39 (4 H, d, $J=8.9$ Hz), 10.98 (1 H, s).

Synthesis of 1,3-di(4-fluorobenzyl)imidazolium chloride:²

Imidazole (50 mg, 0.735 mmol), 4-fluorobenzyl chloride (182 μ L) and K_2CO_3 (122 mg) in acetonitrile (7.5 mL) for 72 h gave 165 mg (70%) of a yellow gum. 1H NMR ($CDCl_3$, 500 MHz): δ 5.51 (4 H, s), 7.00 (2 H, tt, $J=8.7$, 2.6 Hz), 7.34 (2 H, s), 7.49 (1 H, dd, $J=8.7$, 5.0 Hz), 11.02 (1 H, br. s.).

Synthesis of 1,3-di(3,5-dimethoxybenzyl)imidazolium chloride:³

Imidazole (50 mg, 0.735 mmol), 3,5-dimethoxybenzyl chloride (288 mg) and K_2CO_3 (122 mg) in acetonitrile (7.5 mL) for 5 d gave 205 mg (69%) of an orange gum. 1H NMR ($CDCl_3$, 500 MHz): δ 3.73 (12 H, s), 5.39 (4 H, s), 6.39 (2 H, t, $J=2.3$ Hz), 6.56 (4 H, d, $J=2.3$ Hz), 7.18 (2 H, s), 11.20 (1 H, s).

Synthesis of 1-benzyl-3-methylimidazolium chloride:⁴

Methylimidazole (60 mg, 0.735 mmol) and benzyl chloride (100 μ L, 0.882 mmol) in acetonitrile (5 mL) were heated to 70 °C for 72 h. After evaporation of the solvent in vacuo the residue was washed several times with Et_2O to yield 132 mg (86%) of a pale yellow gum. 1H NMR ($CDCl_3$, 500 MHz): δ 3.98 (3 H, s), 5.54 (2 H, s), 7.29 - 7.34 (3 H, m), 7.37 (1 H, t, $J=1.7$ Hz), 7.41 - 7.46 (2 H, m), 7.51 (1 H, t, $J=1.7$ Hz), 10.51 (1 H, s).

Synthesis of *trans*-[dichlorido-bis(1,3-di(4-methoxybenzyl)imidazol-2-ylidene)]platinum(II) (**1b**):⁵

A solution of 1,3-di(4-methoxybenzyl)imidazolium chloride (60 mg, 0.154 mmol) in CH_2Cl_2 was treated with silver(I) oxide (18 mg, 77 μ mol), and the resulting mixture was stirred at room temperature for 24 h. Then K_2PtCl_4 (32 mg, 77 μ mol) was added and the reaction was allowed to stir for additional 24 h. The suspension was filtered, the filtrate was concentrated in vacuo, and the residue was recrystallized from CH_2Cl_2 /hexane. Yield 38 mg (56%) white crystals of m.p. 194 °C (decomp.). 1H NMR ($CDCl_3$, 500 MHz): δ 3.76 (12 H, s), 5.74 (8 H, s), 6.63 (4 H, s), 6.83 (8 H, d, $J=8.5$ Hz), 7.43 (8 H, d, $J=8.5$ Hz); ^{13}C NMR ($CDCl_3$, 126 MHz): δ 53.0, 55.2, 114.0, 120.1, 128.6, 129.9, 159.3, 167.2 (NHC). EI-MS: m/z 883 (M^+ , 5%), 847 (12, -Cl), 810 (35, -2x Cl), 501 (17), 308 (23), 241 (28), 121 (100).

Table S 1: X-ray structural data of platinum carbene complexes **5a**, **d**, **h** and **8a**

	5a (CCDC1481381)	5d (CCDC1481378)	5h (CCDC1481379)	8a (CCDC1481380)
Empirical formula	C ₃₄ H ₃₂ Cl ₂ N ₄ Pt	C ₃₄ H ₂₈ Cl ₂ F ₂ N ₄ Pt	C ₃₉ H ₄₂ Cl ₄ N ₄ O ₄ Pt	C ₅₃ H ₅₃ Cl ₄ N ₄ O ₂ PPt
Formula weight	762.62	796.59	967.65	1145.85
Temperature	133 K	133 K	133 K	133 K
Wavelength	0.71069 Å	0.71069 Å	0.71069 Å	0.71069 Å
Crystal system	monoclinic	monoclinic	monoclinic	triclinic
Space group	P2 ₁ /c	C2/c	P2 ₁ /c	P-1
Unit cell dimensions	a = 7.5380(3) Å	a = 15.6790(6) Å	a = 11.1330(4) Å	a = 11.4460(4) Å
	b = 33.6480(12) Å	b = 14.1220(6) Å	b = 29.7780(14) Å	b = 11.7520(4) Å
	c = 12.1810(5) Å	c = 15.1390(8) Å	c = 12.1160(4) Å	c = 19.7120(8) Å
	α = γ = 90°	α = γ = 90°	α = γ = 90°	α = 75.959(3)°
	β = 95.951(3)°	β = 113.895(5)°	β = 101.539(3)°	β = 74.604 (3)° γ = 73.708(3)°
Volume	3072.9(2) Å ³	3064.8(3) Å ³	3935.5(3) Å ³	2412.88(16) Å ³
Z	4	4	4	2
Density (calcd)	1.648 Mg/m ³	1.726 Mg/m ³	1.633 Mg/m ³	1.577 Mg/m ³
Absorption coefficient	4.77 mm ⁻¹	4.80 mm ⁻¹	3.88 mm ⁻¹	3.21 mm ⁻¹
F(000)	1504	1560	1928	1152
Crystal size / mm	0.16 × 0.11 × 0.08	0.21 × 0.14 × 0.08	0.15 × 0.12 × 0.08	0.25 × 0.18 × 0.11
Theta range (data col.)	3.6–54.5°	4.1–53.1°	4.4–55.3°	3.7–53.2°
Index ranges	–9 ≤ h ≤ 9	–19 ≤ h ≤ 19	–7 ≤ h ≤ 13	–14 ≤ h ≤ 14
Index ranges	–42 ≤ k ≤ 0	–17 ≤ k ≤ 17	–36 ≤ k ≤ 36	–14 ≤ k ≤ 14
Index ranges	–15 ≤ l ≤ 15	–18 ≤ l ≤ 18	–14 ≤ l ≤ 14	–24 ≤ l ≤ 24
Reflections collected	12924	19249	23066	34049
Independent reflexes	6540 [R _{int} =0.040]	3070 [R _{int} =0.073]	7701 [R _{int} =0.069]	9655 [R _{int} =0.099]
Completeness to qmax	99.4%	99.4%	99.7%	98.9%
Absorption correction	numerical	numerical	numerical	numerical
Max / min transmission	0.740 / 0.454	0.506 / 0.248	0.848 / 0.652	0.712 / 0.424
Refinement method	Full-matrix least-squares on F ²	Full-matrix least-squares on F ²	Full-matrix least-squares on F ²	Full-matrix least-squares on F ²
Data / restraints / param	6540 / 0 / 370	3070 / 18 / 204	7701 / 18 / 475	9655 / 4 / 602
Goodness-of-fit on F ²	0.766	0.984	0.934	0.994
Final R indices	R ₁ = 0.0276	R ₁ = 0.0267	R ₁ = 0.0575	R ₁ = 0.0582
[I > 2σ(I)]	wR ₂ = 0.0601	wR ₂ = 0.0639	wR ₂ = 0.1494	wR ₂ = 0.1538
R indices	R ₁ = 0.0471	R ₁ = 0.0350	R ₁ = 0.0931	R ₁ = 0.0794
(all data)	wR ₂ = 0.0579	wR ₂ = 0.0625	wR ₂ = 0.1342	wR ₂ = 0.1436
Largest diff. peak / hole	1.40/– 1.21 eÅ ⁻³	2.30/– 1.11 eÅ ⁻³	1.89/– 2.14 eÅ ⁻³	3.43/– 1.47 eÅ ⁻³

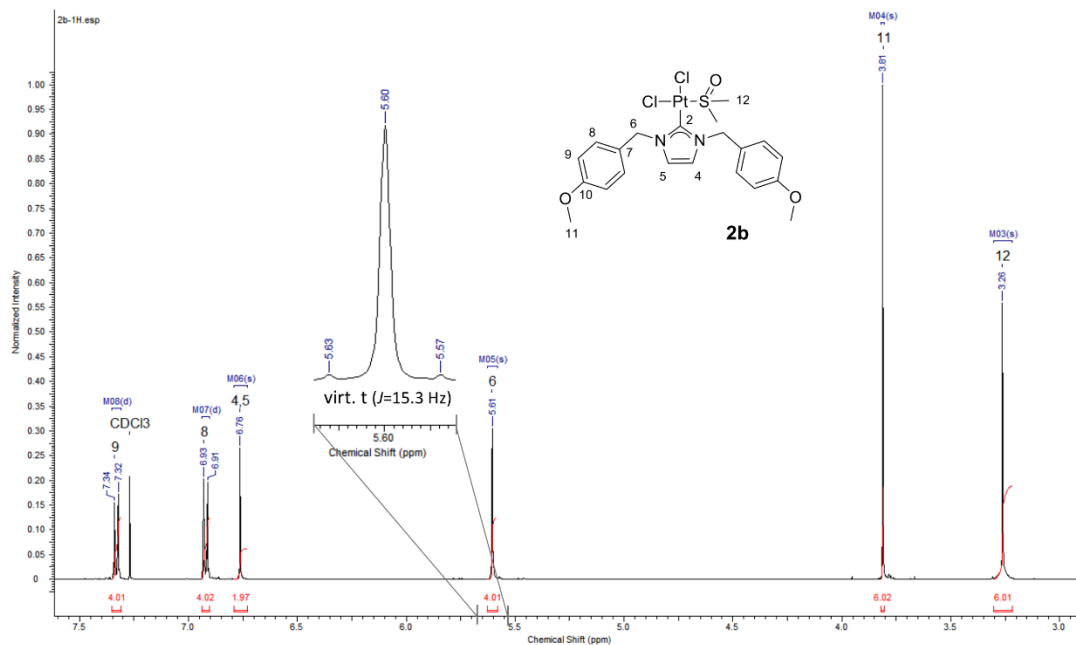


Fig. S 1: $^1\text{H-NMR}$ spectrum (500 MHz, CDCl_3) of complex **2b**.

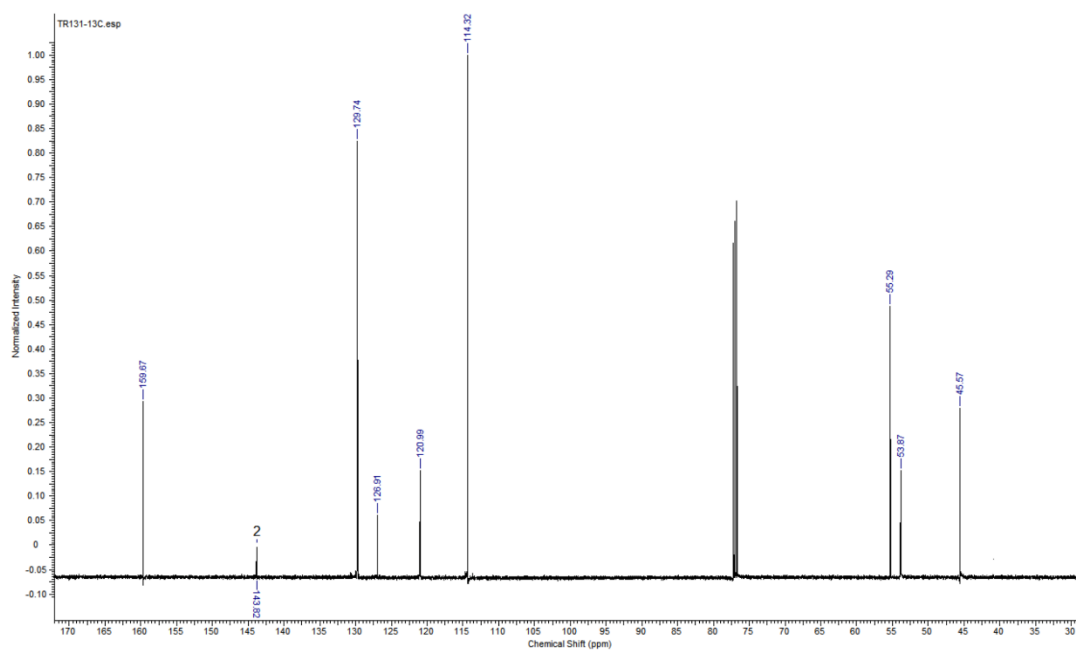


Fig. S 2: $^{13}\text{C-NMR}$ spectrum (126 MHz, CDCl_3) of complex **2b**.

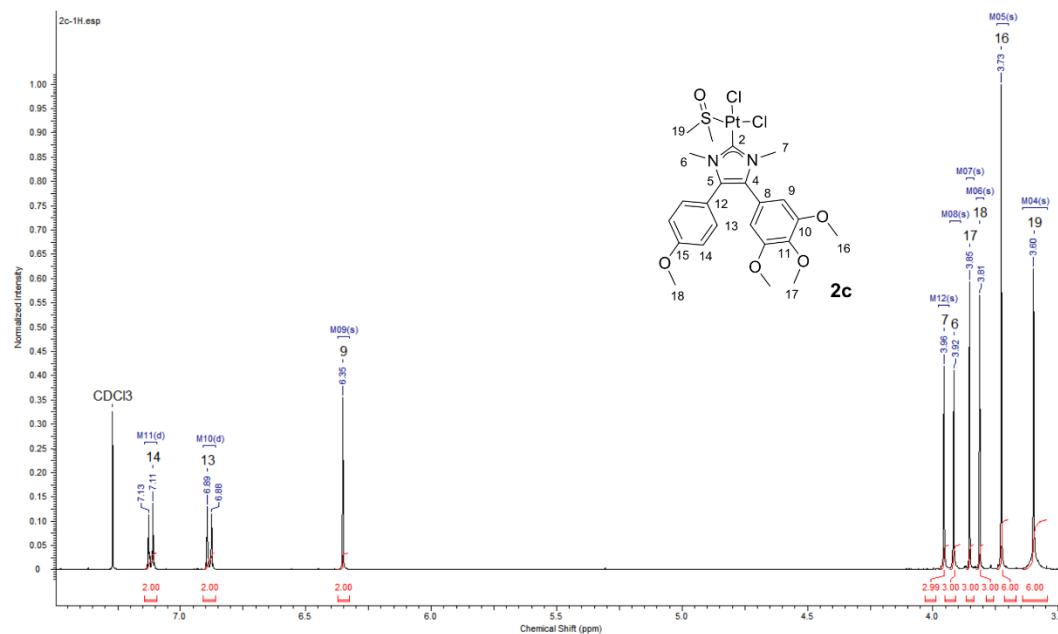


Fig. S 3: ^1H -NMR spectrum (500 MHz, CDCl_3) of complex **2c**.

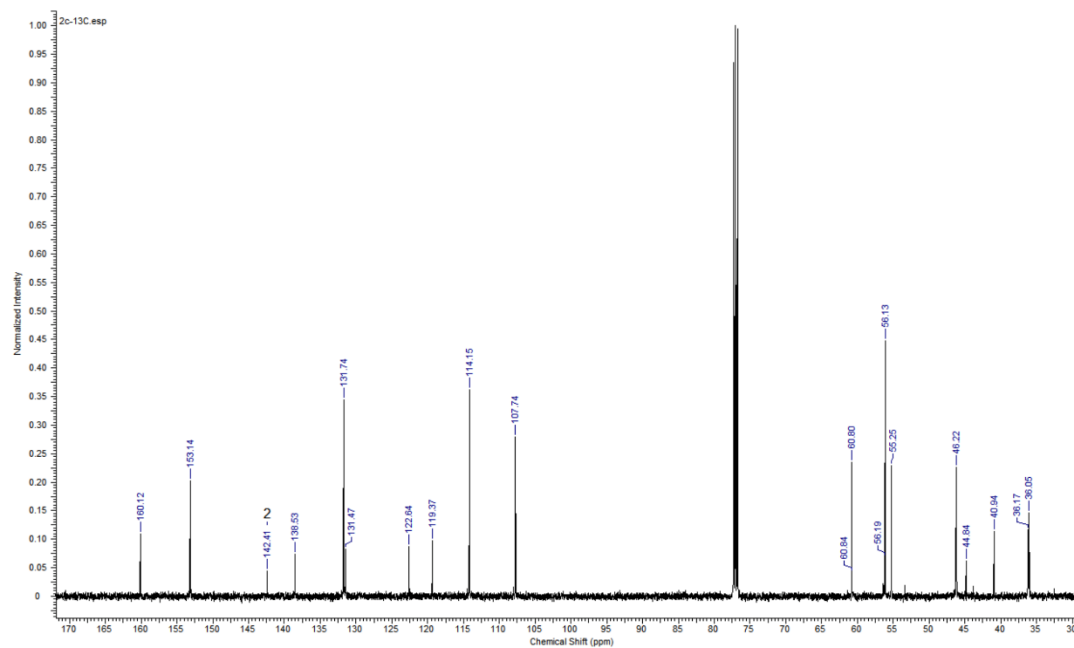


Fig. S 4: ^{13}C -NMR spectrum (126 MHz, CDCl_3) of complex **2c**.

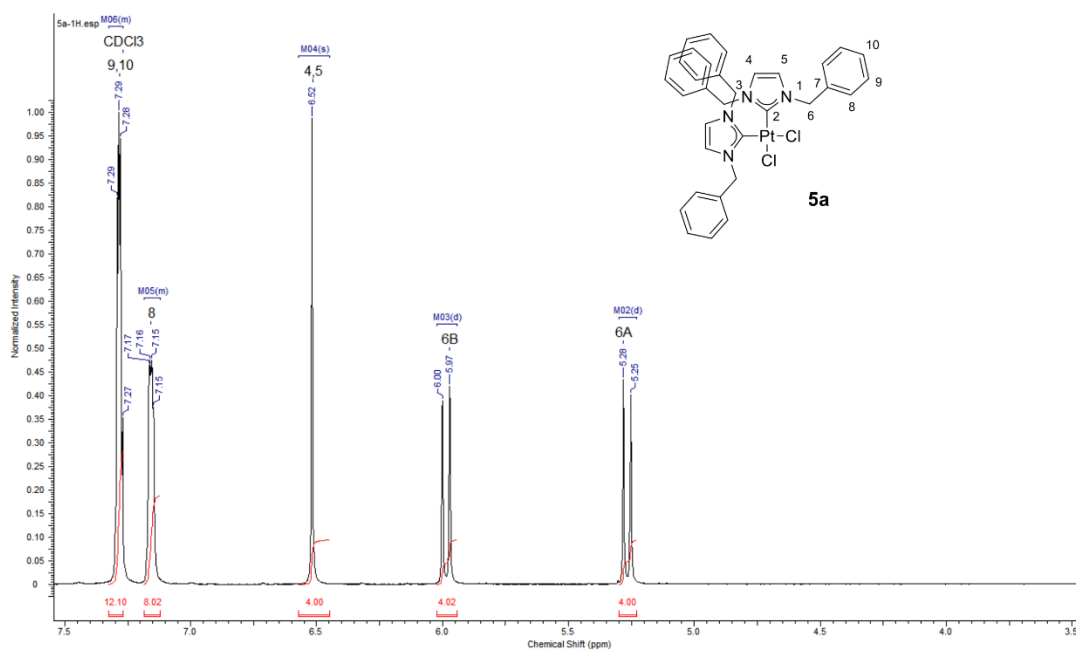


Fig. S5: ^1H -NMR spectrum (500 MHz, CDCl_3) of complex 5a.

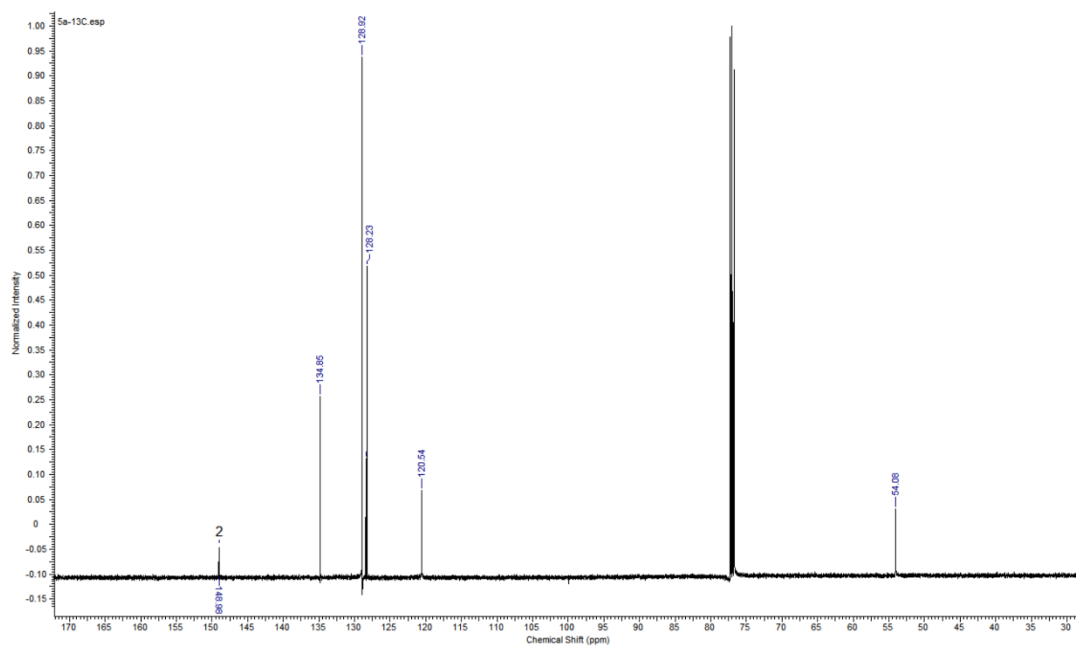


Fig. S 6: ^{13}C -NMR spectrum (126 MHz, CDCl_3) of complex 5a.

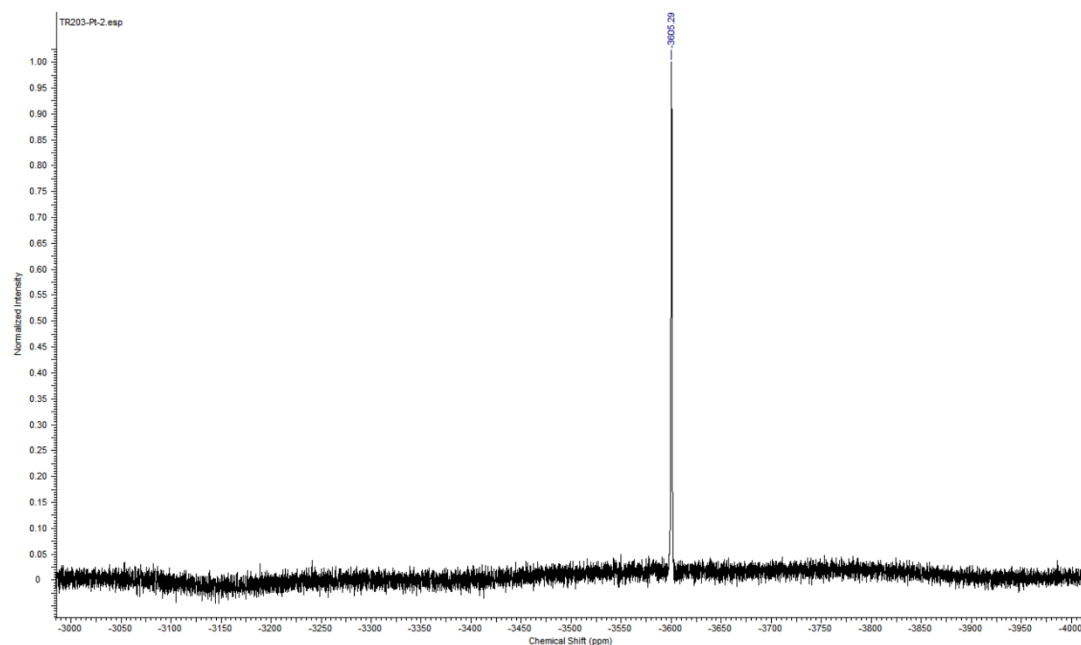


Fig. S 7: ^{195}Pt -NMR spectrum (CDCl_3) of complex **5a**.

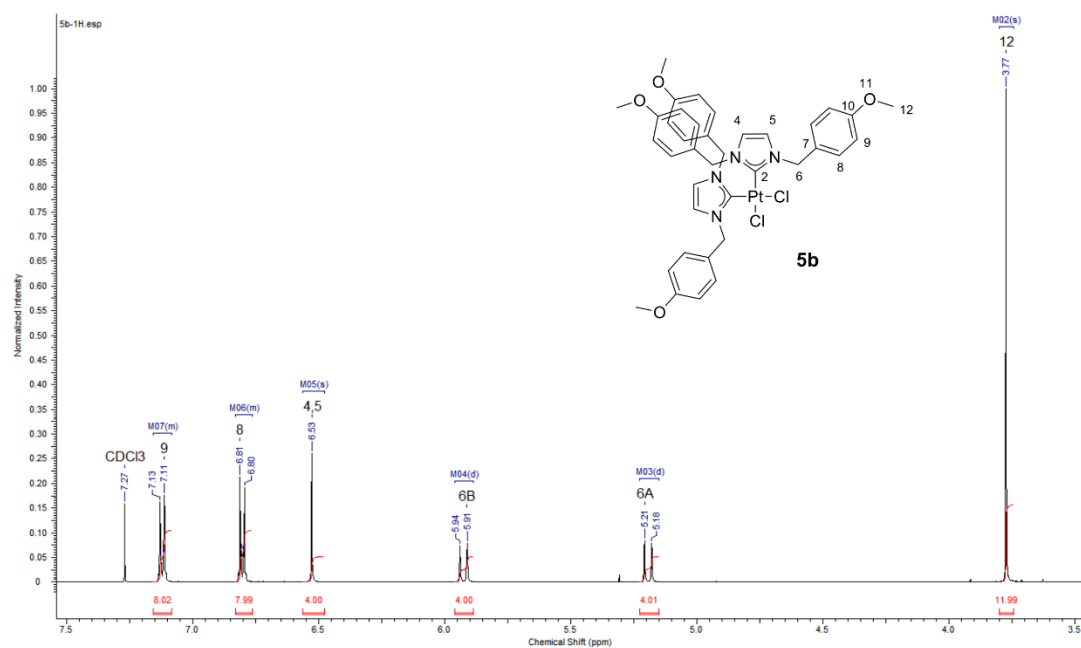


Fig. S8: ^1H -NMR spectrum (500 MHz, CDCl_3) of complex **5b**.

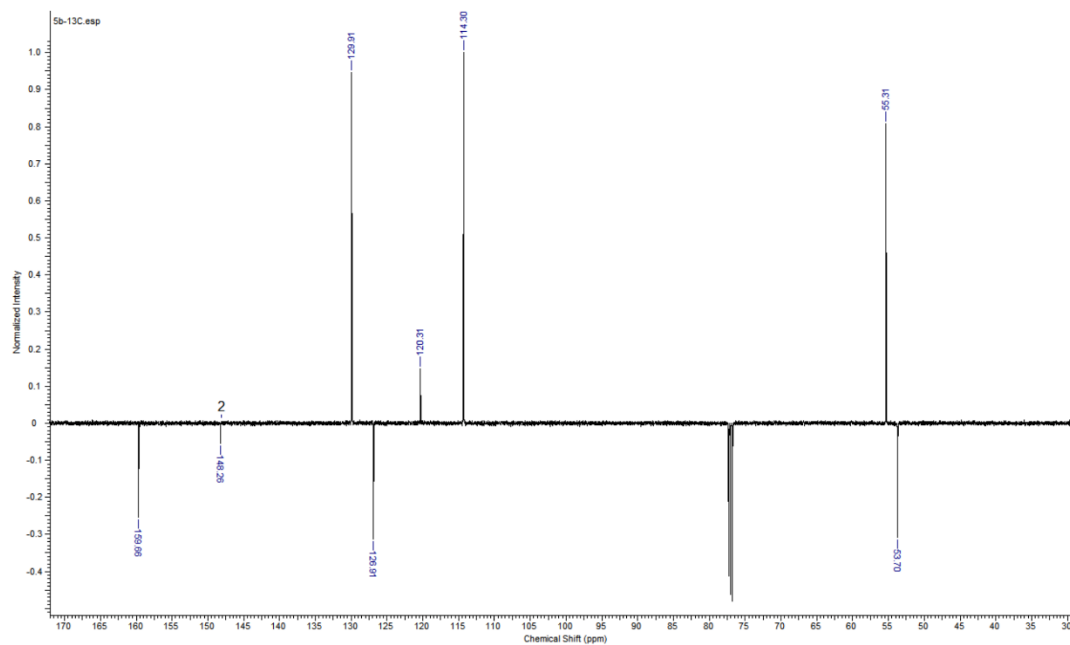


Fig. S 9: ^{13}C -ATP-NMR spectrum (126 MHz, CDCl_3) of complex **5b**.

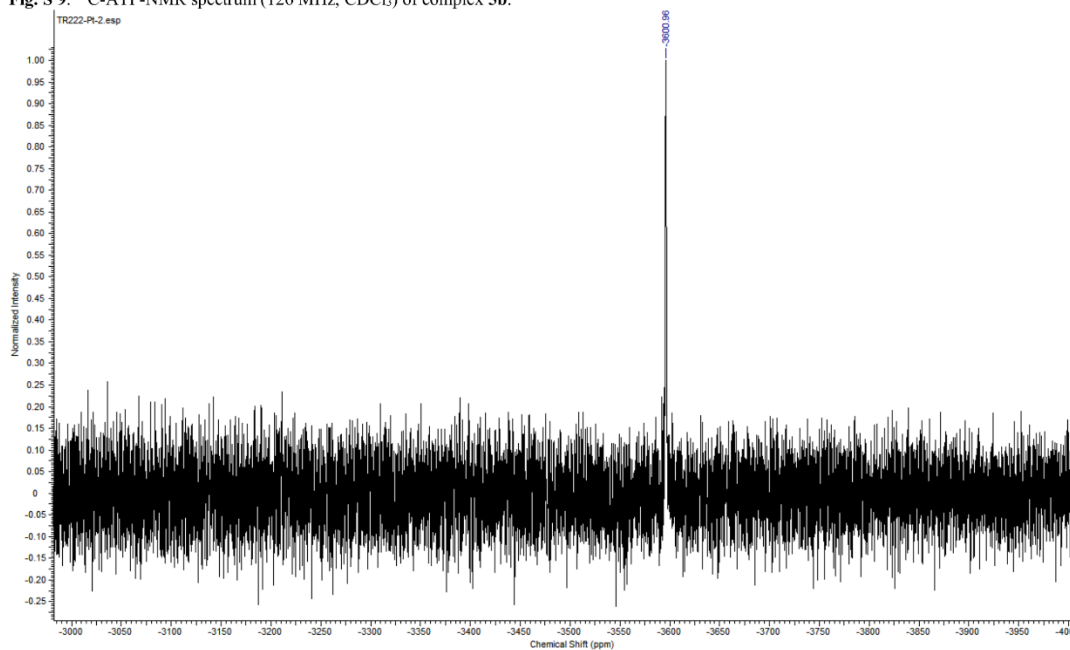


Fig. S 10: ^{195}Pt -NMR spectrum (CDCl_3) of complex **5b**.

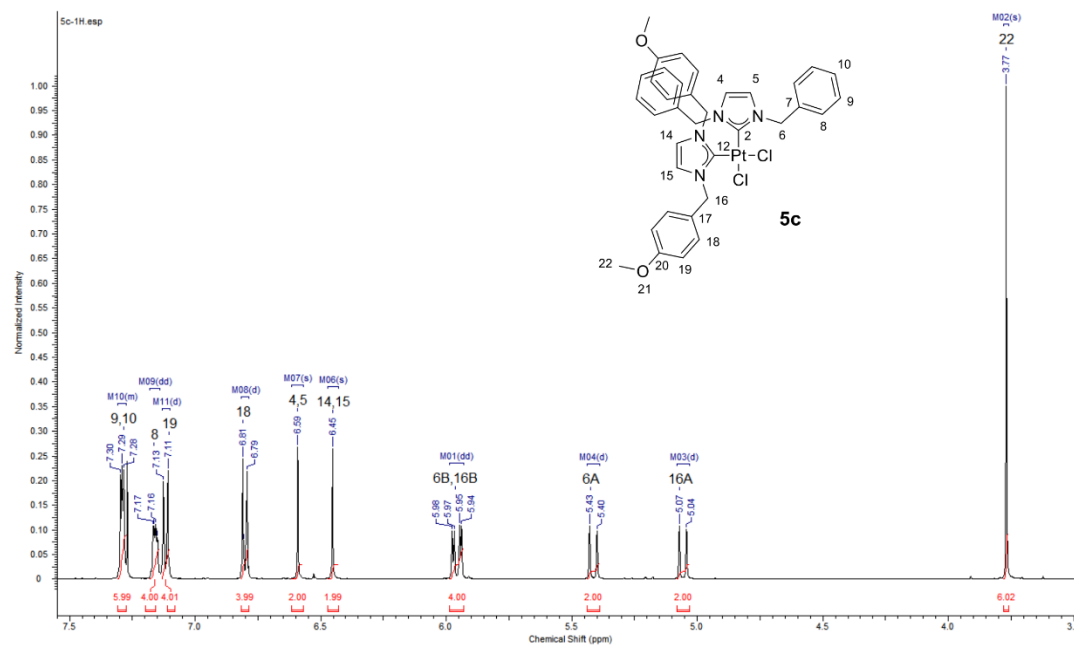


Fig. S11: ^1H -NMR spectrum (500 MHz, CDCl_3) of complex **5c**.

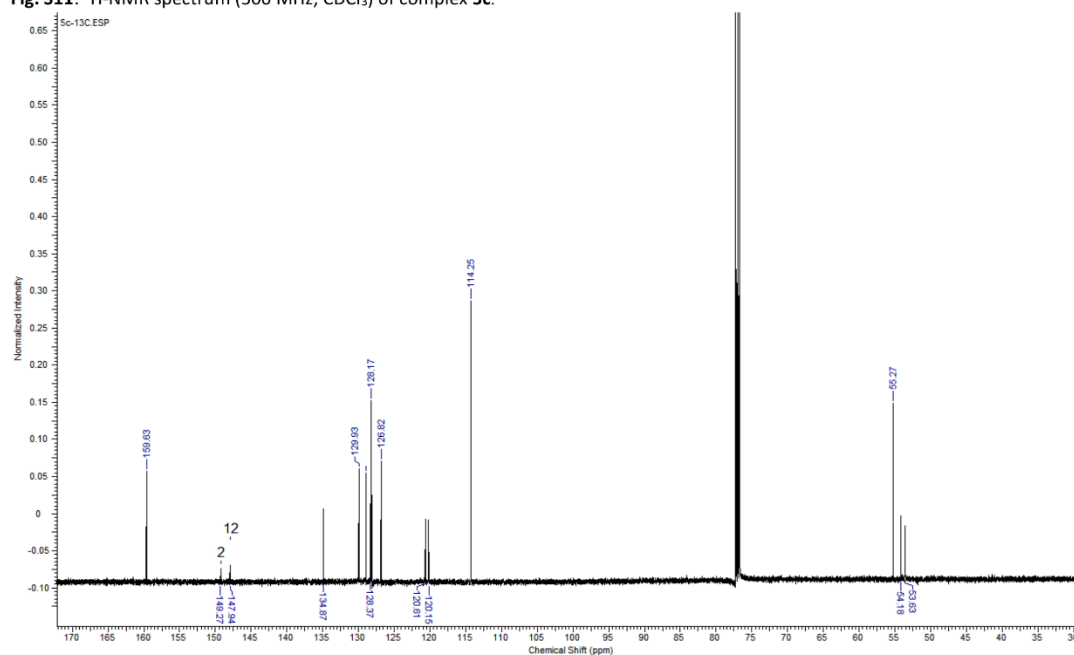


Fig. S12: ^{13}C -NMR spectrum (126 MHz, CDCl_3) of complex **5c**.

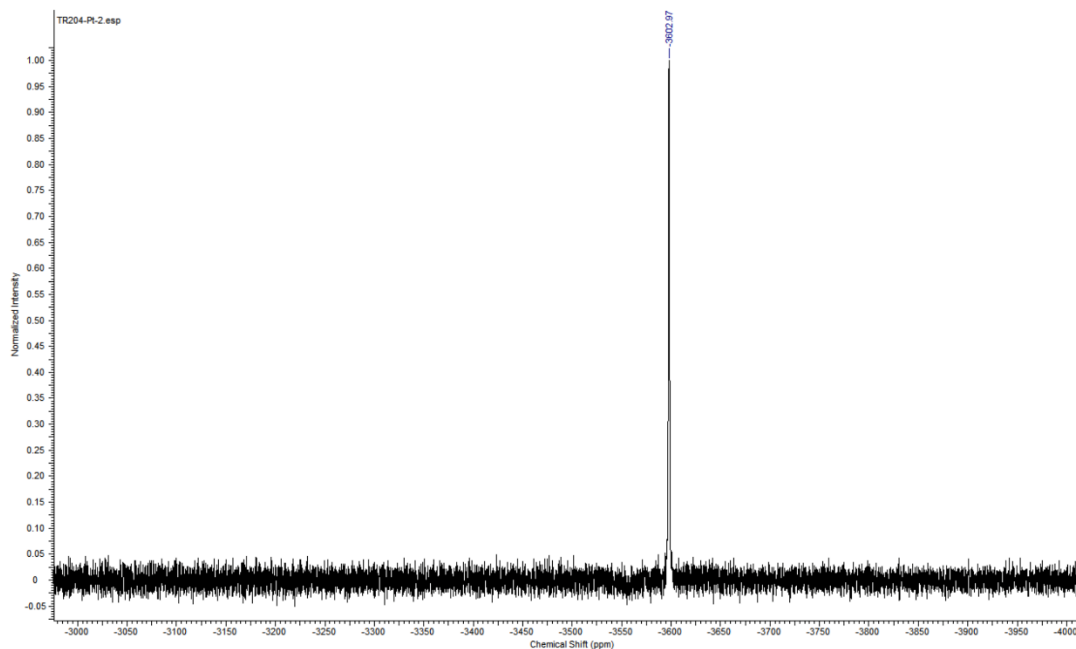


Fig. S 13: ^{195}Pt -NMR spectrum (CDCl_3) of complex **5c**.

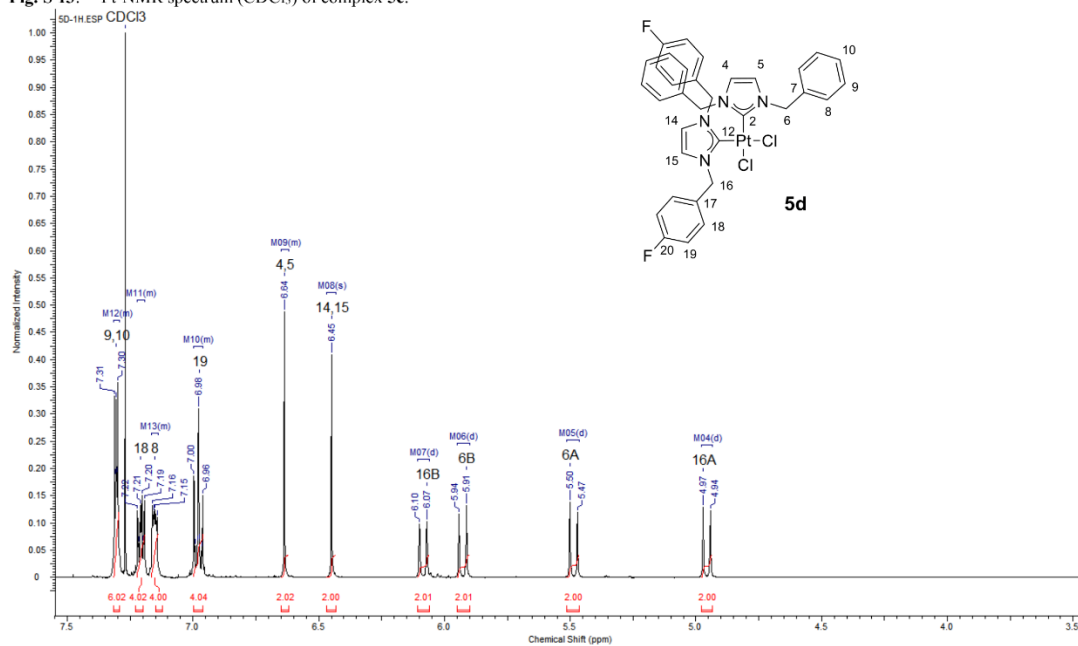
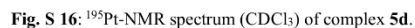
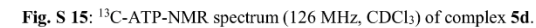


Fig. S14: ^1H -NMR spectrum (500 MHz, CDCl_3) of complex **5d**.



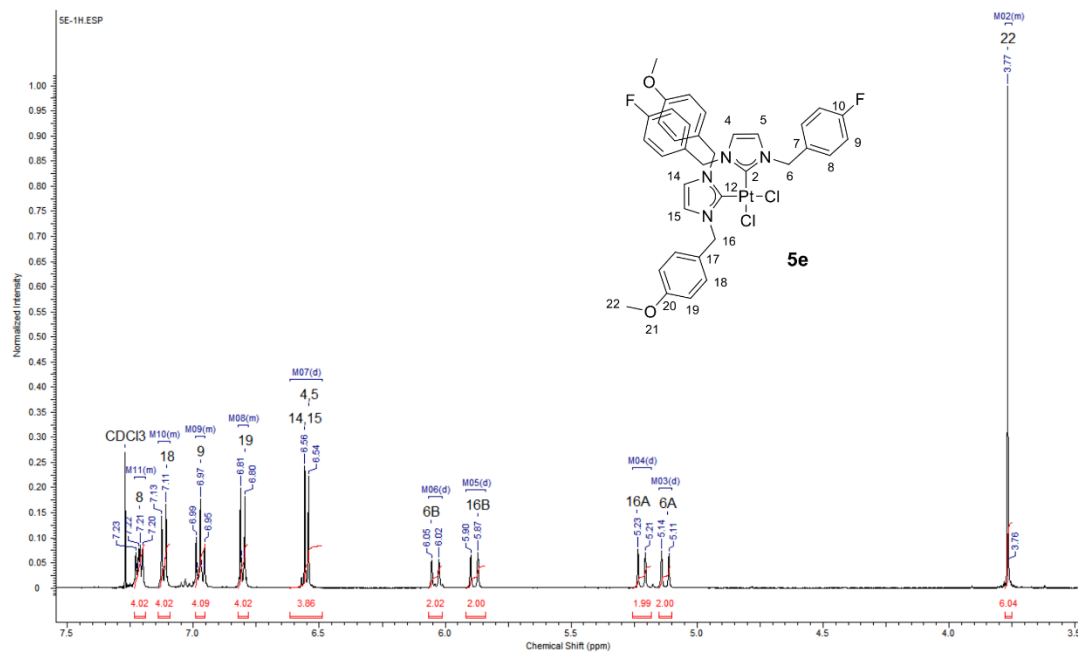


Fig. S17: ^1H -NMR spectrum (500 MHz, CDCl_3) of complex **5e**.

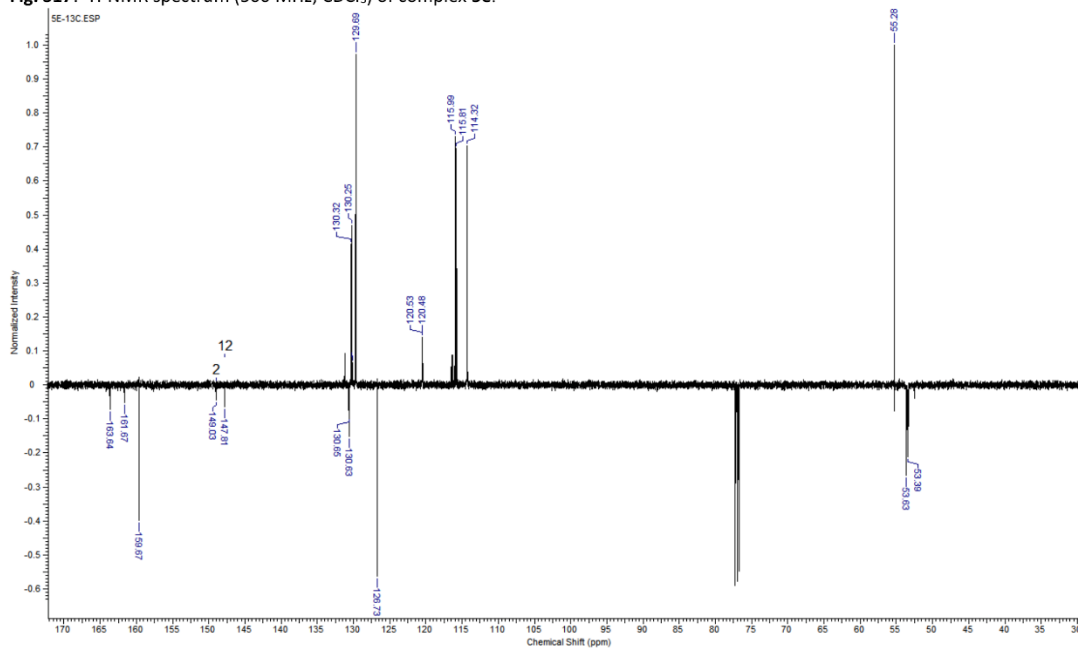


Fig. S18: ^{13}C -ATP-NMR spectrum (126 MHz, CDCl_3) of complex **5e**.

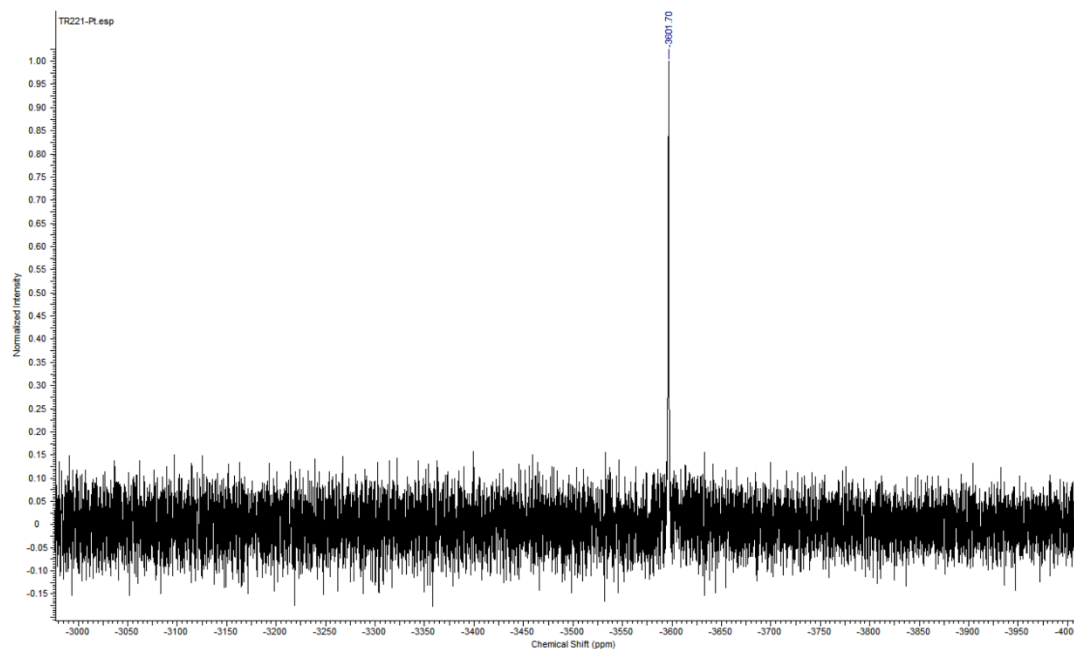


Fig. S 19: ^{195}Pt -NMR spectrum (CDCl_3) of complex **5e**.

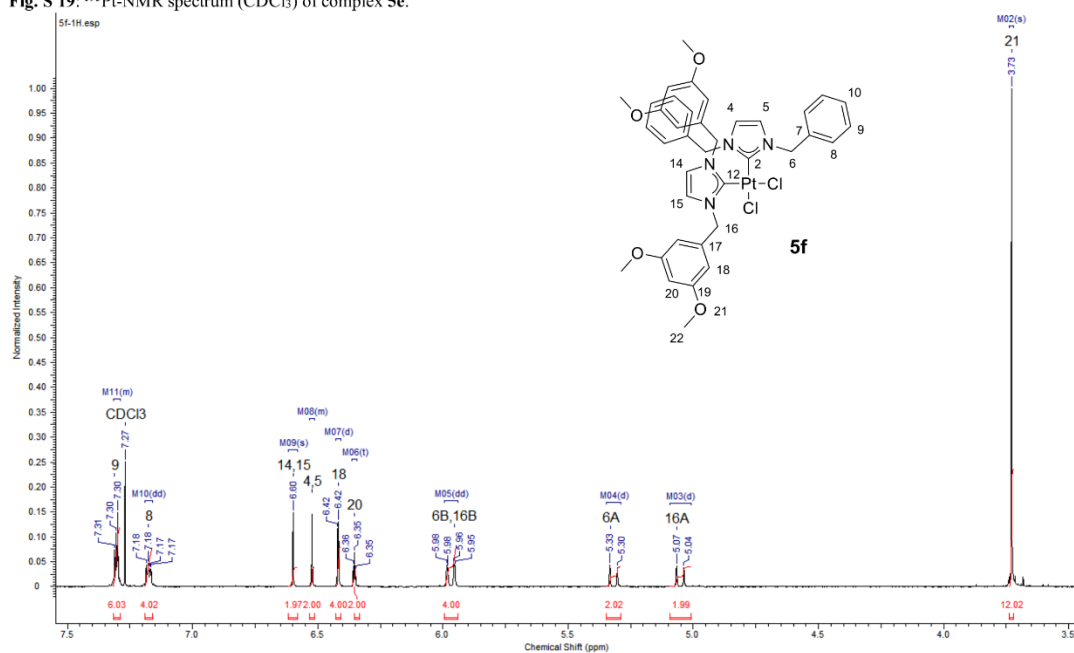


Fig. S20: ^1H -NMR spectrum (500 MHz, CDCl_3) of complex **5f**.

S13

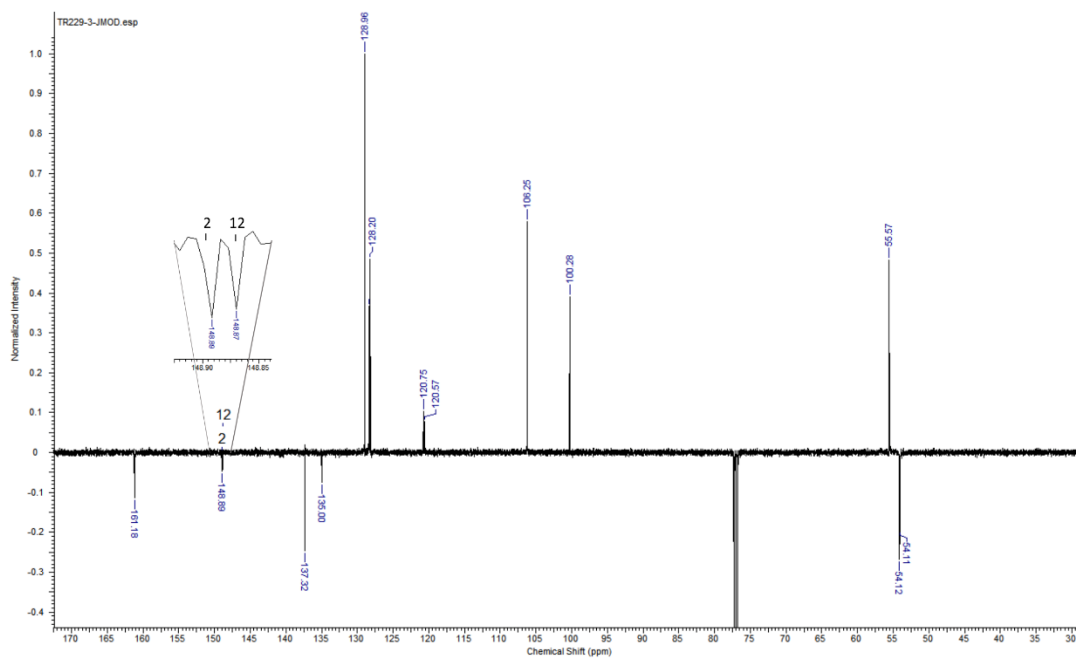


Fig. S 21: ^{13}C -ATP-NMR spectrum (126 MHz, CDCl_3) of complex 5f.

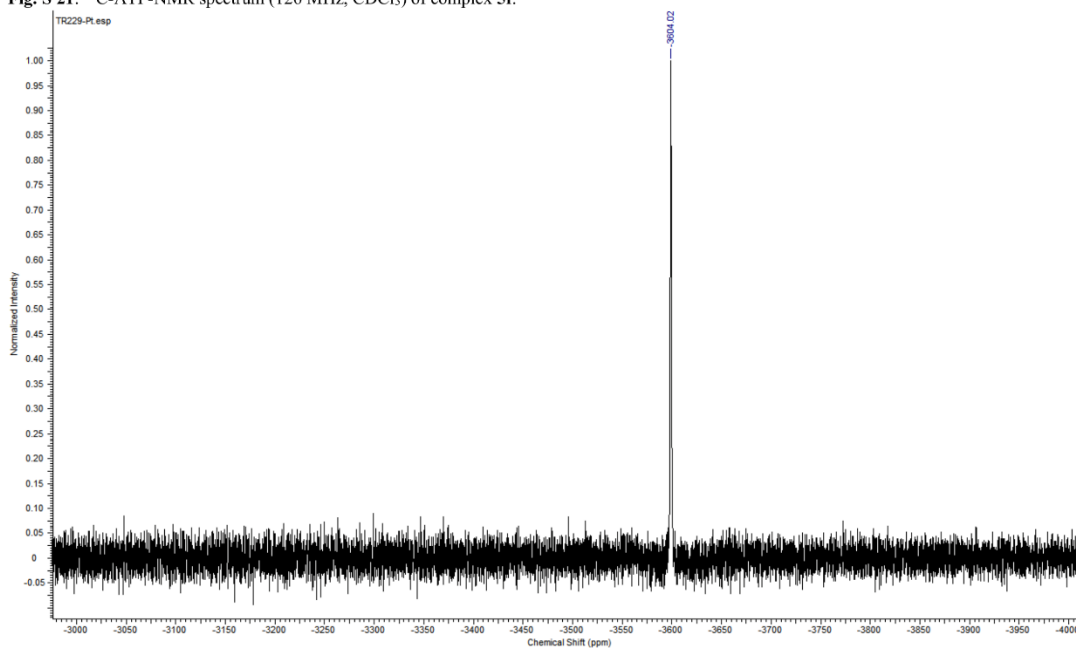


Fig. S 22: ^{195}Pt -NMR spectrum (CDCl_3) of complex 5f.

S14

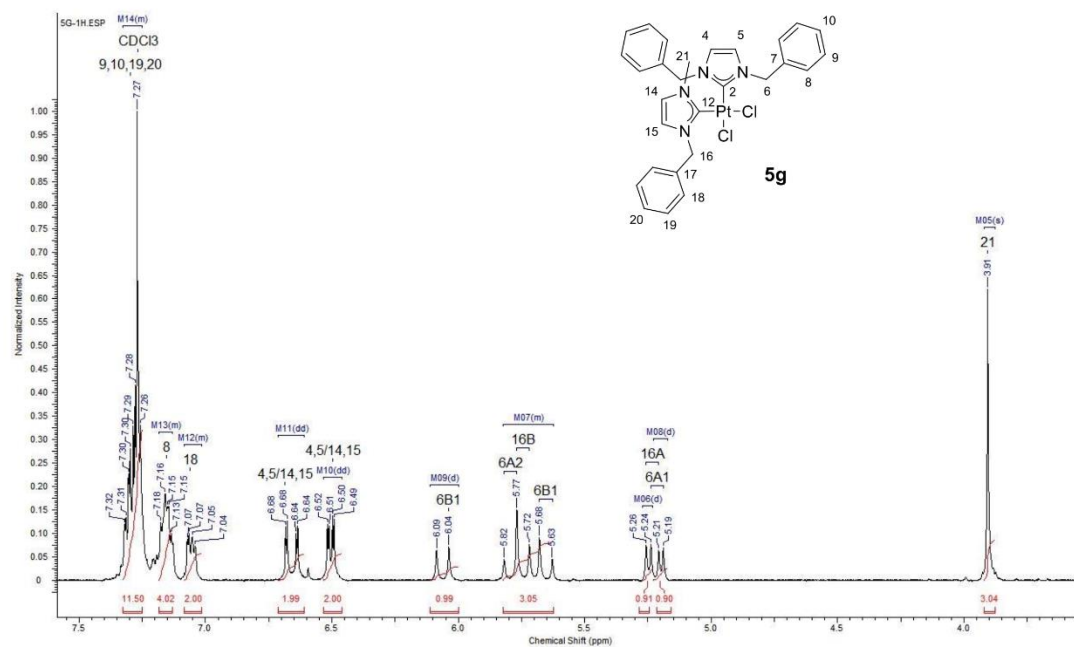


Fig. S23: ^1H -NMR spectrum (500 MHz, CDCl_3) of complex **5g**.

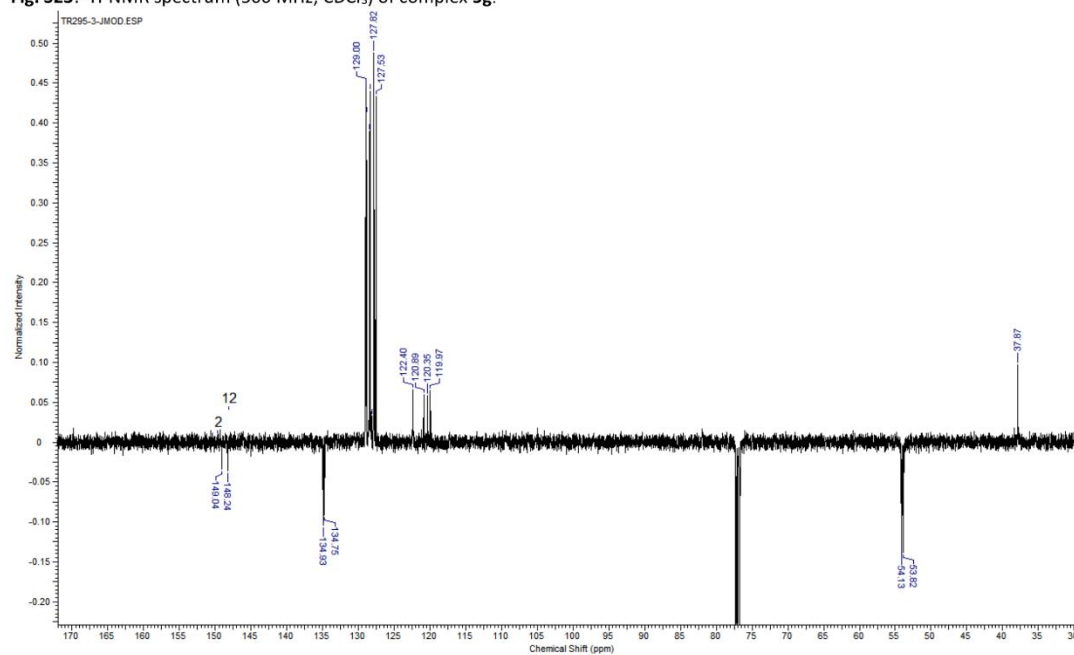


Fig. S 24: ^{13}C -ATP-NMR spectrum (126 MHz, CDCl_3) of complex **5g**.

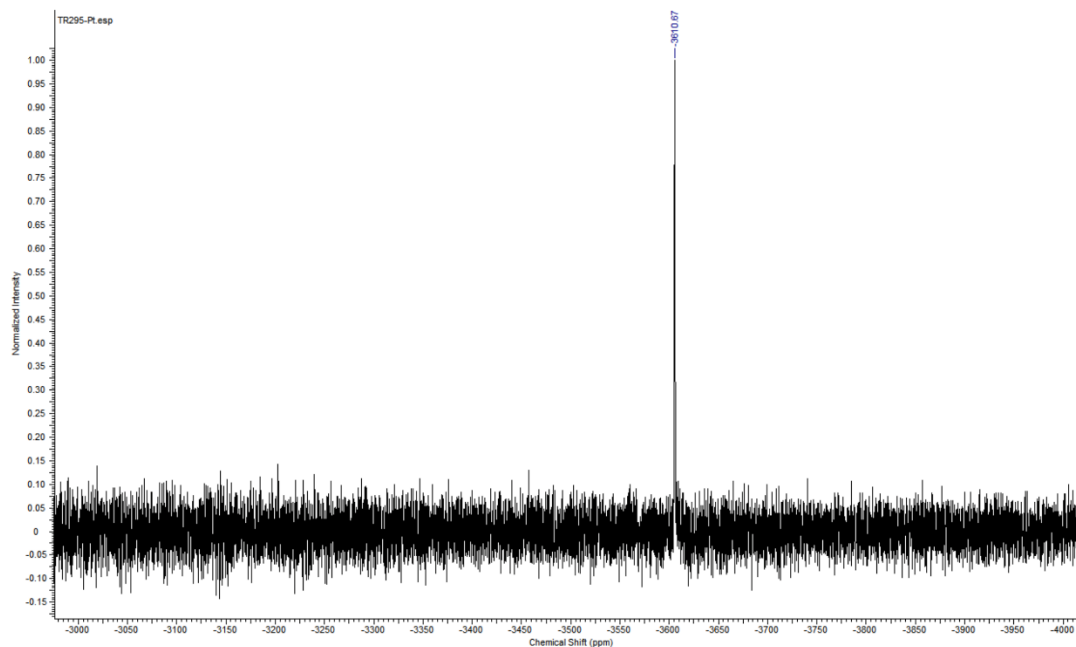


Fig. S 25: ^{195}Pt -NMR spectrum (CDCl_3) of complex **5g**.

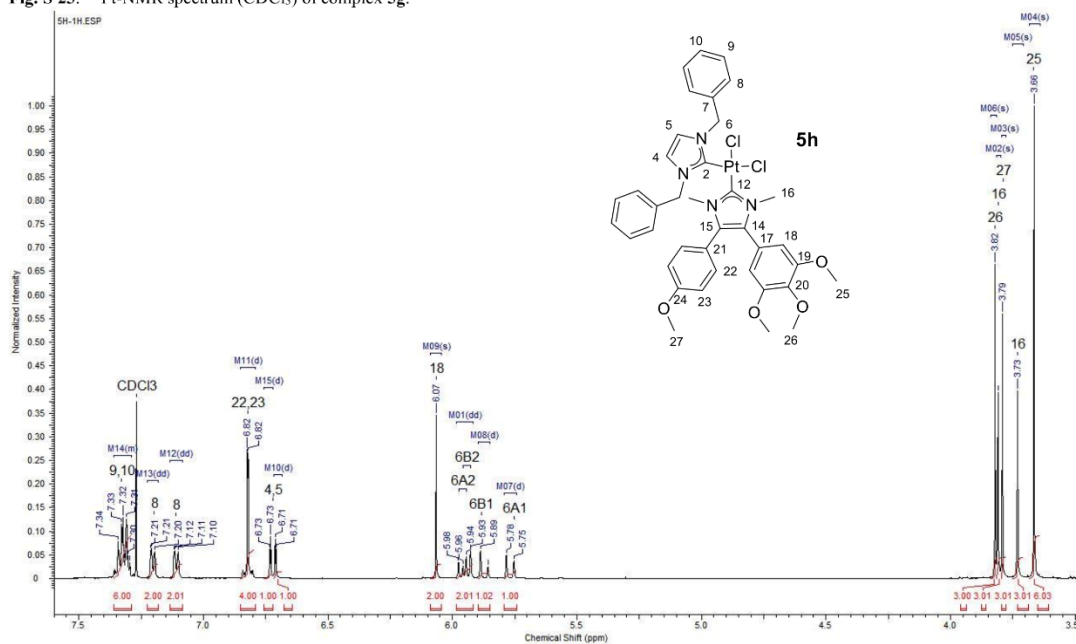


Fig. S26: ^1H -NMR spectrum (500 MHz, CDCl_3) of complex **5h**.

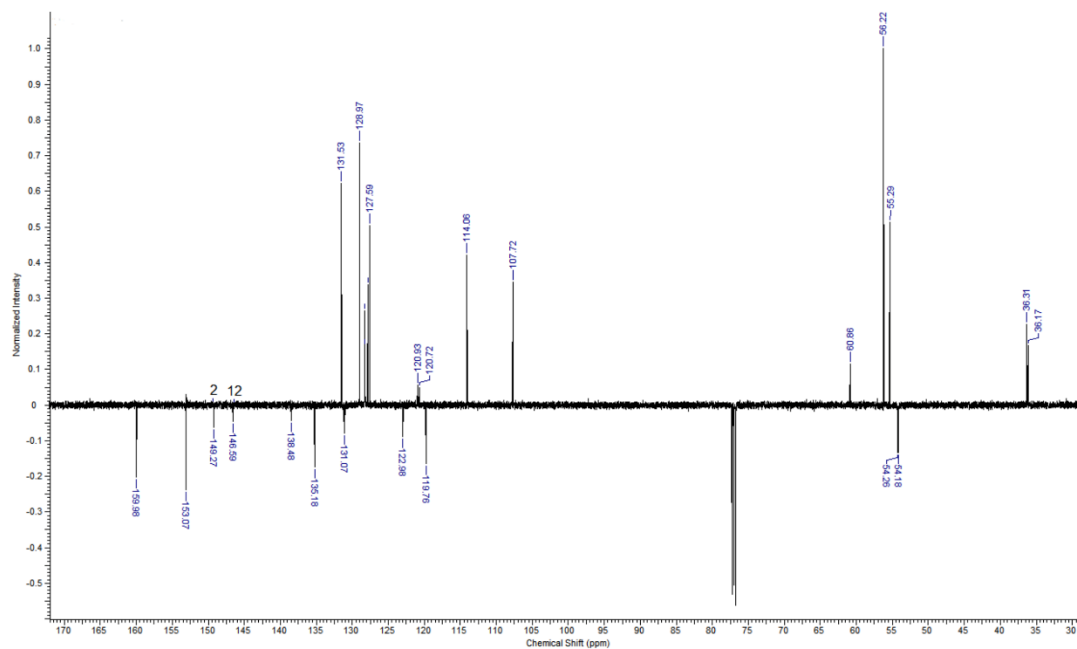


Fig. S 27: ^{13}C -ATP-NMR spectrum (126 MHz, CDCl_3) of complex **5h**.

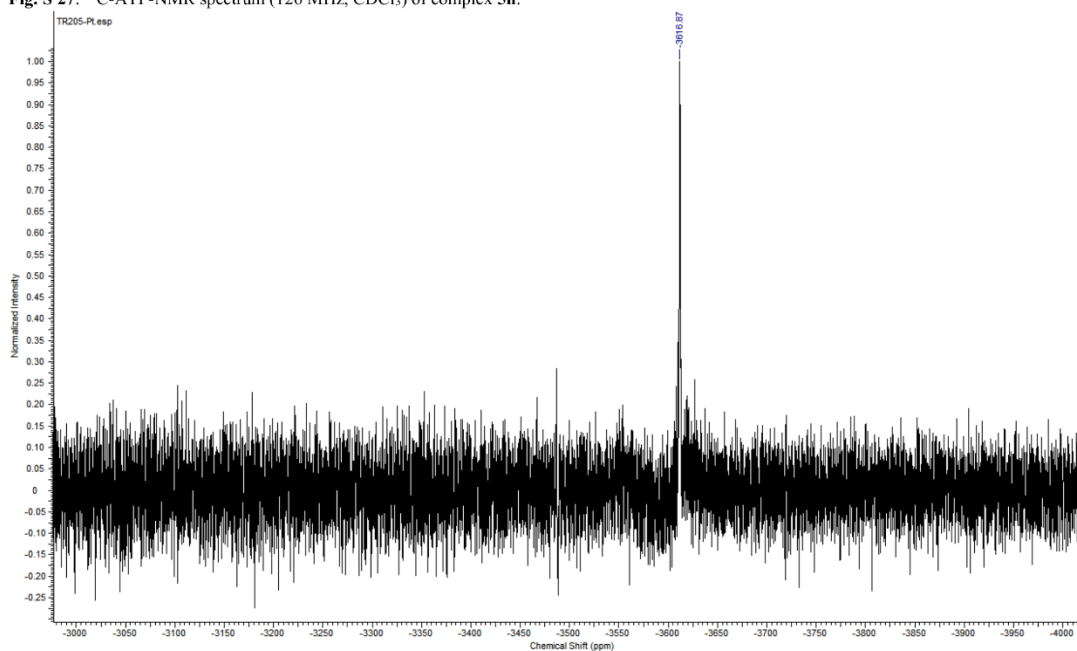


Fig. S 28: ^{195}Pt -NMR spectrum (CDCl_3) of complex **5h**.

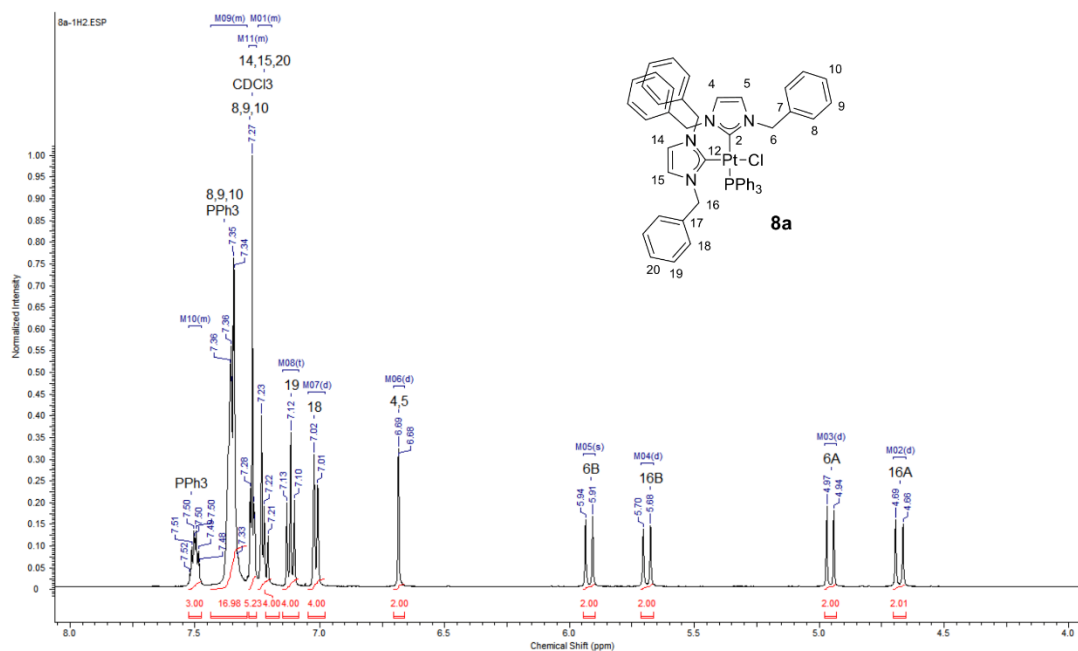


Fig. S 29: ^1H -NMR spectrum (500 MHz, CDCl_3) of complex **8a**.

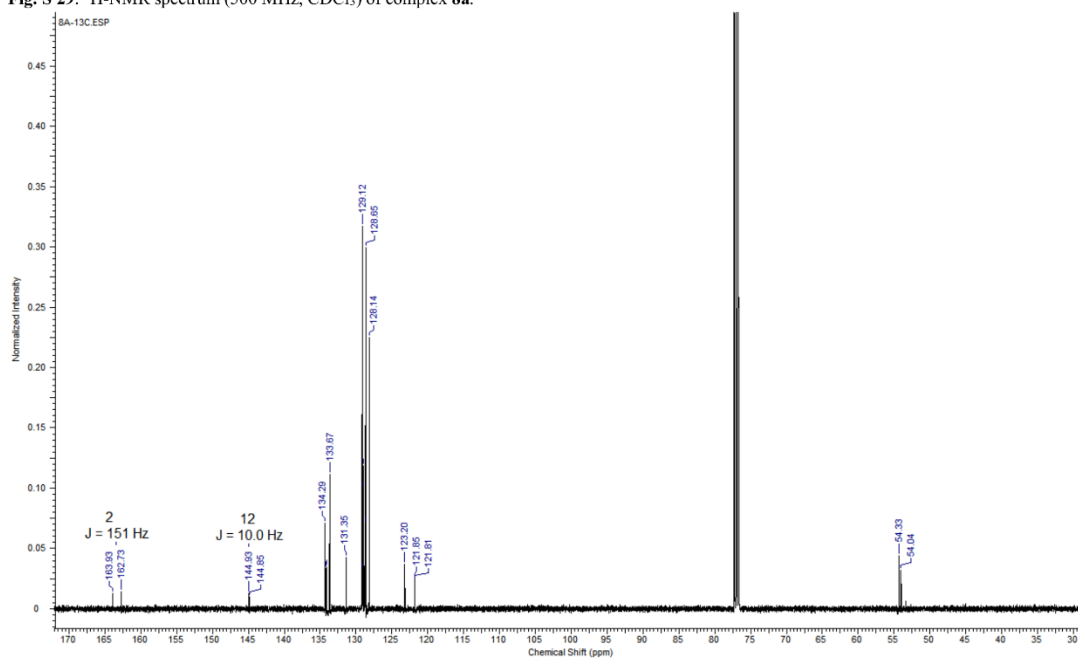


Fig. S 30: ^{13}C -NMR spectrum (126 MHz, CDCl_3) of complex **8a**.

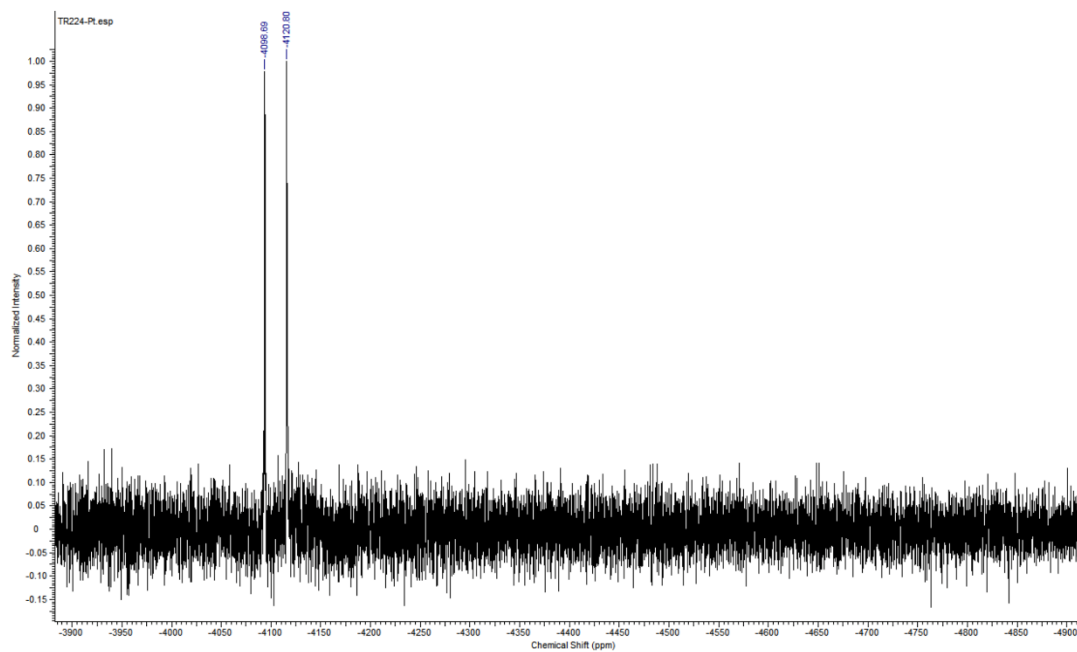


Fig. S 31: ^{195}Pt -NMR spectrum (CDCl_3) of complex **8a**.

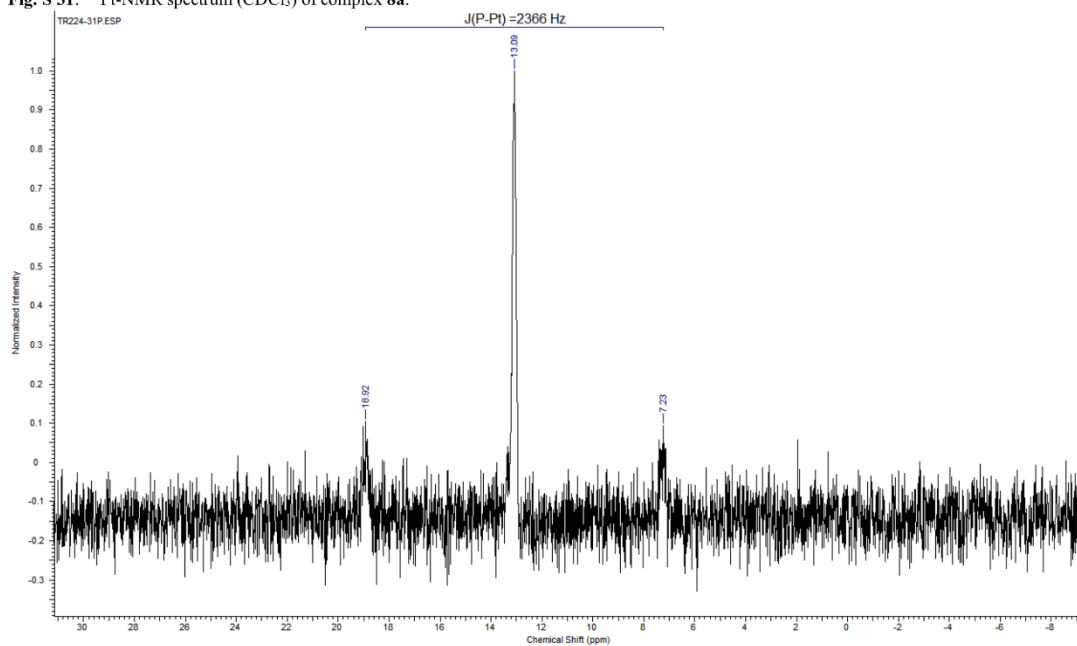


Fig. S 32: ^{31}P -NMR spectrum (202 MHz, CDCl_3) of complex **8a**.

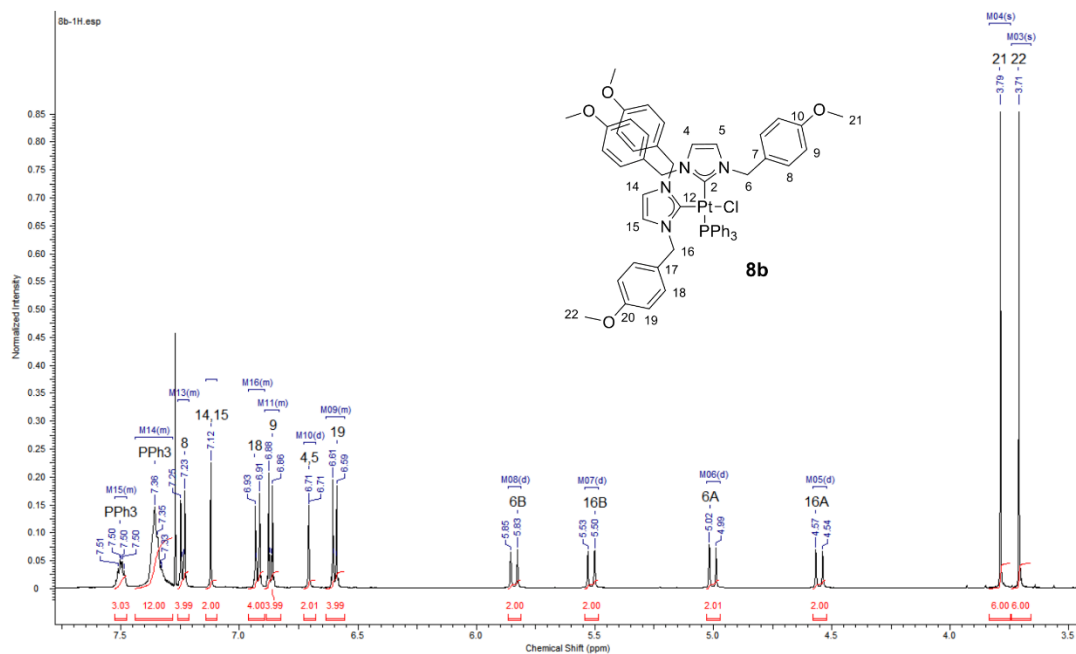


Fig. S 33: ^1H -NMR spectrum (500 MHz, CDCl_3) of complex **8b**.

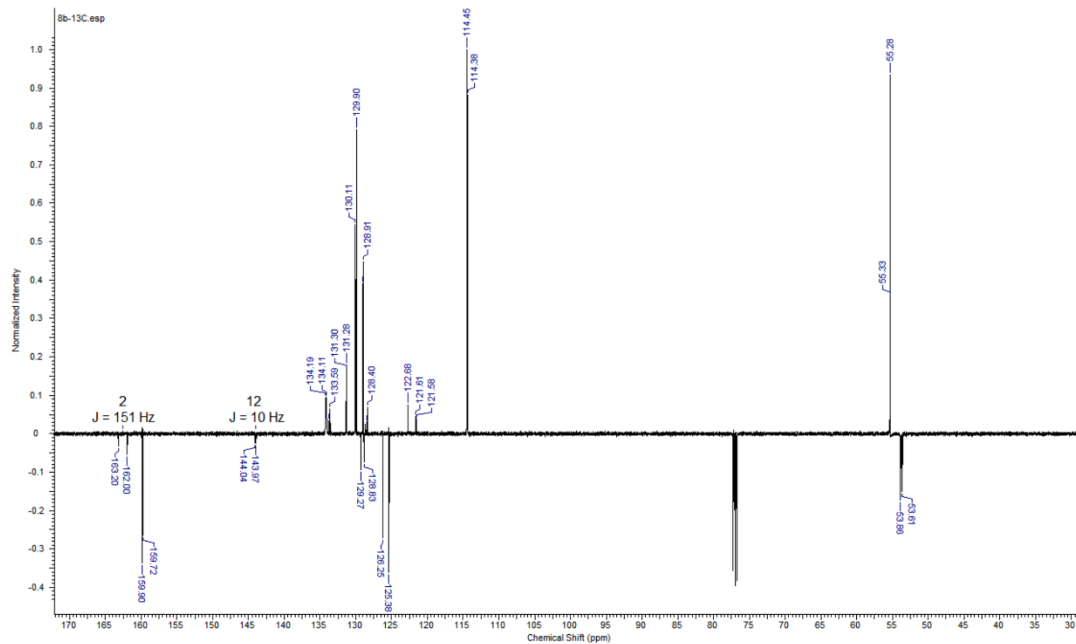


Fig. S 34: ^{13}C -ATP-NMR spectrum (126 MHz, CDCl_3) of complex **8b**.

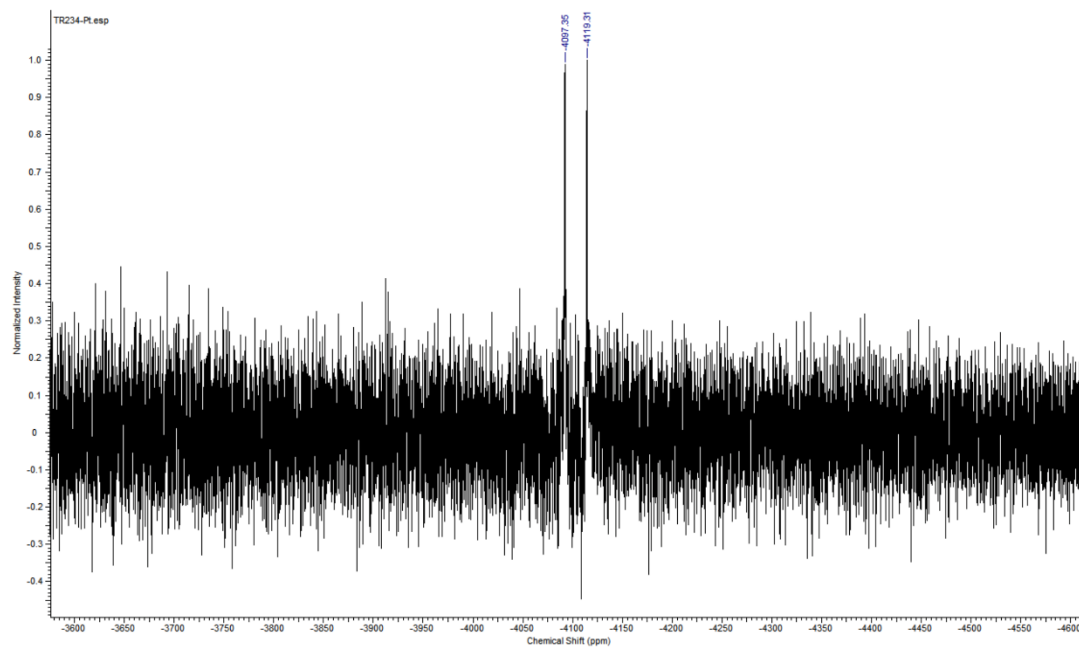


Fig. S 35: ^{195}Pt -NMR spectrum (CDCl_3) of complex **8b**.

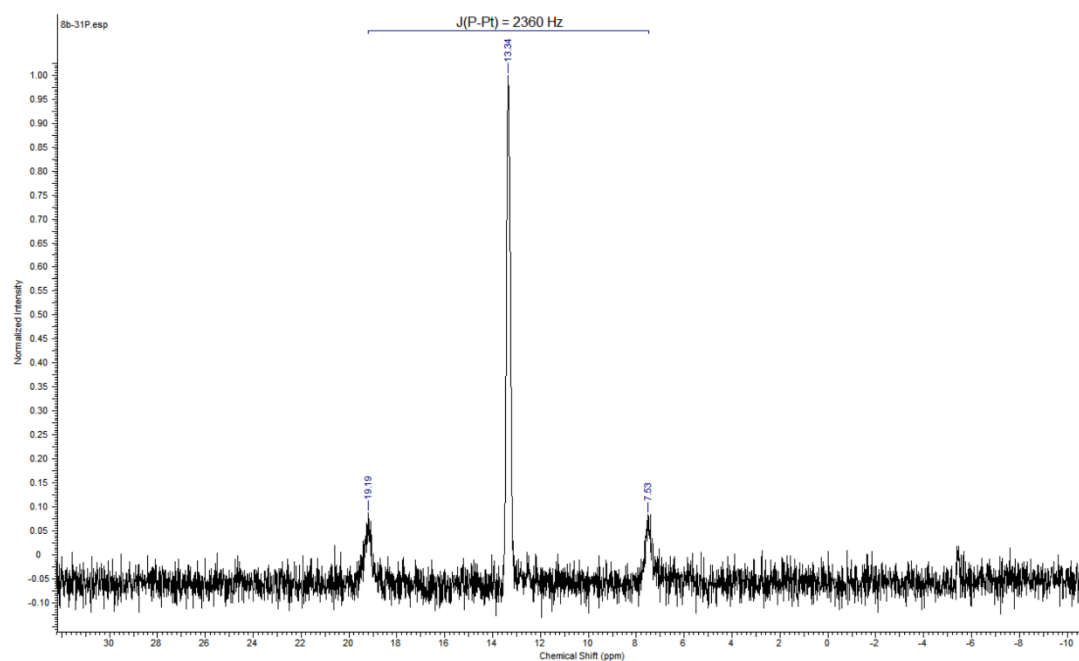


Fig. S 36: ^{31}P -NMR spectrum (202 MHz, CDCl_3) of complex **8b**.

S21

References

- ¹ M. Bouhrara, E. Jeanneau, L. Veyre, C. Coperet, C. Thieuleux, *Dalton Trans.*, 2011, **40**, 2995.
- ² L. Naya, D. Vazquez-García, A. Fernandez, M. Lopez-Torres, I. Marcos, O. Lenis, M. Pereira, J. Vila, J. Fernandez, *J. Organomet. Chem.*, 2014, **772-773**, 192–201.
- ³ K. Fujita, K. Inoue, J. Sato, T. Tsuchimoto and H. Yasuda, *Tetrahedron*, 2016, **72**, 1205–1212.
- ⁴ H. Shirota, H. Matsuzaki, S. Ramati and J. Wishart, *J. Phys. Chem. B*, 2015, **119**, 9173–9187.
- ⁵ J. Muenzner, T. Rehm, B. Biersack, A. Casini, I. de Graaf, P. Worawutputtapong, A. Noor, R. Kempe, V. Brabec, J. Kasparkova and R. Schobert, *J. Med. Chem.*, 2015, **58**, 6283–6292.

5.3 Publikation II

Antitumoral effects of mitochondria-targeting neutral and cationic *cis*-
[bis(1,3-dibenzylimidazol-2-ylidene)(L)Cl]Pt(II) complexes

*Matthias Rothmund,^{a,†} Sofia I. Bär,^{a,†} Tobias Rehm, Hana Kostrhunova,^b Viktor Brabec,^b Rainer Schobert^{*a}*

^aOrganic Chemistry Laboratory, University of Bayreuth, Universitätsstr. 30, 95440 Bayreuth

^bInstitute of Biophysics, Academy of Sciences of the Czech Republic, CZ-61265 Brno, Czech Republic

*e-mail: Rainer.Schobert@uni-bayreuth.de

† These authors contributed equally to this work

Dalton Trans. 2020, 49, 8901 – 8910.

PAPER



Cite this: *Dalton Trans.*, 2020, **49**, 8901

Antitumoral effects of mitochondria-targeting neutral and cationic *cis*-[bis(1,3-dibenzylimidazol-2-ylidene)Cl(L)]Pt(II) complexes†

Matthias Rothemund,^{‡,a} Sofia I. Bär,^{‡,a} Tobias Rehm,^a Hana Kostrhunova,^b Viktor Brabec^{ib} and Rainer Schobert^{ib} ^{*,a}

Recently, we opened a synthetic access to antitumoral platinum complexes of the type *cis*-[(NHC)¹(NHC)²Pt^{II}Cl(L)] which interact with DNA in a way correlated to the complex charge and to the sterical accessibility of the leaving chlorido ligand. We now identified mitochondria rather than nuclei as the cellular target of the neutral dichlorido complex **1** (L = Cl) and the delocalized lipophilic cationic phosphine complex **2** (L = PPh₃), both carrying the same *cis*-bis(1,3-dibenzylimidazol-2-ylidene) ligands. Their uptake into 518A2 melanoma cells was concentration-dependent and distinctly greater for complex **2** which was also more cytotoxic against sensitive cancer cell lines with submicromolar IC₅₀ values. Both complexes interfered strongly with various forms of DNA *in vitro*, but only complex **2** caused a melanoma cell cycle arrest in G1-phase, setting both apart from the S-phase arresting drug cisplatin. Studies of the intracellular localisation of **1** and **2** were carried out with their alkyne-tagged analogues **6** and **7**, which showed identical patterns of cancer cell cytotoxicity, cell cycle interference and effects on mitochondria. Click reactions with 7-hydroxycoumarin azide, colocalisation with Mitotracker™ and confocal microscopy, proved complexes **6** and **7** to accumulate mainly in the mitochondria rather than the nuclei of melanoma cells. Complex **1** and even more so complex **2** reduced the mitochondrial membrane potential and also increased the cellular ROS levels. As a consequence, both complexes caused stress fibre formation in the F-actin cytoskeleton of melanoma cells, most distinctly so complex **2** which also activated the apoptotic cascade mediated by capases-3 and -7.

Received 7th May 2020,
Accepted 15th June 2020

DOI: 10.1039/d0dt01664k

rsc.li/dalton

Introduction

The serendipitous discovery of the biological effects of *cis*-diamminodichloridoplatinum(II) (cisplatin; CDDP) by Rosenberg *et al.* almost five decades ago led to an intensive worldwide study and screening of congeneric platinum coordination complexes, culminating in the FDA approval of the mainstay tumor therapeutics carboplatin and oxaliplatin.¹ In recent years, the interest of medicinal chemists in antitumoral metalodrugs was rekindled by the growing evidence that organoplatinum complexes carrying *N*-heterocyclic carbene (NHC) ligands offer more means of fine-tuning and optimising their pharmacological properties due to the variability of both the

N-heterocycle and its substituents.² Recently, we reported on the synthesis of platinum(II) complexes of type *cis*-[(NHC)¹(NHC)²Pt^{II}Cl(L)] bearing two – optionally different – *cis*-oriented (benz)imidazol-2-ylidene ligands. Preliminary tests showed their modes of antitumoral action to be dependent not only on these NHC ligands but also decisively on their secondary ligands L and their overall charge. Fig. 1 depicts two typical complexes.^{3,4} The neutral complex **1**, like derivatives with further residues on the phenyl rings not shown here, was

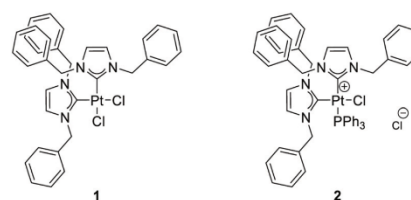


Fig. 1 Structures of complexes **1** (L = Cl) and **2** (L = PPh₃) of the type *cis*-[bis(1,3-dibenzylimidazol-2-ylidene)Pt^{II}Cl(L)].⁴

^aOrganic Chemistry Laboratory, University of Bayreuth, Universitätsstrasse 30, 95440 Bayreuth, Germany. E-mail: Rainer.Schobert@uni-bayreuth.de

^bCzech Academy of Sciences, Institute of Biophysics, Kralovopolska 135, CZ-61265, Czech Republic

†Electronic supplementary information (ESI) available: NMR spectra of **6** and **7**, uptake of complexes **1** and **2** by 518A2 melanoma cells, electrophoretic mobility shift assays of **1**, **2**, **6**, and **7**, *etc.* See DOI: 10.1039/d0dt01664k

‡These authors contributed equally to this work.

cytotoxic with IC_{50} values generally in the low micromolar range, and gave rise to a band shift of plasmid DNA in electrophoretic mobility shift assays (EMSA) comparable to cisplatin. Exchange of a chlorido ligand for triphenylphosphine afforded cationic complexes like **2**, which were more cytotoxic against cancer cells with IC_{50} values in the nanomolar range, and which caused an aggregation rather than coordination of DNA *in vitro*.⁴

Investigations of related neutral mono-NHC complexes of type *cis*-[(benzimidazol-2-ylidene)Pt^{II}Cl₂(L)] and cationic complexes *trans*-[(benzimidazol-2-ylidene)Pt^{II}Cl(L)₂]⁺Cl[−] gave a more nuanced picture.⁵ While the cationic complexes were also more cytotoxic against cancer cells than the neutral ones, DNA interaction of the latter *in vitro* depended decisively on the ligands L.⁵ In order to find out whether cellular DNA is an actual target of *cis*-[(1,3-dibenzylimidazol-2-ylidene)₂Pt^{II}Cl(L)] complexes **1** and **2** and to further elucidate their modes of action, we synthesized their 4-ethynylbenzyl derivatives **6** and **7** for intracellular localisation *via* alkyne-azide click reactions.⁶

Results and discussion

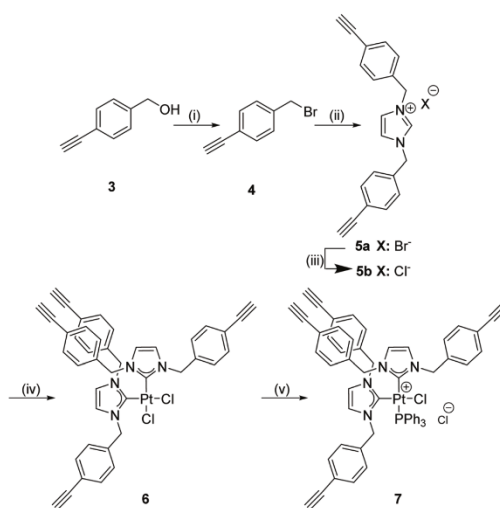
Synthesis and characterization

4-Ethynylbenzyl bromide **4** was synthesized from the corresponding benzyl alcohol **3**, NBS and PPh₃. It was reacted with imidazole under basic conditions to give the imidazolium bromide **5a**. To prevent anionic exchange during the next steps, bromide **5a** was converted to the imidazolium chloride **5b**. The latter was deprotonated with KO^tBu to generate the free carbene, which was trapped with half an equivalent of *cis*-[Pt^{II}Cl₂(DMSO)₂] to afford the desired *cis*-(bis-NHC)Cl₂Pt^{II} complex **6**. *cis*-[Pt^{II}Cl₂(DMSO)₂] can be prepared by adding a three-fold excess of DMSO to K₂PtCl₄ in water and allowing the solution to stand at room temperature until yellow crystals precipitate.⁷ Cationic complex **7** was obtained from reaction of complex **6** with an excess of PPh₃ (Scheme 1).

As for complexes **1** and **2**, the NMR spectra of the new alkyne derivatives confirmed their *cis* configuration and the perpendicular orientation of their imidazole rings with respect to the PtCl(L) plane. The ¹H NMR spectra reflected the inequivalency of the geminal protons of each benzylic CH₂ group giving rise to two (for **6**) or four (for **7**) doublets which were 0.73 ppm apart in the case of **6** and 0.71/0.74 ppm for complex **7**. In the ¹³C NMR spectra the carbene carbons of complex **6** peaked at 146.7 ppm and those of complex **7** appeared as doublets at 145.8 ppm with ²J_{CP} = 10 Hz (*cis* to PPh₃) and at 163.2 ppm with ²J_{CP} = 151 Hz (*trans* to PPh₃).

Biological evaluation

Inhibition of cancer cell proliferation. Complexes **1** and **2** had previously been tested for antiproliferative effects on various cancer cell lines as members of a larger series of similar NHC platinum(II) complexes with distinct antitumoral activity. We now tested them, using the same MTT-assay,



Scheme 1 Syntheses of bis[1,3-(4-ethynylbenzyl)imidazol-2-ylidene] Pt^{II} complexes **6** and **7**. Reagents and conditions: (i) NBS, PPh₃, CH₂Cl₂, 40 °C, 3 h, 96%; (ii) imidazole, K₂CO₃, MeCN, 80 °C, 16 h, 100%; (iii) Ag₂CO₃, HNO₃, EtOH, rt, 2 h, then HCl, 68%; (iv) *cis*-[Pt^{II}Cl₂(DMSO)₂], KO^tBu, CH₂Cl₂, rt, 24 h, 40%; (v) PPh₃, CH₂Cl₂, rt, 2 h, 82%.

against further cell lines such as the colon cancer cell line HCT116^{wt}, its p53-deficient mutant HCT116^{−/−}, the non-malignant human fibroblasts HDFa, and the multi-drug resistant cervix carcinoma cell line KB-V1^{Vbl}, pre-incubated with verapamil, a competitive inhibitor of the P-gp1 efflux transporter overexpressed in this cell line. In parallel, we also tested the ethynyl-tagged complexes **6** and **7**, to find out whether their cytotoxic pattern across this cell line panel is comparable to that of their analogues **1** and **2** and so ensure their suitability as surrogates for complexes **1** and **2** in intracellular localisation studies *via* alkyne-azide click reactions. As previously reported for other cancer cell lines,^{4,5} complex **2** bearing a sterically demanding triphenylphosphine residue and a positive charge, was more cytotoxic than neutral dichlorido complex **1**, with IC_{50} values in the nanomolar or lower micromolar range also against the cell lines listed in Table 1. This pattern was also observed for the alkynyl-tagged complexes **6** and **7**, which showed IC_{50} values similar to those of their congeners **1** and **2**, albeit with a few conspicuous exceptions. All four complexes showed a reduced cytotoxicity against HCT116^{−/−} cells lacking functional tumor suppressor protein p53, which plays an important role in cell cycle progression and in apoptosis activation.⁸ Unlike its non-ethynylated parent complex **1**, the neutral complex **6** was virtually inactive against HCT116^{−/−} cells. These results suggest a similarity in the mode of action with cisplatin, which is known to activate p53 upon extensive DNA damage.⁹ Inhibition of the P-gp1 efflux pump of multi-drug resistant Kb-V1^{Vbl} cervix carcinoma cells by pre-incubation with verapamil, which is used clinically as a re-sensi-

Table 1 Means \pm SD of IC₅₀ values [μ M] of cisplatin and compounds **1**, **2**, **6**, **7** in MTT assays against human cell lines^a after 72 h of incubation as calculated from four independent measurements. * Data taken from ref. 4. ** Data taken from ref. 10

IC ₅₀ (72 h) [μ M]	518A2	HT-29	HCT116 ^{wt}	HCT116 ^{-/-}	EaHy926	Kb-V1 ^{Vbl}	Kb-V1 ^{Vbl+vpmb}	HDFa	SI ^b
Cisplatin	2.6 \pm 0.7*	8.3 \pm 0.5*	5.7 \pm 0.3*	9.2 \pm 0.5*	21.1 \pm 2.5	2.2 \pm 0.3**	0.23 \pm 0.08*	>50	>9.0
1	6.2 \pm 0.4*	14.6 \pm 1.4*	2.3 \pm 0.8	14.1 \pm 0.9	6.8 \pm 1.6*	11.7 \pm 0.8*	6.3 \pm 0.6	4.5 \pm 0.5	0.6
2	0.86 \pm 0.05*	0.82 \pm 0.06*	0.51 \pm 0.04	1.6 \pm 0.1	0.48 \pm 0.01*	7.3 \pm 1.2*	0.99 \pm 0.16	3.1 \pm 0.4	4.2
6	5.6 \pm 0.2	13.12 \pm 1.0	1.1 \pm 0.1	>50	12.5 \pm 2.2	25.9 \pm 3.4	>50	>50	>7.5
7	1.2 \pm 0.2	0.66 \pm 0.26	0.14 \pm 0.03	2.0 \pm 0.3	0.63 \pm 0.10	34.1 \pm 3.8	34.5 \pm 4.2	3.4 \pm 1.9	5.1

^a 518A2 – melanoma, HT-29 – colon adenocarcinoma, HCT116^{wt} – colon carcinoma (wildtype), HCT116^{-/-} – colon carcinoma (p53 knock-out mutant), EaHy926 – endothelial hybrid, Kb-V1^{Vbl} – cervix carcinoma, HDFa – human dermal fibroblasts. ^b Vbl – vinblastine, vpmb – verapamil, SI – selectivity index.

tizer of refractory tumours, led to an enhanced activity of complexes **1** and **2** but not of the alkynyl-tagged complexes **6** and **7**, indicating that the latter are no substrates of P-gp1.

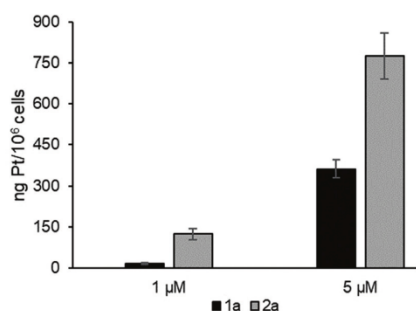
To determine the selectivity of the complexes for tumour cells, we tested them for their toxicity against the non-malignant fibroblast cells HDFa and calculated a selectivity index (SI) by dividing their IC₅₀ against the fibroblasts by the average IC₅₀ values against the unadulterated cancer cell lines 518A2, HT-29, and HCT116^{wt}. Like cisplatin, complex **6** was inactive against the HDFa cells and thus can be regarded highly cancer cell selective. Complexes **2** and **7** also showed a marked selectivity for cancer cells, whereas complex **1** was somewhat selective only towards HCT116^{wt} colon cancer cells.

Cellular uptake. To find out whether the greater cytotoxicity of the cationic complex **2** stems from an actual increase in toxicity due to the positive charge and the bulkier phosphine ligand or from an enhanced uptake into the cells, we measured the platinum content of 518A2 cells after 8 h of incubation with complexes **1** and **2** (1 μ M and 5 μ M) by ICP-MS (Fig. 2; cf. SI for exact values). The observed divergence in uptake rates of complexes **1** and **2** by a concentration-dependent factor of 2.5 (for 5 μ M) to 7 (for 1 μ M) reflects the previously measured⁴ difference in their IC₅₀ values against this cell line fairly well, i.e. 6.2 μ M for **1** and 0.86 μ M for **2**. This suggests that they do not differ much in their intrinsic antiproliferative activities.

Such ostensible hikes in cytotoxicity upon increasing the charge and bulkiness, and hence the uptake rates, were previously reported by us⁵ for related benzimidazol-2-ylidene complexes of platinum and more systematically by Osella *et al.*¹¹ for cisplatin, carboplatin, oxaliplatin and close congeners.

DNA-interaction. While the canonical mechanism of action of cisplatin and related coordination complexes of platinum(II) rests upon coordinative bonds to DNA bases, cross-link formation and eventually cell cycle arrest and apoptosis,¹² evidence has accumulated that NHC-complexes of platinum may interact with DNA in a different way, implying DNA aggregation rather than coordination and electrostatic rather than covalent bonding.^{3–5} Therefore the DNA interaction of complexes **1**, **2**, **6** and **7** was investigated *in vitro* by electrophoretic mobility shift assays (EMSA) with circular plasmid DNA. All complexes showed similar band shift patterns in EMSA experiments (Fig. S8†) as previously tested neutral and cationic imidazol-2-ylidene^{3,4} and some benzimidazol-2-ylidene complexes.⁵ The neutral complexes **1** and **6** gave rise to band shifts of the compact covalently closed circular (ccc) form reminiscent of those caused by cisplatin, while the cationic complexes **2** and **7** did not shift the bands of the ccc form at concentrations up to 10 μ M, yet at higher concentrations led to precipitation of DNA aggregates in the agarose gel pockets. In other words, the neutral complexes **1** and **6** appear to interact with DNA like cisplatin by forming coordination complexes with DNA bases, while the cationic complexes **2** and **7** are likely to aggregate DNA *via* electrostatic attraction. In ethidium bromide saturation assays complexes **1** and **2** caused a distinct concentration-dependent reduction of the fluorescence of ethidium bromide intercalated in linear salmon sperm DNA, exceeding that by cisplatin markedly (Fig. 3). It is reasonable to assume that the complexes **1** and **2** interact with DNA like some of the structurally related benzimidazol-2-ylidene platinum(II) complexes investigated by us earlier.⁵ These bound to DNA quickly *via* electrostatic attraction to its negatively charged backbone which over time was replaced by tighter coordinative bonding.

Cell cycle analysis. Previously, we found that certain imidazol-2-ylidene and benzimidazol-2-ylidene complexes of platinum(II) interfered with the cell cycle of cancer cells differently

**Fig. 2** Platinum content of 518A2 melanoma cells after 8 h incubation with 1 μ M or 5 μ M of complexes **1** and **2**, measured *via* ICP-MS.

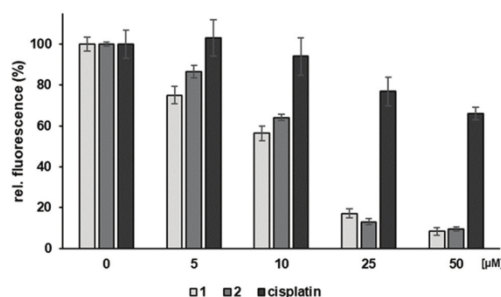


Fig. 3 Relative fluorescence intensities of ethidium bromide, intercalated in linear salmon sperm DNA after 2 h treatment with **1**, **2** or cisplatin in different concentrations. Experiments were conducted in triplicate for each substance and concentration.

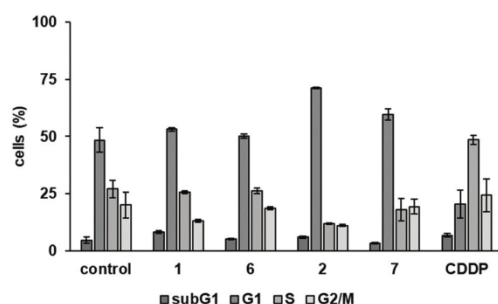


Fig. 4 Cell cycle analysis of 518A2 melanoma cells after 24 h incubation at 37 °C with 5 μM of **1** or **6**, 500 nM of **2** or **7**, and 2 μM of CDDP as a positive control. DMF was used as a negative control. Data shown are based on three independent experiments per substance and concentration.

from cisplatin which typically induces an S-phase or a twofold S-phase *cum* G2/M-phase arrest.^{3,5} We now studied the effects of complexes **1**, **2**, **6**, **7**, and cisplatin on the cell cycle of 518A2 melanoma cells (Fig. 4). While CDDP stops the cell cycle of 518A2 melanoma cells during the S-phase, the neutral complexes **1** and **6** had virtually no effect on the distribution of cells in the individual phases of the cell cycle, apart from a marginal rise in the G1-phase population. In contrast, the cationic complex **2** and its ethynyl-substituted derivative **7** initiated a pronounced G1-phase arrest of the melanoma cell cycle, fully in line with earlier results for other cationic imidazol-2-ylidene platinum(II) complexes.³ Two conclusions can be drawn: first, both types of complexes **1/6** and **2/7** had effects different from that of cisplatin, and second, the similarity of the effects of complexes **1** and **2** and their respective ethynyl-tagged derivatives **6** and **7** justifies the use of the latter as surrogates in localisation studies.

Colocalisation. To test if the compounds accumulate in the nucleus or if the differences in their modes of action from that

of cisplatin originate from a different target location, we treated 518A2 melanoma cells with the ethynyl-substituted complexes **6** and **7** (30 min, 30 μM). The intracellular distribution was visualized *via* Cu(I)-catalysed click reaction with 3-azido-7-hydroxycoumarin in a mixture of CuSO₄ and ascorbic acid in BSA buffer. This gave a turquoise fluorescent triazole. Confocal microscopy of the treated cells, co-stained with Mitotracker™ (ThermoFisher) found both complexes mainly to be located at the mitochondria (Fig. 5). Using the framed cells in Fig. 5, the Pearson correlation coefficient (PC) and Li's colocalisation quotient (LICQ) were calculated as a measure of colocalisation accuracy, using imageJ and the colocalisation plugin JaCoP.^{13,14} Both complexes showed high PC values (a value of 1 corresponds to complete colocalisation) and LICQ values (a value of 0.5 corresponds to complete colocalisation) for the localisation of complexes **6** (PC: 0.89, LICQ: 0.46) and **7** (PC: 0.90, LICQ: 0.47) at the mitochondria of the selected cells. This stands in stark contrast to the tendency of most known platinum complexes to accumulate in the nucleus, but falls in line with reports on charged and lipophilic complexes addressing other cellular targets than nuclear DNA.^{15–17} There are also many reports on complexes, predominantly of gold, of the type “delocalized lipophilic cations” (DLC) accumulating in mitochondria.^{18–22} DLCs are able to pass lipid layers and selectively accumulate in mitochondria which feature a negative inner transmembrane potential.^{23–25}

Changes of the mitochondrial membrane potential Ψ and of ROS levels. The accumulation of complexes **6** and **7** in mitochondria suggests that their closely related congeners **1** and **2** might also operate by a mitochondria-associated mechanism of action. The integrity of the mitochondrial membrane potential $\Delta\Psi$ (MMP $\Delta\Psi$) is a prerequisite for cellular functionality. $\Delta\Psi$ is built up by a H⁺-gradient across the inner mitochondrial membrane and drives the ATP synthesis by oxidative phosphorylation.²⁶ The impact of complexes **1**, **2**, **6**, and **7** on the MMP was evaluated using the cationic dye tetramethyl rhodamine methyl ester (TMRM), which accumulates proportionally to $\Delta\Psi$ in the mitochondria. All complexes led to a significant decrease of $\Delta\Psi$ with the parent complexes **1** and **2** slightly more so than their alkyne-tagged derivatives **6** and **7** (Fig. 6). A reduced $\Delta\Psi$ lowers the amount of TMRM accumulating inside the mitochondria and consequently leads to a reduced fluorescence signal. Disruptions of the mitochondrial functionality often lead to an increase of cellular ROS levels, which play a pivotal role in cellular signaling, up to the point where they can activate p21, causing a G1-arrest and an upstream activation of p53.^{27,28} Typical intracellular sources of ROS are peroxisomes, which are relevant to the oxidative metabolism of long-chained fatty acids. During this metabolic pathway H₂O₂ is formed as a side product. Furthermore, mitochondria are a main source of intracellular ROS due to the mitochondrial respiratory chain.^{28,29} Cancer cells in general show elevated levels of ROS due to their increased proliferation rate and thus are prone to ROS-induced cell death.³⁰ Therefore, effects of all four complexes on the intracellular ROS level of 518A2 melanoma cells were determined, using the fluorescent

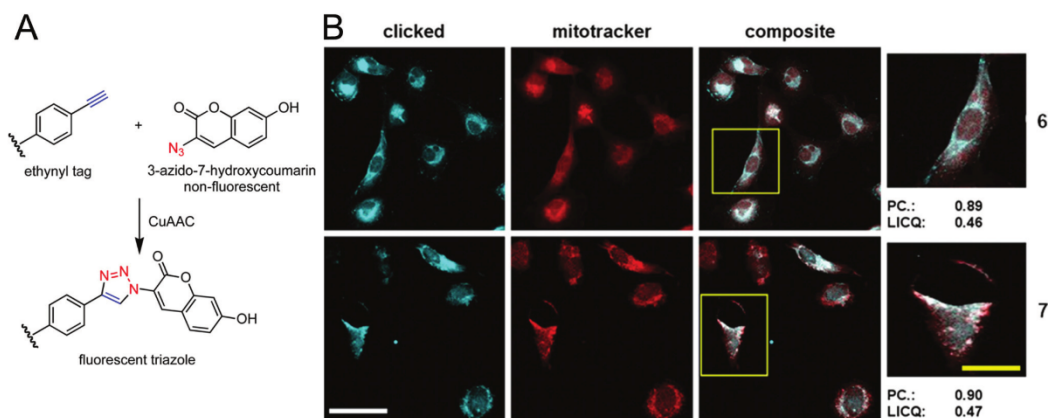


Fig. 5 A: Schematic copper(i)-catalysed 1,3-dipolar azide–alkyne cycloaddition (CuAAC; click reaction) of ethynyl-substituted complexes **6** or **7** with 3-azido-7-hydroxycoumarin in a mixture of CuSO_4 and ascorbic acid in BSA buffer to give turquoise fluorescent triazoles. B: Localisation of complexes **6** and **7** in 518A2 melanoma cells visualized via click reaction (turquoise) and documented by confocal fluorescence microscopy and co-staining of the mitochondria with Mitotracker™ (red) 30 min after incubation with 30 μM of the complexes. Pearson's coefficient (PC) and Li's colocalisation quotient (LICQ) were calculated for the marked cells (yellow box), using imageJ and JaCoP.^{13,14} Scale: white: 50 μm , yellow 25 μm .

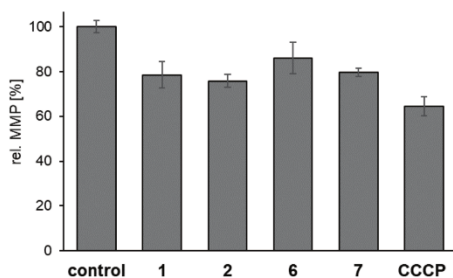


Fig. 6 Relative MMP $\Delta\Psi$ of 518A2 melanoma cells, determined by fluorescence of the cationic lipophilic dye TMRM, after treatment with complexes **1**, **2**, **6**, and **7** (each 10 μM , 1 h). Carbonyl cyanide *m*-chlorophenylhydrazone (CCCP, 10 μM) was used as a positive control and DMF treated negative controls were set to 100%. Means \pm SDs were calculated from three independent experiments.

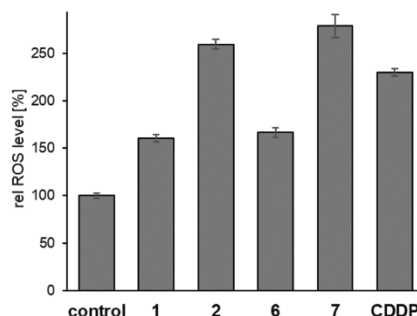


Fig. 7 Increase of the intracellular ROS levels of 518A2 melanoma cells, measured with DCFH-DA assays, after 1 h incubation at 37 $^{\circ}\text{C}$ with 10 μM of **1**, **2**, **6**, **7** or CDDP as a positive control. DMF was used as a negative control. Means \pm SD were calculated from three independent experiments.

dye DCFH-DA, which is converted inside the cells to a non-fluorescent dye, while in the presence of ROS it is oxidized to highly fluorescent dichlorofluorescein. Treatment with each of the complexes **1**, **2**, **6** or **7** led to an increase in the ROS level which was most pronounced for the cationic complexes **2** and **7** (Fig. 7), in keeping with the greater cellular uptake of complex **2** when compared with that of neutral complex **1**. Within the two pairs of corresponding un-tagged and alkyne-tagged complexes **1/6** and **2/7**, the ROS promoting effect of the respective alkyne derivative, *i.e.* **6** or **7**, was slightly greater than that of the corresponding untagged complex, *i.e.* **1** or **2**. The ROS level elevation by the neutral complexes **1** and **6** was obviously insufficient to cause a G1 arrest, typical of ROS induced cellular death,^{22,23} as shown in Fig. 4.

Effects on the cytoskeleton. Changes in cell cycle progression, mitochondrial function, and ROS levels are often associated with changes in the structure of different components of the cytoskeleton. *Via* immunofluorescence staining of the microtubules and actin filaments of 518A2 melanoma cells the effects of the complexes **1**, **2**, **6**, and **7** on these cytoskeletal components were investigated. All complexes induced visible changes in the cytoskeleton of 518A2 melanoma cells (Fig. 8). In comparison to cells treated with DMF only, cells treated with 3 μM or 6 μM of complex **1** showed stress fibre formation throughout the cells and beginning decomposition of the actin filaments. The microtubules appeared slightly more diffuse than in the negative control and protruding more from

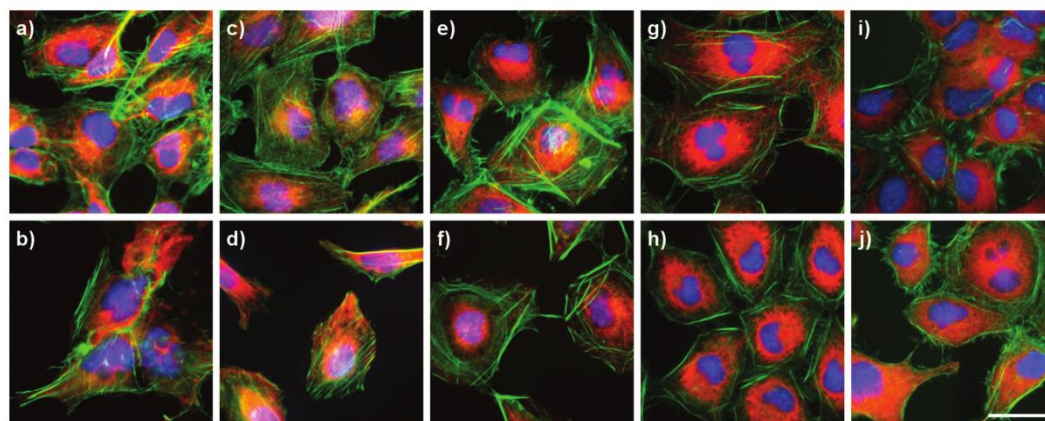


Fig. 8 Fluorescence staining of the nuclei (DAPI, blue), F-actin (Acti-stain™, green) and microtubules (Alexa Fluor 546, red) of 518A2 melanoma cells after 24 h of incubation with (a) DMF as control, (b) combretastatin-A4 as a positive control (25 nM), (c) **1** (3 μ M), (d) **1** (6 μ M), (e) **2** (400 nM), (f) **2** (800 nM), (g) **6** (3 μ M), (h) **6** (6 μ M), (i) **7** (500 nM), (j) **7** (1 μ M). Scalebar: 30 μ m. Images shown are representative of at least four independent experiments.

a point near the nucleus (Fig. 8c and d). Complex **2** led to similar changes in the cytoskeleton already at nanomolar concentrations. The tubulin network appeared to be even more concentrated around the nucleus and the actin stress fibre filaments formed thick bundles beneath the cell walls, almost tracing the cell membrane (Fig. 8e and f). The effects of complexes **6** and **7** largely resembled those of their analogues **1** and **2** (Fig. 8g–j), although they showed no interaction with purified tubulin (Fig. S9†). Stress fibre formation is often linked to a ROS-induced G1-phase arrest of the cell cycle,²⁸ as observed for complexes **2** and **7** (Fig. 4). The less distinct stress fibre formation induced by complexes **1** and **6** is in line with their missing cell cycle arrest. Further downstream in the mechanism of action, a strong cytoskeletal disruption is likely to accelerate the activation of caspase-3, resulting in cell apoptosis.³¹

Caspase-3/-7 mediated apoptosis induction. Since any deregulation of the mitochondrial function, as that ascertained for complexes **1**, **2**, **6** and **7** may trigger cytochrome c release and thus eventually apoptosis,³² these complexes were also investigated for their ability to activate the effector caspases-3 and -7 (Fig. 9) by means of a fluorescence based caspase-3/-7 assay. While the neutral complexes **1** and **6** did not induce the activation of caspases-3/-7, complex **2** almost quadrupled and complex **7** more than doubled the amount of active caspases, surpassing the positive control staurosporine, albeit only in a concentration nearly ten times its IC_{50} (72 h). The lack of caspase-3/-7 induction by complexes **1** and **6** fits in well with the lower uptake of **1** and the lower ROS production rates by complexes **1** and **6** in 518A2 melanoma cells and with their missing interference with their cell cycle. Maybe, complexes **1** and **6** induce cell death *via* a caspase-independent mitochondria-associated pathway.³³

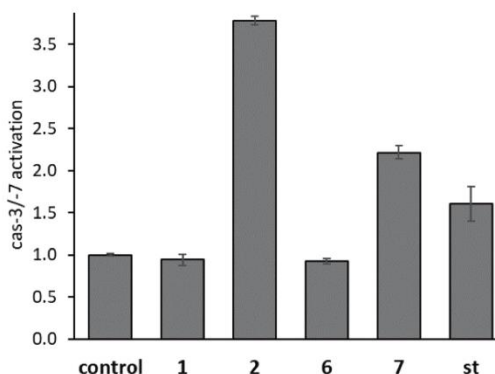


Fig. 9 Activation of caspases-3/-7 in 518A2 melanoma cells after 4 h of incubation with 10 μ M of **1**, **2**, **6** and **7** or 2 μ M staurosporine (st) as a positive control in comparison DMF as a negative control, measured using the Apo-ONE® homogenous caspase-3/7 assay kit (Promega). Values were corrected for the cell viability as obtained from MTT assays (>80% for all experiments). Means \pm SD were calculated from three independent experiments.

Materials and methods

Chemical synthesis

General. All chemicals and reagents were purchased from Sigma Aldrich, Fluka, Merck, Acros Alfa Aesar, or ABCR and were used without further purification. Melting points are uncorrected; NMR spectra were run on a 500 MHz spectrometer; chemical shifts are given in ppm (δ) and referenced relative to the internal solvent signal; ^{195}Pt NMR shifts are quoted relative to $\Xi(^{195}\text{Pt}) = 21.496784$ MHz, K_2PtCl_4 was used

as external standard ($\delta = -1612.81$); for ^{31}P NMR spectra H_3PO_4 was used as an external standard; mass spectra: direct inlet, EI, 70 eV; absorbance and fluorescence measurements: Tecan F200; flow cytometry: Beckman Coulter Cytomics FC 500, fluorescence microscopy: Zeiss Axioplan 2 and Leica Confocal TCS SP5.

1-(Bromomethyl)-4-ethynylbenzene (4). Under dry conditions and an argon atmosphere, 4-ethynylbenzyl alcohol **3** (400 mg, 3.03 mmol) in dry CH_2Cl_2 (30 mL) was treated with *N*-bromosuccinimide (1.078 g, 6.05 mmol, 2 eq.) and PPh_3 (1.588 g, 6.05 mmol, 2 equiv.) After stirring for 3 h at 40 °C the mixture was poured on water (100 mL) and the aqueous phase was extracted with CH_2Cl_2 . The combined organic layers were washed with brine, dried with Na_2SO_4 and evaporated. The product was purified by column chromatography (SiO_2 , hexane/ethyl acetate 2:1). Yield: 564 mg (2.89 mmol, 96%), yellow oil. ^1H NMR (500 MHz, CDCl_3): δ 3.11 (s, 1 H, $\text{C}\equiv\text{CH}$), 4.48 (s, 2 H, CH_2), 7.36 (d, $J = 8.2$ Hz, 2 H, *m*-Ph), 7.47 (d, $J = 7.9$ Hz, 2 H, *o*-Ph); ^{13}C NMR (125 MHz, CDCl_3): δ 32.7 (CH_2), 78.0 (C_q), 83.1 (C_q), 122.2 (C_q), 129.0 (Ar), 132.5 (Ar), 138.4 (C_q).

1,3-Di(4-ethynylbenzyl)imidazolium bromide (5a). A mixture of **4** (564 mg, 2.89 mmol, 2.3 equiv.), imidazole (85.6 mg, 1.26 mmol), K_2CO_3 (174 mg, 1.26 mmol, 1 equiv.), and acetonitrile (25 mL) was stirred for 17 h at 80 °C. After evaporation of the solvent the residue was taken up in CH_2Cl_2 , washed with water and dried over Na_2SO_4 . The product was precipitated by adding hexane. Yield: 477 mg (1.26 mmol, 100%), amber solid of m.p. 232 °C. ^1H NMR (500 MHz, $\text{DMSO}-d_6$): δ 4.28 (s, 2 H, $\text{C}\equiv\text{CH}$), 5.46 (s, 4 H, CH_2), 7.43 (d, $J = 8.2$ Hz, 4 H, *m*-Ph), 7.54 (d, $J = 8.2$ Hz, 4 H, *o*-Ph), 7.84 (d, $J = 1.5$ Hz, 2 H, Imi-4,5), 9.39 (s, 1 H, 2-H); ^{13}C NMR (125 MHz, CDCl_3): δ 51.7 (CH_2), 81.8 (C_q), 82.9 (C_q), 122.2 (C_q), 123.0 (Imi-4,5), 128.7 (Ar), 132.3 (Ar), 135.4 (Imi-2), 136.6 (C_q); *m/z* (EI): 297, 182, 115.

1,3-Di(4-ethynylbenzyl)imidazolium chloride (5b). To **5a** (115 mg, 305 μmol) in ethanol (6 mL) were added Ag_2CO_3 (96 mg, 348 μmol , 1.14 equiv.) and three drops HNO_3 (65%). After stirring for 3.5 h at room temperature the silver halides were filtered off and the filtrate was treated with HCl (75 μL , 2.3 equiv.), neutralized with NaHCO_3 and filtered again. After removal of the solvent, desolving of the residue in CH_2Cl_2 and another filtration step, the product was precipitated with hexane. Yield: 69 mg (207 μmol , 68%); colorless solid. ^1H NMR (500 MHz, $\text{DMSO}-d_6$): δ 4.28 (2 H, s, $\text{C}\equiv\text{CH}$), 5.44 (4 H, s, $\text{N}-\text{CH}_2$), 7.42 (4 H, d, $J = 8$ Hz, *m*-Ph), 7.54 (4 H, d, $J = 8$ Hz, *o*-Ph), 7.83 (2 H, d, $J = 2$ Hz, 4,5-H), 9.36 (1 H, s, 2-H).

***cis*-[Dichlorido-bis(1,3-di(4-ethynylbenzyl)imidazol-2-ylidene)]platinum(II) (6).** A solution of *cis*- $[\text{Pt}^{\text{II}}\text{Cl}_2(\text{DMSO})_2]$ (39 mg, 90 μmol) and 1,3-di(4-ethynylbenzyl)imidazolium chloride (69 mg, 207 μmol , 2.3 equiv.) in dry CH_2Cl_2 (10 mL) under argon atmosphere was treated with KO^tBu (30 mg, 270 μmol , 3 equiv.). After stirring for 24 h at room temperature, the solution was filtered to remove solid by-products, the filtrate was concentrated *in vacuo*, and the remaining solid was first crystallized from $\text{CH}_2\text{Cl}_2/\text{Et}_2\text{O}$ and then purified by column chromatography (silica gel, $\text{CH}_2\text{Cl}_2 + 1\% \rightarrow 2.5\%$ methanol). Yield:

31 mg (36 μmol , 40%); colorless solid of m.p. >360 °C (dec.). Elemental analysis (%): calc. for $\text{C}_{42}\text{H}_{34}\text{N}_4\text{Cl}_2\text{Pt}$ (860.75): C, 58.61; H, 3.98; N, 6.51. Found: C, 58.47; H, 4.19; N, 5.94. ^1H NMR (500 MHz, $\text{DMSO}-d_6$): δ 4.20 (4 H, s, $\text{C}\equiv\text{CH}$), 5.22 (4 H, d, $J = 15.3$ Hz, CH_2), 5.85 (4 H, d, $J = 15.3$ Hz, CH_2), 6.95 (4 H, s, Imi), 7.24 (8 H, d, $J = 8.2$ Hz, Ar), 7.43 (8 H, d, $J = 8.2$ Hz, Ar); ^{13}C NMR (125 MHz, $\text{DMSO}-d_6$): δ 52.5 (CH_2), 81.2 ($\text{C}\equiv\text{CH}$), 83.2 (C_q), 121.2 (C_q), 121.7 (Imi), 127.9 (Ar), 131.9 (Ar), 136.8 (C_q), 146.7 (NCN); ^{195}Pt NMR ($\text{DMSO}-d_6$): δ -3583 ppm; *m/z* (EI): 662, 648, 453, 312, 277, 115, 36.

***cis*-[Chlorido-bis(1,3-di(4-ethynylbenzyl)imidazol-2-ylidene)(triphenylphosphine)]platinum(II) chloride (7).** A solution of complex **6** (15 mg, 17.5 μmol) and triphenylphosphine (24 mg, 92 μmol , 5 equiv.) in CH_2Cl_2 /methanol (9 mL/1 mL) was stirred at room temperature for 72 h. The crude product was crystallized from $\text{CH}_2\text{Cl}_2/\text{Et}_2\text{O}$. Yield: 16 mg (14.3 μmol , 82%); colorless solid of m.p. 237 °C (dec.). ^1H NMR (500 MHz, $\text{DMSO}-d_6$): δ 4.25 (4 H, d, $J = 7.9$ Hz, $\text{C}\equiv\text{CH}$), 4.79 (2 H, d, $J = 15.7$ Hz, CH_2), 4.97 (2 H, d, $J = 15.1$ Hz, CH_2), 5.50 (2 H, d, $J = 15.7$ Hz, CH_2), 5.71 (2 H, d, $J = 15.1$ Hz, CH_2), 6.81 (4 H, d, $J = 7.9$ Hz, Imi), 7.08 (4 H, d, $J = 5.0$ Hz, Ar), 7.14 (4 H, d, $J = 7.9$ Hz, Ar), 7.30 (4 H, d, $J = 7.9$ Hz, Ar), 7.41–7.46 (16 H, m, Ar), 7.57 (3 H, t, $J = 6.6$ Hz, *p*- PPh_3); ^{13}C NMR (125 MHz, $\text{DMSO}-d_6$): δ 53.3 (CH_2), 53.6 (CH_2), 81.9 (C_q), 82.1 (C_q), 83.3 (C_q), 122.0 (C_q), 123.2 (Imi), 123.6 (Imi), 127.9 (Ar), 128.5 (Ar), 129.3 (d, $J = 55.4$ Hz, *P*-C), 129.4 (d, $J = 12$ Hz, PPh_3), 131.9 (Ar), 132.5 (d, $J = 12$ Hz, PPh_3), 134.3 (PPh_3), 135.3 (Ar- C_q), 136.6 (Ar- C_q), 145.8 (d, $J = 10$ Hz, $\text{NC}^{\text{cis}}\text{P}$), 163.2 (d, $J = 151$ Hz, $\text{NC}^{\text{trans}}\text{P}$); ^{31}P NMR ($\text{DMSO}-d_6$): δ 12.9 (s, $J = 2356$ Hz); ^{195}Pt NMR ($\text{DMSO}-d_6$): δ -4112 (d, $J = 2401$ Hz).

Biological evaluation

Cell culture conditions and stock solutions. The 518A2 melanoma cells (Department of Radiotherapy & Radiobiology, University Hospital Vienna, Austria), the HT-29 (DSMZ ACC-299), HCT116 (DSMZ ACC-581) colon carcinoma cells, the EaHy926 (ATCC CRL-2922) endothelial cells, the HDFa (ATCC® PCS-201-012™) human dermal fibroblasts, the Kb-V1 (DSMZ ACC-149) cervix carcinoma cells were cultivated in Dulbeccos Modified Eagle Medium (Gibco, ThermoFisher), supplemented with 10% fetal bovine serum (Biocrom) and 1% Antibiotic-Antimycotic (Gibco, ThermoFisher) at 37 °C, 95% humidity and 5% CO_2 . For a stable multi-drug resistance the Kb-V1 cells were treated regularly with 340 nM vinblastine. The platinum complexes used in the biological assays were dissolved in DMF (10 mM) and freshly diluted appropriately with sterile water. If not indicated otherwise all incubation steps of the bioassays were conducted under cell culture conditions.

Inhibition of cell growth (MTT assay).³⁴ Via the MTT (3-(4,5-dimethylthiazol-2-yl)-2,5-diphenyltetrazolium bromide, Glentham life sciences) based proliferation assay, the complexes **1**, **2**, **6** and **7** were investigated for their anti-proliferative effect on the aforementioned cell lines. Cells were seeded at 0.05×10^6 cells per mL (cpm) or at 0.1×10^6 cpm (HDFa) into the wells of 96-well microtiter plates (100 μL per well) and

incubated for 24 h. Appropriate dilutions in H₂O of the complexes or equal amounts of the solvent were added into the wells (final concentrations 100 μ M–5 nM) and the cells were further incubated for 72 h. Before staining of the viable cells the plates were centrifuged (300g, 5 min, 4 °C) and the old medium was discarded. 50 μ L of a 0.05% MTT solution (PBS) were added to each well. Subsequent to another 2 h of incubation the plates were centrifuged as before and the MTT solution was discarded again. To dissolve the cells and the formed violet water-insoluble formazan, 25 μ L of an SDS/DMSO solution (10%, 0.6% AcOH) were added to each well and the plates were further incubated for at least 1 h. The absorbances at 570 nm (formazan) and at 630 nm (background) were measured. The absorbance of formazan is directly linked to the amount of metabolically active (viable) cells in the wells. The absorbance of the wells treated with the solvent was set to 100% viable cells, and the percentage of viable cells in the wells treated with the platinum complexes was calculated accordingly. IC₅₀ values were determined using Graphpad Prism, means and SD were calculated from four independent experiments.

Uptake into 518A2 melanoma cells via ICP-MS. 518A2 melanoma cells were seeded at a density of 2×10^6 cells per dish and grown overnight. The cells were treated with **1** or **2** at final concentrations of 1 μ M and 5 μ M for 8 hours. The cells were harvested, washed twice with PBS, counted and pelleted. Cell pellets were lysed using the microwave digestion system (MARS5, CEM) with HCl. The platinum content was determined with ICP-MS.

Ethidium bromide saturation assay (EtdBr assay). The DNA interaction of **1** and **2** with linear salmon sperm DNA (ThermoFisher) was investigated utilizing the increase of fluorescence upon intercalation of ethidium bromide between the bases of DNA.³⁵ Alterations of the DNA structure by, e.g. small molecules change the ethidium bromide fluorescence. 1 μ g of salmon sperm DNA in TE-buffer (Tris/HCl 10 mM, EDTA 1 mM, pH 8.0) was treated with 5 μ M, 10 μ M, 25 μ M, 50 μ M or the solvent (equal to 50 μ M) for 2 h at 37 °C inside the wells of a 96-well black well plate. EtdBr-DNA adduct fluorescence was measured at λ_{ex} = 535 nm and λ_{em} = 595 nm. The background fluorescence was measured from samples prepared analogously but without the DNA and was subtracted from the sample values. Changes in the fluorescence intensity of the wells containing the DNA treated with the compounds were calculated in relation to the fluorescence of the wells treated with the solvent (set to 100%). Means and SD were calculated from triplicates.

Cell cycle analysis. The effects of **1**, **2**, **6** and **7** on the cell cycle progression of 518A2 melanoma cells were investigated via flow cytometry. 518A2 cells were seeded into the wells of 6-well microtiter plates (0.05×10^6 cpm, 3 mL per well). After an incubation period of 24 h appropriate dilutions of the test complexes or the solvent were added into the wells to give final concentrations of 5 μ M (**1**, **6**), 500 nM (**2**, **7**) or 2 μ M (CDDP). After 24 h of incubation the medium of each well was transferred into precooled centrifugation tubes (on ice) and the

cells were washed with 1 mL PBS. After trypsination (500 μ L per well) the cells were transferred into the respective tube and the wells were washed multiple times with PBS to transfer the remaining cells as well. The cells were pelleted by centrifugation (300g, 5 min, 4 °C). The pellet was resuspended with 1 mL ice-cold EtOH (70%) and the cells were fixed for at least 1 h on ice. The cellular DNA was stained with propidium iodide (PI) buffer (50 μ g mL⁻¹ PI, 0.1% sodium citrate, 50 μ g mL⁻¹ RNase A, freshly added) for 30 min at 37 °C before, depending on pellet size, 300–500 μ L PBS were added. The PI fluorescence, *i.e.* the amount of DNA inside the cells, was measured via flow cytometry. Using the CXP analysis software, provided by Beckman Coulter, the distribution of the cell population of each well between the phases of the cell cycle (G1, S, G2/M, sub-G1) was determined. Means and SD were calculated from triplicates.

Colocalisation. 518A2 cells (0.05×10^6 cpm) were seeded onto cover slips (borosilicate glass, Carl Roth) inside the wells of 24-well microtiter plates (0.5 mL per well) and incubated for 24 h. The medium was removed and the cells were washed once with 1 mL PBS before 500 μ L (250 nM in FBS-free DMEM) of Mitotracker™ Red CM-H₂Xros (ThermoFisher Scientific) were added into each well and the cells were incubated for 30 min at 37 °C. The staining solution was discarded and the cells were washed twice with 1 mL PBS before they were overlaid with complete DMEM medium (500 μ L per well). The cells were treated with **6** or **7** at a final concentration of 30 μ M for 30 min at 37 °C before fixation, blocking and permeabilization was done analogously to the fluorescence staining of the cytoskeleton. 200 μ L of click working solution (2 mM CuSO₄, 5 mM sodium ascorbate, 0.1 mM 3-azido-7-hydroxycoumarin, 1% BSA in PBS) were added into each well. The cells were incubated for 30 min at RT in the dark before the click solution was discarded and the cells were washed three times with 1% BSA in PBS for 5 min. The coverslips were embedded in mowiol mounting medium. Confocal fluorescence images were taken at 1 Airy and colocalisation parameters were calculated for one cell using the ImageJ Plugin JaCOP.^{13,14}

Mitochondrial membrane potential assay. For the examination of the effect on the mitochondrial membrane potential (MMP) of complexes **1** and **2** the cationic dye tetramethylrhodamine methyl ester (TMRM) was used. TMRM accumulates in mitochondria in quantities proportional to the MMP. For the assay melanoma cells 518A2 (0.25×10^6 cpm) were seeded in a black 96-well plate (Brand pureGrade™) and a transparent 96-well plate, for corresponding MTT-assay (100 μ L per well), and incubated for 24 h. The medium was then replaced by standard assay buffer (80 mM NaCl, 75 mM KCl, 25 mM D-glucose, 25 mM HEPES, pH 7.4) (90 μ L per well). Test compounds in standard assay buffer were added (10 μ L per well) to obtain the desired final concentration. Carbonylcyanide *m*-chlorophenylhydrazone (CCCP), a known decoupling agent of oxidative phosphorylation, was used as a positive control, followed by an incubation period of 1 h. Then, a TMRM solution (2 μ M in standard assay buffer) was added (10 μ L per well) and cells were further incubated for

10 min at rt. Cells were washed three times with PBS (160 μ L per well), PBS was added (100 μ L per well) and the fluorescence of the TMRM remaining inside the cells was measured after 15 min (ex/em 535/590 nm). The fluorescence signal was standardized relative to the cell viability as determined by a concomitant MTT-assay.

Reactive oxygen species (ROS) assay. ROS were detected using the 2,7-dichlorofluorescein diacetate (DCFH-DA) assay which is based on the oxidation of the dye by ROS inside the cells to give the highly fluorescent 2,7-dichlorodihydrofluorescein. In case of oxidative stress, cellular levels of ROS rise and cause oxidative damages. Melanoma cells (518A2) were seeded in a black 96-well plate (0.1×10^6 cpm, 100 μ L per well) and incubated for 24 h under standard cell culture conditions. The medium was replaced by serum-free medium, containing DCFH-DA (20 μ M), followed by an incubation for 30 min. The cells were washed twice with PBS and fresh serum-free medium was added, before the cells were treated with test compounds **1** or **2** for 1 h. Solvent served as a negative, and hydrogen peroxide as a positive control. Next, the cells were washed twice with PBS, fresh PBS was added (100 μ L per well) and the fluorescence was measured (ex/em 485/535 nm). The fluorescence intensity values were corrected for the amount of viable cells as determined *via* MTT assays, and were calculated in relation to the control which was set as 100%.

Fluorescence staining. 518A2 (0.05×10^6 cpm) or EaHy926 (0.1×10^6 cpm) cells were seeded onto cover slips (borosilicate glass, Carl Roth) inside the wells of 24-well microtiter plates (0.5 mL per well) and incubated for 24 h. Dilutions of **1**, **2**, **6**, **7** or combretastatin-A4 in H_2O were added into each well and the cells were incubated for another 24 h. For fixation of the cells the medium was discarded and the cells were washed with 1 mL PBS (37 $^{\circ}C$) for 30 s, the cells were incubated with 3.7% formaldehyde (PBS) for 20 min at rt. The formaldehyde solution was removed, and the cells were washed three times with PBS (1 mL) to completely remove the formaldehyde as it could interfere with the fluorescence staining. Blocking and permeabilization of the cells was done with 500 μ L of 1% BSA in PBS (0.5% Triton X-100) for 30 min at rt. For staining of the microtubules, the cells inside each well were incubated with 200 μ L of 1% BSA in PBS containing the primary antibody mouse anti- α -tubulin (Invitrogen, 1:300) for 1 h at 37 $^{\circ}C$. The solution was discarded, and the wells were washed three times with 1 mL PBS before the secondary antibody goat anti-mouse Alexa Fluor 546 (Invitrogen, 1:300) was added (200 μ L per well, 1% BSA in PBS). After another incubation step (1 h) in the dark at rt the solution was discarded again, and the wells were washed three times with PBS (1 mL). For staining of the actin components of the cytoskeleton, cells were incubated with 200 μ L of 100 nM (PBS) of Acti-stainTM (Cytoskeleton) for 1 h in the dark at rt. The staining solution was discarded and the cells in each well were washed twice with 1 mL PBS and overlaid with 500 μ L sterile water before the coverslips were embedded in mowiol mounting medium (+1 μ g mL⁻¹ DAPI). The condition of the cytoskeleton was documented by fluorescence microscopy.

Caspases-3/-7 activation. Using the Apo-One[®] homogeneous caspase-3/-7 assay kit (Promega), complexes **1**, **2**, **6** and **7** were tested for their ability to activate the apoptosis-associated caspases-3 and -7. 518A2 melanoma cells were seeded at 0.1×10^6 cpm into the wells of a 96-black well plate (67.5 μ L per well) and the plate was incubated for 24 h under standard cell culture conditions. The cells were treated with 10 μ M of **1**, **2**, **6** and **7**, 2 μ M of the positive control staurosporine (st) or equivalent amounts of the solvent as negative control for 4 h at 37 $^{\circ}C$. The substrate (100 \times) was diluted in assay buffer, provided in the kit. The substrate dilution was added to the wells (75 μ L per well). After 2 h of incubation at rt in the dark the fluorescence of the processed substrate was measured at λ_{ex} = 499 nm and λ_{em} = 527 nm. A second microtiter plate was treated analogously for MTT assays.

Conclusions

The aim of this in-depth study was to identify the structural factors that govern the uptake rates and sites of accumulation in cancer cells, the molecular targets, and the modes of antitumoral action of two closely related *cis*-[bis(1,3-dibenzylimidazol-2-ylidene)Pt^{II}Cl(L)] complexes sharing the same lipophilic NHC ligands while differing in their overall charge (neutral vs. cationic) and the bulkiness of their secondary ligands (Cl₂ vs. Cl, PPh₃). Both complexes **1** (L = Cl) and **2** (L = PPh₃) interacted strongly with purified DNA *in vitro*, modifying its morphology in EMSA and ethidium bromide assays to a greater extent than cisplatin. The uptake into melanoma cells was significantly greater for complex **2** than for complex **1**, possibly because of its DLC character, or by being a substrate of the organic cation transporters (OCT). Surprisingly, their ethynyl-tagged analogues **6** and **7**, regardless of their initial charge, accumulated at the mitochondria rather than the nuclei of the melanoma cells, which might be due to their DLC character overriding the tendency of Pt(II) to form coordination complexes with DNA bases. All complexes **1**, **2**, **6** and **7** impaired the functionality of the mitochondria by decreasing their membrane potential and thus elevating the levels of reactive oxygen species. In the case of complexes **2** and **7**, but not **1** and **6**, with the lipophilicity and bulkiness of the PPh₃ residue being the discriminating factor, these effects are great enough to induce a G1-phase arrest of the melanoma cell cycle and a remodeling of the actin filaments to stress fibres. The elevated ROS levels are presumably also causative for the activation of caspase-3/-7 mediated apoptosis in the case of complexes **2** and **7**. Their consistently lower IC₅₀ values in MTT-assays against various cancer cell lines are in keeping with this mechanistic rationale.

The upshot of this study is that NHC-platinum(II) complexes may be used to selectively target mitochondria rather than nuclei and DNA, thus bypassing the notorious DNA-repair associated resistance against platinum tumour therapy.

Paper

Dalton Transactions

Conflicts of interest

There are no conflicts of interest.

Acknowledgements

R. S. thanks the Deutsche Forschungsgemeinschaft (DFG) for a grant (Scho 402/12-2), V. B. was supported by the Czech Science Foundation (grant 18-09502S). We thank Franziska Gillsch (University Bayreuth) for providing a new batch of complex 7.

Notes and references

- 1 (a) B. Rosenberg, L. Van Camp, J. E. Trosko, *et al.*, *Nature*, 1969, **222**, 385; (b) B. Rosenberg and L. Van Camp, *Cancer Res.*, 1970, **30**, 1799; (c) S. Dilruba and G. V. Kalayda, *Cancer Chemother. Pharmacol.*, 2016, **77**, 1103.
- 2 (a) S. Bellemin-Lapomnaz, *Eur. J. Inorg. Chem.*, 2020, **2020**, 10; (b) T. Zou, C.-N. Lok, P.-K. Wan, *et al.*, *Curr. Opin. Chem. Biol.*, 2018, **43**, 30.
- 3 J. K. Muenzner, T. Rehm, B. Biersack, *et al.*, *J. Med. Chem.*, 2015, **58**, 6283.
- 4 T. Rehm, M. Rothmund, J. K. Muenzner, *et al.*, *Dalton Trans.*, 2016, **45**, 15390.
- 5 T. Rehm, M. Rothmund, A. Bär, *et al.*, *Dalton Trans.*, 2018, **47**, 17367.
- 6 L. Yang, C. Chumsac, J. B. Kaplan, *et al.*, *Bioconjugate Chem.*, 2017, **28**, 2302.
- 7 (a) J. H. Price, A. N. Williamson, R. F. Schramm, *et al.*, *Inorg. Chem.*, 1972, **11**, 1280; (b) N. I. Dodoff, D. Koval-Demertzi, M. Kubiak, *et al.*, *Z. Naturforsch., B: J. Chem. Sci.*, 2006, **61**, 1110.
- 8 J. Chen, *Cold Spring Harbor Perspect. Med.*, 2016, **6**, a026104.
- 9 B. S. Cummings and R. G. Schnellmann, *J. Pharmacol. Exp. Ther.*, 2002, **302**, 8.
- 10 M. Gold, Y. Mujahid, K. Ahmed, *et al.*, *J. Biol. Inorg. Chem.*, 2019, **24**, 647.
- 11 A. Ghezzi, M. Aceto, C. Cassino, E. Gabano and D. Osella, *J. Inorg. Biochem.*, 2004, **98**, 73.
- 12 (a) J. Reedijk and P. H. Lohman, *Pharm. Weekbl., Sci.*, 1985, **7**, 173; (b) M. H. Hanigan and P. Devarajan, *Cancer Ther.*, 2003, **1**, 47.
- 13 M. D. Abramoff, P. J. Magalhães and S. J. Ram, *Biophotonics Int.*, 2004, **11**, 36.
- 14 S. Bolte and F. P. Cordelières, *J. Microsc.*, 2006, **224**, 213.
- 15 Z. Zhu, Z. Wang, C. Zhang, *et al.*, *Chem. Sci.*, 2019, **10**, 3089.
- 16 G. M. Tozer, C. Kanthou, C. S. Parkins, *et al.*, *Int. J. Exp. Pathol.*, 2002, **83**, 21.
- 17 L. Vincent, P. Kermani, L. M. Young, *et al.*, *J. Clin. Invest.*, 2005, **115**, 2992.
- 18 S. Trapp and R. Horobin, *Eur. Biophys. J.*, 2005, **34**, 959.
- 19 B. Bertrand and A. Casini, *Dalton Trans.*, 2014, **43**, 4209.
- 20 A. Casini and L. Messori, *Curr. Top. Med. Chem.*, 2011, **11**, 2647.
- 21 L. Oehninger, R. Rubbiani and I. Ott, *Dalton Trans.*, 2013, **42**, 3269.
- 22 S. J. Berners-Price and A. Filipovska, *Aust. J. Chem.*, 2008, **61**, 661.
- 23 C. I. Yeo, K. K. Ooi and E. R. T. Tiekink, *Molecules*, 2018, **23**, 1410.
- 24 S. B. Aher, P. N. Muskawar, K. Thenmozhi, *et al.*, *Eur. J. Med. Chem.*, 2014, **81**, 408.
- 25 J. S. Modica-Napolitano and J. R. Aprile, *Adv. Drug Delivery Rev.*, 2001, **49**, 63.
- 26 P. D. Boyer, B. Chance, L. Ernster, *et al.*, *Annu. Rev. Biochem.*, 1977, **46**, 955.
- 27 B. Liu, Y. Chen and D. K. St Clair, *Free Radicals Biol. Med.*, 2008, **44**, 1529.
- 28 J. Boonstra and J. A. Post, *Gene*, 2004, **337**, 1.
- 29 V. Adam-Vizi and C. Chinopoulos, *Trends Pharmacol. Sci.*, 2006, **27**, 639.
- 30 G.-Y. Liou and P. Storz, *Free Radical Res.*, 2010, **44**, 479.
- 31 Y. Yamazaki, M. Tsuruga, D. Zhou, *et al.*, *Exp. Cell Res.*, 2000, **259**, 64.
- 32 S. A. Lakhani, A. Masud, K. Kuida, *et al.*, *Science*, 2006, **311**, 847.
- 33 M. Donovan and T. G. Cotter, *Biochim. Biophys. Acta*, 2004, **1644**, 133.
- 34 T. Mosmann, *J. Immunol. Methods*, 1983, **65**, 55.
- 35 J.-B. Lepecq and C. Paoletti, *J. Mol. Biol.*, 1967, **27**, 87.

Electronic Supplementary Material (ESI) for Dalton Transactions.
This journal is © The Royal Society of Chemistry 2020

Supporting Information

Antitumoral effects of mitochondria-targeting neutral and cationic *cis*-[bis(1,3-dibenzylimidazol-2-ylidene)Cl(L)]Pt(II) complexes

Matthias Rothmund,¹ Sofia I. Bär,¹ Tobias Rehm,¹ Hana Kostrhunova,²
Victor Brabec,² Rainer Schobert^{1,*}

[1] Organic Chemistry Laboratory, University of Bayreuth, Universitätsstr. 30, 95447 Bayreuth, Germany

[2] Czech Academy of Sciences, Institute of Biophysics, Kralovopolká 135, CZ-61264, Czech Republic.

Table of content:

NMR spectra of 6 and 7 (Figures S1-S7)	S2
Uptake of 1 and 2 into 518A2 cells via ICP-MS	S5
Experimental procedure of electrophoretic mobility shift assays (EMSA)	
with complexes 1 , 2 , 6 , 7 and cisplatin	S6
Agarose gels of EMSA with 1 , 2 , 6 , 7 and cisplatin (Figure S8)	S6
Experimental procedure for tubulin polymerisation assay with 6 , 7 and CA-4	S7
Tubulin polymerisation assays with 6 , 7 and CA-4 (Figure S9)	S7

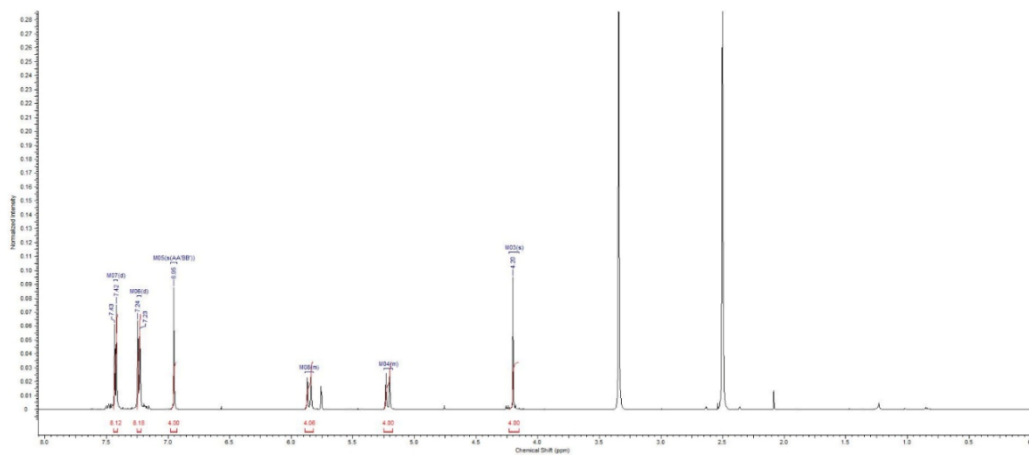


Figure S1. ^1H -NMR spectrum (500 MHz, $\text{DMSO-}d_6$) of complex **6**.

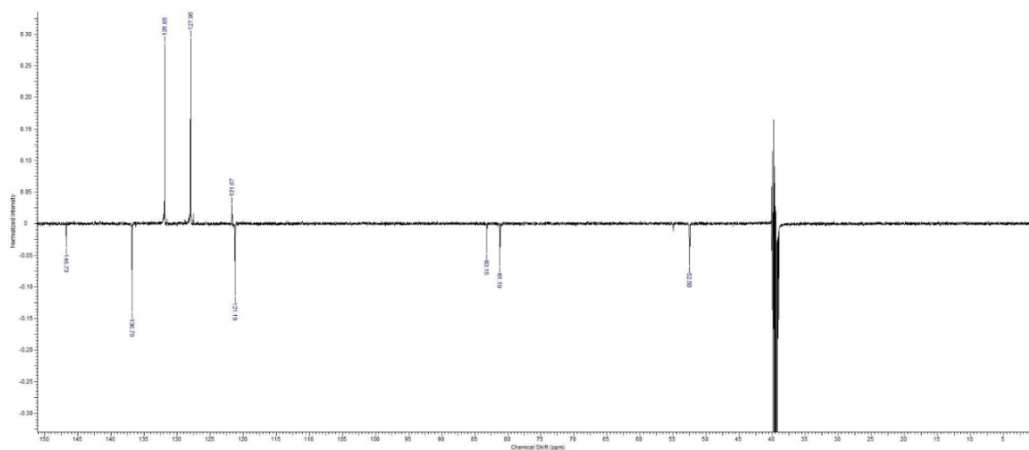


Figure S2. ^{13}C -NMR spectrum (125 MHz, $\text{DMSO}-d_6$) of complex **6**.

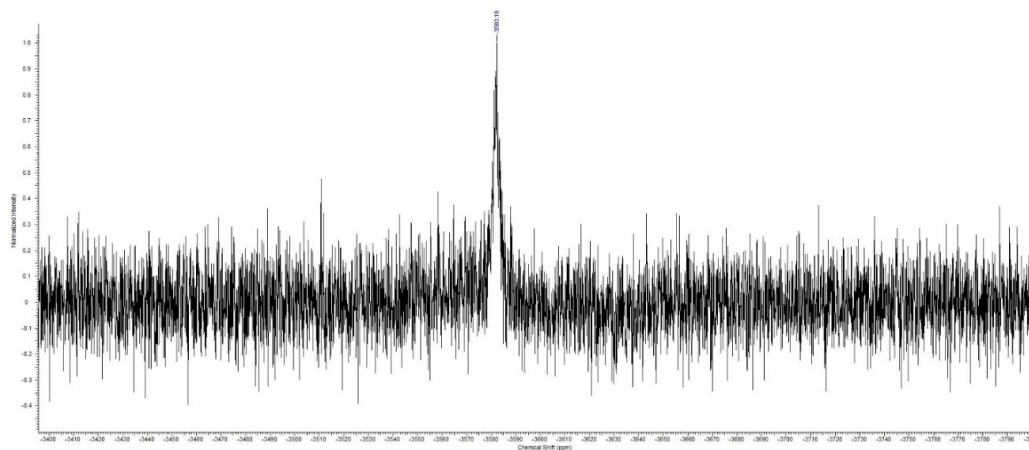


Figure S3. ^{195}Pt -NMR spectrum ($\text{DMSO}-d_6$) of complex 6.

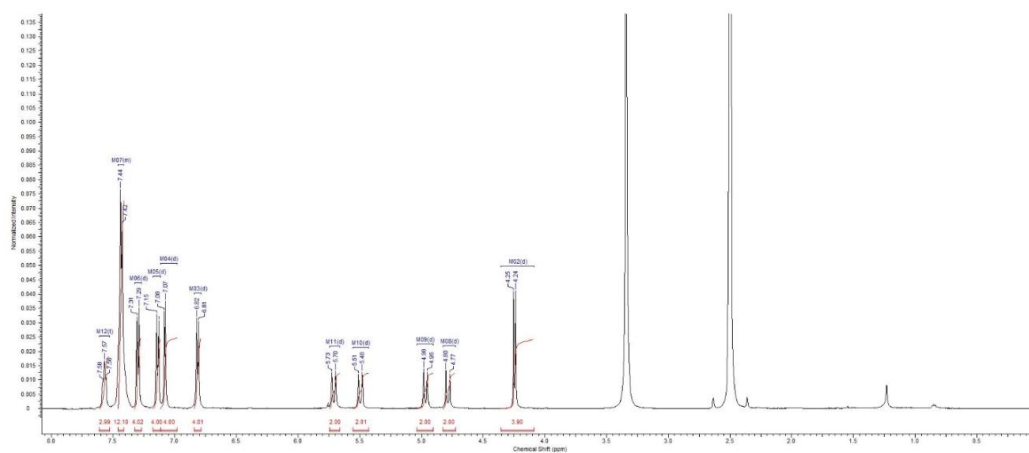


Figure S4. ^1H -NMR spectrum (500 MHz, $\text{DMSO}-d_6$) of complex 7.

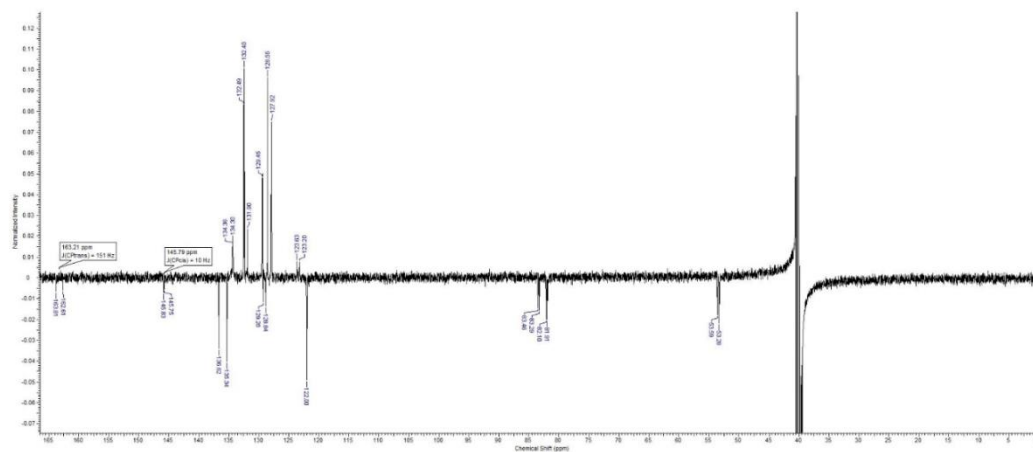


Figure S5. ^{13}C -NMR spectrum (125 MHz, $\text{DMSO-}d_6$) of complex 7.

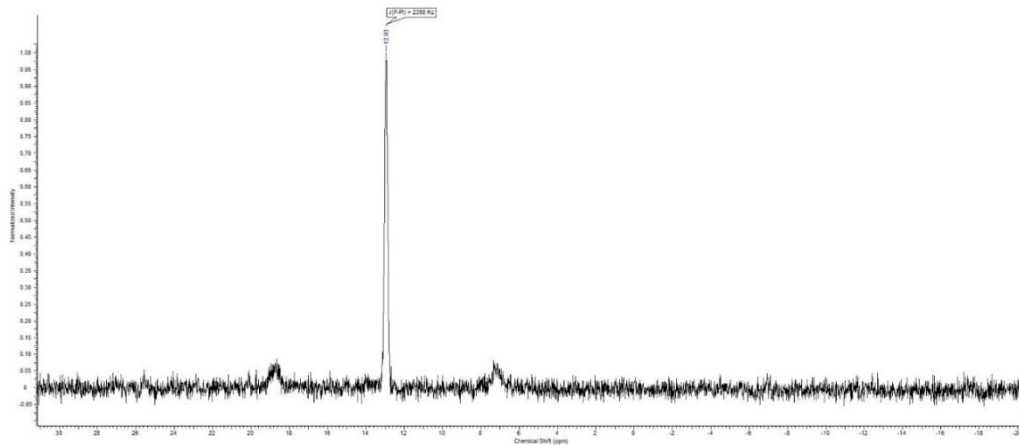


Figure S6. ^{31}P -NMR spectrum ($\text{DMSO-}d_6$) of complex 7.

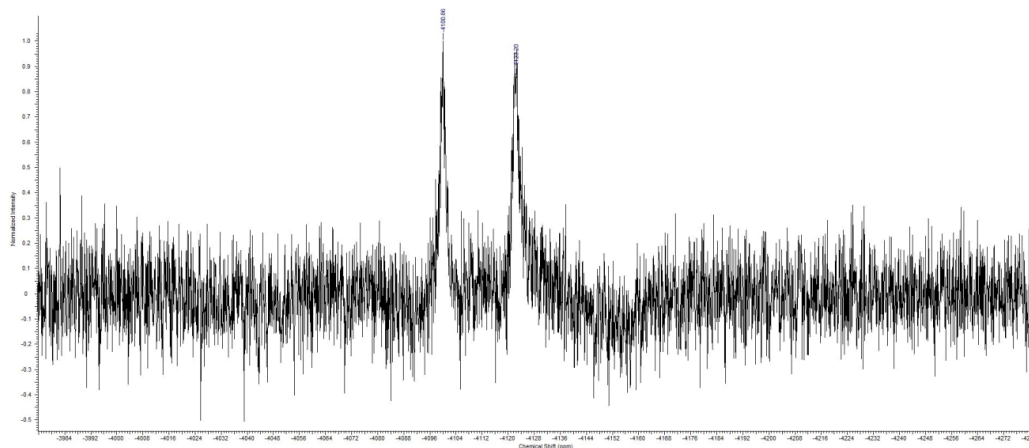


Figure S7. ^{195}Pt -NMR spectrum ($\text{DMSO-}d_6$) of complex 7.

Uptake of 1 and 2 into 518A2 cells via ICP-MS

Table S1. Uptake of 1 or 2 in 518A2 melanoma cells, after 8 h of incubation with 1 or 5 μM of the complexes.

	ng Pt/ 10^6 cells	
	1 μM	5 μM
1	17.4 ± 3.9	362 ± 33
2	124 ± 21	774 ± 83

Experimental procedure of electrophoretic mobility shift assays (EMSA) with complexes 1, 2, 6, 7 and cisplatin

The effects of **1**, **2**, **6**, and **7** on the topology of circular pBR322 plasmid DNA were investigated via EMSA. Changes in the running behaviour of the DNA bands during agarose gel electrophoresis indicate an interaction between the platinum complexes and the plasmid DNA, forcing it from the compact covalently closed circular (ccc) form into the bulkier open circular form. 1.5 µg of pBR322 plasmid DNA (> 90% in the ccc form, ThermoFisher) in TE-buffer (*cf.* EtdBr Assay) were treated with 0, 5, 10, 25 or 50 µM of the platinum complexes (final sample volume 20 µL) for 24 h at 37 °C. After addition of 5×DNA sample buffer (Tris/HCl 10 mM, 25% glycerine, bromphenol blue, pH 8.0, sterile filtered) agarose gelelectrophoresis (1% in Tris/HCl 4.5 mM, boracic acid 4.5 mM, EDTA 1.25 mM, pH 8.3) was run at 66 V for 4 h. DNA bands were stained for 30 min with EtdBr and documented with a UV transilluminator.

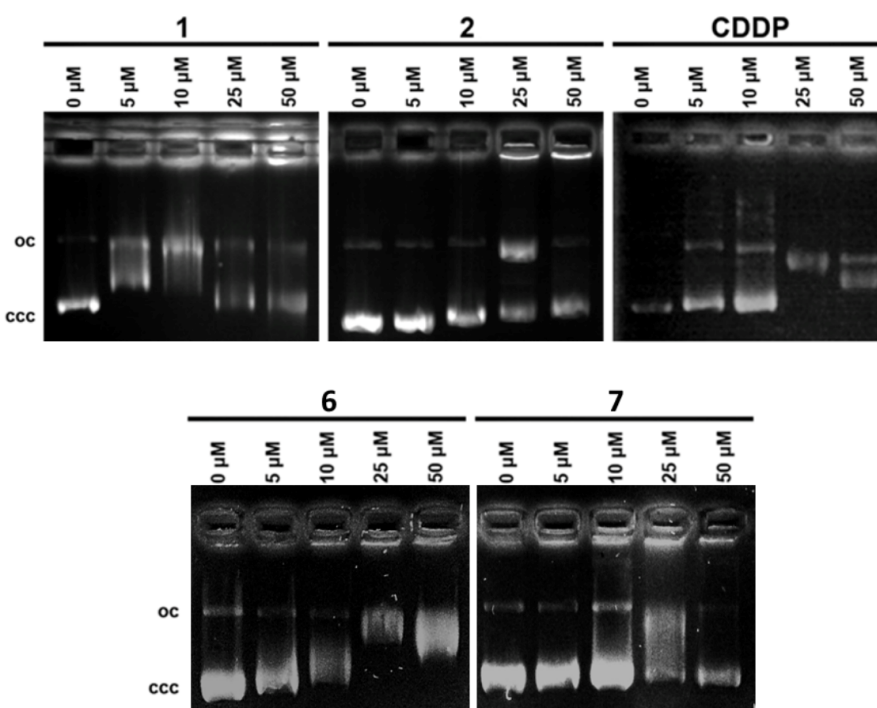
Agarose gels of EMSA with 1, 2, 6, 7 or cisplatin

Figure S8. Agarose gel of EMSA with pBR322 plasmid DNA after 24 h of incubation with **1**, **2**, **6**, **7** or cisplatin at 0, 5, 10, 25 or 50 µM.

Experimental procedure for tubulin polymerisation assays of 6, 7 and CA-4

The tubulin binding capacity of complexes **6**, **7** as well as of the known tubulin polymerisation inhibitor CA-4, which served as a control, was investigated using the tubulin polymerisation assay which was conducted in clear black 96-well plates (Brand). A 2-fold polymerisation buffer was freshly prepared by adding 20% glycerol and GTP (end concentration 3 mM) to BRB80-Buffer. To 50 μL /well 2-fold polymerisation buffer were added 11.1 μL of 10-fold substance solution and gently mixed. The corresponding solvent and combretastatin A4 served as controls. The microplate reader was pre-heated to 37 $^{\circ}\text{C}$ and 50 μL /well of purified pig brain solution was added. The progression of the optical density at 340 nm was observed in 20 sec intervals for at least 120 min, using a Tecan Microplate reader. The assay was conducted twice per compound and concentration, and mean values of each double determination were calculated. The values of the optical density were plotted against time in 5 min intervals.

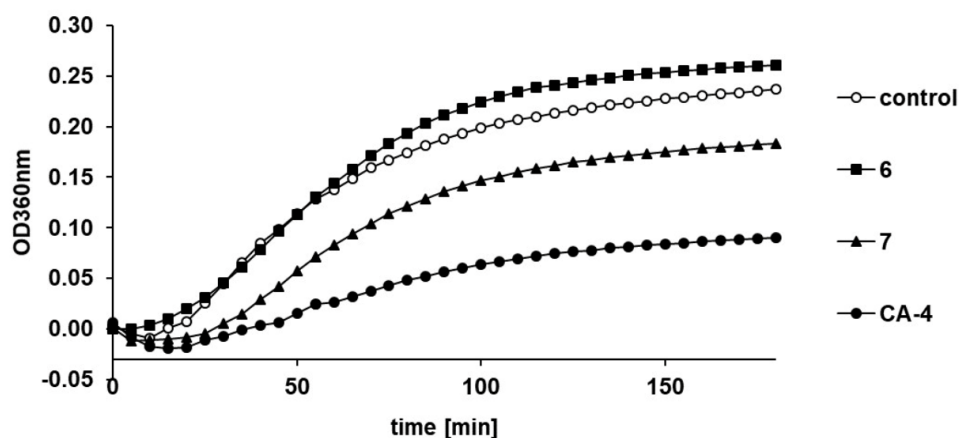
Tubulin polymerisation assays with 6, 7 and CA-4

Figure S9. Progression of polymerisation of purified tubulin monomers in response to treatment with 10 μM each of complexes **6** and **7** and combretastatin A4 for 3 h; mean values of double determinations

5.4 Publikation III

N,N-Dialkylbenzimidazol-2-ylidene platinum complexes - effects of alkyl residues and acillary *cis*-ligands on anticancer activity

*Tobias Rehm,^{‡a} Matthias Rothmund,^{‡a} Alexander Bär,^a Thomas Dietel,^b Rhett Kempe,^b Hana Kostrhunova,^c Viktor Brabec,^c Jana Kasparkova,^{*c} und Rainer Schobert^{*a}*

^aDepartment of Chemistry, University Bayreuth, Universitaetsstr. 30, 95440 Bayreuth, Germany

^bLehrstuhl fuer Anorganische Chemie II, University Bayreuth, Universitaetstr. 30, 95440 Bayreuth, Germany

^cInstitute of Biophysics, Academy of Sciences of the Czech Republic, CZ-61265 brno, Czech Republic

*e-mail: Rainer.Schobert@uni-bayreuth.de; jana@ibp.cz

[‡] These authors contributed equally to this work

Dalton Trans. 2018, 47, 17367 – 17381.



Cite this: *Dalton Trans.*, 2018, **47**, 17367

N,N-Dialkylbenzimidazol-2-ylidene platinum complexes – effects of alkyl residues and ancillary *cis*-ligands on anticancer activity†

Tobias Rehm,^{‡a} Matthias Rothmund,^{‡a} Alexander Bär,^a Thomas Dietel,^{id b} Rhett Kempe,^b Hana Kostrhunova,^{id c} Viktor Brabec,^{id c} Jana Kasparkova^{id *c} and Rainer Schobert^{id **a}

Eleven complexes of [(1,3-dialkylbenzimidazol-2-ylidene) L_n Cl $_{3-n}$] $Pt^{(n-1)+}$, with L_n = DMSO (**8**), Ph_3P (**9**), $(Ph_3P)_2$ (**10**), and alkyl = Me (**a**), Et (**b**), Bu (**c**), octyl (**d**), were synthesised and tested for cellular accumulation, cytotoxicity, interference with the tumour cell cycle, and interaction with DNA. The delocalised lipophilic cationic bisphosphane complexes **10** were on average found to be more cytotoxic in MTT assays against a panel of seven cancer cell lines than the neutral DMSO and monophosphane complexes **8** and **9**. The uptake of complexes **10**, at least into HCT116 colon carcinoma cells, was also significantly greater than that of analogues **8** and **9**. Their cytotoxicities did not differ significantly with the *N*-alkyl side chain length. The complexes that were most active, with sub-micromolar IC_{50} (72 h) values against HCT116^{wt} cells, that is **8b**, **9b**, **10a–c**, worked by a mode of action that was dependent on the functional p53, yet were still far more active than cisplatin in both of the HCT116^{wt} and HCT116^{−/−} variants. In detailed binding analyses **8c**, **9c** and **10a–c** showed a lower affinity to DNA and different binding modes when compared to cisplatin, preferably forming mono-adducts with DNA and distorting it to a lower extent. Also, unlike cisplatin, they arrested the HCT116 cells of both variants predominantly in the G1 phase.

Received 16th August 2018.
Accepted 13th November 2018
DOI: 10.1039/c8dt03360a

rsc.li/dalton

Introduction

Since its approval in 1979, cisplatin (**1**, CDDP) has established itself as the leading anti-cancer drug for several cancer entities. In nearly 40 years only six more approved platinum drugs have arisen from intensive scientific research. Although these drugs offer quite a few advantages over cisplatin, such as increased tumour specificity and reduced unwanted side effects, they are still hampered by their high toxicity and adverse effects in patients, as well as a tendency to elicit tumoral drug resistance.¹

A common strategy to overcome these negative effects is the variation of the spectator and the leaving ligands, for example,

in the case of cisplatin, the substitution of the ammine residues by mono- or bidentate amines and/or the exchange of the chlorido ligands by chelating carboxylic acids. Since the turn of the millennium, ever more diverse ligands with targeting functions or bioactivity of their own have been attached to Pt^{II} complexes and Pt^{IV} prodrugs.²

With the advent of the stable *N*-heterocyclic carbenes (NHCs), first being made accessible by Arduengo *et al.*,³ a genuinely new ligand motif became available that allowed the stereoelectronic fine-tuning of catalysts⁴ and the pharmacological optimisation of metallodrugs. Owing to their ease of synthesis, their structural variability and their chemical stability, *N*-heterocyclic carbene (NHC) complexes of metals⁵ as diverse as silver,⁶ gold,⁷ copper,⁸ ruthenium⁹ and platinum¹⁰ have become an ever-growing branch of medicinal chemistry.

N-Heterocyclic carbenes are often teamed up in square planar Pt^{II} complexes with other ligands such as amines,^{10a,b} pyridines^{10c} or pnictogen ligands^{10d,e} (PPh_3 , $AsPh_3$, $SbPh_3$). In the past, we have concentrated on Pt^{II} complexes carrying DMSO or phosphane ligands *cis* to benzylated imidazol-2-ylidene ligands, for example **2–4**.^{10d} We have also developed a protocol to introduce a second, optionally different, NHC ligand in the *cis*-position to the first one as shown in complex **5** (Fig. 1).¹¹ We have now found that complexes with *N*-alkylated

^aDepartment of Chemistry, University Bayreuth, Universitätsstrasse 30, 95440 Bayreuth, Germany. E-mail: Rainer.Schobert@uni-bayreuth.de

^bLehrstuhl fuer Anorganische Chemie II, University Bayreuth, Universitätsstrasse 30, 95440 Bayreuth, Germany

^cInstitute of Biophysics, Academy of Sciences of the Czech Republic, CZ-61265 Brno, Czech Republic. E-mail: jana@ibp.cz

† Electronic supplementary information (ESI) available: Ligand synthesis; NMR spectra; X-ray structural data, values for cellular accumulation, cell cycle analysis in HCT116 cells. CCDC 1857511–1857513. For ESI and crystallographic data in CIF or other electronic format see DOI: 10.1039/c8dt03360a

‡ These authors contributed equally to this work.

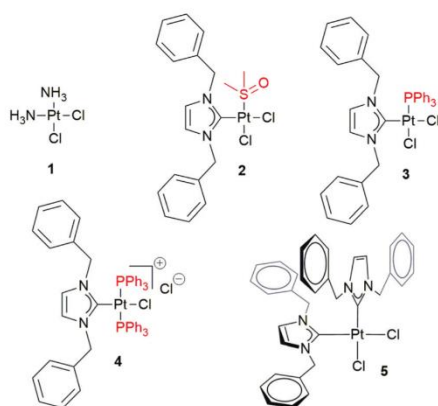


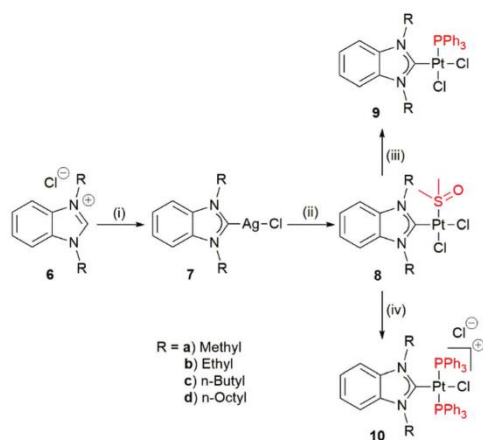
Fig. 1 Structures of cisplatin (1) and the NHC complexes 2–5.

benzimidazoles rather than imidazole ligands show some advantages, including a better solubility combined with chemical stability and the tendency to form easy to purify, and easy to weigh out, crystalline complexes. The aim of this study was to evaluate the influence of structural changes, for example the alkyl chain length, overall size, lipophilicity, and steric encumbrance of the benzimidazol-2-ylidene complexes of Pt^{II}, on the effects of the complexes on cancer cells. To this end, we synthesised the ligand precursors **6a–d** and their downstream complexes of types **8–10** (Scheme 1). By extending the length of the *N*-alkyl chain from the methyl to the ethyl, butyl and up to the octyl we gradually increased the size and lipophilicity of the NHC ligands and their respective platinum complexes. A comparison of the complex patterns *cis*-[Cl₂(NHC)(DMSO)Pt^{II}], *cis*-[Cl₂(NHC)(PPh₃)Pt^{II}] and *trans*-[Cl(NHC)(PPh₃)₂Pt^{II}Cl][−], analogous to 2–4, should allow a prediction of the influence of the lipophilicity, steric encumbrance, and charge on the biological properties of similar NHC-Pt^{II} anticancer drugs. Eleven such NHC-platinum(II) complexes with benzimidazol-2-ylidene ligands of varying size and lipophilicity were prepared and studied. Complex **10d** was inaccessible as it decomposed upon attempted isolation.

Results and discussion

Synthesis and characterisation

Benzimidazolium salts with methyl, ethyl, butyl, and octyl residues were obtained by treating benzimidazole with K₂CO₃ and either iodomethane, iodoethane, 1-bromobutane, or 1-bromooctane, respectively. They were converted to their chlorides **6a–d** to prevent anion exchange during the following steps. Treating them with Ag₂O in CH₂Cl₂ for at least 24 h afforded the NHC silver(I) complexes **7a–d** after filtration and crystallisation. As complex **7a** was poorly soluble it could not be separated from the silver residues and was therefore converted to the platinum complex **8a** without purification. The formation



Scheme 1 Synthesis of complexes **8a–d**, **9a–d** and **10a–c**. (i) Ag₂O, CH₂Cl₂, rt; (ii) K₂PtCl₄, DMSO, 60 °C; (iii) PPh₃, CH₂Cl₂; (iv) PPh₃, CH₂Cl₂, rt; **10c**: CH₃CN, 60 °C; **10d**: unstable, decomposed upon attempted isolation.

of the silver carbene complex **7d** took several days, probably owing to the bulkiness of its NHC ligand.

Transmetalation to the respective *cis*-[(NHC)(DMSO)Pt^{II}Cl₂] complexes **8** was achieved by adding the silver complexes **7** to K₂PtCl₄ in DMSO to give *cis*-Pt(DMSO)₂Cl₂ as a reactive intermediate. The crude silver complex **7a** of uncertain purity was treated only with 0.9 equivalents of K₂PtCl₄ to prevent contamination of the product complex **8a** by leftover *cis*-Pt(DMSO)₂Cl₂. After extraction and crystallisation all of the complexes of **8** were obtained in good yield and a purity sufficient for biochemical assessment.

For the synthesis of the phosphane complexes of types **9** and **10** we intended to apply the same protocols as for the preparation of the imidazol-2-ylidene analogues **3** and **4**. Complex **3** had been obtained by substitution of the labile DMSO ligand of complex **2** with 1.1 equivalents of PPh₃ in CH₂Cl₂ at room temperature within 90 min. The conversion of complex **2** to the cationic bisphosphane complex **4** required stirring with five equivalents of PPh₃ for 30 min. However, the benzimidazol-2-ylidene complexes **9** and **10** were not accessible in this way. When treated with 1.1 equivalents of PPh₃ only 50% of the DMSO complex **8a**, bearing a 1,3-dimethylbenzimidazol-2-ylidene ligand, reacted to afford the exclusively bisphosphane complex **10a**, but none of the monophosphane complex **9a**, which is obviously more reactive than **8a**. To prepare complex **9a** in an acceptable yield, a solution of PPh₃ was added slowly to a highly diluted solution of **8a**. The product was then separated and purified using column chromatography and crystallisation. When the sterically more hindered *N,N*-diethyl substituted analogue **8b** was reacted overnight with five equivalents of PPh₃, the monophosphane complex **9b** was isolated in good yield besides only trace amounts of the cationic bisphosphane complex **10b**. To gain

the latter in a moderate yield **8b** was stirred with 10 equivalents of PPh_3 for a full five days, followed by careful crystallisation. Unsurprisingly, the sterically even more hindered DMSO complex **8c**, bearing a 1,3-dibutylbenzimidazol-2-ylidene ligand, when reacted with 10 equivalents of PPh_3 for several days afforded the monophosphane complex **9c** exclusively. The cationic bisphosphane complex **10c** could be prepared in acceptable yield only by heating the DMSO complex **8c** with 20 equivalents of PPh_3 in acetonitrile at 80 °C for four days. Similarly, the DMSO complex **8d**, bearing a 1,3-dioctylbenzimidazol-2-ylidene ligand, reacted with five equivalents of PPh_3 in CH_2Cl_2 at room temperature for 16 h to give monophosphane complex **9d**. A second PPh_3 was incorporated only upon heating with a large excess of PPh_3 in acetonitrile at 80 °C. Attempts to isolate the bisphosphane complex **10d** always gave mixtures of **10d**, **9d** and PPh_3 . ^{31}P NMR spectra revealed that in solution, with an excess of phosphane, the signals for **9d** and PPh_3 at 9.1 ppm and -5.5 ppm, respectively, would disappear over time to generate more **10d** at 18.9 ppm, as shown in

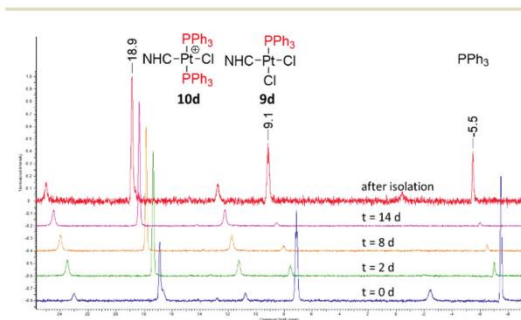


Fig. 2 ^{31}P NMR spectra of reactions over time between PPh_3 and **9d** to give **10d**, and for the decomposition products obtained upon attempts to isolate it from the "t = 14 d" sample.

Fig. 2. Repeated attempts to isolate the cationic product from such solutions, with only traces of **9d** and PPh_3 left, led to equilibrated mixtures again, or even pure **9d** in significant amounts. This indicates that **10d** is stable in solution only in the presence of an excess of PPh_3 and decomposes upon isolation. It was therefore not possible to purify this compound for biological studies.

The new Pt^{II} complexes **8**, **9** and **10** were characterised using ^1H , ^{13}C , ^{195}Pt and ^{31}P nuclear magnetic resonance (NMR) spectroscopy, as well as mass spectrometry and elemental analysis. Single crystal X-ray structure analyses were performed for complexes **8b**, **9c** and **10a** (Fig. 3).

The completion of the formation of the DMSO complexes **8** can be seen from the equivalent benzimidazole and DMSO signals in the ^1H NMR spectra. For **8b–d** the $\text{N}-\text{CH}_2$ protons of the side chains were inequivalent and gave rise to two sets of signals. As seen before with the benzylated imidazole ligands,^{10d} this confirms the *cis* configuration of the NHC and DMSO ligands as well as a perpendicular orientation of the benzimidazole relative to the plane spanned by the $\text{PtCl}_2(\text{DMSO})$ fragment. This effect recurs for **9b–d**, while the spectra of the symmetric complexes **10** show no inequivalent protons.

To monitor the formation of complexes **9** and **10** and to also verify their conformation, ^{31}P NMR spectroscopy is a convenient technique. The neutral complexes **9** exhibit a signal between 8.83 and 9.19 ppm with coupling constants ranging from 3861 to 3901 Hz. The cationic complexes **10** with two equivalent PPh_3 moieties show a signal between 17.7 and 18.9 ppm, coupling with a $J_{\text{P-Pt}} = 2478$ Hz to 2486 Hz typical of the *trans*-configured phosphanes.^{10d,e}

The same Pt–P couplings are present in the ^{195}Pt NMR spectra. Complexes **8a–d** give a singlet around -3554 to -3566 ppm, complexes **9** show the expected doublets at -4017 to -4018 ppm and **10** shows triplets at -4378 to -4383 ppm. With $J_{\text{Pt-P}} = 3871\text{--}3895$ Hz for **9** and $2486\text{--}2490$ Hz for **10** the

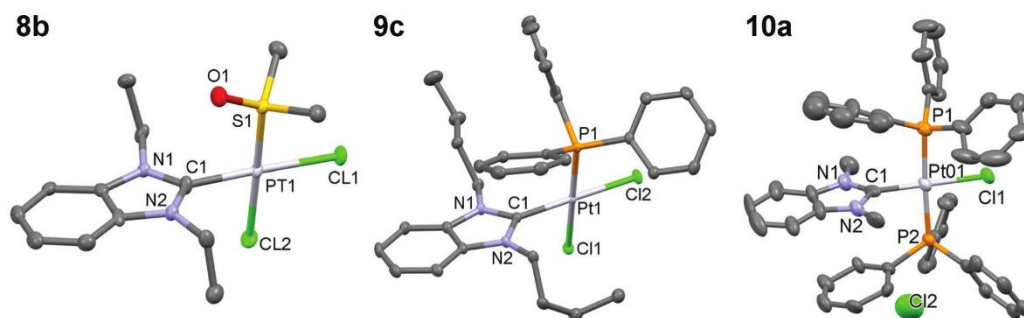


Fig. 3 Molecular structures of complexes **8b**, **9c** and **10a** as thermal ellipsoid representations at the 50% probability level (H atoms omitted). Selected bond lengths [Å] and angles [°]: **8b**: Pt1–Cl1 2.3447(19), Pt1–Cl2 2.332(2), Pt1–C1 1.983(7), Pt1–S1 2.202(2), Cl1–Pt1–Cl2 90.35(7), Cl1–Pt1–C1 177.6(2), Cl2–Pt1–C1 86.9(2), Cl2–Pt1–S1 178.84(7), C1–Pt1–S1 92.1(2), N1–C1–N2 107.7(6); **9c**: Pt1–C1 1.980(2), Pt1–P1 2.2345(8), Pt1–Cl1 2.3603(8), Pt1–Cl2 2.3480(8), C1–Pt1–P1 95.34(7), C1–Pt1–Cl1 86.76(7), C1–Pt1–Cl2 175.80(6), P1–Pt1–Cl1 175.686(19), P1–Pt1–Cl2 88.09(4), Cl1–Pt1–Cl2 89.65(3), N1–C1–N2 106.70(19); **10a**: Pt1–Cl1 2.349(3), Pt1–C1 1.959(10), Pt1–P1 2.309(3), Pt1–P2 2.311(3), C1–Pt1–Cl1 179.4(4), C1–Pt1–P1 92.2(3), C1–Pt1–P2 90.7(3), P1–Pt1–P2 176.87(10), P1–Pt1–Cl1 87.77(10), P2–Pt1–Cl1 89.33(9), N1–C1–N2 105.3(9).

coupling constants agree with those obtained from the ^{31}P NMR spectra and with the literature values of similar complexes.^{10d,e} In the ^{13}C NMR spectra the carbene signals are of special interest. They were found at around 154 ppm for complexes **8**, between 160.6 ppm and 162.0 ppm for **9**, and between 158.0 and 159.9 ppm for the cationic complexes **10**.

Crystallography

Crystals suitable for X-ray diffraction analyses were grown by slow infusion of hexane or diethyl ether into saturated solutions of **8b**, **9c** or **10a** in CH_2Cl_2 kept at 4 °C. Fig. 3 shows their molecular structures. The distances between the platinum and the carbene carbon atoms were in the range of 1.959 to 1.983 Å. The Pt–Cl distances lay between 2.347 to 2.349 Å for those *trans* to the NHC ligand, while the *cis* coordinated varied from 2.332 Å in the DMSO-complex **8b** to 2.360 Å in **9c** *trans* to a phosphine. In cationic **10a**, Pt–P distances were both around 2.31 Å, while in neutral **9c**, this was 2.234 Å and the Pt–S bond in **8b** was even shorter at 2.202 Å. The bond angles between the carbene and the *cis*-phosphine or DMSO ligand were slightly above 90° with a maximum of 95.3° for **9c**.

Cytotoxicity

The new benzimidazol-2-ylidene Pt^{II} complexes **8a–d**, **9a–d**, **10a–c**, and CDDP as a reference, were evaluated using a MTT-assays for their *in vitro* cytotoxicity against a panel of seven cancer cell lines of various entities, including a p53 knock-out mutant (HCT116^{−/−}) and the two multi-drug resistant (*mdr*) cell lines Kb-V1^{Vbl} and MCF-7^{Topo}. The complexes showed a structure-dependent cytotoxicity, with IC_{50} values ranging from inactive ($\text{IC}_{50} > 100 \mu\text{M}$) to low nanomolar (Table 1). A trend emerged with respect to the three complex types **8**, **9**, and **10**, reminiscent of that previously observed for the imidazol-2-ylidene complexes **2–4**.^{10d} Substitution of the DMSO ligand in complexes **8** by a PPh_3 ligand led to a slight increase of the overall cytotoxicity of the resulting complexes **9** in some cell

lines, while the addition of a second PPh_3 ligand, as seen in the cationic complexes **10**, gave rise to low nanomolar IC_{50} values against most cell lines. The efficacy of complexes **10** was superior to that of CDDP in all cell lines except for the resistant Kb-V1^{Vbl} cervix carcinoma cell line.

There was no clear trend for the effect of the *N*-alkyl side chain length on the cytotoxicity of the individual complex types **8**, **9**, and **10** over all of the tested cell lines. The neutral *N*-methyl derivatives **8a** and **9a** were inactive ($\text{IC}_{50} > 100 \mu\text{M}$) in all tested cell lines, while the lipophilic delocalised cation **10a** was highly active with low nanomolar IC_{50} values in all but the cervix carcinoma cell line. The *N*-ethyl substituted complex **8b** was the most active DMSO complex in all of the cell lines bar the 518A2 melanoma in which it was virtually inactive. Its high cytotoxicity in the slow-growing colon carcinoma cell lines DLD-1 and HCT116^{wt}, as well as in the re-sensitised cervix carcinoma cell line Kb-V1^{Vbl+Vpm}, is worthy of note. Elongation of the side chain as in **8c** and **8d** had no distinct effect.

Amongst the generally bigger and more lipophilic monophosphine complexes the *N*-ethyl substituted **9b** was roughly as active as its *N*-butyl analogue **9c** while complex **9d**, the biggest and most lipophilic, was distinctly less active. The delocalised lipophilic cations **10** were less affected by changes at their NHC ligands and showed similar IC_{50} values in the nanomolar range, or the low micromolar range in the case of complex **10c**.

Judging by their IC_{50} values, the complexes **8b–d**, **9b–d** and **10a–c** were as active against the *mdr* breast cancer cell line MCF-7^{Topo} as against all other cell lines, suggesting that they are not recognised as substrates by the breast cancer resistance protein (BCRP) which is overexpressed in this cell line.^{13a} In contrast, all of these complexes were conspicuously less effective against the *mdr* cervix carcinoma cell line Kb-V1^{Vbl} which overexpresses P-glycoprotein 1 (P-gp1), presumably because they are substrates of this efflux transporter.^{13b,c} To corroborate this assumption, the IC_{50} values were determined

Table 1 Mean \pm SD of IC_{50} (72 h) values [μM] of complexes **8**, **9**, **10a–c** and CDDP in MTT assays against human cancer cell lines^a as calculated from four independent measurements

Compounds	IC_{50} (72 h) [μM]								r^{p53} ^b
	518A2 ^a	HT-29 ^a	DLD-1 ^a	HCT116 ^{wt a}	HCT116 ^{−/− a}	MCF-7 ^{Topo a}	Kb-V1 ^{Vbl a}	Kb-V1 ^{Vbl+Vpm a}	
8a	>100	>100	>100	>100	n.d.	n.d.	n.d.	n.d.	—
8b	>50	8.6 \pm 1.7	0.24 \pm 0.03	0.12 \pm 0.01	5.9 \pm 0.5	6.5 \pm 1.6	25.2 \pm 0.6	0.28 \pm 0.06	−0.979
8c	7.6 \pm 0.2	29.4 \pm 0.9	12.7 \pm 0.9	8.1 \pm 0.7	6.0 \pm 0.2	10.1 \pm 0.3	21.2 \pm 0.5	0.25 \pm 0.09	0.356
8d	3.1 \pm 0.1	11.6 \pm 0.5	11.0 \pm 1.0	3.9 \pm 0.3	9.9 \pm 0.7	8.1 \pm 0.4	28.3 \pm 6.8	4.5 \pm 0.9	−0.627
9a	>100	>100	>100	>100	n.d.	n.d.	n.d.	n.d.	—
9b	1.8 \pm 0.2	1.9 \pm 0.4	1.5 \pm 0.1	0.91 \pm 0.09	3.7 \pm 0.3	3.9 \pm 0.3	20.4 \pm 1.2	5.6 \pm 0.3	−0.755
9c	2.5 \pm 0.1	1.3 \pm 0.0	0.61 \pm 0.06	2.6 \pm 0.8	2.4 \pm 0.4	1.5 \pm 0.1	11.5 \pm 0.3	1.6 \pm 0.3	0.058
9d	11.0 \pm 0.3	11.0 \pm 0.5	9.4 \pm 0.7	12.3 \pm 1.2	12.3 \pm 0.5	14.5 \pm 3.1	14.1 \pm 2.8	4.5 \pm 0.9	−0.002
10a	0.21 \pm 0.03	0.17 \pm 0.01	0.30 \pm 0.06	0.15 \pm 0.01	0.28 \pm 0.03	0.10 \pm 0.01	18.5 \pm 0.9	1.10 \pm 0.2	−0.464
10b	0.29 \pm 0.04	0.16 \pm 0.04	0.45 \pm 0.14	0.20 \pm 0.03	0.50 \pm 0.04	0.29 \pm 0.05	4.6 \pm 0.2	0.12 \pm 0.02	−0.599
10c	0.24 \pm 0.03	0.08 \pm 0.01	2.6 \pm 0.1	0.15 \pm 0.01	2.1 \pm 0.2	1.1 \pm 0.1	2.6 \pm 0.2	0.13 \pm 0.03	−0.928
CDDP	2.6 \pm 0.7	8.3 \pm 0.5	5.5 \pm 0.2	5.7 \pm 0.3	9.2 \pm 0.5	13.5 \pm 1.7	0.13 \pm 0.01	0.23 \pm 0.08	−0.380

^a 518A2 – melanoma, HT-29 – colon adenocarcinoma, DLD-1 – Dukes type C colorectal adenocarcinoma, HCT116^{wt} – colon carcinoma (wildtype); HCT116^{−/−} – colon carcinoma (p53 knock-out mutant); MCF-7^{Topo} – mamma carcinoma, Kb-V1^{Vbl} – cervix carcinoma. ^b p53 dependency of IC_{50} values in HCT116 cells, indicated by $r^{\text{p53}} = (\text{IC}_{50}^{\text{wt}}/\text{IC}_{50}^{\text{−/−}}) - 1$.

once more in the presence of the competitive P-gp1 inhibitor verapamil and found to be significantly lower when compared to those obtained without added verapamil (Table 1, second column from the right).

p53 dependency

To investigate the dependency of the cytotoxic activity on p53, which represents one activator of the apoptotic cascade after DNA damage and prolonged cell cycle arrest, and which is normally activated upon treatment with CDDP,^{14,15} the IC₅₀ values of **8b–d**, **9b–d**, **10a–c** and CDDP were determined in the HCT116^{wt} p53 knock-out mutant cell line and the p53 dependency factor $r^{p53} = (IC_{50}^{wt}/IC_{50}^{-/-}) - 1$ was calculated (Table 1). In Fig. 4 the r^{p53} values are depicted as bars to illustrate the differences in the IC₅₀ values in the wildtype (wt) and the p53 knock-out mutant (−/−). The longer the bar the greater the effect that the deletion of p53 has on the cytotoxic activity of each complex. Bars in the negative range indicate a lower cytotoxicity in the p53^{−/−} mutant in comparison to the wildtype cells, bars in the positive range indicate a higher cytotoxicity. Owing to the inactivity of **8a** and **9a** against the wildtype cell line these complexes were not tested in the p53 negative cell line. Except for **9d**, all tested compounds seemed to be dependent on p53 to various degrees. The cationic complexes **10a–c** showed a correlation between the length of the *N*-alkyl residues and the difference between the toxicity in the wildtype cells and the p53^{−/−} cells.

Cellular uptake

In order to check whether the observed differences in the cytotoxicities of the new complexes are a consequence of different uptake rates and intracellular concentrations, the latter were measured *via* inductively coupled plasma mass spectrometry (ICP-MS) in HCT116^{wt} cells treated with **8a–c**, **9a–d**, **10a–c** and CDDP. These complexes cover the whole spectrum of chain

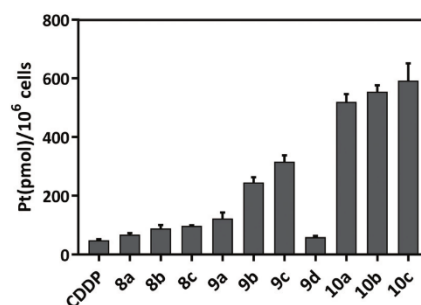


Fig. 5 Intracellular platinum levels in HCT116^{wt} colon carcinoma cells after 5 h of incubation with 8 μ M of Pt(II) complexes CDDP, **8a–c**, **9a–d** and **10a–c**, measured *via* ICP-MS. Mean \pm SD from three independent experiments. Exact values can be found in ESI Table S2.†

length, variation of the secondary ligands (DMSO, PPh₃, (PPh₃)₂), and a potential positive charge. Fig. 5 shows the amount of Pt (pmol per 10⁶ cells) taken up by the cells after 5 h of incubation with the compounds (*cf.* ESI† for values \pm SD).

Complexes **8a–c**, carrying DMSO as an ancillary ligand, are not taken up much better than CDDP. The increased toxicity of **8b** for example, over that of CDDP or **8a** is owed to mechanistic reasons rather than the uptake rates. Within the group of complexes **9**, the uptake rises with the growing length of the *N*-alkyl chain from methyl (**9a**) to butyl (**9c**). However, the *N*-octyl substituted complex **9d** is taken up to a far lesser extent, ranging between that of CDDP and **9a**. However, when the cytotoxicities of **9b–d** measured against HCT116^{wt} were adjusted to their uptake rates the resulting relative 'intrinsic' cytotoxicities were found to be quite similar.

A comparison of complexes **8**, **9** and the charged complex **10**, shows that the exchange of the secondary ligands (DMSO or Cl) for one or two phosphanes vastly promotes the cellular uptake of the platinum complexes, independent of the chain length. Almost six times as much of the bisphosphino complex **10c** was taken up as that of **8a–c** and about 12 times as much as the of CDDP. Consequently, the 'intrinsic' cytotoxicities against HCT116^{wt} differed less markedly than the actual measured ones. The upshot is that we found a weak correlation between the uptake and the *N*-alkyl side chain length for complexes **a–d**, yet no decisive influence was found for the side chains ranging from ethyl to octyl on the cytotoxicity.

DNA interaction

EMSA and ethidium bromide assays. One of the main targets of CDDP is the nuclear DNA. By intra- and inter-strand crosslinking, CDDP drastically changes the DNA morphology, and essential cellular processes, such as DNA replication or protein expression are hindered, and ultimately apoptotic mechanisms are activated.^{14c} We examined the potential DNA interaction of complexes **8**, **9**, **10** and CDDP using ethidium bromide saturation assays with salmon sperm DNA (Fig. 6 top) and electrophoretic mobility shift assays (EMSA) with circular

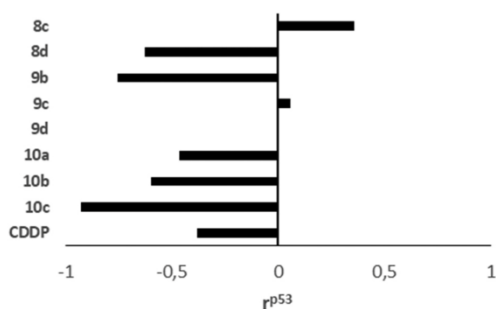


Fig. 4 Comparison of the IC₅₀ values (72 h) of **8c–d**, **9b–d**, **10a–c**, and CDDP against the HCT116 colon carcinoma cells with wildtype p53 (wt) and the p53 knock out mutant (−/−) *via* the dependency factor r^{p53} which is defined as $(IC_{50}^{wt}/IC_{50}^{-/-}) - 1$. The further r^{p53} deviates from zero, the wider apart the two IC₅₀ values are set. Negative r^{p53} values indicate a lower cytotoxicity of the compound in the knock out mutant, positive values indicate a higher cytotoxicity.

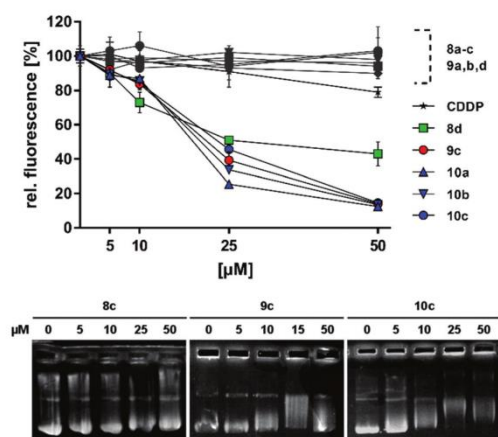


Fig. 6 Top: Ethidium bromide – DNA adduct fluorescence after 2 h of incubation with complexes **8**, **9**, **10** or CDDP, relative to a vehicle control (set to 100%). Mean \pm SD calculated from 3 independent measurements. Bottom: EMSA of circular pBR322 plasmid DNA after 24 h of incubation with 0, 5, 25 and 50 μ M of **8c**, **9c** or **10c**. Staining of DNA bands was performed using ethidium bromide.

pBR322 plasmid DNA (Fig. 6 bottom). Complexes **8a–c** neither reduced the ethidium bromide (EtBr) fluorescence after incubation with salmon sperm DNA, nor caused any band shifts or aggregations of the plasmid DNA in EMSA. This coincides nicely with the lack of DNA affinity that we found recently for the related complexes **2**.^{10d} Although **9a**, **9b** and **9d** showed no impact in the EtBr saturation assay, complex **9c** reduced the EtBr fluorescence to a similar extent as the charged complexes **10**. Despite the negative result from the EtBr saturation assay, **9b** (ethyl) induced, like **9c** (butyl), a band shift in the EMSA at a concentration of 25 μ M. However, complex **9d**, carrying the longest *N*-alkyl side chain, showed virtually no effect in the EMSA. The positive charge of complexes **10** likely facilitates their interaction with the negatively charged phosphate backbone of the DNA,¹⁶ resulting in a reduction of the EtBr fluorescence to about 15% of the vehicle control value, and a band shift in the EMSA as well as the formation of DNA aggregates, which are too bulky to leave the pockets of the agarose gel during electrophoresis.

Kinetics and DNA base preferences. As neither the EMSA nor the ethidium bromide saturation assays gave detailed information on the DNA–complex interaction, more sophisticated biophysical methods were applied, with a focus on complexes **8c**, **9c** and **10a–c** which cover the whole spectrum of ancillary ligands (DMSO, PPh_3 , $(\text{PPh}_3)_2$) while sharing a butyl chain, but also allow us to gauge the influence of the side chain length.

The speed and degree of platination of double-stranded calf thymus (ct) DNA was investigated using its incubation with defined concentrations of the respective complexes, dialysis against water or high salt buffer (0.1 M NaCl), and measure-

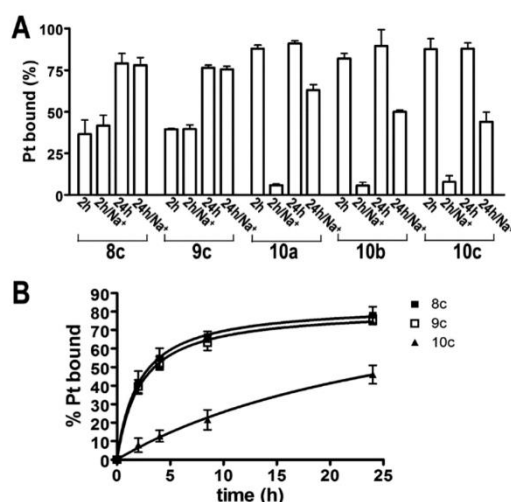


Fig. 7 (A) Quantification of Pt from **8c**, **9c** and **10a–c** bound to DNA in 0.01 M NaClO_4 at 37 °C after 2 or 24 h. Samples were dialysed against water (columns 2 h and 24 h) or against 0.1 M NaCl (columns 2 h/Na⁺ or 24 h/Na⁺). The platinum content associated with the DNA was determined using FAAS. (B) Progress of DNA platination by **8c**, **9c**, and **10c**. Samples, withdrawn after indicated time intervals were exhaustively dialysed against 0.1 M NaCl and analysed using FAAS.

ment of the Pt content using flame atomic absorption spectroscopy (FAAS) after 2 and 24 h. As indicated in Fig. 7A, there was a significant difference in the DNA binding between the neutral complexes **8c** and **9c** and the cationic compounds **10a–c**. After a short incubation time, approximately 40% of **8c** and **9c** were bound to the DNA, while ca. 80% were associated with it after 24 h. The amount of platinum bound to the DNA did not change after dialysis with a high salt buffer. In contrast, complexes **10a–c** associated much faster with DNA, but when the treated DNA samples were dialysed after 2 h against a buffer of high ionic strength, the amount of Pt that stuck to the DNA was much lower (ca. 5%). These results indicate that complexes **10a–c** associate to DNA in a fast, though initially mainly electrostatic, manner. Under the conditions of a high Na⁺ concentration, these electrostatic attractions are disrupted by saturation of the negatively charged phosphate backbone of the DNA, and only the Pt coordinatively bound to the DNA remains. The coordinative binding of **10a–c** is much slower than that of **8c** and **9c**, this is probably due to the steric hindrance of the two bulky PPh_3 groups of **10** (Fig. 7B). Next, we investigated the preferences of complexes **8c**, **9c**, and **10a–c** for binding to particular nucleotide sequences by exposing them to various synthetic single-stranded homopolydeoxyribonucleotides. All of the tested complexes bound readily to single-stranded poly(dG) and, to a lesser extent, to poly(dA), but virtually not at all to the single-stranded poly(dT) or poly(dC) (cf. ESI† for exact values), in keeping with the base sequence preferences of cisplatin.¹⁷

DNA stability. The capability of **8c**, **9c**, **10a–c** to distort and destabilise dsDNA was assessed by measuring the absorbance of the platinated ct DNA at 260 nm as a function of the temperature. The Pt/nucleotide ratio was set to $r_b = 0.03$ and the samples were dialysed against 0.1 M NaCl and, subsequently, against 0.01 M NaClO₄ to get rid of any unbound complex molecules. The effect of the resulting DNA platination on its melting temperature (T_m) was measured in samples with low (0.01 M) and high (0.1 M) concentrations of Na⁺. In contrast to CDDP, the complexes **8c**, **9c**, and **10a–c** had a slightly increased T_m at low Na⁺ concentrations (*cf.* ESI Fig. S41,† left). At high Na⁺ concentrations the T_m decreased as with CDDP, but not to the same degree (*cf.* ESI Fig. S41,† right). The observation that the T_m values of DNA modified by **8c**, **9c**, and **10a–c** decreased at a higher salt concentration (0.1 M) is consistent with the presence of conformational alterations induced by these complexes that destabilise the duplex. At higher salt concentrations (0.1 M), the negative DNA phosphate groups are already efficiently neutralised by the cations present in the medium, so that any stabilising electrostatic contribution by the coordinated positively charged platinum fragments is less pronounced than in a medium of a lower salt concentration. However, the destabilisation caused by **8c**, **9c**, and **10a–c** was less prominent than that induced by cisplatin, indicating a lower extent of DNA distortion. In contrast, at low salt concentrations, in which the negative charges of the DNA phosphate groups are not sufficiently neutralised by the Na⁺ counterions, the electrostatic stabilising effects of **8c**, **9c**, and **10a–c** override their destabilising effects stemming from conformational distortions. These results suggest that the Pt(II)-benzimidazole complexes induce conformational distortions in dsDNA that differ from those induced by CDDP.

DNA distortion and unwinding. The DNA morphology alterations upon binding of the investigated Pt(II) complexes were further assessed according to their effects on the fluorescence of DNA-terbium ion (Tb³⁺) adducts and on the unwinding of pSP73 double helical plasmid DNA. Tb³⁺ fluorescence has been used to investigate local perturbations induced in double-helical DNA by various physical or chemical agents including platinum(II) complexes. The fluorescence of Tb³⁺ ions is strongly enhanced when they are bound to unplatinated guanine (G) residues in distorted DNA regions.¹⁸ Ct DNA was treated with the complexes at r_b values of 0.03. Unbound platinum was removed by dialysis as described in the materials and methods. The platinated DNA samples were treated with TbCl₃, and subsequently, the fluorescence of the Tb³⁺-DNA adducts was measured (*cf.* ESI Fig. S42†). The treatment of DNA with complexes **8c**, **9c**, and **10a–c** resulted in a slight enhancement of the terbium fluorescence, which was, however, less pronounced than that induced by CDDP. These results confirm that DNA adducts of these Pt(II)-benzimidazole complexes give rise to local conformational alterations in double-stranded DNA which are less distorting than those of CDDP.

To determine the effect of the DNA adducts of **8c**, **9c**, and **10a–c** on the unwinding of double-helical DNA in more detail

than before (*cf.* Fig. 6), the degree of supercoiling of the negatively supercoiled pSP73 plasmid DNA was analysed by agarose gel electrophoresis (*cf.* ESI Fig. S43†).¹⁹ Any unwinding and reduction of the supercoils in a closed circular plasmid affects its electrophoretic mobility. The decrease of the mobility during electrophoresis allows the quantification of the mean unwinding angle θ per adduct. It can be calculated as $\theta = -18\sigma/r_b(c)$, in which σ is the superhelical density and $r_b(c)$ is the value of r_b at which the supercoiled and nicked forms comigrate.¹⁹ Under the conditions used in these experiments, the value for σ of the plasmid DNA was calculated to be -0.029 on the basis of the data for CDDP, for which the $r_b(c)$ was determined in this study and $\theta = 13^\circ$ was calculated.¹⁹ Using this approach, the DNA unwinding angles were determined to be $6.2 \pm 0.5^\circ$, $6.1 \pm 0.3^\circ$, $5.6^\circ \pm 0.5^\circ$, $6 \pm 1^\circ$, and $6.6 \pm 1.0^\circ$ for **8c**, **9c**, **10a**, **10b**, and **10c**, respectively, which are thus significantly smaller than that found for cisplatin (13°), but very similar to those of the monofunctional complexes [Pt(NH₃)₃Cl]Cl and [Pt(dien)Cl]Cl, for which unwinding angles of 6° have been measured.¹⁹ Interestingly, none of the complexes tested in this work increased the mobility of the relaxed form (oc) as CDDP does. It has been shown that the bifunctional binding of CDDP and other platinum complexes to DNA shortens and condenses the DNA helix.²⁰ The observation that the binding of **8c**, **9c**, and **10a–c** does not affect the mobility of oc DNA suggests that these complexes predominantly form DNA mono-adducts, even though **8c** and **9c** contain two leaving chloride ligands.

DNA interstrand crosslinking. Apart from the stabilising effect of the coordinated positively charged platinum complex fragments, and the destabilising conformational distortions, crosslinks are a third factor that significantly affect the thermal stability of DNA. It has been shown that interstrand crosslinks (ICLs) in DNA markedly increase its melting temperature by preventing the dissociation of the strands.²¹ For complexes **10a–c**, which contain only one leaving chloride ligand, the formation of ICLs in double helical DNA is unlikely, in contrast to complexes **8c** and **9c** which feature two replaceable chlorido ligands. We tested the ability of complexes **8c**, **9c**, and **10a–c**, as well as CDDP, to crosslink pSP73KB DNA which had been linearized and ³²P-labeled. The electrophoretic autoradiograms shown in Fig. 8 reveal that CDDP, even at very low concentrations r_b , gave rise to distinct interstrand-crosslinked DNA bands which migrate more slowly through the denaturing agarose gel than single stranded (ss) DNA. In contrast, complexes **8c** and **9c** caused comparably fainter ICL DNA bands, even when applied at r_b values ten times of those for CDDP. Although the frequency of the ICLs caused by CDDP was 6%, it was far less than 1% for complexes **8c** and **9c**. With complex **10c**, as with **10a** and **10b** (not shown), no ICL DNA bands were detected. It should be noted, though, that the absence of DNA crosslinking is not necessarily an indication of a lower biological activity. It has been shown that DNA adducts of monofunctional anticancer Pt(II) complexes, such as pyriplatin, phenanthriplatin, or *cis*-[Pt(NH₃)₂[3,5-dichloro-*N*-(3-chloro-4-(quinolin-6-yl-oxy)phenyl)-

Paper

View Article Online

Dalton Transactions

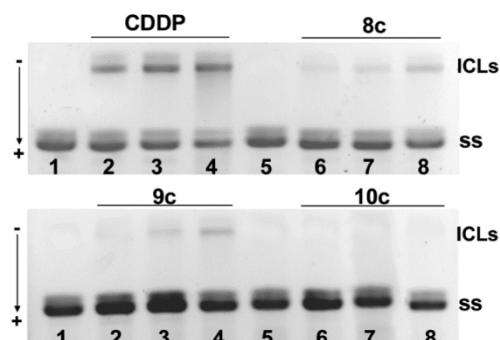


Fig. 8 Autoradiograms of a denaturing agarose gel of linear pSP73 DNA modified by CDDP or complexes **8c**, **9c**, **10c**. Interstrand crosslinked DNA (upper bands, ICLs) migrates more slowly during electrophoresis than single-stranded DNA (bottom bands, ss). Top: CDDP $r_b = 0, 0.001, 0.0015, 0.002$; **8c** $r_b = 0, 0.01, 0.015, 0.02$; Bottom: **9c**, **10c** $r_b = 0, 0.01, 0.015, 0.02$.

2-hydroxybenzamide]Cl}NO₃, bearing bulkier aromatic ligands,²² effectively inhibit the RNA-polymerisation that is considered to be crucial for the biological activity of Pt complexes.²³ Moreover, a less distinct DNA distortion might help to hide the DNA lesions from the repair machinery.²⁴

Cell cycle analysis

The binding of small molecules to the DNA and the resulting damages affect various cellular DNA-dependent processes, such as protein expression, DNA replication and mitosis. Changes in the DNA integrity often lead to an arrest of the cell cycle progression of the cells. Key players during the cell cycle arrest and the activation of the apoptotic cascade are the “guardian of the genome” p53 and the CDK1 inhibitor p21, a major target of activated p53.¹⁵ Using propidium iodide staining and flow cytometry, we tested the *N*-butyl substituted complexes **8c**, **9c**, and **10c** for their effect on the cell cycle progression of HCT116^{wt} cells (Fig. 9) and p53 knock-out mutant HCT116^{-/-} cells (cf. ESI, Fig. S44†). No distinct changes in the cell cycle progression were observed upon treatment of the wildtype cells with the DMSO complex **8c**, while in the p53 knock-out mutant cells treatment led to a G2/M phase arrest. In contrast, both phosphane complexes **9c** and **10c** at a concentration as low as 500 nM induced a strong G1 phase arrest in the wildtype and the mutant cell lines after 24 h, indicating a mode of action that differs from that of CDDP, which caused an arrest in the S phase.

Upshot: SAR and mode of action

Some structure-uptake and structure-activity relations emerged from our studies. The uptake of the delocalised lipophilic cationic complexes **10** by HCT116 colon carcinoma cells was conspicuously greater than that of the neutral analogues **8** and **9**. The complexes **10** were also—on average—more cytotoxic in the MTT assays against the panel of seven cancer cell

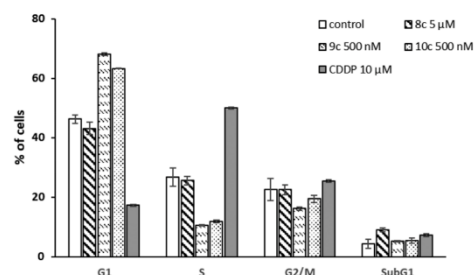


Fig. 9 Effects of **8c** (10 μ M), **9c** (500 nM), **10c** (500 nM) and CDDP (10 μ M) on the progression of the cell cycle of HCT116^{wt} colon carcinoma cells after 24 h of treatment. The bars represent the percentages of cells in each phase of the cell cycle (G1, S and G2/M) and dead cells (sub-G1). Analysis was performed via propidium iodide staining and flow cytometry, values represent mean \pm SDs of three experiments.

lines. With the exception of **9d**, the uptake rates of all three complex types into the HCT116 cells increased with the length of their *N*-alkyl substituents. However, this effect was not mirrored by the course of their cytotoxicities against most of the tested cancer cell lines which were somewhat erratic. Neutral *N*-methyl substituted complexes **8a** and **9a** were virtually inactive against all tested cancer cell lines, while the *N*-ethyl substituted complex **8b** stood out as being specifically efficacious against slow-growing colon carcinoma cell lines, where it reached IC₅₀ values like the cationic complexes **10**. The complexes that were most active with sub-micromolar IC₅₀ (72 h) values against HCT116^{wt} cells were **8b**, **9b**, **10a–c**, which worked by a mode of action that was dependent on the functional p53, which was evident from their reduced activity against the HCT116^{-/-} cancer cells. They were also far more active than cisplatin in both of the HCT116 variants. In a cell-free context, DNA was a major target for all of the new benzimidazol-2-ylidene complexes, although their molecular interactions differed considerably. Neutral complexes **8** and **9** appear to bind swiftly to DNA at G-residues in a coordinative manner, whereas the cationic complexes **10** quickly pre-associate with DNA by electrostatic attraction, which is only slowly replaced by coordinative binding. The DNA adducts formed eventually in either case are characterised by monofunctional platination, causing lesions which distort dsDNA to a much lesser extent than those caused by cisplatin. This might go hand in hand with reduced side effects in animals or humans. Also, unlike cisplatin, complexes **10** and **9c** arrested the HCT116 cells of both variants in the G1 phase.

Conclusions

The replacement of imidazol-2-ylidene by benzimidazol-2-ylidene ligands in antitumoral platinum(II) complexes with otherwise identical ancillary and leaving ligands changes their chemistry (synthesis, stability, and solubility) more than their biological profile (DNA interaction, cancer cell cycle inter-

ference, dependency of the cytotoxicity on the ancillary ligands and on charge). However, their selectivity and individual efficacies against particular cancer entities may differ significantly. What makes the new *N,N*-dialkylbenzimidazol-2-ylidene platinum complexes interesting as drug candidates is their highly structure-dependent cytotoxicity against cancer cells, in combination with reduced morphology changes to DNA, which bode well for the management of unwanted side effects in patients when compared to cisplatin.

To achieve a rational structure-based optimisation of their drug-like properties, in subsequent studies we need to clarify their uptake pathways and their intracellular distribution, and in particular the potential contribution of antimetochondrial effects by the cationic complexes **10**.

Experimental

Materials and methods

All chemicals and reagents were purchased from Sigma Aldrich, Alfa Aesar, ChemPur or ABCR and were used without further purification. Synthetic double-helical polydeoxyribonucleotides poly (dA), poly (dT), poly (dC), and poly (dG) were purchased from Boehringer-Mannheim. Restriction endonuclease EcoRI and the Klenow fragment of DNA polymerase I were purchased from New England Biolabs. EtBr and agarose were purchased from Merck KgaA. $\text{TbCl}_3 \cdot 6\text{H}_2\text{O}$ was purchased from Fluka Chemie and $[\alpha\text{-}^{32}\text{P}]\text{ATP}$ was obtained from MP Biomedicals. Melting points are uncorrected; NMR spectra were run on a 500 MHz spectrometer; chemical shifts are given in ppm (δ) and referenced relative to the internal solvent signal; ^{195}Pt NMR shifts are quoted relative to $\Xi(^{195}\text{Pt}) = 21.496784$ MHz, K_2PtCl_4 was used as an external standard ($\delta = -1612.81$); mass spectra: direct inlet, EI, 70 eV; elemental analyses: Vario EL III elemental analyser; X-Ray diffractometer: STOE-IPDS II; absorption and fluorescence measurements: Tecan Infinite F200; absorption for DNA melting: Varian Cary 4000 UV-vis spectrophotometer; FAAS measurements: Varian AA240Z Zeeman atomic absorption spectrometer equipped with a GTA 120 graphite tube atomizer; flow cytometry: Beckman Coulter Cytomics FC500. All biotested compounds were >95% pure by elemental analysis. Benzimidazolium salts were synthesised according to the literature procedures as described in the ESI.†¹²

Syntheses and characterisation

Synthesis of NHC silver complexes 7. Solutions of the benzimidazolium chlorides in CH_2Cl_2 were treated with Ag_2O (0.5 eq.) and stirred for 24 h to 3 days in the dark. After filtration, the product complexes **7** were precipitated by addition of Et_2O or hexane.

Chlorido(1,3-diethylbenzimidazol-2-ylidene) silver(i) (7b). **6b** (400 mg, 1.90 mmol), Ag_2O (950 mg, 0.95 mmol, 0.5 eq.), CH_2Cl_2 (40 mL), 24 h; yield: 526 mg (1.66 mmol, 87%); colourless solid; ^1H NMR (500 MHz, CDCl_3): δ 1.49 (6H, t, $J = 7.2$ Hz,

CH_3), 4.57 (4H, q, $J = 7.2$ Hz, CH_2), 7.44–7.50 (2H, m, BI), 7.83–7.89 (2H, m, BI).

*Chlorido(1,3-di-*n*-butylbenzimidazol-2-ylidene) silver(i) (7c).* **6c** (320 mg, 1.40 mmol), Ag_2O (159 mg, 0.70 mmol, 0.5 eq.), CH_2Cl_2 (35 mL), 24 h; yield: 407 mg (1.09 mmol, 78%); amber solid; ^1H NMR (500 MHz, CDCl_3): δ 0.97 (6H, t, $J = 7.3$ Hz, CH_3), 1.48–1.39 (4H, m, $\text{CH}_3\text{--CH}_2$), 2.01–1.90 (4H, m, $\text{NCH}_2\text{--CH}_2$), 4.54 (4H, t, $J = 7.2$ Hz, N--CH_2), 7.41 (2H, dd, $J = 6.1$, 3.0 Hz, BI), 7.53 (2H, dd, $J = 6.0$, 3.1 Hz, BI).

Chlorido(1,3-dioctylbenzimidazol-2-ylidene) silver(i) (7d). **6d** (240 mg, 633 μmol), Ag_2O (147 mg, 633 μmol , 1 eq.), CH_2Cl_2 (15 mL), 3 d; yield: 238 mg (489 μmol , 77%); beige solid; ^1H NMR (500 MHz, CDCl_3): δ 0.84 (6H, t, $J = 6.9$ Hz, CH_3), 1.19–1.29 (12H, m, CH_2), 1.30–1.37 (4H, m, NCCCCCH_2), 1.37–1.44 (4H, m, NCCCCCH_2), 1.98 (4H, quin, $J = 7.4$ Hz NCCCCCH_2), 4.53 (4H, t, $J = 6.5$ Hz, NCH_2), 7.43 (2H, dd, $J = 6.1$, 3.2 Hz, BI), 7.53 (2H, dd, $J = 6.1$, 3.2 Hz, BI).

Synthesis of *cis*-[Cl₂(DMSO)(1,3-dialkylbenzimidazol-2-ylidene)]Pt^{II} complexes 8. A solution of silver complex **7** in DMSO was treated with K_2PtCl_4 (1 eq.) and heated at 60 °C in the dark for 20 h. After addition of CH_2Cl_2 the precipitating AgCl was filtered off, the filtrate was washed with H_2O and brine, and dried over Na_2SO_4 . Residual DMSO was removed *in vacuo* and by crystallising the product from CH_2Cl_2 with Et_2O or hexane.

cis-[Dichlorido(1,3-dimethylbenzimidazol-2-ylidene)(dimethylsulfoxid)]platinum(II) (8a). As the solubility of **7a** was not sufficient to allow its separation from the by-products, **8a** was synthesised from **6a** directly. Ag_2O (106 mg, 456 μmol , 0.5 eq.) was added to a solution of **6a** (250 mg, 912 μmol) in CH_2Cl_2 (20 mL) and the mixture was stirred in the dark for 19 h. After removal of the solvent, the residue was suspended in DMSO (30 mL) and treated with K_2PtCl_4 (341 mg, 821 μmol , 0.9 eq.). After 24 h at 60 °C in the dark, the reaction was worked up as described above. Yield: 353 mg (720 μmol , 79%); colourless crystals of melting point (mp) 262 °C; elemental analysis (%): calc. for $\text{C}_{11}\text{H}_{16}\text{N}_2\text{SOPtCl}_2$ (490.31): C, 26.95; H, 3.29; N, 5.71. Found: C, 27.24; H, 3.99; N, 6.26. ^1H NMR (500 MHz, CDCl_3): δ 3.57 (6H, s, DMSO), 4.23 (6H, s, NCH_3), 7.37 (2H, dd, $J = 6.1$, 3.1 Hz, BI), 7.44 (2H, dd, $J = 6.1$, 3.1 Hz, BI); ^{13}C NMR (125 MHz, CDCl_3): δ 34.7 (NCH_3), 46.3 (DMSO), 110.9 (BI), 124.3 (BI), 134.2 (BI- C_q), 154.8 (NHC); ^{195}Pt NMR (108 MHz, CDCl_3): δ -3565.9; m/z (EI): 491 [M^+], 413, 377, 340, 78.

cis-[Dichlorido(1,3-diethylbenzimidazol-2-ylidene)(dimethylsulfoxid)]platinum(II) (8b). **7b** (449 mg, 1.41 mmol), K_2PtCl_4 (587 mg, 1.41 mmol, 1.0 eq.), DMSO (40 mL); yield: 639 mg (1.23 mmol, 87%); colourless crystals of mp 270 °C; elemental analysis (%): calc. for $\text{C}_{13}\text{H}_{20}\text{N}_2\text{SOPtCl}_2$ (518.37): C, 30.12; H, 3.89; N, 5.40. Found: C, 30.75; H, 4.203; N, 5.96. ^1H NMR (500 MHz, CDCl_3): δ 1.63 (6H, t, $J = 7.3$ Hz, CH_3), 3.57 (6H, s, DMSO), 4.83 (4H, q, $J = 7.3$ Hz, CH_2), 7.35 (2H, dd, $J = 6.1$, 3.1 Hz, BI), 7.46 (2H, dd, $J = 6.1$, 3.1 Hz, BI); ^{13}C NMR (125 MHz, CDCl_3): δ 14.5 (CH_3), 43.8 (CH_2), 46.4 (DMSO), 111.4 (BI), 124.0 (BI), 133.4 (BI- C_q), 153.5 (NHC); ^{195}Pt NMR (108 MHz, CDCl_3): δ -3561.4; m/z (EI): 518 [M^+], 440, 404, 173, 78. *Crystal data:* $\text{C}_{13}\text{H}_{20}\text{N}_2\text{Cl}_2\text{OptS}$, $M = 518.36$, triclinic, space group $\bar{P}1$,

$a = 8.675(5)$ Å, $b = 9.264(5)$ Å, $c = 10.601(5)$ Å, $\alpha = 91.874(5)^\circ$, $\beta = 103.182(5)^\circ$, $\gamma = 94.722(5)^\circ$, $V = 825.5(8)$ Å³, $Z = 2$, $\lambda = 0.71069$ Å, $\mu = 8.945$ mm⁻¹, $T = 133$ K; 7449 reflections measured, 3177 unique; $R[F^2 > 2\sigma(F^2)] = 0.0329$ and $R_w = 0.0851$, GOF = 1.032. CCDC 1857512.†

cis-[Dichlorido(1,3-di-*n*-butylbenzimidazol-2-ylidene)(dimethylsulfoxide)]platinum(II) (**8c**). **7c** (143 mg, 382 µmol), K₂PtCl₄ (158 mg, 382 µmol, 1.0 eq.), DMSO (12 mL); yield: 203 mg (353 µmol, 93%); colourless crystals of mp 227 °C; elemental analysis (%): calc. for C₁₇H₂₈NSO₂Cl₂ (574.47): C, 30.12; H, 3.89; N, 5.40. Found: C, 30.75; H, 4.20; N, 5.96. ¹H NMR (500 MHz, CDCl₃): δ 1.04 (6H, t, $J = 7.4$ Hz, CH₃), 1.60–1.51 (4H, m, NCCCH₂), 2.04–1.94 (2H, m, NCCCH₂), 2.19–2.09 (2H, m, NCCCH₂), 3.56 (6H, s, DMSO), 4.64 (2H, ddd, $J = 14.0$, 10.2, 6.0 Hz, NCH₂), 4.75 (2H, ddd, $J = 14.1$, 10.3, 5.6 Hz, NCH₂), 7.33 (2H, dd, $J = 6.1$, 3.1 Hz, BI), 7.44 (2H, d, $J = 9.2$ Hz, BI); ¹³C NMR (125 MHz, CDCl₃): δ 14.0 (CH₃), 20.5 (CH₃–CH₂), 31.4 (NCCCH₂), 46.3 (DMSO), 48.6 (NCH₂), 111.4 (BI), 123.9 (BI), 133.8 (BI–C_q), 153.7 (NCN); ¹⁹⁵Pt NMR (CDCl₃): δ –3554.2; m/z (EI): 574 [M⁺], 538, 501, 421, 229, 78.

cis-[Dichlorido(1,3-diocetylbenzimidazol-2-ylidene)(dimethylsulfoxide)]platinum(II) (**8d**). **7d** (230 mg, 473 µmol), K₂PtCl₄ (196 mg, 473 µmol, 1.0 eq.), DMSO (15 mL); yield: 295 mg (430 µmol, 91%); colourless solid of mp 132 °C; elemental analysis (%): calc. for C₂₅H₄₄N₂Cl₂SO₂ (686.68): C, 43.73; H, 6.46; N, 4.08. Found: C, 44.36; H, 6.77; N, 4.36. ¹H NMR (500 MHz, CDCl₃): δ 0.89 (6H, t, $J = 6.87$ Hz, CH₃), 1.25–1.36 (12H, m, CH₂), 1.36–1.44 (4H, m, NCCCH₂), 1.48–1.56 (4H, m, NCCCH₂), 1.94–2.07 (2H, m, NCCCH₂), 2.09–2.20 (2H, m, NCCCH₂), 3.56 (6H, s, DMSO), 4.58–4.68 (2H, m, NCH₂), 4.71–4.81 (2H, m, NCH₂), 7.31–7.38 (2H, m, BI–H), 7.42–7.47 (2H, m, BI–H); ¹³C NMR (125 MHz, CDCl₃): δ 14.1 (CH₃), 22.6 (CH₂), 27.1 (CH₂), 29.2 (CH₂), 29.3 (CH₂), 29.3 (CH₂), 31.6 (NCCCH₂), 46.2 (DMSO), 48.72 (NCH₂), 111.3 (BI), 123.8 (BI), 133.6 (C_q), 153.5 (NHC); ¹⁹⁵Pt NMR: δ –3556; m/z (EI): 686 [M⁺], 533, 358, 230, 131, 78.

Synthesis of *cis*-[Cl₂(PPh₃)₂](1,3-dialkylbenzimidazol-2-ylidene)Pt^{II} complexes **9**

cis-[Dichlorido(1,3-dimethylbenzimidazol-2-ylidene)(triphenylphosphane)]platinum(II) (**9a**). A solution of triphenylphosphane (29 mg, 112 µmol, 1.1 eq.) in CH₂Cl₂ (15 mL) was added over 15 min to a solution of complex **8a** (50 mg, 102 µmol) in CH₂Cl₂ (30 mL) and the resulting mixture was stirred at room temperature for a further 15 min. The volatiles were removed *in vacuo* and the remaining crude product was purified using column chromatography (silica gel, 2% MeOH in CH₂Cl₂). The product was crystallised from CH₂Cl₂/Et₂O. Yield: 22 mg (32.6 µmol, 32%); colourless crystalline solid of mp 346 °C. Elemental analysis (%): calc. for C₂₇H₂₅N₂Cl₂P₂ (674.46): C, 48.08; H, 3.74; N, 4.15. Found: C, 47.71; H, 4.03; N, 4.14. ¹H NMR (500 MHz, CDCl₃): δ 3.83 (6H, s, CH₃), 7.07–7.15 (2H, m, BI), 7.16–7.26 (8H, m, BI and PPh₃), 7.29–7.37 (3H, m, PPh₃), 7.60 (6H, t, $J = 9.5$ Hz, PPh₃); ¹³C NMR (125 MHz, CDCl₃): δ 34.1 (CH₃), 109.9 (BI), 123.1 (BI), 128.29 (d, $J = 11.8$ Hz, *o*-PPh₃), 129.4 (d, $J = 63.5$ Hz, *ipso*-PPh₃), 131.1 (d, $J = 1.82$ Hz, *p*-PPh₃), 134.0 (d, $J = 10.9$ Hz, *m*-PPh₃), 134.1 (BI–C_q), 162.0 (d,

$J = 7.27$ Hz, NCN); ³¹P NMR (CDCl₃): δ 8.83 ($J = 3893$ Hz); ¹⁹⁵Pt NMR (CDCl₃): δ –4017 (d, $J = 3895$ Hz); m/z (EI): 675 [M⁺], 640, 603, 263, 184, 148, 109.

cis-[Dichlorido(1,3-diethylbenzimidazol-2-ylidene)(triphenylphosphane)]platinum(II) (**9b**). Triphenylphosphane (131 mg, 500 µmol, 5 eq.) was added to a solution of complex **8b** (50 mg, 97 µmol) in CH₂Cl₂ (5 mL) and the resulting mixture was stirred at room temperature for 21 h. After precipitation from CH₂Cl₂/hexane the product was purified using column chromatography (silica gel, 1% MeOH in CH₂Cl₂). Yield: 29 mg (41 µmol, 43%); colourless solid of mp 323 °C. Elemental analysis (%): calc. for C₂₉H₂₉N₂Cl₂P₂ (702.52): C, 49.58; H, 4.16; N, 3.99. Found: C, 49.19; H, 4.10; N, 3.70. ¹H NMR (500 MHz, CDCl₃): δ 1.46 (6H, t, $J = 7.2$ Hz, CH₃), 3.84 (2H, dq, $J = 14.5$, 7.2 Hz, NCH₂), 4.85 (2H, dq, $J = 14.5$, 7.2 Hz, NCH₂), 7.12 (2H, dd, $J = 6.1$, 3.1 Hz, BI), 7.24–7.16 (8H, m, BI, *o*-PPh₃), 7.31 (3H, t, $J = 7.2$ Hz, *p*-PPh₃), 7.64–7.53 (6H, m, *m*-PPh₃); ¹³C NMR (125 MHz, CDCl₃): δ 14.0 (CH₃), 43.4 (NCH₂), 110.3 (BI), 123.0 (BI), 128.2 (d, $J = 10.9$ Hz, *o*-PPh₃), 129.0 (d, $J = 64.5$ Hz, *ipso*-PPh₃), 131.0 (d, $J = 2.72$ Hz, *p*-PPh₃), 133.3 (BI–C_q), 133.9 (d, $J = 10.9$ Hz, *m*-PPh₃), 160.6 (d, $J = 7.26$ Hz, NCN); ³¹P NMR (CDCl₃): δ 8.85 ($J = 3861$ Hz); ¹⁹⁵Pt NMR (CDCl₃): δ –4016 (d, $J = 3873$ Hz); m/z (EI): 702 [M⁺], 666, 630, 455, 262.

cis-[Dichlorido(1,3-di-*n*-butylbenzimidazol-2-ylidene)(triphenylphosphane)]platinum(II) (**9c**). Triphenylphosphane (114 mg, 434 µmol, 5 eq.) was added to a solution of complex **8c** (50 mg, 86.9 µmol) in CH₂Cl₂ (5 mL) and the resulting mixture was stirred at room temperature for 30 min. The volatiles were removed *in vacuo* and the remaining crude product was purified by crystallisation from CH₂Cl₂/hexane. Yield: 48 mg (63.3 µmol, 73%); colourless crystalline solid of mp 248 °C; elemental analysis (%): calc. for C₃₃H₃₇N₂Cl₂P₂ (758.62): C, 52.25; H, 4.92; N, 3.69. Found: C, 52.75; H, 4.69; N, 3.58. ¹H NMR (500 MHz, CDCl₃): δ 0.94 (6H, t, $J = 7.3$ Hz, CH₃), 1.35–1.48 (4H, m, NCCCH₂), 1.63–1.73 (2H, m, NCCCH₂), 2.00–2.14 (2H, m, NCCCH₂), 3.78–3.87 (2H, m, NCH₂), 4.54–4.64 (2H, m, NCH₂), 7.11 (2H, dd, $J = 6.0$, 3.2 Hz, BI), 7.15–7.24 (8H, m, BI and PPh₃), 7.33 (3H, t, $J = 7.3$ Hz, PPh₃), 7.48–7.66 (6H, m, PPh₃); ¹³C NMR (125 MHz, CDCl₃): δ 13.7 (CH₃), 20.4 (NCCCH₂), 30.7 (NCCCH₂), 48.3 (NCH₂), 110.4 (BI), 123.0 (BI), 128.2 (d, $J = 10.9$ Hz, *o*-PPh₃), 129.1 (d, $J = 62.7$ Hz, *ipso*-PPh₃), 131.1 (d, $J = 1.82$ Hz, *p*-PPh₃), 133.7 (BI–C_q), 134.0 (d, $J = 10.9$ Hz, *m*-PPh₃), 160.7 (d, $J = 7.26$ Hz, NCN); ³¹P NMR (CDCl₃): δ 9.19 ($J = 3901$ Hz); ¹⁹⁵Pt NMR: δ –4018 (d, $J = 3871$ Hz); m/z (EI): 758 [M⁺], 722, 685, 262, 229, 183, 108. *Crystal data*: C₃₃H₃₇Cl₂N₂P₂, $M = 758.63$, triclinic, space group $P\bar{1}$, $a = 9.1067(18)$ Å, $b = 12.792(3)$ Å, $c = 13.803(3)$ Å, $\alpha = 88.02(3)^\circ$, $\beta = 87.59(3)^\circ$, $\gamma = 71.06(3)^\circ$, $V = 1519.2(6)$ Å³, $Z = 2$, $\lambda = 0.71073$ Å, $\mu = 4.872$ mm⁻¹, $T = 133$ K; 21 191 reflections measured, 5813 unique; $R[F^2 > 2\sigma(F^2)] = 0.0183$ and $R_w = 0.0447$, GOF = 1.030. CCDC 1857511.†

cis-[Dichlorido(1,3-diocetylbenzimidazol-2-ylidene)(triphenylphosphane)]platinum(II) (**9d**). Triphenylphosphane (95 mg, 364 µmol, 5 eq.) was added to a solution of complex **8d** (50 mg, 73 µmol) in CH₂Cl₂ (20 mL) and the resulting mixture was stirred at room temperature for 24 h. After crystallisation

from CH_2Cl_2 /hexane the crude product was purified using column chromatography (silica gel, 1% MeOH in CH_2Cl_2). Yield: 60 mg (68 μmol , 93%); colourless crystalline solid of mp 168 °C. Elemental analysis (%): calc. for $\text{C}_{41}\text{H}_{53}\text{N}_2\text{Cl}_2\text{P}_2\text{Pt}$ (870.84): C, 56.55; H, 6.13; N, 3.22. Found: C, 57.14; H, 6.03; N, 3.22. ^1H NMR (500 MHz, CDCl_3): δ 0.91 (6H, t, J = 6.9 Hz, CH_3), 1.26–1.39 (20H, m, CH_2), 1.63–1.72 (2H, m, NCCH_2), 2.04–2.13 (2H, m, NCCH_2), 3.78–3.88 (2H, m, NCH_2), 4.52–4.78 (2H, m, NCH_2), 7.10 (2H, dd, J = 6.9, 3.05 Hz, BI), 7.16–7.25 (8H, m, BI and PPh_3), 7.33 (3H, t, J = 6.7 Hz, PPh_3), 7.51–7.64 (6H, m, PPh_3); ^{13}C NMR (125 MHz, CDCl_3): δ 14.1 (CH_3), 22.6 (CH_2), 27.3 (CH_2), 28.8 (CH_2), 29.1 (NCCH_2), 29.3 (CH_2), 31.6 (CH_2), 48.6 (NCH_2), 110.4 (BI), 122.9 (BI), 128.1 (d, J = 11.8 Hz, *o*- PPh_3), 129.2 (d, J = 62.7 Hz, *ipso*- PPh_3), 131.0 (d, J = 2.7 Hz, *p*- PPh_3), 134.0 (d, J = 10.9 Hz, *m*- PPh_3), 160.7 (d, J = 8.17 Hz, NCN); ^{31}P NMR (CDCl_3): δ 9.17 (J = 3874 Hz); ^{195}Pt NMR (CDCl_3): δ -4018 (d, J = 3879 Hz); m/z (EI): 870 [M^+], 834, 797, 564, 533, 341, 262, 183, 108.

Synthesis of *trans*-[Cl(1,3-dialkylbenzimidazol-2-ylidene)] Pt^+Cl^- complexes **10**

trans-[Chlorido(1,3-dimethylbenzimidazol-2-ylidene)bis(triphenylphosphane)]platinum(II) chloride (**10a**). Triphenylphosphane (80 mg, 306 μmol , 3 eq.) was added to a solution of complex **8a** (50 mg, 102 μmol) in CH_2Cl_2 (5 mL) and the resulting mixture was stirred at room temperature for 30 min. The volatiles were removed *in vacuo* and the remaining crude product was purified by crystallisation from CH_2Cl_2 /hexane. Yield: 80 mg (90 μmol , 83%); colourless crystalline solid of mp 310 °C; elemental analysis (%): calc. for $\text{C}_{48}\text{H}_{47}\text{N}_2\text{P}_2\text{PtCl}_2$ (979.84): C, 57.70; H, 4.30; N, 2.99. Found: C, 57.98; H, 5.04; N, 3.43. ^1H NMR (500 MHz, CDCl_3): δ 3.54 (6H, s, CH_3), 7.20 (2H, dd, J = 6.1, 3.1 Hz, BI), 7.29 (12H, t, J = 7.5 Hz, *o*- PPh_3), 7.32 (2H, dd, J = 6.1, 3.1 Hz, BI), 7.37 (6H, t, J = 7.4 Hz, *p*- PPh_3), 7.51 (12H, dd, J = 12.4, 6.0 Hz, *m*- PPh_3); ^{13}C NMR (125 MHz, CDCl_3): δ 35.1 (CH_3), 111.1 (BI), 124.3 (BI), 127.5 (t, J = 29.5 Hz, *ipso*- PPh_3), 128.9 (t, J = 5.5 Hz, *o*- PPh_3), 131.8 (*p*- PPh_3), 133.7 (t, J = 5.9 Hz, *m*- PPh_3), 133.9 (BI- C_q), 159.9 (t, J = 10.0 Hz, NCN); ^{31}P NMR (CDCl_3): δ 17.7 (J = 2478 Hz); ^{195}Pt NMR (CDCl_3): δ -4378 (t, J = 2490 Hz); m/z (EI): 908 [M^+], 673, 653, 602, 262, 183. *Crystal data*: $\text{C}_{45}\text{H}_{40}\text{ClN}_2\text{P}_2\text{PtCl}$, M = 936.72, monoclinic, space group $P2_1/c$, a = 12.578 (5) Å, b = 10.790 (5) Å, c = 32.126 (5) Å, α = 90°, β = 94.531(5)°, γ = 90°, V = 4346 (3) Å³, Z = 4, λ = 0.71069 Å, μ = 3.46 mm⁻¹, T = 133 K; 32457 reflections measured, 6540 unique; $R[F^2 > 2\sigma(F^2)]$ = 0.0276 and R_w = 0.0601, GOF = 0.766. CCDC 1857513.†

trans-[Chlorido(1,3-diethylbenzimidazol-2-ylidene)bis(triphenylphosphane)]platinum(II) chloride (**10b**). Triphenylphosphane (252 mg, 960 μmol , 10 eq.) was added to a solution of complex **8b** (50 mg, 96 μmol) in CH_2Cl_2 (10 mL) and the resulting mixture was stirred at room temperature for 5 d. The volatiles were removed *in vacuo* and the remaining crude product was purified by crystallisation from CH_2Cl_2 /Et₂O. Yield: 22 mg (22.8 μmol , 24%); colourless solid of mp 297 °C; elemental analysis (%): calc. for $\text{C}_{50}\text{H}_{51}\text{N}_2\text{Cl}_2\text{P}_2\text{Pt}$ (1007.89): C, 58.51; H, 4.60; N, 2.90. Found: C, 58.59; H, 4.66; N, 2.89. ^1H NMR (500 MHz, CDCl_3): δ 0.83 (6H, t, J = 7.3 Hz, CH_3), 3.86 (4H, q,

J = 7.2 Hz, CH_2), 7.20–7.42 (24H, m, BI and PPh_3), 7.43–7.54 (10H, m, PPh_3); ^{13}C NMR (125 MHz, CDCl_3): δ 13.0 (CH_3), 44.2 (CH_2), 111.5 (BI), 124.6 (BI), 127.1 (t, J = 25.5 Hz, *ipso*- PPh_3), 129.0 (t, J = 5.5 Hz, *o*- PPh_3), 132.0 (*p*- PPh_3), 133.5 (BI- C_q), 133.7 (*m*- PPh_3), 158.0 (t, J = 9.5 Hz, NCN); ^{31}P NMR (CDCl_3): δ 18.9 (J = 2485 Hz); ^{195}Pt NMR (CDCl_3): δ -4383 (t, J = 2490 Hz); m/z (EI): 702, 667, 630, 456, 297, 262, 183, 108.

trans-[Chlorido(1,3-di-*n*-butylbenzimidazol-2-ylidene)bis(triphenylphosphane)]platinum(II) chloride (**10c**). Triphenylphosphane (456 mg, 1.74 mmol, 20 eq.) was added to a solution of complex **8b** (50 mg, 87 μmol) in CH_2Cl_2 (10 mL) and the resulting mixture was stirred at 80 °C for 4 days. The volatiles were removed *in vacuo* and the remaining crude product was purified by crystallisation from CH_2Cl_2 /Et₂O and subsequent column chromatography (silica gel, CH_2Cl_2 with 2–5% MeOH). Yield: 29 mg (28 μmol , 33%); colourless solid of mp 114 °C; elemental analysis (%): calc. for $\text{C}_{51}\text{H}_{52}\text{N}_2\text{Cl}_2\text{P}_2\text{Pt}$ (1020.91): C, 60.00; H, 5.13; N, 2.74. Found: C, 59.26; H, 5.11; N, 3.06. ^1H NMR (500 MHz, CDCl_3): δ 0.70 (6H, t, J = 7.0 Hz, CH_3), 1.12–1.23 (8H, m, CH_2), 3.62–3.70 (4H, m, NCH_2), 7.15 (2H, dd, J = 6.5, 3.1 Hz, BI), 7.18–7.42 (22H, m, BI and PPh_3), 7.42–7.57 (10H, m, PPh_3); ^{13}C NMR (125 MHz, CDCl_3): δ 13.3 (CH_3), 20.4 (CH_2CH_3), 30.2 (NCCH_2), 49.1 (CH_2), 111.2 (BI), 124.8 (BI), 127.2 (t, J = 29.1 Hz, *ipso*- PPh_3), 129.0 (t, J = 5.5 Hz, *o*- PPh_3), 132.1 (*p*- PPh_3), 133.6 (BI- C_q), 133.9 (*m*- PPh_3), 158.4 (t, J = 10.0 Hz, NCN); ^{31}P NMR (CDCl_3): δ 18.9 (J = 2486 Hz); ^{195}Pt NMR (CDCl_3): δ -4379 (t, J = 2486 Hz); m/z (EI): 758, 723, 685, 456, 262, 229, 183, 108.

X-ray data collection and structural determination

Diffractometer used: STOE-STADIVARI; data collection and cell refinement by: STOE-X-Area. The single crystal samples were measured with Mo-K α and the reflections collected at 133 K. The structures were solved by direct methods using SIR97 and refined by full matrix least-squares on F^2 for all data using SHELXL2016/6. All hydrogen atoms were added at calculated positions and refined using a riding model. Anisotropic thermal displacement parameters were used for all non-hydrogen atoms. Further details of the data collection and reliability factors are listed together with the analytical data in the ESI (Table S1†). Supplementary crystallographic data were deposited with The Cambridge Crystallographic Data Centre CCDC under no. 1857512 (**8b**), 1857511 (**9c**), 1857513 (**10a**).†

Biological evaluation

Cell culture conditions and stock solutions. Cells of 518A2 melanoma, HT-29, DLD-1, HCT116^{wt} and HCT116p53^{-/-} colon carcinoma, MCF-7^{Topo} mamma carcinoma, and Kb-V1^{Vbl} cervix carcinoma were kept in DMEM. All cell lines were cultured at 37 °C, 95% humidity and 5% CO₂. To maintain the *mdr* characteristics of the MCF-7^{Topo} and Kb-V1^{Vbl} cell lines, they were regularly treated with either topotecan or vinblastine. Dilutions of platinum(II) complexes **8**, **9** and **10a–c** were made from 10 mM stock solutions (DMSO) in sterile ddH₂O, dilutions of CDDP from a 3.3 mM stock solution in 150 mM saline.²⁵ Plasmid pSP73 (2464 bp) was isolated

according to standard procedures and banded twice in CsCl equilibrium density gradients.

Growth inhibition assay (MTT-assay). For the investigation of the cytotoxicity an MTT (3-(4,5-dimethylthiazole-2-yl)-2,5-diphenyltetrazoliumbromide) based proliferation assay was performed. Cells were seeded into 96-well plates (0.05×10^6 cells per mL for 518A2, HT-29, HCT116, MCF-7^{Topo} and Kb-V1^{Vbl}, and 0.1×10^6 cells per mL for DLD-1) and incubated for 24 h under cell culture conditions to ensure their adhesion. On the next day the cells were treated with a series of appropriate dilutions (final concentrations ranging from 5 nM, resp. 5 pM, to 100 μ M) of **8**, **9**, **10a-c** and CDDP. As a negative control (100% vital cells) the assay was performed analogously with the respective vehicle. The cells were incubated for a further 72 h under cell culture conditions, centrifuged (300g, 4 °C) and the media were exchanged for 50 μ L of a 0.05% MTT solution in PBS. The cells were incubated for another 2 h at 37 °C before the plates were again centrifuged as before and the MTT solution was discarded. The water insoluble formazan was dissolved by addition of 25 μ L of an SDS/DMSO solution (10%; 0.6% AA) to each well. After 1 h of incubation at 37 °C the absorption was measured at 570 nm, and the background absorption at 630 nm. The formazan absorption correlates directly with the number of viable cells. The IC₅₀ values were determined with *GraphPad Prism* and means \pm SD were calculated from six independent measurements.

Inhibition of P-gp1. The determination of the cytotoxicity of **8b-d**, **9b-d** and **10a-c** in Kb-V1^{Vbl} cervix carcinoma cells in the presence of verapamil, a competitive inhibitor of P-gp1, was conducted analogously to the normal MTT-assay, but with DMEM containing 24 μ M of verapamil (10 mM stock solution in 70% EtOH).

Cellular uptake. The uptake of complexes **8a-c**, **9a-d**, **10a-c** and CDDP by HCT116^{wt} cells was measured *via* ICP-MS. The cells were seeded on 100 mm tissue culture dishes (3×10^6 cells per dish in 7 mL of growth medium) and incubated at 37 °C. Confluent cells were treated with the compounds at final equimolar concentrations (8 μ M) for 5 h. The attached cells were harvested by trypsinisation and the viability of the cells was tested by a trypan blue exclusion assay. Viabilities of the cells ranged from 76 to 97%, both viable and dead fractions were used for the experiment. The cell pellets were subsequently washed twice with cold PBS and cells were counted by using a TC10 Automated Cell Counter (Bio-Rad). The cells were digested by using a microwave acid (HCl, 11 M) digestion system (MARSS, CEM) to give a fully homogenised solution. The final platinum content in the samples was determined using ICP-MS.

DNA interaction

Ethidium bromide saturation assay. Inside the wells of a black 96-well plate 1 μ g salmon sperm DNA in 100 μ L of freshly sterile-filtered TE buffer (10 mM Tris/HCl, 1 mM EDTA pH 8.5) was incubated with 5, 10, 25 and 50 μ M of **8**, **9**, **10a-c** or CDDP for 2 h at 37 °C (final sample volume 111.1 μ L). Control samples were prepared analogously with DMSO to the

highest concentration. To determine the background fluorescence, samples were prepared analogously with equal amounts of TE buffer instead of the DNA stock solution. 100 μ L of ethidium bromide in TE-buffer (10 μ g mL⁻¹) was added to each well and the plate was incubated in the dark for 5 min at room temperature. The ethidium bromide fluorescence was measured at $\lambda_{\text{ex}} = 535$ nm and $\lambda_{\text{em}} = 590$ nm. The background signal was subtracted from the respective sample signals and the fluorescence intensities relative to the control (set to 100%) were calculated. Each measurement was run in triplicate. Reduction of the fluorescence indicates an interaction of **8**, **9**, **10a-c** or CDDP with the DNA and thus a hindrance of ethidium bromide intercalation.

Electrophoretic mobility shift assay (EMSA). Circular pBR322 plasmid DNA (1.5 μ g) in TE buffer was incubated for 24 h with 0, 5, 10, 25 and 50 μ M of complexes **8**, **9** or **10a-c** at 37 °C (final sample volume: 20 μ L). On the next day DNA sample buffer (5 \times , Tris/HCl, pH 8.0; 25% glycerol) was added to each sample and an agarose gel electrophoresis (1% in TBE buffer; 90 mM Tris/HCl, pH 8.3; 90 mM boric acid; 2.5 mM EDTA) was run at 66 V for 4 h. The DNA was stained with ethidium bromide and the plasmid bands were visualised *via* a UV transilluminator.

DNA platination analysis. Calf thymus DNA (1 mM) was incubated with **8c**, **9c** or **10a-c** (100 μ M) in 10 mM NaClO₄ in the dark at 37 °C. After 2, 4 or 24 h, aliquots were withdrawn and exhaustively dialysed against water or, alternatively, against 0.1 M NaCl and subsequently against water. The amount of platinum associated with the DNA was assessed using FAAS. The percentage of Pt bound to DNA was calculated as the ratio of Pt associated with DNA and the total amount of platinum present in the sample.

DNA melting point analysis. DNA was modified with Pt complexes for 24 h in 10 mM NaClO₄ at 37 °C. The DNA was dialysed against 0.1 M NaCl to remove the unbound platinum and subsequently against the medium required for further analysis. An aliquot of the sample was used to determine the level of DNA platination (r_b) using FAAS. The DNA melting curves of unplatinated or platinated DNA were recorded by measuring the absorbance at 260 nm in a medium containing 10 mM or 0.1 M Na⁺ with 1 mM Tris-HCl/0.1 mM EDTA, pH 7.4, using a Varian Cary 4000 UV-vis spectrophotometer equipped with a thermoelectrically controlled cell holder and quartz cells with a pathlength of 1 cm. The melting temperature (T_m) was determined as the temperature corresponding to a maximum on the first derivation profile of the melting curves.

Tb³⁺ fluorescence. Ct DNA was modified with Pt complexes in 10 mM NaClO₄ at 37 °C. After 24 h of incubation, DNA was dialysed against 0.1 M NaCl and then against 10 mM NaClO₄. The level of DNA platination was verified using FAAS. The terbium fluorescence was measured using a previously described method.¹⁸ Briefly, the samples of platinated or unplatinated DNA (2.5×10^{-5} M) were incubated with 5×10^{-5} M TbCl₃ for 60 min at 25 °C. Subsequently, the fluorescence intensity was measured in a 1 cm quartz cell using a Varian Cary Eclipse spectrofluorophotometer. Excitation and emission wavelengths

were set to 290 and 546 nm, respectively, the slit widths were 5 nm, and the integration time was set to 5 s.

Unwinding of negatively supercoiled DNA. The unwinding of closed circular supercoiled pSP73 plasmid DNA was assayed using an agarose gel mobility shift assay.¹⁹ Plasmid DNA (pSP73) was incubated with the platinum complex for 24 h, precipitated by ethanol to remove unbound Pt, and redissolved in TAE buffer (0.04 M Tris-acetate, 1 mM EDTA, pH 7.0). An aliquot of the precipitate was subjected to electrophoresis on 1% agarose gels running at 25 °C in the dark with TAE buffer. The gels were stained with EtBr, followed by photography with a transilluminator. Another aliquot was used to determine the r_b values using FAAS. The unwinding angle θ , induced per platinum–DNA adduct, was calculated based upon the r_b value at which the transformation of the supercoiled to a relaxed form of the plasmid was complete.¹⁹

Interstrand cross-link formation assay. The complexes **8c**, **9c**, **10a–c** and CDDP were incubated at different concentrations (CDDP r_b = 0, 0.001, 0.0015, 0.002; **8c**, **9c**, **10c** r_b = 0, 0.01, 0.015, 0.02) for 24 h with 500 ng of pSP73KB DNA after it had been linearized by EcoRI and 3'-end-labeled by means of a Klenow fragment of DNA polymerase I and [α -32P]dATP. After incubation, the reaction was stopped by addition of NaCl to a final concentration of 0.1 M and samples were precipitated. The sediments were dissolved in 10 mM NaClO₄, and the number of interstrand crosslinks was analysed using electrophoresis under denaturing conditions on an alkaline agarose gel (1%). After the electrophoresis had been completed, the gels were dried and visualised using a FUJIFILM BAS 2500 bio-imaging analyser. The intensities of the bands corresponding to single strands of DNA and interstrand cross-linked duplex were quantified using AIDA image analysis software. The frequency of ICLs, was calculated as % ICL/Pt = XL/4910 \times r_b (the pSP73KB plasmid contained 4910 nucleotide residues), in which % ICL/Pt is the number of ICLs per adduct and XL is the number of ICLs per molecule of the linearized DNA duplex and was calculated assuming a Poisson distribution of the ICLs as XL = $-\ln A$. In which A is the fraction of molecules running as a band corresponding to the non-crosslinked DNA. The values of r_b were determined using FAAS by measuring the amount of free, unbound platinum in the supernatants after precipitation of the samples; the amount of platinum bound to DNA, r_b , was calculated by subtracting the amount of platinum remaining in the solution from the total amount of platinum present in the reaction.

Cell cycle analysis. The cell cycle analysis of the HCT116 cells was performed *via* flow cytometry of the treated HCT116^{wt} and HCT116^{-/-} cells. They were seeded at 0.1×10^6 cells per mL into the wells of a 6-well plate and incubated for 24 h under cell culture conditions. Appropriate dilutions of **8c**, **9c**, **10c** and CDDP in ddH₂O (30.3 μ L) were added to each well (final concentrations: **8c** 5 μ M, **9c** and **10c** 500 nM, CDDP 10 μ M). The cells were incubated for another 24 h under cell culture conditions. On the next day the medium from each well was transferred into a centrifugation tube and the cells were washed with 1 mL PBS. After transferring the PBS to the

respective tubes, the cells were trypsinised for *ca.* 2 min at 37 °C. The detached cells were transferred into the tubes and centrifuged (300g, 4 °C, 5 min). The supernatant was discarded and the cells were fixed in 1 mL of ice-cold 70% EtOH for 1 h at 4 °C.

For propidium iodide staining, the cells were centrifuged (400g, room temperature, 5 min), the supernatant was discarded, and the pellet was layered with 1 mL PBS. After 5 min the cells were again centrifuged and the PBS discarded. The cells were resuspended in 200 μ L of a PI staining solution (0.1% sodium citrate, 50 μ g mL⁻¹ propidium iodide, 50 μ g mL⁻¹ RNase A) for 30 min at 37 °C. The distribution of the cells in the different phases of the cell cycle was measured *via* flow cytometry.

Conflicts of interest

There are no conflicts to declare.

Acknowledgements

RS thanks the Deutsche Forschungsgemeinschaft for a grant (Scho 402/12), JK, HK and VB thank the Czech Science Foundation and Ministry of Education of the Czech Republic for grant (18-09502S and LTC17003), and MR thanks the Bayreuth University Graduate School for financial support. We also thank the COST Action CM1105 'Functional metal complexes that bind to biomolecules' for financial support.

References

- (a) A.-M. Florea and D. Büsselberg, *Cancers*, 2011, **3**, 1351–1371, DOI: 10.3390/cancers3011351; (b) S. Dasari and P. B. Tchounwou, *Eur. J. Pharmacol.*, 2014, **740**, 364–378, DOI: 10.1016/j.ejphar.2014.07.025.
- (a) K. M. Deo, D. L. Ang, B. McGhie, A. Rajamanickam, A. Dhiman, A. Khoury, J. Holland, A. Bjelosevic, B. Pages, C. Gordon and J. R. Aldrich-Wright, *Coord. Chem. Rev.*, 2018, **375**, 148–163, DOI: 10.1016/j.ccr.2017.11.014; (b) T. C. Johnstone, K. Suntharalingam and S. J. Lippard, *Chem. Rev.*, 2016, **116**, 3436–3486, DOI: 10.1021/acs.chemrev.5b00597.
- A. J. Arduengo, R. L. Harlow and M. Kline, *J. Am. Chem. Soc.*, 1991, **113**, 361–363, DOI: 10.1021/ja00001a054.
- X. Bantreil, J. Broggi and S. P. Nolan, *Annu. Rep. Prog. Chem., Sect. B*, 2009, **105**, 232–263, DOI: 10.1039/b822056p.
- (a) L. Oehninger, R. Rubbiani and I. Ott, *Dalton Trans.*, 2013, **42**, 3269–3284, DOI: 10.1039/c2dt32617e; (b) W. Liu and R. Gust, *Coord. Chem. Rev.*, 2016, **329**, 191–213, DOI: 10.1016/j.ccr.2016.09.004.
- (a) S. Patil, A. Deally, B. Gleeson, H. Müller-Bunz, F. Paradisi and M. Tacke, *Metallomics*, 2011, **3**, 74–88, DOI: 10.1039/c0mt00034e; (b) R. A. Haque, S. Y. Choo, S. Budagumpi, M. A. Iqbal and A. Al-Ashraf Abdullah,

- Eur. J. Med. Chem.*, 2015, **90**, 82–92, DOI: 10.1016/j.ejmech.2014.11.005.
- 7 (a) R. Rubbiani, S. Can, I. Kitanovic, H. Alborzinia, M. Stefanopoulou, M. Kokoschka, S. Monchgesang, W. S. Sheldrick, S. Wölfl and I. Ott, *J. Med. Chem.*, 2011, **54**, 8646–8657, DOI: 10.1021/jm201220n; (b) J. K. Muenzner, B. Biersack, H. Kalie, I. C. Andronache, L. Kaps, D. Schuppan, F. Sasse and R. Schobert, *ChemMedChem*, 2014, **9**, 1195–1204, DOI: 10.1002/cmdc.201400049; (c) J. K. Muenzner, B. Biersack, A. Albrecht, T. Rehm, U. Lacher, W. Milius, A. Casini, J. Zhang, I. Ott, V. Brabec, O. Stuchlikova, I. C. Andronache, L. Kaps, D. Schuppan and R. Schobert, *Chem. – Eur. J.*, 2016, **22**, 18953–18962, DOI: 10.1002/chem.201604246.
- 8 (a) W. Streciwilk, F. Hackenberg, H. Müller-Bunz and M. Tacke, *Polyhedron*, 2014, **80**, 3–9, DOI: 10.1016/j.poly.2013.11.039; (b) M.-L. Teyssot, A.-S. Jarrousse, A. Chevy, A. De Haze, C. Beaudoin, M. Manin, S. P. Nolan, S. Díez-González, L. Morel and A. Gautier, *Chem. – Eur. J.*, 2009, **15**, 314–318, DOI: 10.1002/chem.200801992.
- 9 (a) G. Lv, L. Guo, L. Qiu, H. Yang, T. Wang, H. Liu and J. Lin, *Dalton Trans.*, 2015, **44**, 7324–7331, DOI: 10.1039/c5dt00169b; (b) L. Oehninger, M. Stefanopoulou, H. Alborzinia, J. Schur, S. Ludewig, K. Namikawa, A. Muñoz-Castro, R. W. Köster, K. Baumann, S. Wölfl, W. S. Sheldrick and I. Ott, *Dalton Trans.*, 2013, **42**, 1657–1666, DOI: 10.1039/c2dt32319b.
- 10 (a) M. Skander, P. Retailleau, B. Bourrié, L. Schio, P. Mailliet and A. Marinetti, *J. Med. Chem.*, 2010, **53**, 2146–2154, DOI: 10.1021/jm901693m; (b) E. Chardon, G. Dahm, G. Guichard and S. Bellemin-Laponnaz, *Organometallics*, 2012, **31**, 7618–7621, DOI: 10.1021/om300806g; (c) R. Wai-Yin Sun, A. Lok-Fung Chow, X.-H. Li, J. J. Yan, S. Sin-Yin Chui and C.-M. Che, *Chem. Sci.*, 2011, **2**, 728–736, DOI: 10.1039/c0sc00593b; (d) J. K. Muenzner, T. Rehm, B. Biersack, A. Casini, I. de Graaf, P. Worawutputtpong, A. Noor, R. Kempe, V. Brabec, J. Kasparkova and R. Schobert, *J. Med. Chem.*, 2015, **58**, 6283–6292, DOI: 10.1021/acs.jmedchem.5b00896; (e) M. Bouché, G. Dahm, A. Maise-François, T. Achard and S. Bellemin-Laponnaz, *Eur. J. Inorg. Chem.*, 2016, **17**, 2828–2836, DOI: 10.1002/ejic.201600296.
- 11 T. Rehm, M. Rothmund, J. K. Muenzner, A. Noor, R. Kempe and R. Schobert, *Dalton Trans.*, 2016, **45**, 15390–15398, DOI: 10.1039/c6dt02350a.
- 12 (a) R. Rubbiani, I. Kitanovic, H. Alborzinia, S. Can, A. Kitanovic, L. A. Onambe, M. Stefanopoulou, Y. Geldmacher, W. S. Sheldrick, G. Wolber, A. Prokop, S. Wölfl and I. Ott, *J. Med. Chem.*, 2010, **53**, 8608–8618, DOI: 10.1021/jm100801e; (b) H. Valdés, M. Poyatos, G. Ujaque and E. Peris, *Chem. – Eur. J.*, 2015, **21**, 1578–1588, DOI: 10.1002/chem.201404618; (c) H. Lu and R. L. Brutchey, *Chem. Mater.*, 2017, **29**, 1396–1403, DOI: 10.1021/acs.chemmater.6b05293.
- 13 (a) T. Nakanishi and D. D. Ross, *Chin. J. Cancer*, 2012, **31**, 73–99, DOI: 10.5732/cjc.011.10320; (b) D. Shen, C. Cararelli, *et al.*, *J. Biol. Chem.*, 1986, **261**, 7762–7770; (c) M. M. Cromwell, A. R. Safa, R. L. Felsted, M. M. Gottesman and I. Pastan, *Proc. Natl. Acad. Sci. U. S. A.*, 1986, **83**, 3847–3850, DOI: 10.1073/pnas.83.11.3847.
- 14 (a) P. Bragado, A. Armesilla, A. Silva and A. Porras, *Apoptosis*, 2007, **12**, 1733–1742, DOI: 10.1007/s10495-007-0082-8; (b) Q. Kai, L. Ting, W. Jichao, M. Fandi, W. Zhixin, H. Zichao, W. Yong, S. Sidong, L. Sinan, C. Hulin, D. Yafeng and L. Chang, *J. South. Med. Univ.*, 2013, **33**, 1253–1259, DOI: 10.3969/j.ssn.1673-4254.2013.09.01; (c) N. S. Pellegata, R. J. Antoniono, J. L. Redpath and E. J. Standbridge, *Proc. Natl. Acad. Sci. U. S. A.*, 1996, **93**, 15209–15214, DOI: 10.1073/pnas.93.26.15209.
- 15 G. He, Z. H. Siddik, Z. Huang, R. Wang, J. Koomen, R. Kobayashi, A. R. Khokhar and J. Kuang, *Oncogene*, 2005, **24**, 2929–2943, DOI: 10.1038/sj.onc.1208474.
- 16 (a) S. Tabassum, G. Chandra Sharma, F. Arjmad and A. Azam, *Nanotechnology*, 2010, **21**, 195102–114094, DOI: 10.1088/0957-4484/21/19/195102; (b) V. Vijayanathan, T. Thomas and T. J. Thomas, *Biochemistry*, 2002, **41**, 14085–14094, DOI: 10.1021/bi0203987.
- 17 (a) N. P. Johnson, *Biochem. Biophys. Res. Commun.*, 1982, **104**, 1394–1400, DOI: 10.1016/0006-291X(82)91404-8; (b) A. M. J. Fichtinger-Schepman, J. L. Van der Veer, J. H. J. Den Hartog, P. H. M. Lohman and J. Reedijk, *Biochemistry*, 1985, **24**, 707–713, DOI: 10.1021/bi00324a025; (c) A. Eastman, *Pharmacol. Ther.*, 1987, **34**, 155–166, DOI: 10.1016/0163-7258(87)90009-X.
- 18 Z. Balcarova and V. Brabec, *Biophys. Chem.*, 1989, **33**, 55–61, DOI: 10.1016/0301-4622(89)80007-9.
- 19 M. V. Keck and S. J. Lippard, *J. Am. Chem. Soc.*, 1992, **114**, 3386–3390, DOI: 10.1021/ja00035a033.
- 20 (a) G. L. Cohen, W. R. Bauer, J. K. Barton and S. J. Lippard, *Science*, 1979, **203**, 1014–1016, DOI: 10.1126/science.370979; (b) W. M. Scovell and F. Collart, *Nucleic Acids Res.*, 1985, **13**, 2881–2895.
- 21 R. Zaludova, V. Kleinwachter and V. Brabec, *Biophys. Chem.*, 1996, **60**, 135–142, DOI: 10.1016/0301-4622(96)00010-5.
- 22 (a) K. S. Lovejoy, M. Serova, I. Bieche, S. Emami, M. D'Incalci, M. Broggini, E. Erba, C. Gespach, E. Cvitkovic, S. Faivre, E. Raymond and S. J. Lippard, *Mol. Cancer Ther.*, 2011, **10**, 1709–1719, DOI: 10.1158/1535-7163.MCT-11-0250; (b) G. Y. Park, J. J. Wilson, Y. Song and S. J. Lippard, *Proc. Natl. Acad. Sci. U. S. A.*, 2012, **109**, 11987–11992, DOI: 10.1073/pnas.1207670109; (c) B. Wang, Z. Wang, F. Ai, W. K. Tang and G. Zhu, *J. Inorg. Biochem.*, 2015, **142**, 118–125, DOI: 10.1016/j.jinorgbio.2014.10.003; (d) G. Y. Zhu, M. Myint, W. H. Ang, L. Song and S. J. Lippard, *Cancer Res.*, 2012, **72**, 790–800, DOI: 10.1158/0008-5472.CAN-11-3151.
- 23 R. C. Todd and S. J. Lippard, *Metallomics*, 2009, **1**, 280–291, DOI: 10.1039/b907567d.
- 24 (a) S. Teletchéa, S. Komeda, J.-M. Teuben, M. A. Elizondo-Riojas, J. Reedijk and J. Kozelka, *Chem. – Eur. J.*, 2006, **12**, 3741–3753; (b) J. Mlcouskova, J. Malina, V. Novohradsky, J. Kasparkova, S. Komeda and V. Brabec, *Biochim. Biophys.*

[View Article Online](#)

Dalton Transactions

Paper

Acta, 2012, **1820**, 1502–1511, DOI: 10.1016/j.bbagen.2012.05.014; (c) J. Mlcouskova, J. Kasparkova, T. Suchankova, S. Komeda and V. Brabec, *J. Inorg. Biochem.*, 2012, **114**, 15–23, DOI: 10.1016/j.jinorgbio.2012.04.015.

25 M. D. Hall, K. A. Telma, K.-E. Chang, T. D. Lee, J. P. Madigan, J. R. Lloyd, I. S. Goldlust, J. D. Hoeschele and M. M. Gottesman, *Cancer Res.*, 2014, **74**, 3913–3922, DOI: 10.1158/0008-5472.CAN-14-0247.

Electronic Supplementary Material (ESI) for Dalton Transactions.
This journal is © The Royal Society of Chemistry 2018

Electronic Supporting Information

N,N-Dialkylbenzimidazol-2-ylidene platinum complexes – effects of alkyl residues and ancillary *cis*-ligands on their anticancer activity

Tobias Rehm,^a Matthias Rothmund,^a Alexander Bär,^a Thomas Dietel,^b Rhett Kempe,^b Hana Kostřhunová,^c Viktor Brabec,^c Jana Kasparková,^{*c} and Rainer Schobert^{*a}

^a*Organic Chemistry Laboratory, University Bayreuth, Universitätsstrasse 30, 95440 Bayreuth, Germany.*

E-mail: Rainer.Schobert@uni-bayreuth.de

^b *Lehrstuhl fuer Anorganische Chemie II, University Bayreuth, Universitätsstrasse 30, 95440 Bayreuth, Germany.*

^c *Institute of Biophysics, Academy of Sciences of the Czech Republic, CZ-61265 Brno, Czech Republic.*

E-mail: jana@ibp.cz

Table of content:

General information	S1
Synthesis and characterization of benzimidazolium chlorides	S2
X-ray structural data of complexes 8b , 9c and 10a (Table S1)	S3
NMR spectra of complexes 8a-d , 9a-d and 10a-c (Fig. S1-S40)	S4
Values of cellular accumulation of complexes 8c , 9a-d , 10c and CDDP (Table S2)	S25
Sequence preferences of complexes 8c , 9c and 10a-c (Table S3)	S25
Influence of complexes 8c , 9c , 10a-c and CDDP on the melting point of ct DNA (Fig. S41)	S25
Influence of complexes 8c , 9c , 10a-c and CDDP on the relative Tb ³⁺ ion fluorescence (Fig. S42)	S26
Unwinding of negatively supercoiled pSP73 plasmid DNA by 8c , 9c , 10a-c and CDDP (Fig. S43)	S26
Cell cycle analysis of complexes 8c , 9c and 10c in HCT116 ^{-/-} cells (Fig. S44)	S27
References	S27

*shared corresponding authors.

General information

All the chemicals and reagents were purchased from Sigma Aldrich, Alfa Aesar, ChemPur or ABCR and were used without further purification. Melting points are uncorrected; NMR spectra were run on a 500 MHz spectrometer; chemical shifts are given in ppm (δ) and referenced relative to the internal solvent signal; ^{195}Pt NMR shifts are quoted relative to $\Xi(^{195}\text{Pt}) = 21.496784$ MHz, K_2PtCl_4 was used as external standard ($\delta = -1612.81$); mass spectra: direct inlet, EI, 70 eV; elemental analyses: Vario EL III elemental analyser; X-Ray Diffractometer: STOE-IPDS II. Synthesis of benzimidazolium salts was performed based on literature procedures¹⁻³ as described herein.

Synthesis and characterization of benzimidazolium chlorides 6General procedure:

Benzimidazole (1eq) and the respective alkyl iodides or bromides (5 - 10 eq) in acetonitrile (10 mL/mmol) were treated with K_2CO_3 (1.5 eq) and the mixture was heated to 50 - 70 °C for 1-5 days. After filtration the solvent was evaporated in vacuo and the residue was crystallized from CH_2Cl_2 and hexane.

The resulting benzimidazolium iodides/bromides were then stirred with Ag_2CO_3 (1eq) and conc. HNO_3 (kat.) in Ethanol for 3 h and after filtration of the silver halides the solution was treated with conc. HCl to obtain the respective benzimidazolium chlorides. After neutralization with NaHCO_3 and further filtration the solvent was evaporated, and the solids were resuspended in CH_2Cl_2 to filter off all inorganic residues. The product was then crystallized by adding hexane.

Synthesis of 1,3-dimethylbenzimidazolium chloride:¹

Benzimidazole (472 mg, 4.0 mmol), iodomethane (2.48 mL, 40 mmol, 10 eq) and K_2CO_3 (828 mg, 6.0 mmol, 1.5 eq) in acetonitrile (40 mL) for 5 d at 50 °C gave 1.004 g (92 %) of the benzimidazolium iodide which was treated with Ag_2CO_3 (1.0 g, 3.7 mmol), conc. HNO_3 (100 μL) and conc. HCl (800 μL) in EtOH (80 mL). Yield: 632 mg (87 %) white solid; ^1H NMR (CDCl_3 , 500 MHz): δ 4.21 (6 H, s) 7.67 - 7.71 (2 H, m) 7.71 - 7.76 (2 H, m) 10.75 (1 H, s).

Synthesis of 1,3-diethylbenzimidazolium chloride:¹

Benzimidazole (500 mg, 4.2 mmol), iodoethane (1.26 mL, 21 mmol, 5 eq) and K_2CO_3 (871 mg, 6.3 mmol, 1.5 eq) in acetonitrile (40 mL) for 24 h at 70 °C gave 1.278 g (100 %) of the benzimidazolium iodide which was treated with Ag_2CO_3 (1.16 g, 4.2 mmol), conc. HNO_3 (100 μL) and conc. HCl (800 μL) in EtOH (80 mL). Yield: 880 mg (100 %) white solid; ^1H NMR (CDCl_3 , 500 MHz): δ 1.77 (6 H, t, $J = 7.3$ Hz) 4.70 (4 H, q, $J = 7.3$ Hz) 7.66 - 7.70 (2 H, m) 7.75 - 7.79 (2 H, m) 11.08 (1 H, s).

Synthesis of 1,3-dibutylbenzimidazolium chloride:²

Benzimidazole (2.0 g, 17 mmol), 1-bromobutane (7.2 mL, 68 mmol, 4 eq) and K_2CO_3 (3.5 g, 26 mmol, 1.5 eq) in acetonitrile (150 mL) for 5 d at 70 °C gave 3.635 g (69 %) of the benzimidazolium bromide which was treated with Ag_2CO_3 (3.22 g, 12 mmol), conc. HNO_3 (100 μL) and conc. HCl (800 μL) in EtOH (100 mL). Yield: 2.849 mg (63 %) amber solid; ^1H NMR (CDCl_3 , 500 MHz): δ 0.98 (6 H, t, $J = 7.5$ Hz) 1.44 (4 H, sxt, $J = 7.5$ Hz) 2.02 (4 H, quin, $J = 7.5$ Hz) 4.59 (4 H, t, $J = 7.5$ Hz) 7.64 - 7.68 (2 H, m) 7.70 - 7.74 (2 H, m) 11.46 (1 H, s).

Synthesis of 1,3-dioctylbenzimidazolium chloride:³

Benzimidazole (236 mg, 2.0 mmol), 1-bromooctane (1.74 mL, 10 mmol, 5 eq) and K_2CO_3 (414 mg, 3.0 mmol, 1.5 eq) in acetonitrile (20 mL) for 3 d at 70 °C gave 461 mg (54 %) of the benzimidazolium bromide which was treated with Ag_2CO_3 (300 mg, 1.1 mmol), conc. HNO_3 (30 μ L) and conc. HCl (200 μ L) in EtOH (20 mL). Yield: 398 mg (52 %) white solid; 1H NMR ($CDCl_3$, 500 MHz): δ 0.84 - 0.89 (6 H, m) 1.20 - 1.40 (20 H, m) 2.01 (4 H, quin, J = 7.5 Hz) 4.54 (4 H, t, J = 7.5 Hz) 7.64 - 7.69 (2 H, m) 7.69 - 7.75 (2 H, m) 11.05 (1 H, s).

Table S 1: X-ray structural data of platinum carbene complexes 8b, 9c and 10a.

Crystal data	8b	9c	10a
Chemical formula	$C_{13}H_{20}Cl_2N_2OPtS$	$C_{33}H_{37}Cl_2N_2PPt$	$C_{45}H_{40}ClN_2P_2Pt-Cl$
M_r	518.36	1517.27	936.72
Crystal system, space group	Triclinic, P^1	Triclinic, P^1	Monoclinic, $P2_1/c$
Temperature (K)	133	133	133
a, b, c (Å)	8.675 (5), 9.264 (5), 10.601 (5)	9.1067 (18), 12.792 (3), 13.803 (3)	12.578 (5), 10.790 (5), 32.126 (5)
α, β, γ (°)	91.874 (5), 103.182 (5), 94.722 (5)	88.02 (3), 87.59 (3), 71.06 (3)	90, 94.531 (5), 90
V (Å ³)	825.5 (8)	1519.2 (6)	4346 (3)
Z	2	1	4
$F(000)$	496	752	1864
D_x (Mg m ⁻³)	2085	1.658	1431
Radiation type	Mo $K\alpha$	Mo $K\alpha$	Mo $K\alpha$
No. of reflections for cell measurement	9824	31963	16101
θ range (°) for cell measurement	2.0–28.5	1.5–30.1	1.6–27.7
μ (mm ⁻¹)	8.95	4.87	3.46
Crystal shape	Needles	Block	Platte
Colour	Colourless	Colourless	Colourless
Crystal size (mm)	0.11 × 0.08 × 0.07	0.36 × 0.19 × 0.15	0.20 × 0.09 × 0.08
Data collection			
Diffractometer	STOE-STADIVARI	STOE-STADIVARI	STOE-STADIVARI
Scan method	ω -scan	ω -scan	ω -scan
Absorption correction	Numerical	Numerical	Numerical
	STOE X-RED32	STOE X-RED32	SROE X-RED32
T_{min}, T_{max}	0.680, 0.761	0.553, 0.719	0.863, 0.953
No. of measured, independent and observed [$I > 2\sigma(I)$] reflections	7449, 3177, 2704	21191, 5907, 5605	32457, 8450, 5359
R_{int}	0.042	0.022	0.104
θ values (°)	$\theta_{max} = 26.0, \theta_{min} = 2.0$	$\theta_{max} = 26.0, \theta_{min} = 1.5$	$\theta_{max} = 26.0, \theta_{min} = 1.6$
$(\sin \theta/\lambda)_{max}$ (Å ⁻¹)	0.617	0.617	0.617
Range of h, k, l	$h = -9 \rightarrow 10$ $k = -11 \rightarrow 9$ $l = -13 \rightarrow 11$	$h = -5 \rightarrow 11$ $k = -15 \rightarrow 15$ $l = -16 \rightarrow 17$	$h = -15 \rightarrow 8$ $k = -13 \rightarrow 13$ $l = -39 \rightarrow 37$
Refinement			
Refinement on	F^2	F^2	F^2

S3

$R[F^2 > 2\sigma(F^2)], wR(F^2), S$	0.033, 0.085, 1.03	0.017, 0.040, 1.04	0.072, 0.190, 0.95
No. of reflections	3177	5907	8450
No. of parameters	185	354	471
No. of restraints	0	0	27
H-atom treatment	H-atom parameters constrained	H-atom parameters constrained	H-atom parameters constrained
Weighting scheme	$w = 1/[\sigma^2(F_o^2) + (0.0485P)^2]$ where $P = (F_o^2 + 2F_c^2)/3$	$w = 1/[\sigma^2(F_o^2) + (0.0275P)^2 + 0.1532P]$ where $P = (F_o^2 + 2F_c^2)/3$	$w = 1/[\sigma^2(F_o^2) + (0.1181P)^2]$ where $P = (F_o^2 + 2F_c^2)/3$
$(\Delta/\sigma)_{\max}$	< 0.001	0.001	0.001
$\Delta\rho_{\max}, \Delta\rho_{\min} (e \text{ \AA}^{-3})$	2.52, -2.72	0.45, -1.24	1.99, -2.96

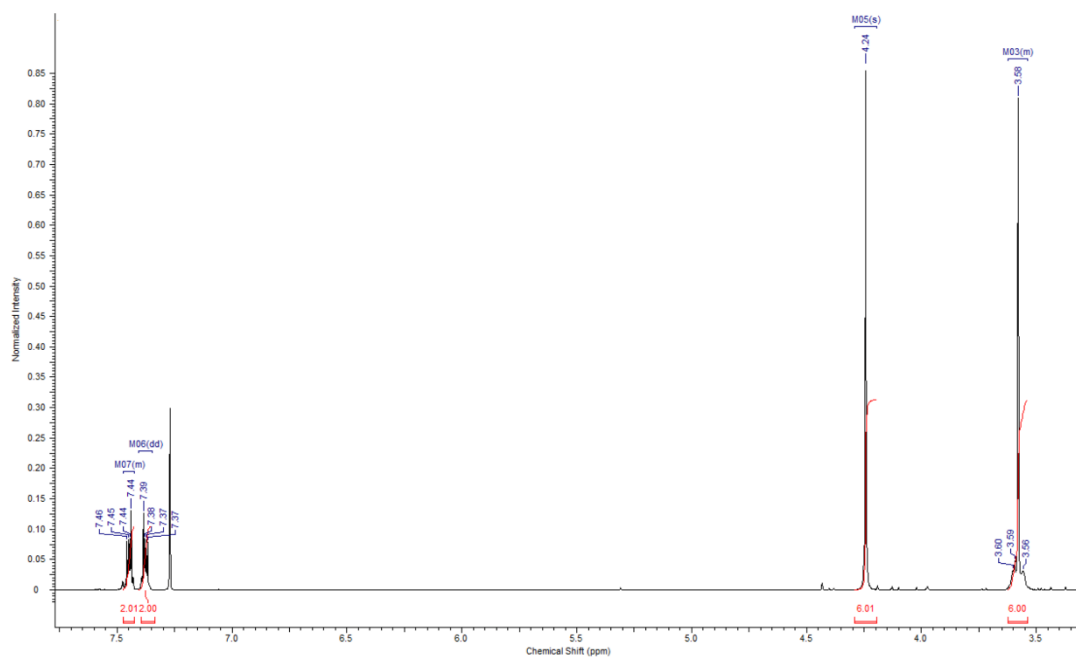


Fig. S1: ^1H -NMR spectrum (500 MHz, CDCl_3) of complex **8a**.

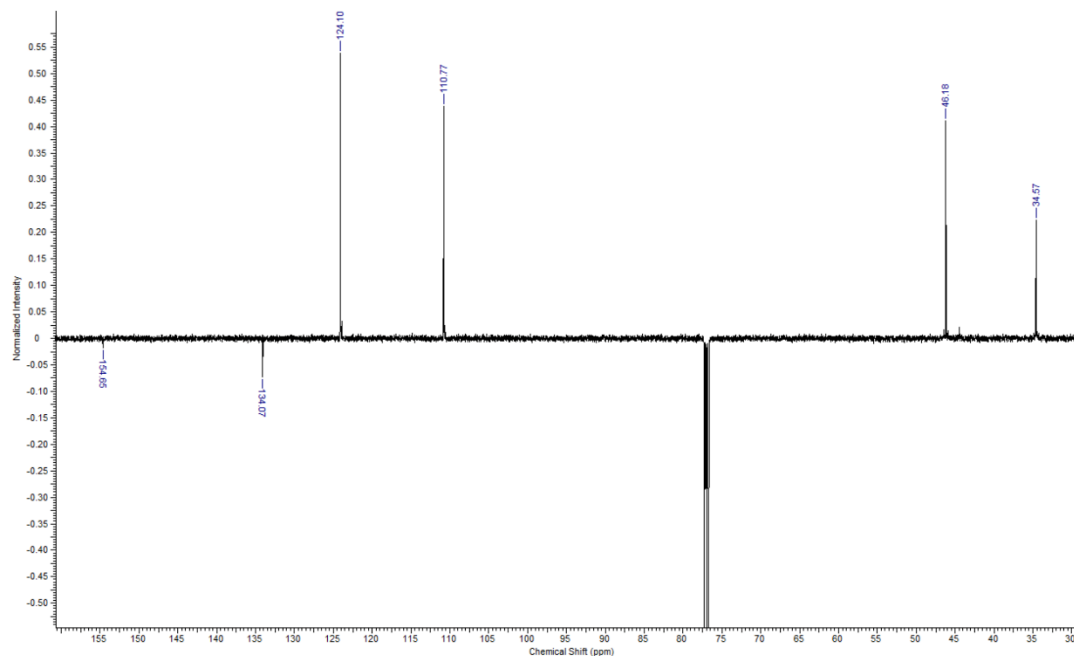


Fig. S 2: ^{13}C -NMR spectrum (126 MHz, CDCl_3) of complex **8a**.

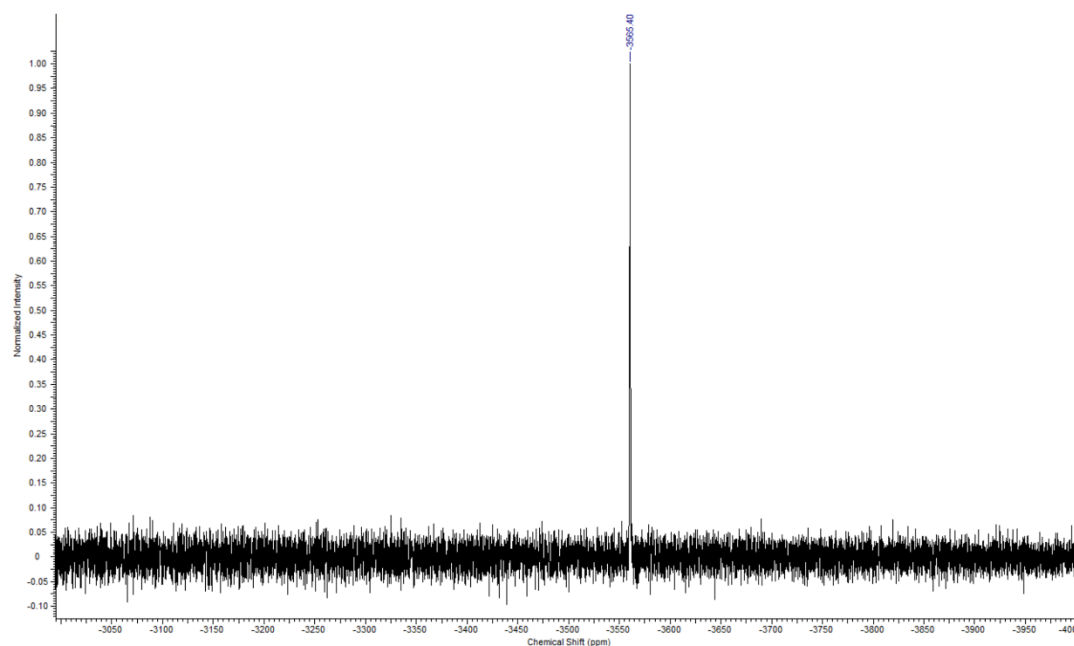


Fig. S 3: ^{195}Pt -NMR spectrum (108 MHz, CDCl_3) of complex **8a**.

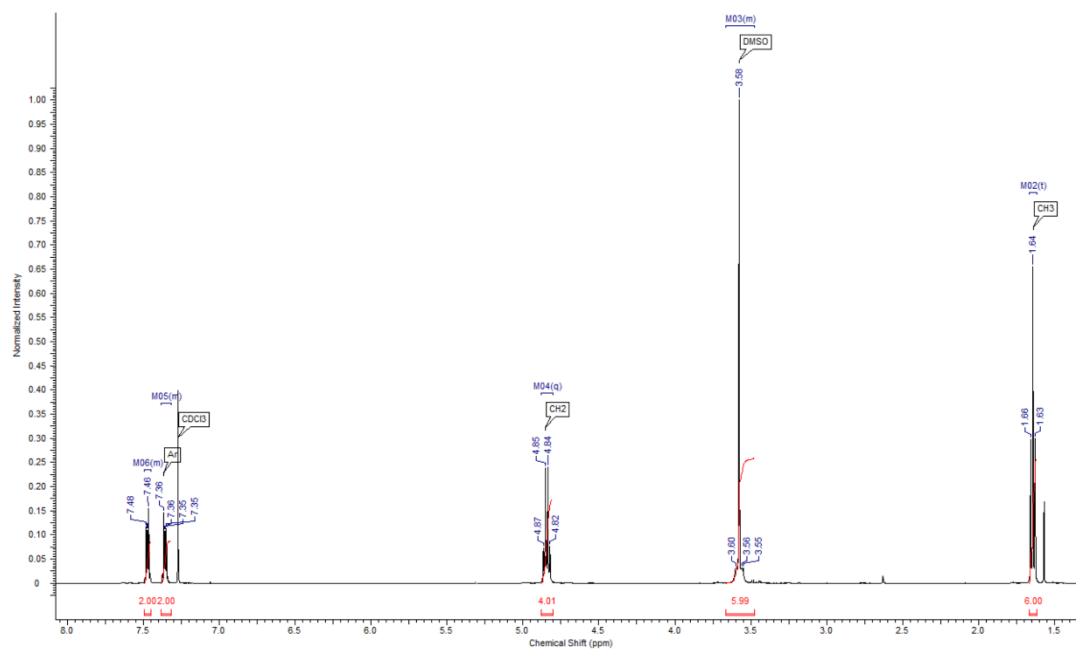


Fig. S 4: ^1H -NMR spectrum (500 MHz, CDCl_3) of complex **8b**.

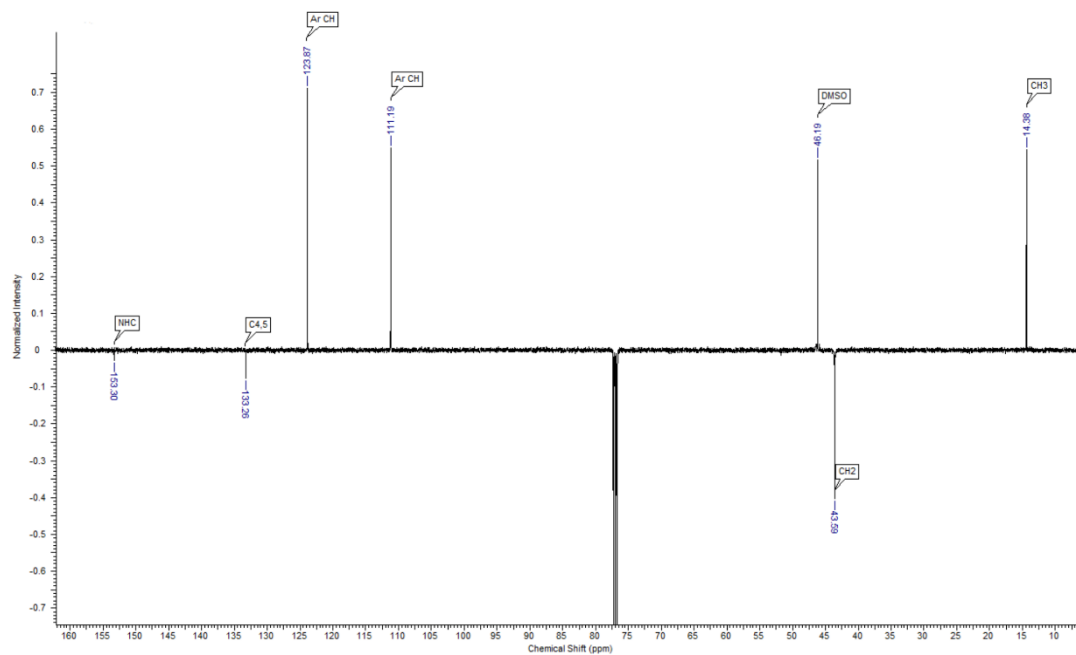


Fig. S 5: ^{13}C -NMR spectrum (126 MHz, CDCl_3) of complex **8b**.

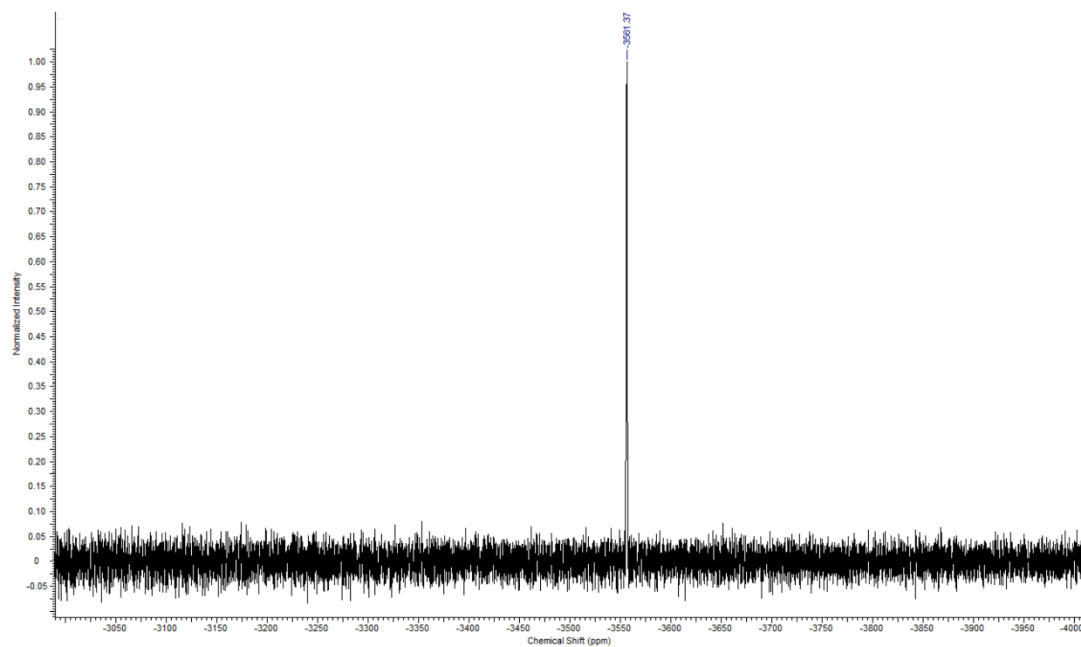


Fig. S 6: ^{195}Pt -NMR spectrum (108 MHz, CDCl_3) of complex **8b**.

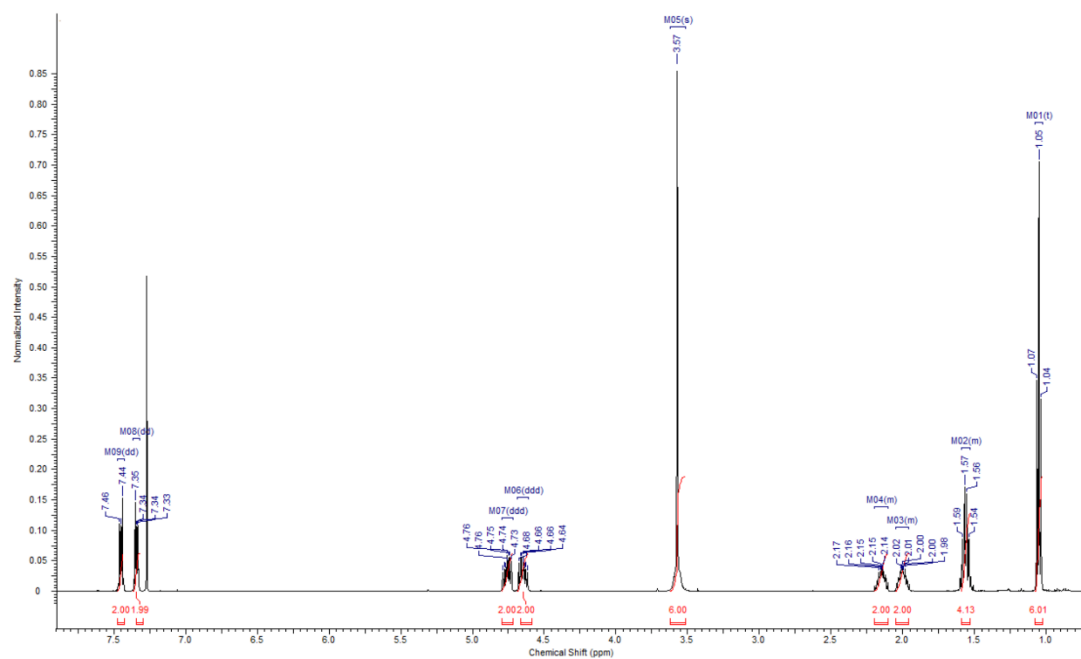


Fig. S 7: ^1H -NMR spectrum (500 MHz, CDCl_3) of complex **8c**.

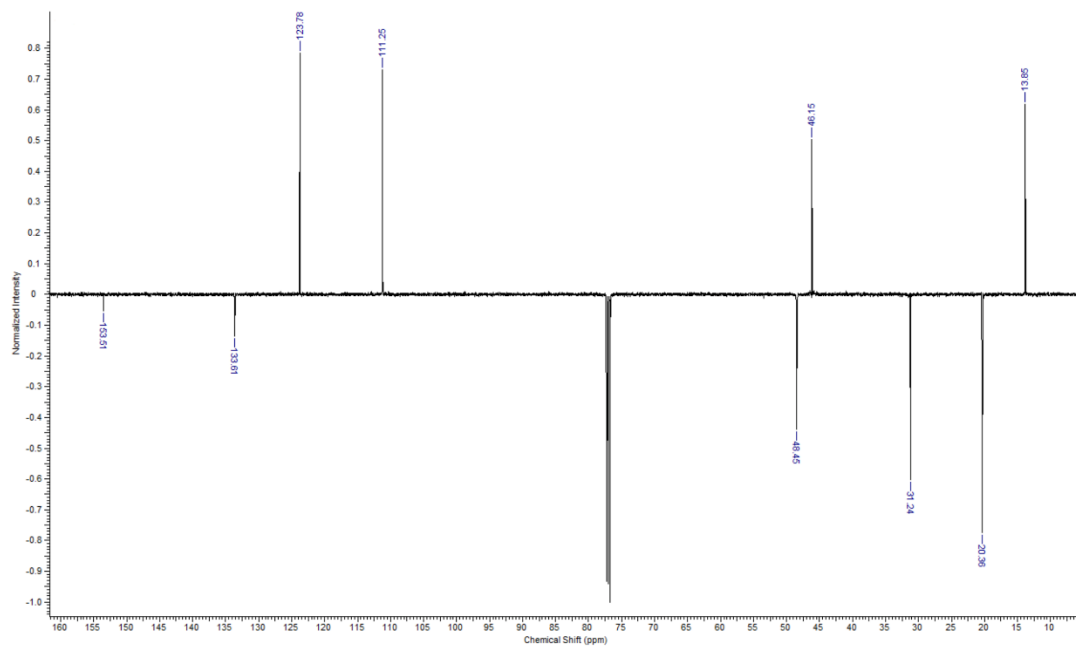


Fig. S 8: ^{13}C -NMR spectrum (126 MHz, CDCl_3) of complex **8c**.

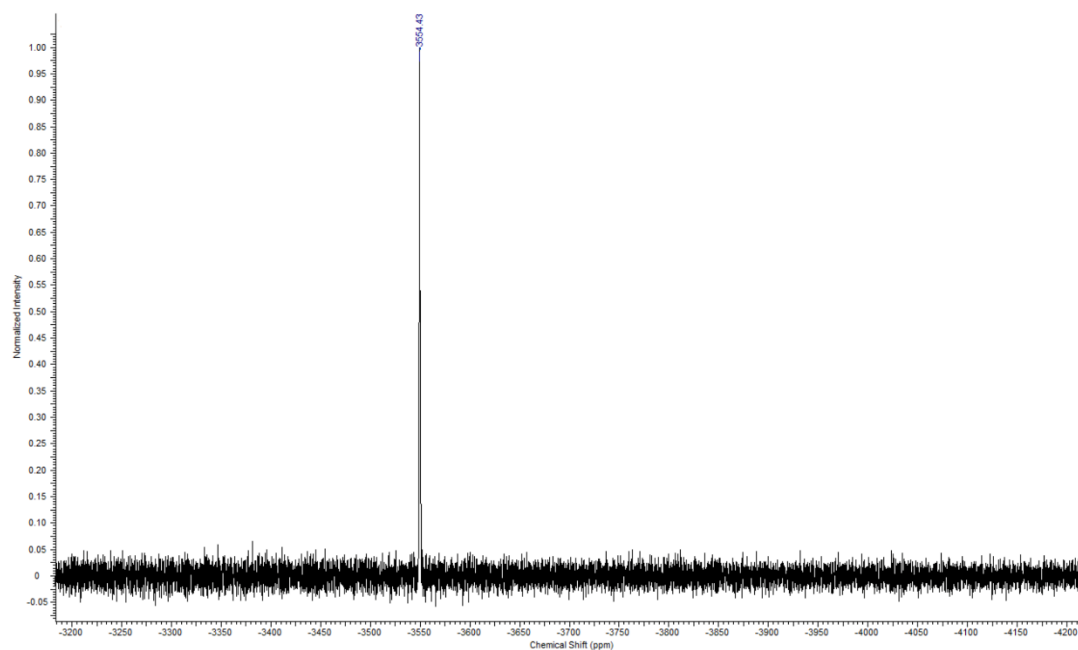


Fig. S 9: ^{195}Pt -NMR spectrum (108 MHz, CDCl_3) of complex **8c**.

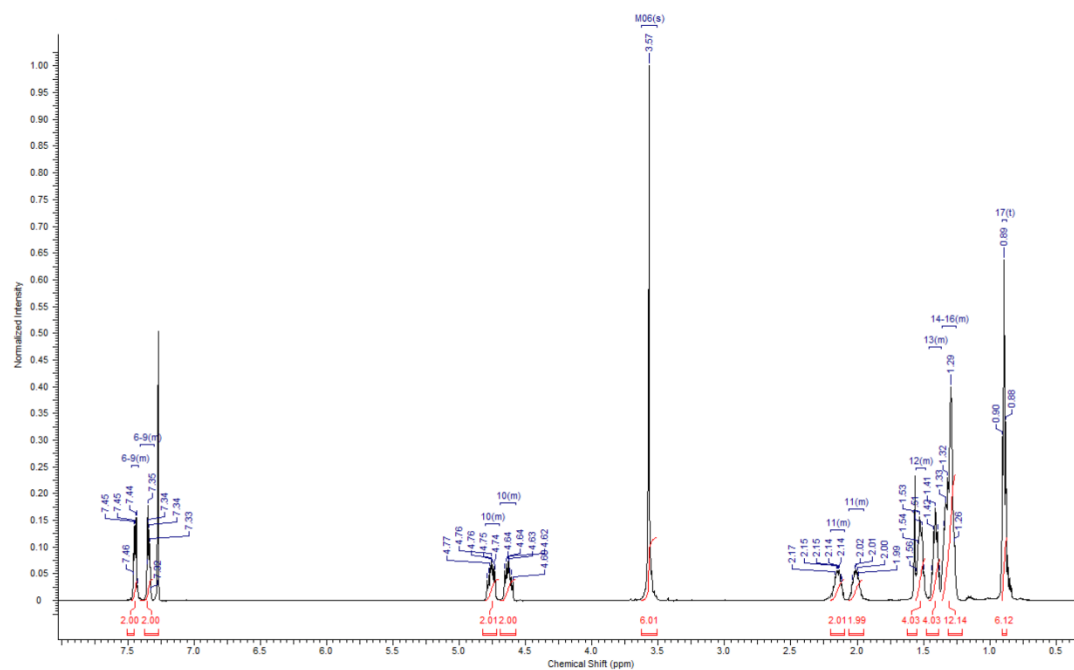


Fig. S 10: ^1H -NMR spectrum (500 MHz, CDCl_3) of complex **8d**.

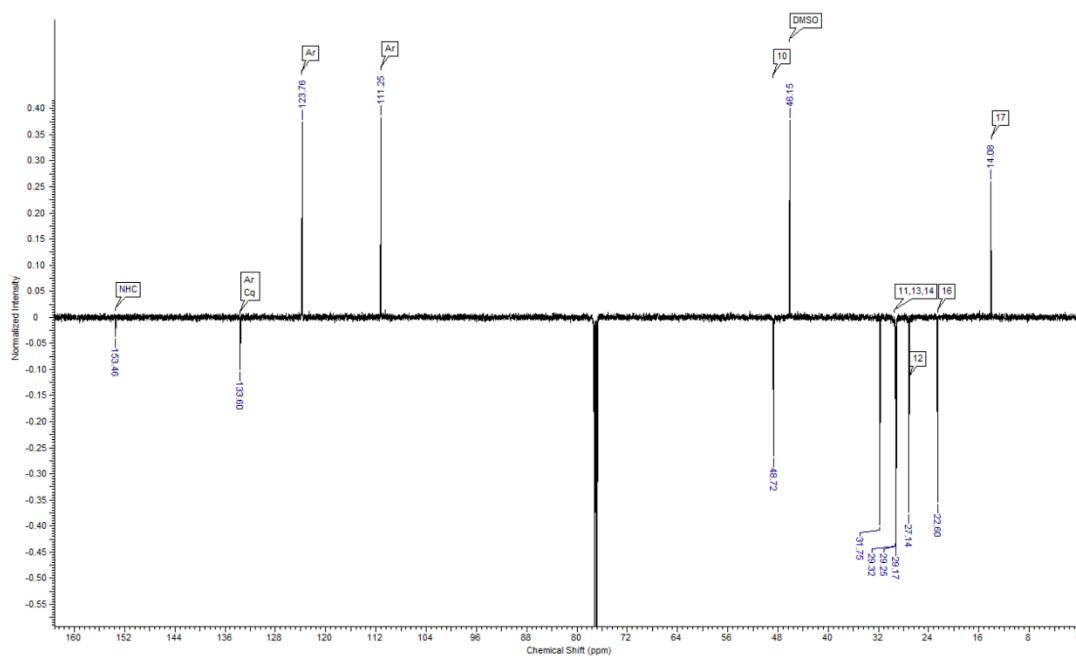


Fig. S 11: ^{13}C -NMR spectrum (126 MHz, CDCl_3) of complex **8d**.

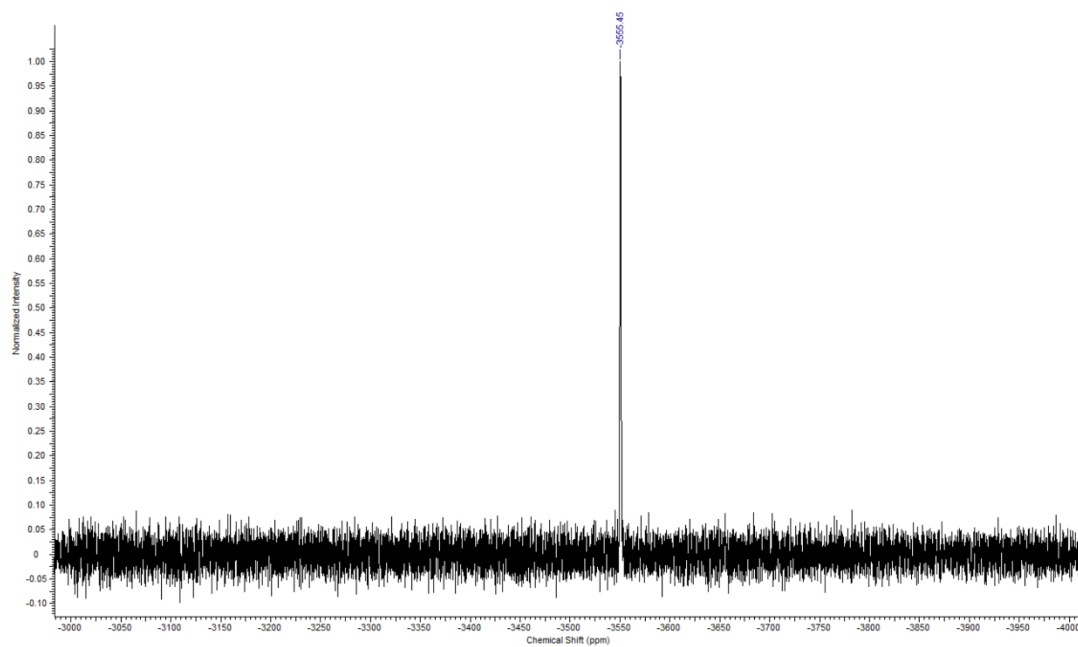


Fig. S 12: ^{195}Pt -NMR spectrum (108 MHz, CDCl_3) of complex **8d**.

S10

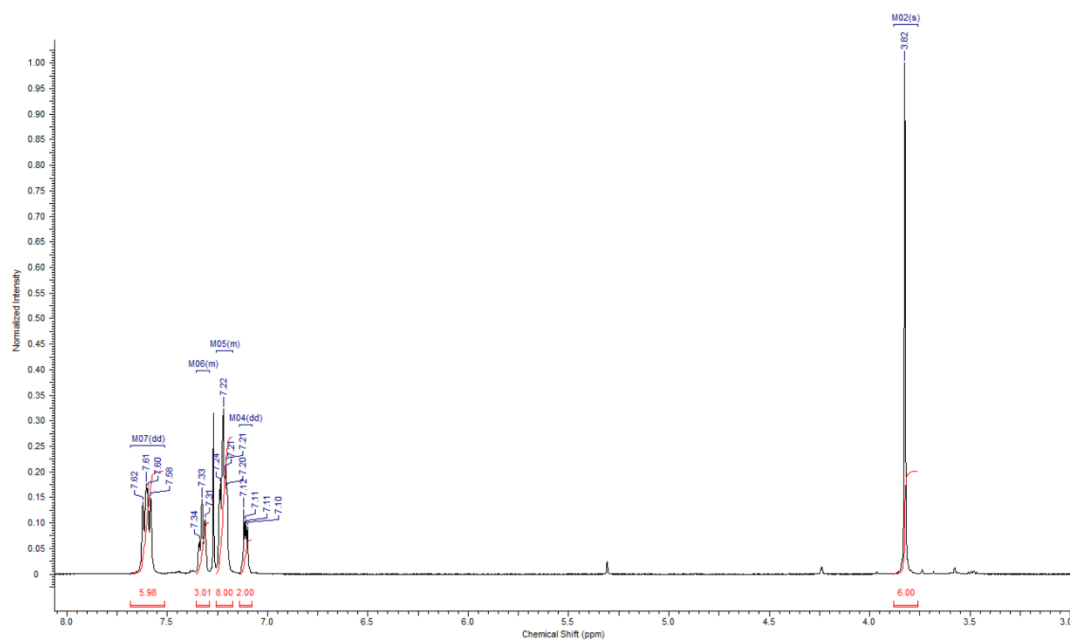


Fig. S 13: ^1H -NMR spectrum (500 MHz, CDCl_3) of complex **9a**.

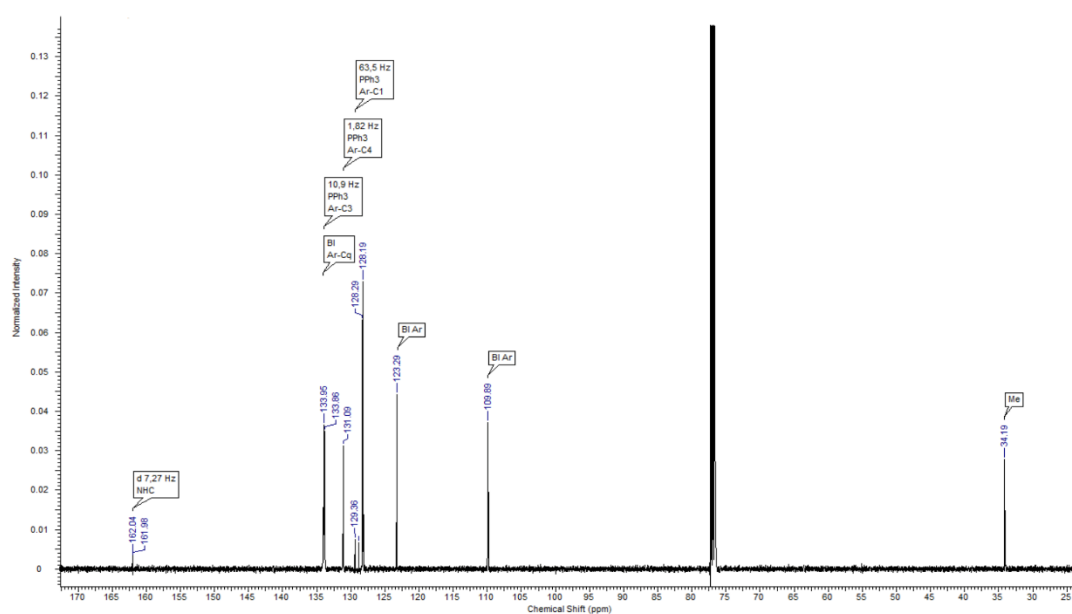


Fig. S 14: ^{13}C -NMR spectrum (126 MHz, CDCl_3) of complex **9a**.

S11

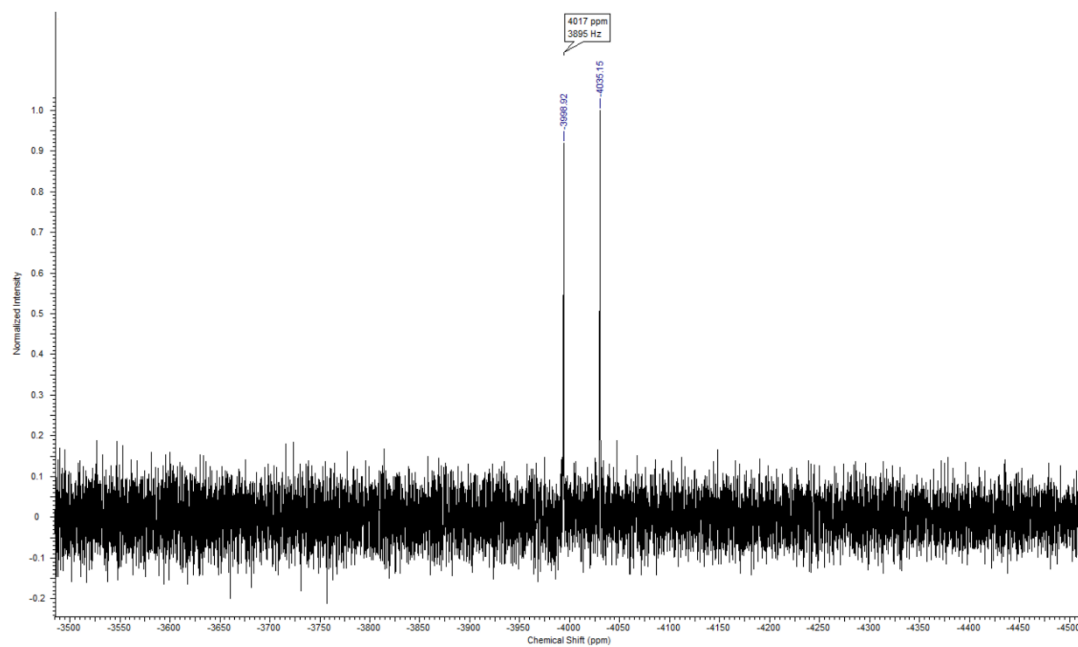


Fig. S 15: ^{195}Pt -NMR spectrum (108 MHz, CDCl_3) of complex **9a**.

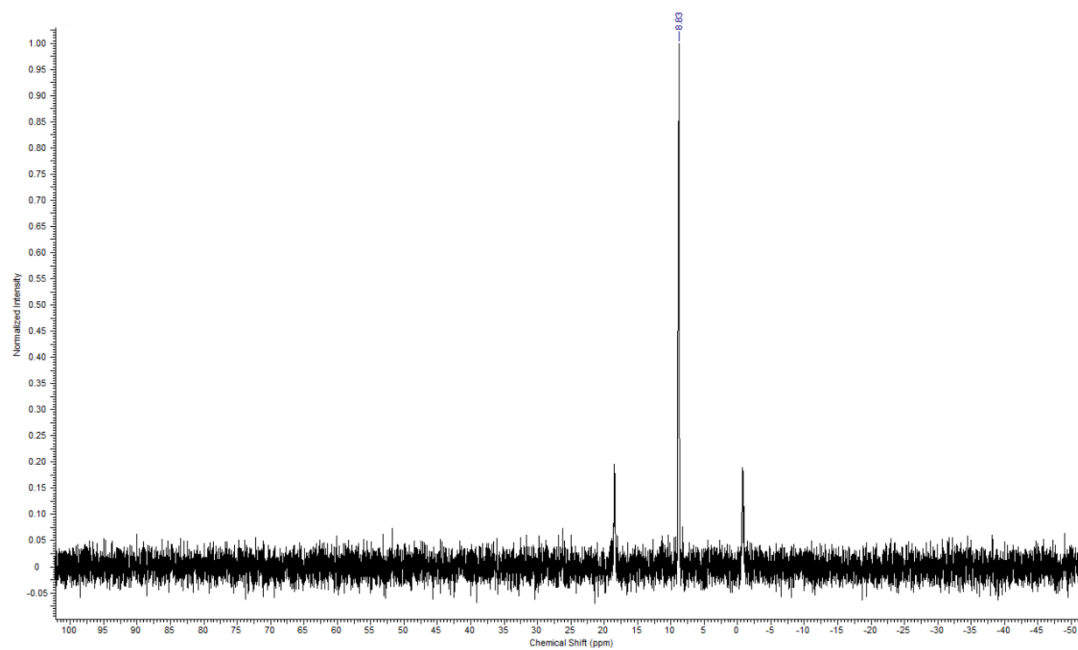


Fig. S 16: ^{31}P -NMR spectrum (202 MHz, CDCl_3) of complex **9a**.

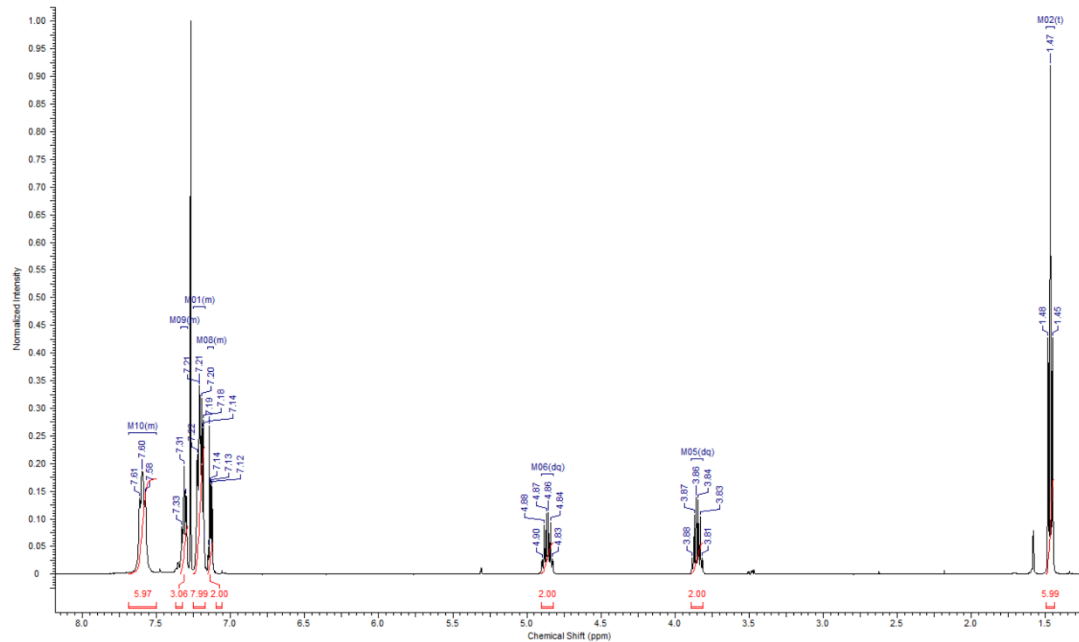


Fig. S 17: ¹H-NMR spectrum (500 MHz, CDCl₃) of complex **9b**.

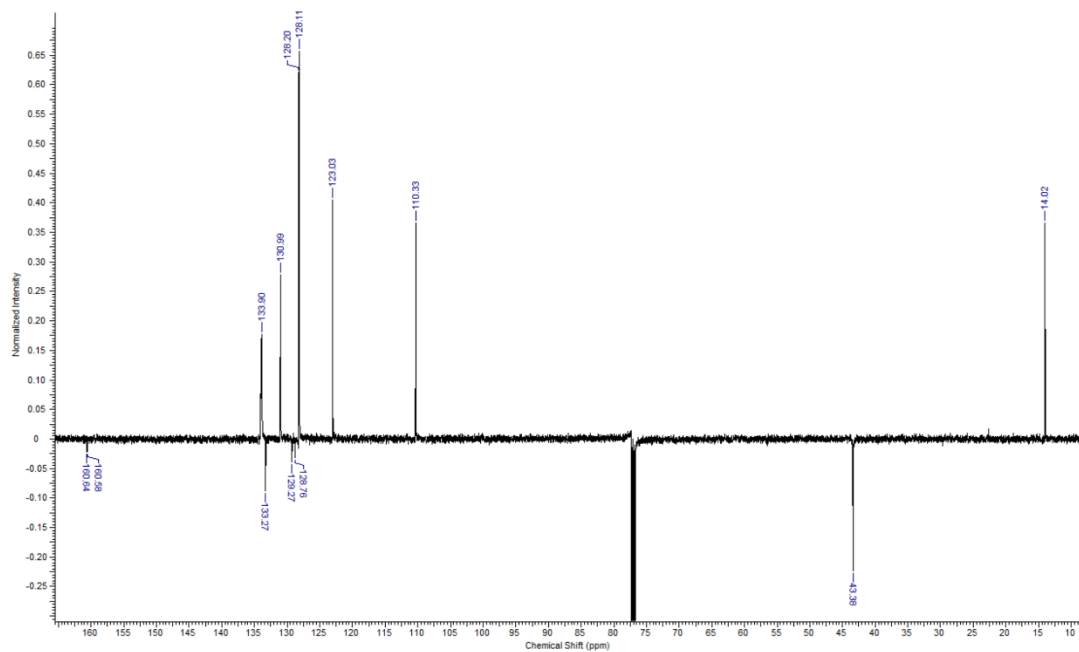


Fig. S 18: ¹³C-NMR spectrum (126 MHz, CDCl₃) of complex **9b**.

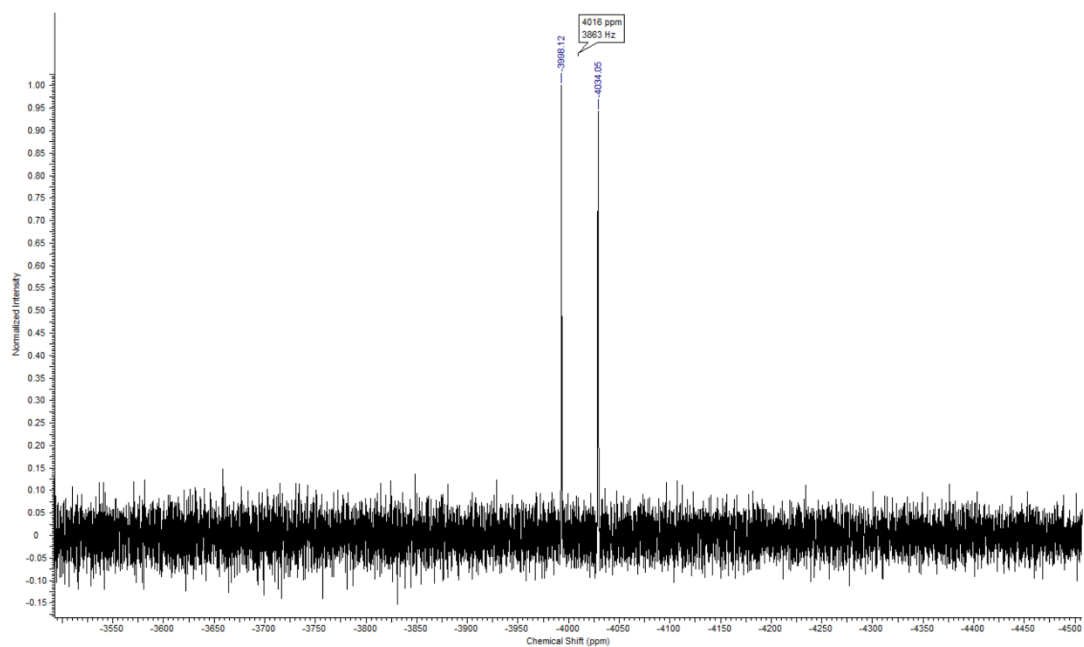


Fig. S 19: ^{195}Pt -NMR spectrum (108 MHz, CDCl_3) of complex **9b**.

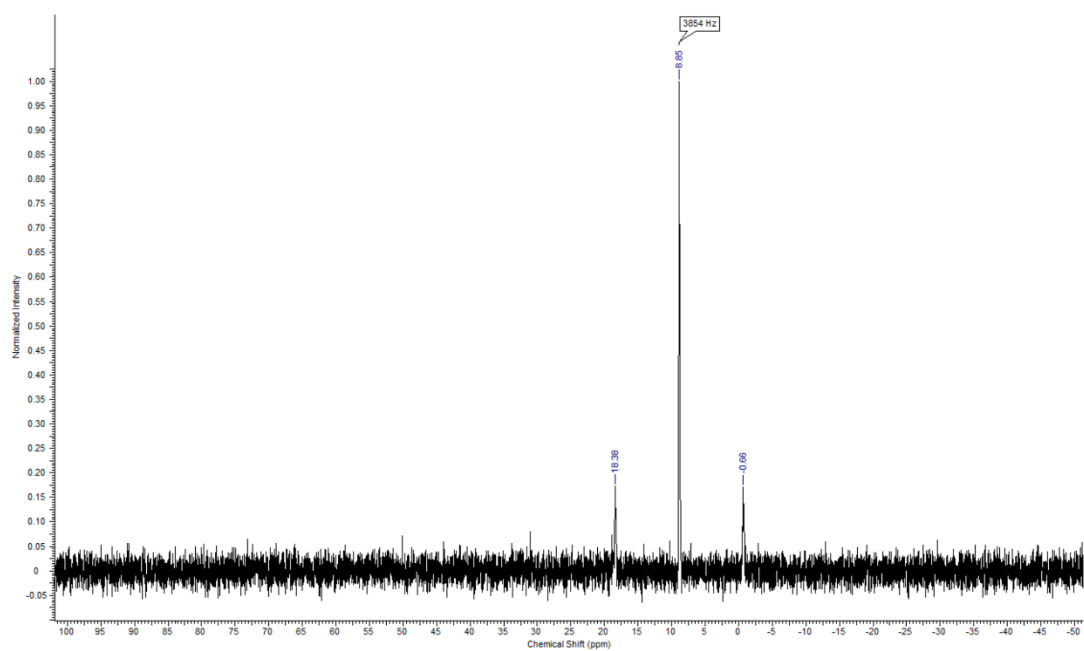
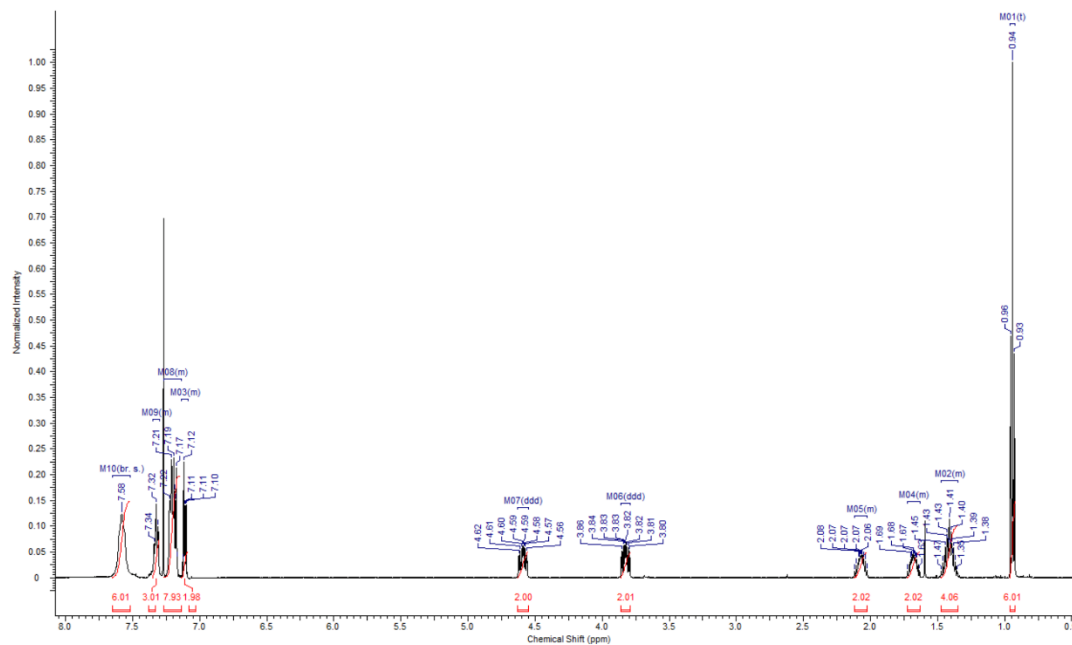
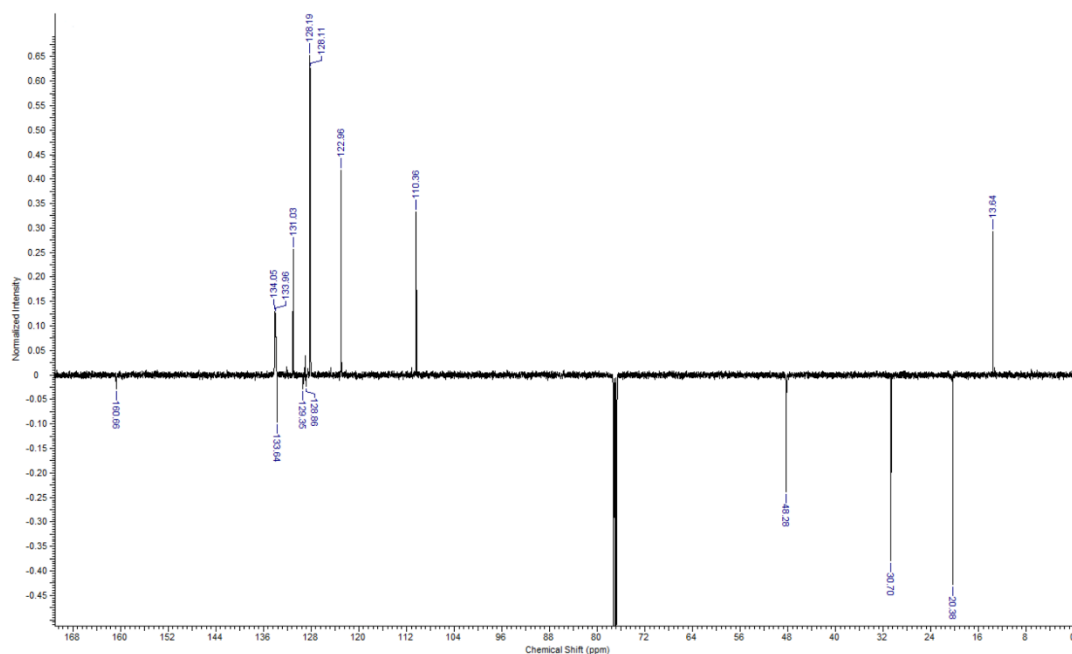


Fig. S 20: ^{31}P -NMR spectrum (202 MHz, CDCl_3) of complex **9b**.

Fig. S 21: ¹H-NMR spectrum (500 MHz, CDCl₃) of complex 9c.Fig. S 22: ¹³C-NMR spectrum (126 MHz, CDCl₃) of complex 9c.

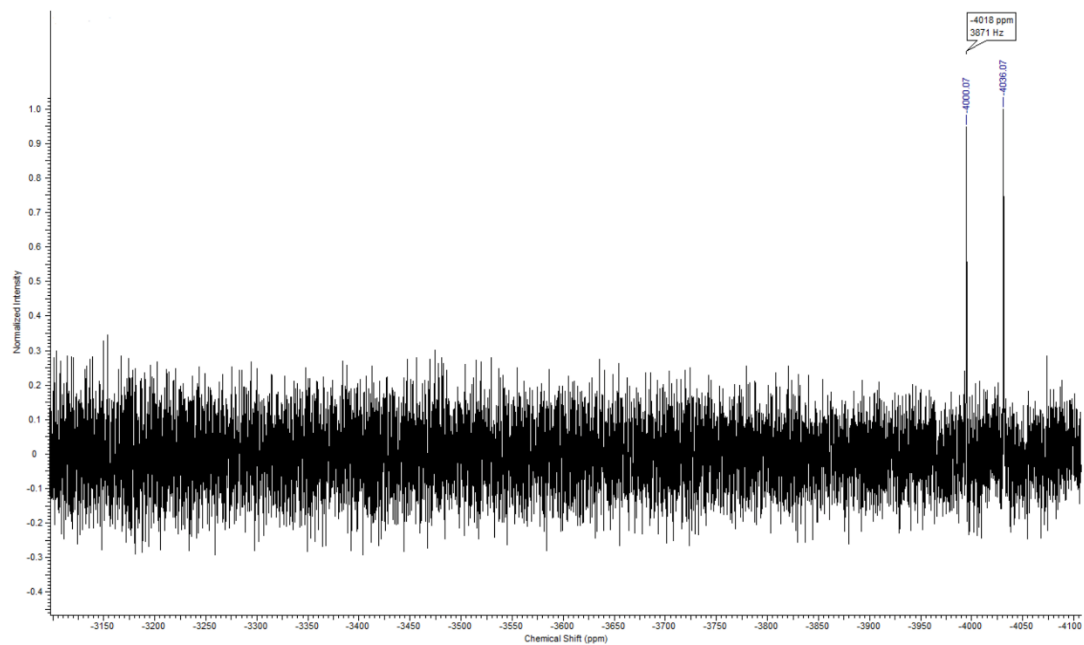


Fig. S 23: ^{195}Pt -NMR spectrum (108 MHz, CDCl_3) of complex **9c**.

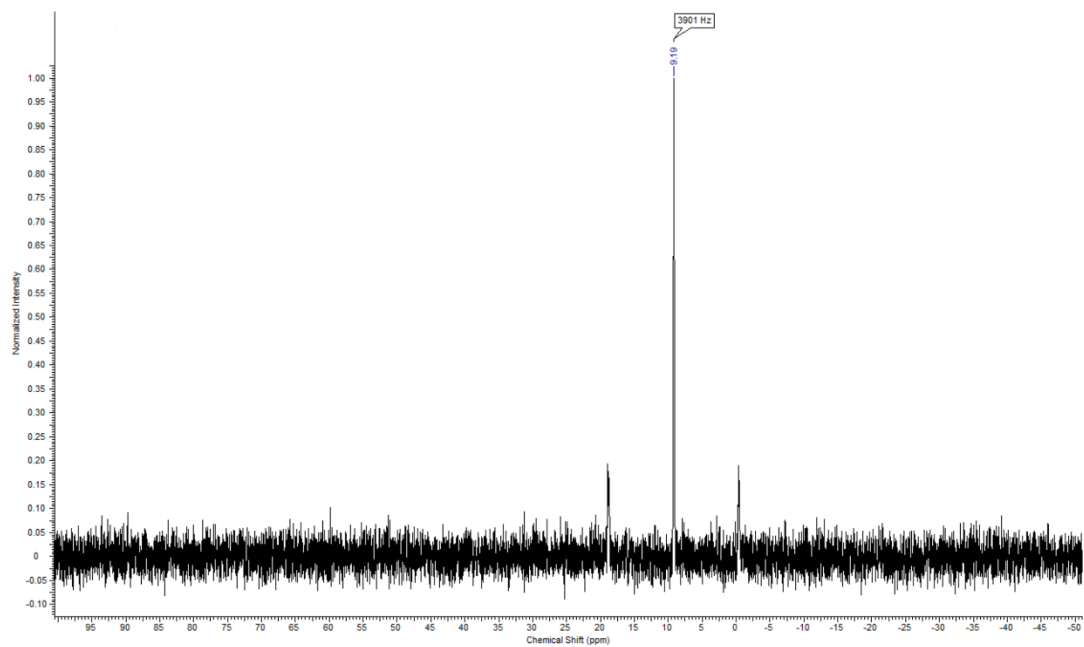


Fig. S 24: ^{31}P -NMR spectrum (202 MHz, CDCl_3) of complex **9c**.

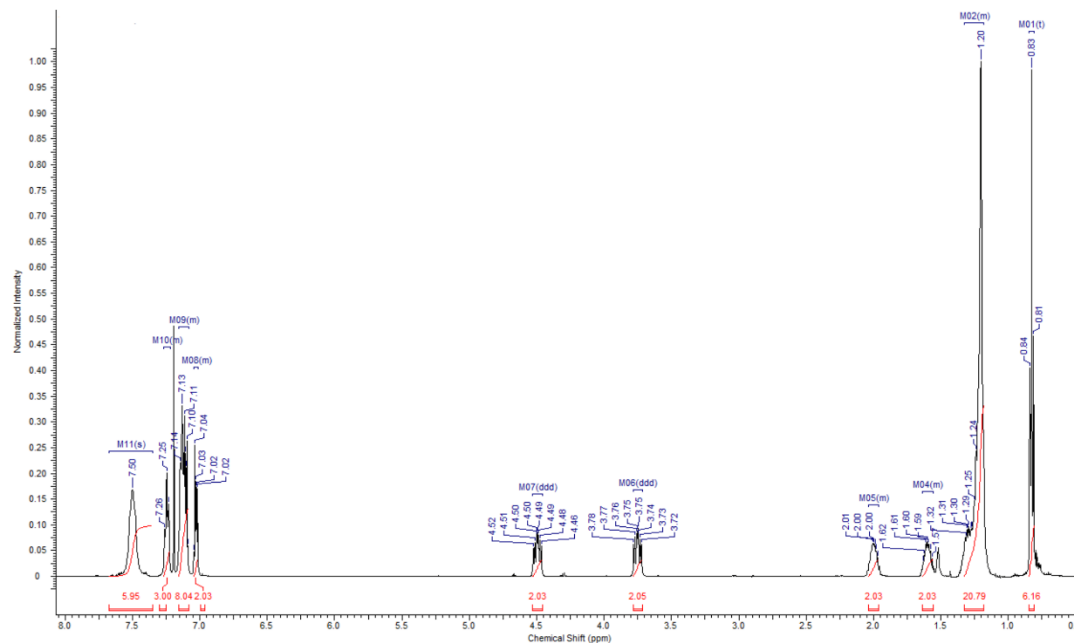


Fig. S 25: ¹H-NMR spectrum (500 MHz, CDCl₃) of complex **9d**.

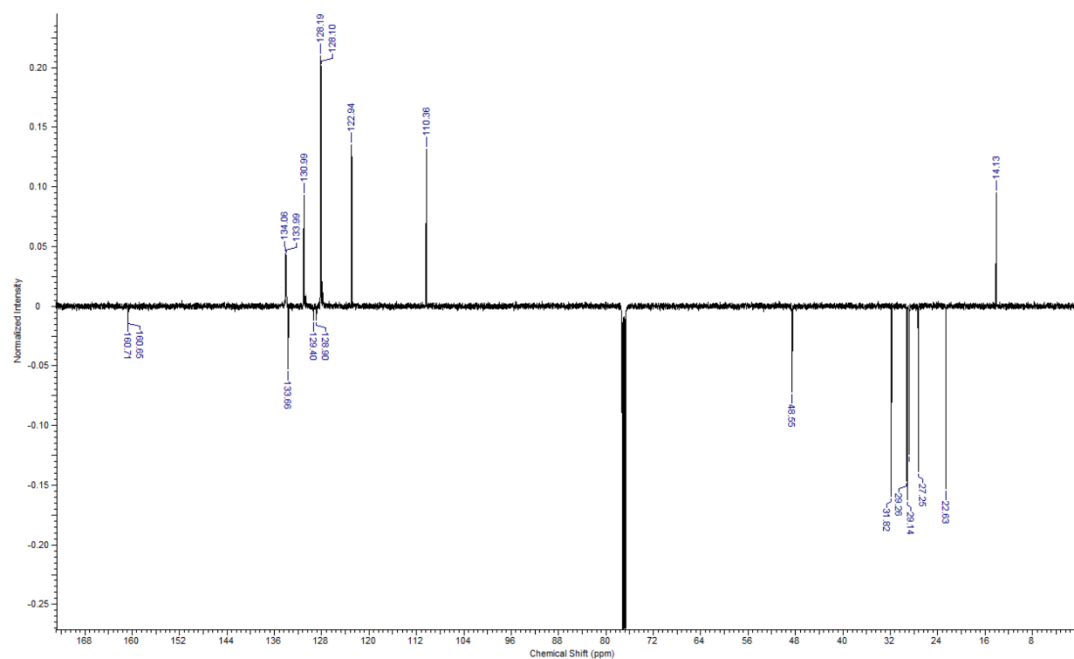


Fig. S 26: ¹³C-NMR spectrum (126 MHz, CDCl₃) of complex **9d**.

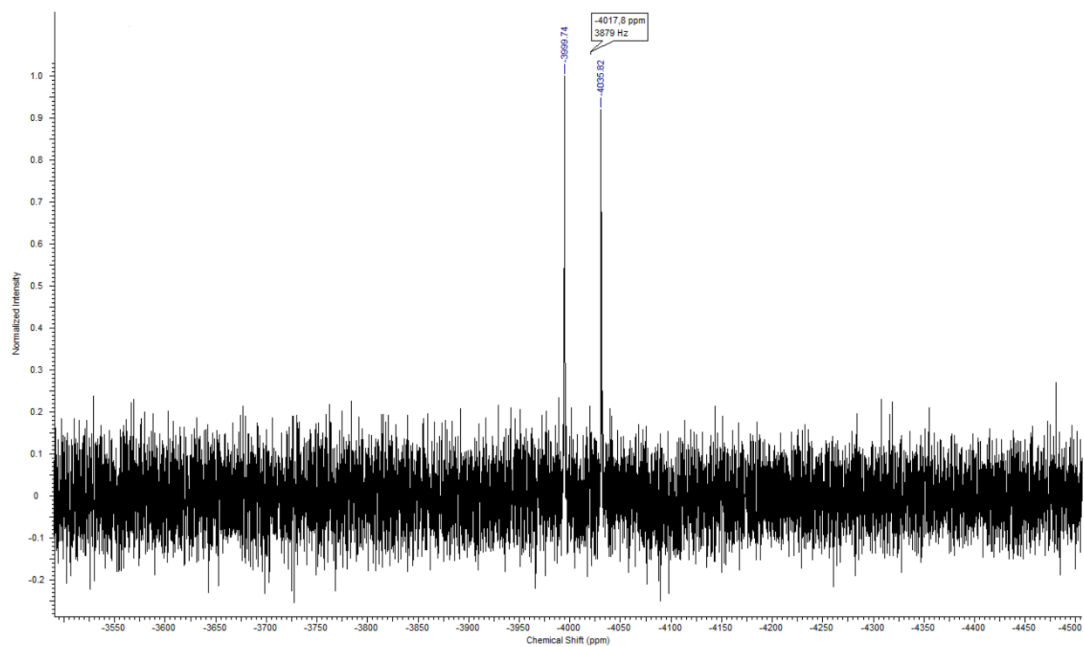


Fig. S 27: ^{195}Pt -NMR spectrum (108 MHz, CDCl_3) of complex **9d**.

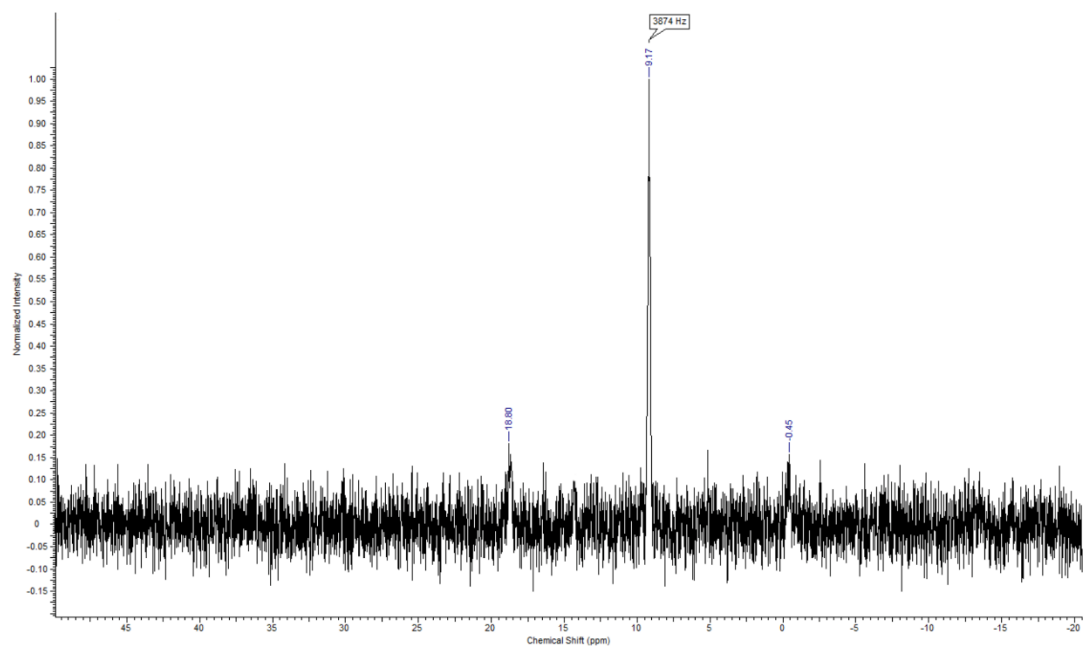


Fig. S 28: ^{31}P -NMR spectrum (202 MHz, CDCl_3) of complex **9d**.

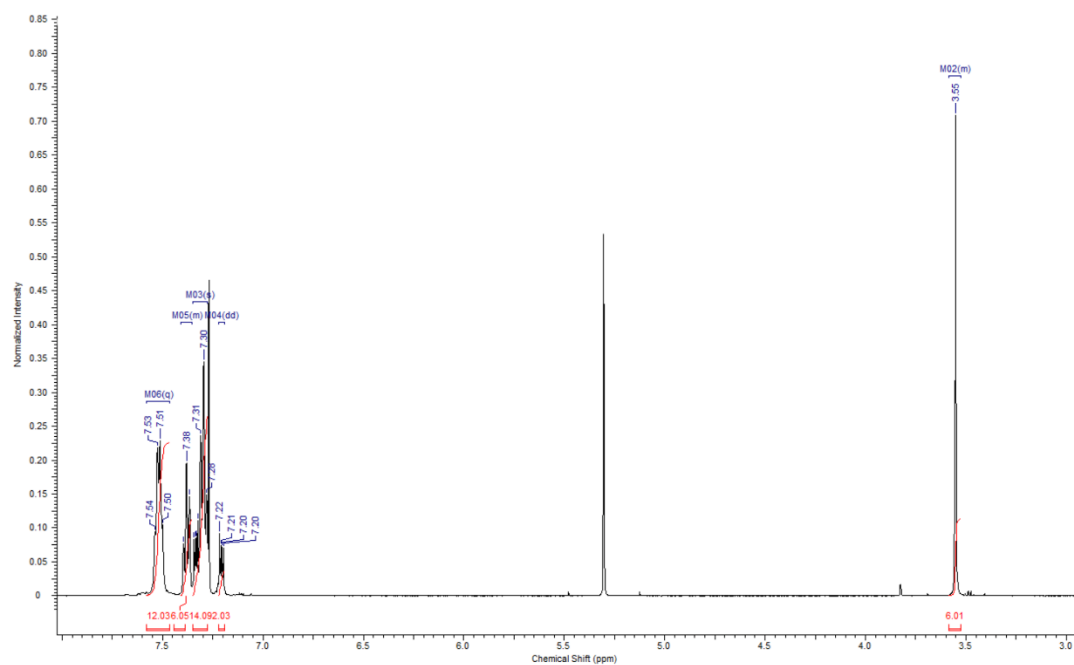


Fig. S 29: ¹H-NMR spectrum (500 MHz, CDCl₃) of complex **10a**.

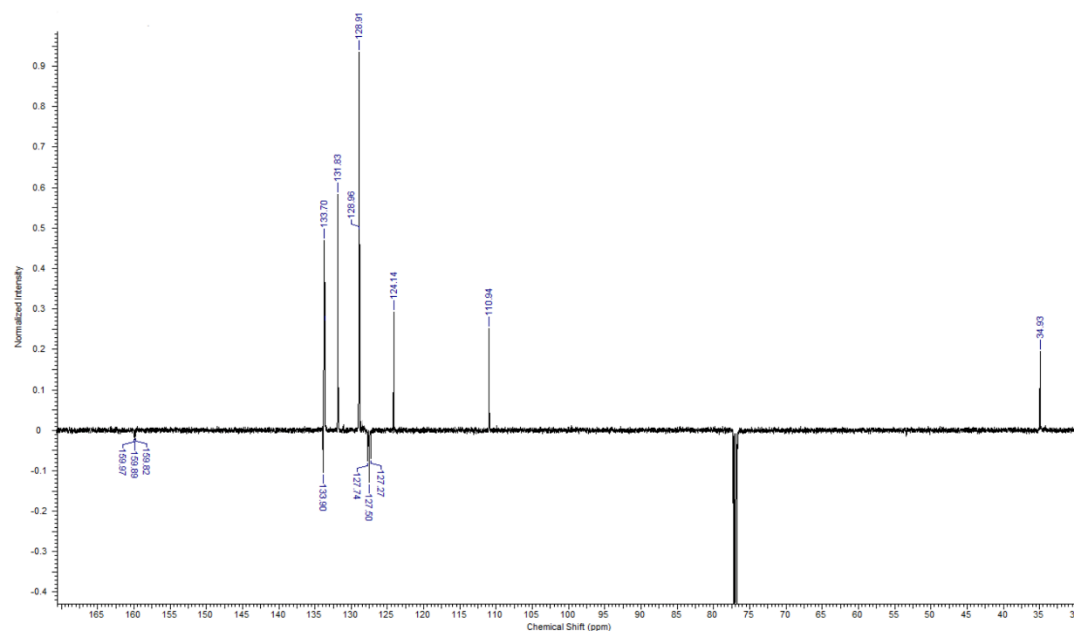


Fig. S 30: ¹³C-NMR spectrum (126 MHz, CDCl₃) of complex **10a**.

S19

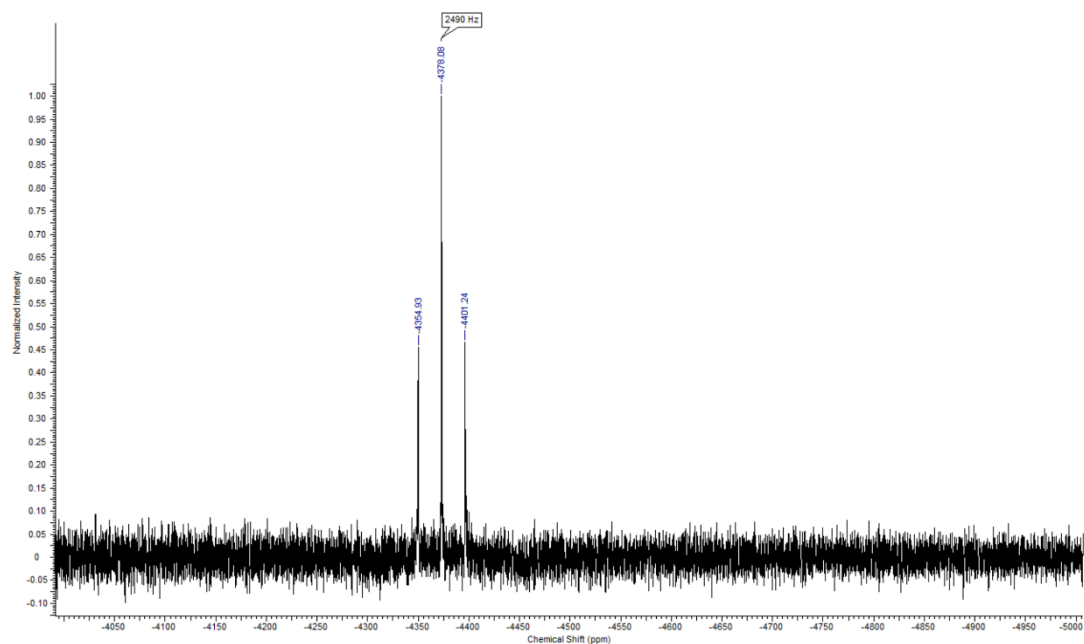


Fig. S 31: ^{195}Pt -NMR spectrum (108 MHz, CDCl_3) of complex **10a**.

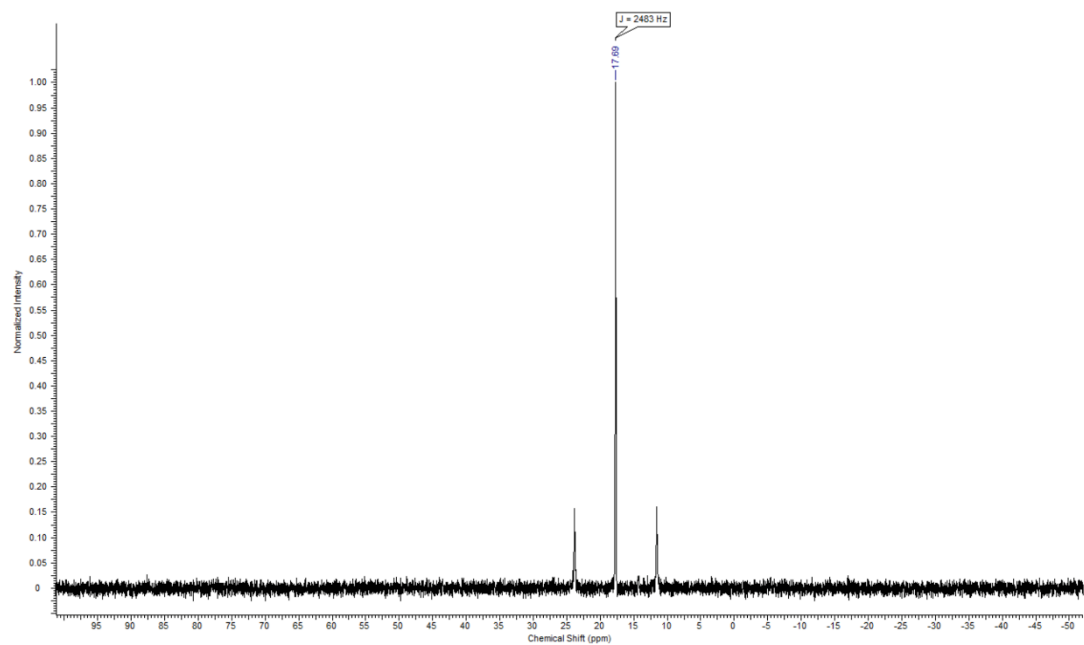


Fig. S 32: ^{31}P -NMR spectrum (202 MHz, CDCl_3) of complex **10a**.

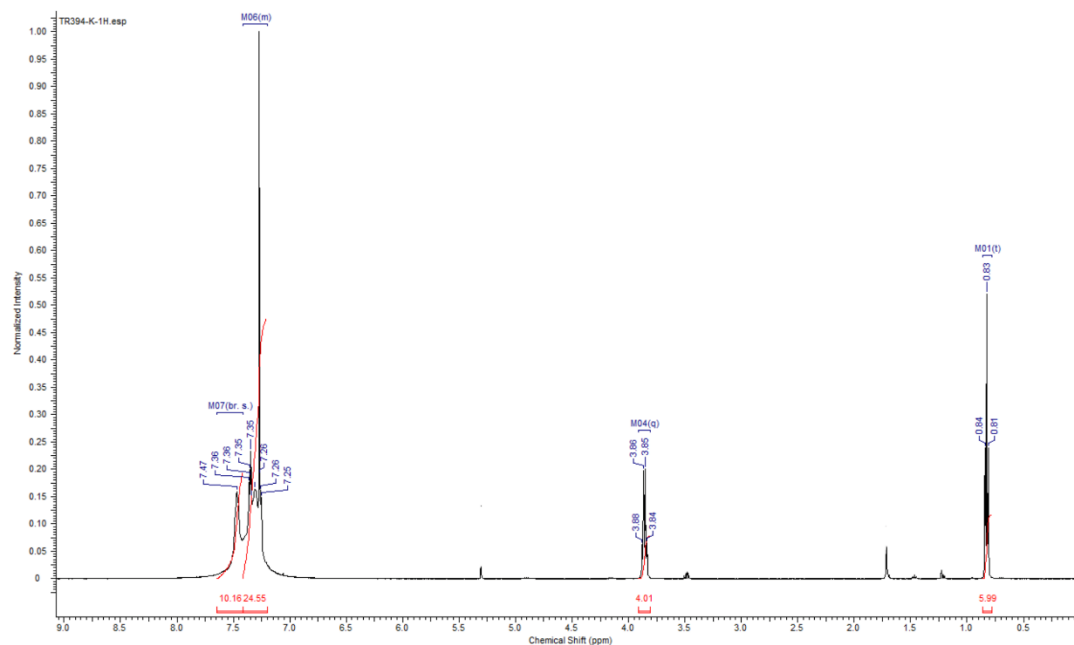


Fig. S 33: ^1H -NMR spectrum (500 MHz, CDCl_3) of complex **10b**.

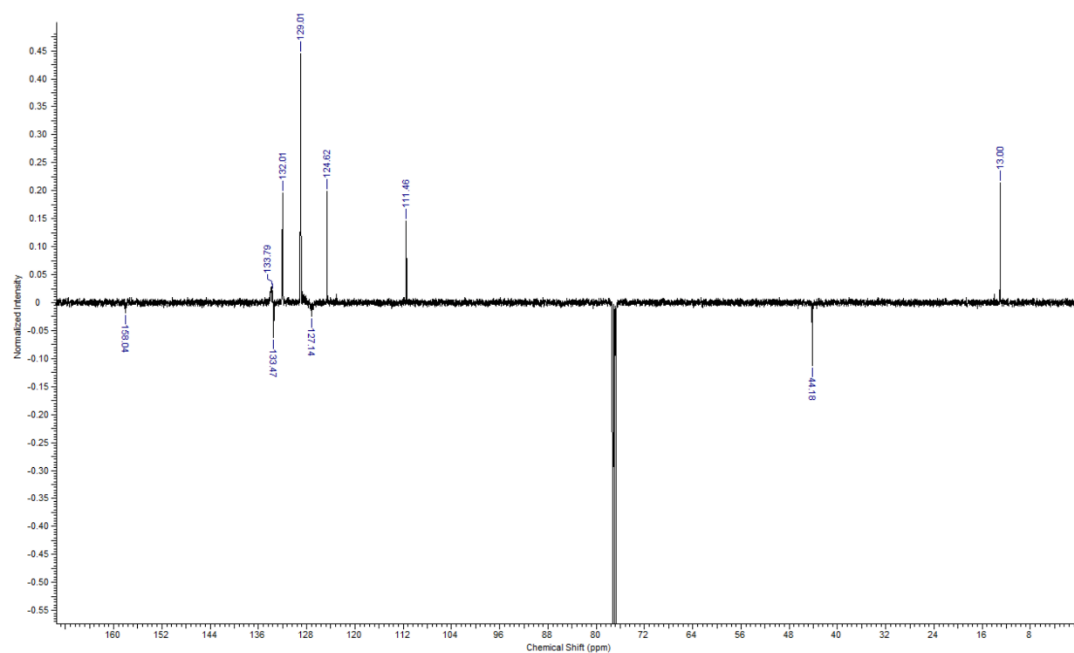


Fig. S 34: ^{13}C -NMR spectrum (126 MHz, CDCl_3) of complex **10b**.

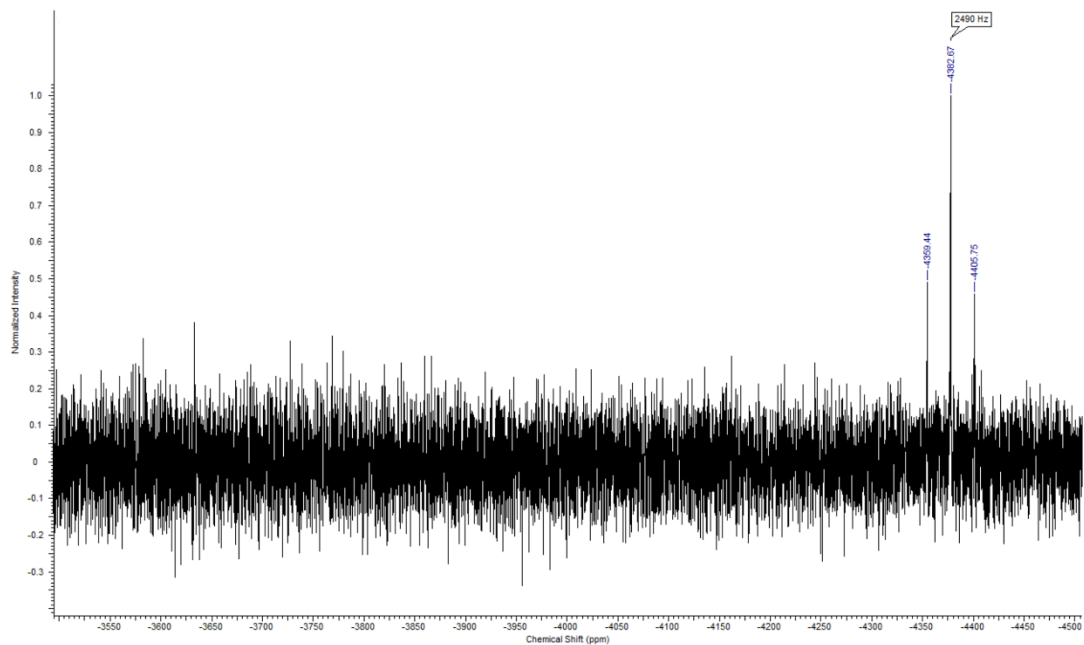


Fig. S 35: ^{195}Pt -NMR spectrum (108 MHz, CDCl_3) of complex **10b**.

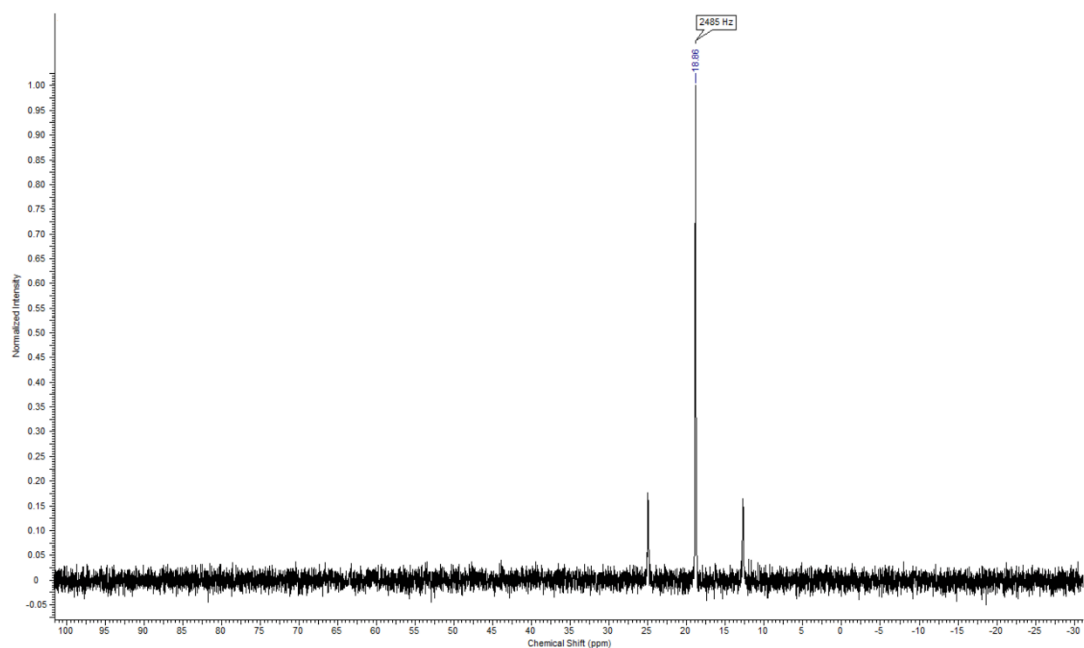


Fig. S 36: ^{31}P -NMR spectrum (202 MHz, CDCl_3) of complex **10b**.

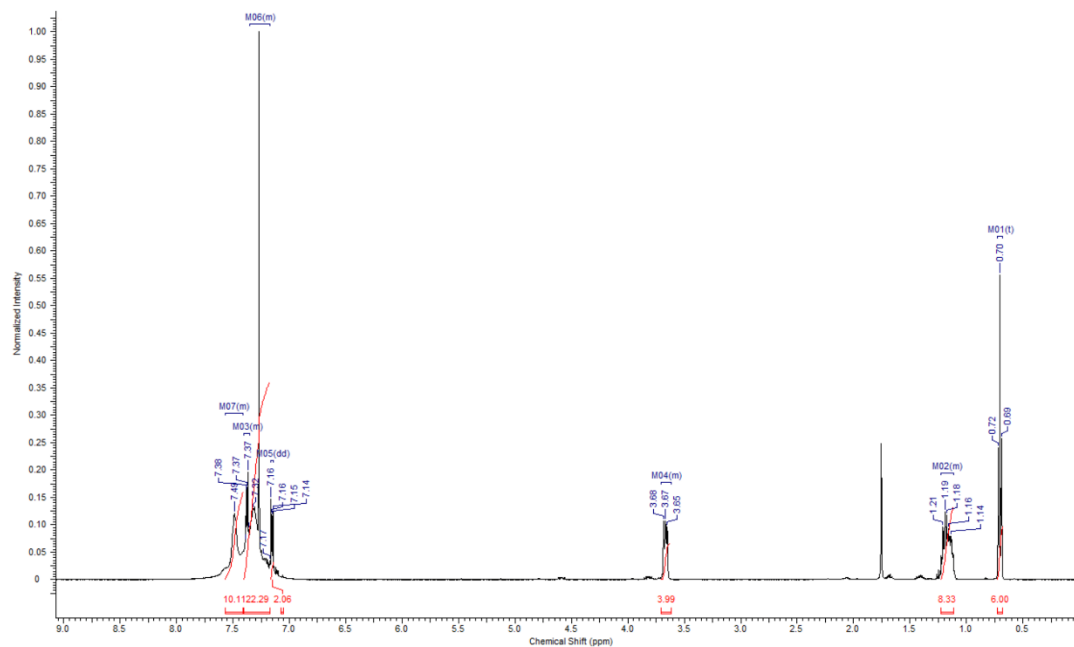
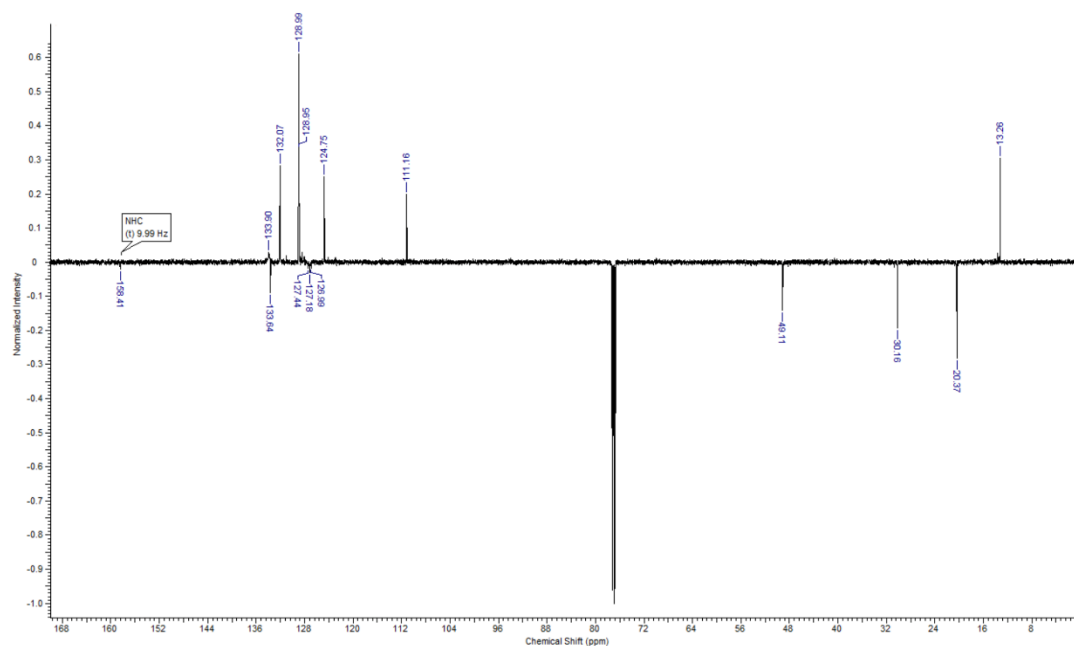


Fig. S 37: ^1H -NMR spectrum (500 MHz, CDCl_3) of complex **10c**.



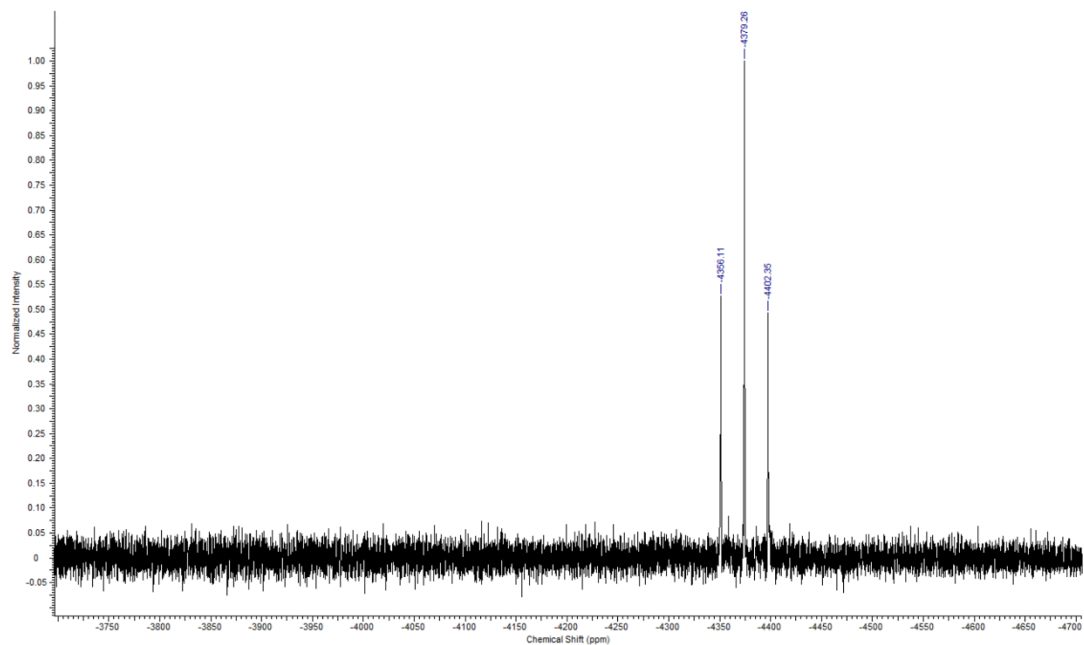


Fig. S 39: ^{195}Pt -NMR spectrum (108 MHz, CDCl_3) of complex 10c.

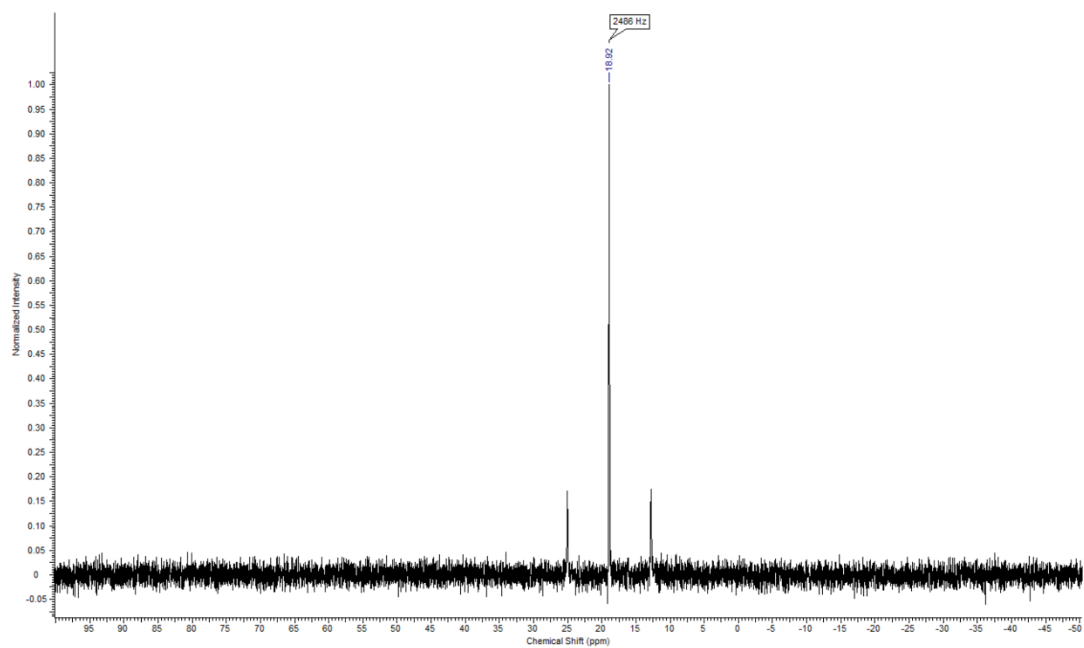


Fig. S 40: ^{31}P -NMR spectrum (202 MHz, CDCl_3) of complex 10c.

Table S 41. Cellular accumulation of cisplatin and tested complexes in HCT116 cells.^a

Compound	pmolPt/10 ⁶ cells
CDDP	49 ± 3
8a	67 ± 5
8b	88 ± 12
8c	97 ± 2
9a	122 ± 21
9b	245 ± 18
9c	316 ± 22
9d	59 ± 4
10a	520 ± 27
10b	555 ± 21
10c	592 ± 59

^aCellular accumulation of Pt from tested compounds (8 μ M in media) in HCT116 cells after 5 h of treatment. Each value in the table is in pmol Pt/10⁶ cells. The results are expressed as the mean \pm SD of three independent experiments.

Table S 3. Binding of **8c**, **9c**, **10a-c** to synthetic polydeoxyribonucleotides determined by FAAS.

	8c	9c	10a	10b	10c
poly (dA)	35%	40%	22%	20%	15%
poly (dC)	5%	3%	1%	1%	2%
poly (dG)	75%	82%	55%	52%	49%
poly (dT)	0.1%	0%	0.3%	0.1%	0.5%

Binding (%) was calculated as a ratio of Pt associated with the polydeoxyribonucleotides after dialysis to the total amount of Pt present in the sample, multiplied by 100.

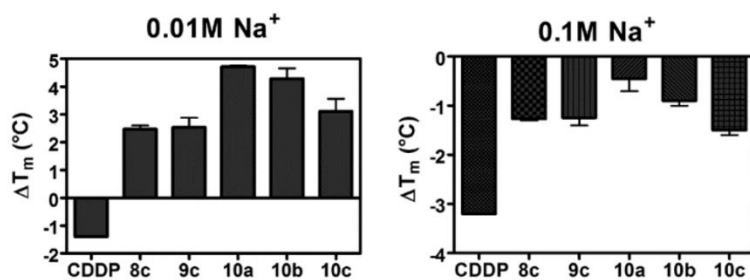


Fig. S 41. ΔT_m values of ct DNA modified by **CDDP**, **8c**, **9c** and **10a-c** at $r_b = 0.03$ measured in 0.01 M (left) or 0.1 M (right) NaClO₄ plus 1 mM Tris/Cl with 0.1 mM EDTA, pH 7.4. ΔT_m is defined as the difference between the T_m values of platinated and nonmodified DNA. Data represent a mean \pm SEM from two independent experiments.

S25

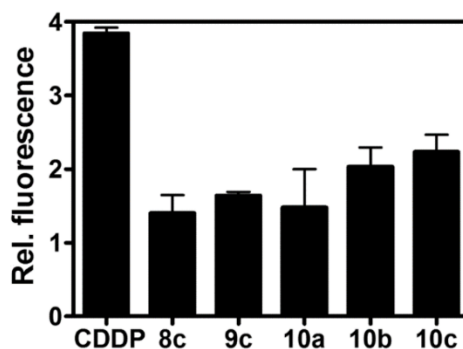


Fig. S 42. Changes in the relative fluorescence of Tb³⁺ ion bound to double-helical ctDNA modified by Pt complexes at $r_b = 0.03$. Tb³⁺ ion fluorescence of untreated DNA was arbitrarily set at 1. Values shown in the graph are the means (\pm SEM) of at least two independent measurements.

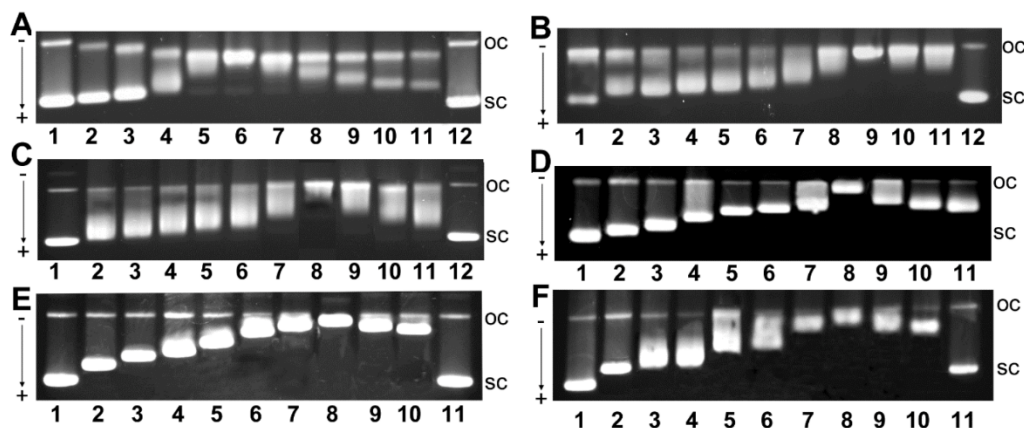


Fig. S 43. Unwinding of supercoiled pSP73 plasmid DNA by CDDP (A), **8c** (B), **9c** (C), **10a** (D), **10b** (E) and **10c** (F). The top bands correspond to the form of nicked plasmid (oc) and the bottom bands to the closed, negatively supercoiled plasmid (sc). A) lanes: 1 and 12, control, nonplatinated DNA; 2, $r_b = 0.005$; 3, $r_b = 0.01$; 4, $r_b = 0.02$; 5, $r_b = 0.03$; 6, $r_b = 0.04$; 7, $r_b = 0.05$; 8, $r_b = 0.06$; 9, $r_b = 0.07$; 10, $r_b = 0.08$; 11, $r_b = 0.09$. B) lanes: 1 and 12, control, nonplatinated DNA; 2, $r_b = 0.03$; 3, $r_b = 0.04$; 4, $r_b = 0.05$; 5, $r_b = 0.056$; 6, $r_b = 0.06$; 7, $r_b = 0.07$; 8, $r_b = 0.077$; 9, $r_b = 0.084$; 10, $r_b = 0.09$; 11, $r_b = 0.1$. C) lanes: 1 and 12, control, nonplatinated DNA; 2, $r_b = 0.055$; 3, $r_b = 0.06$; 4, $r_b = 0.064$; 5, $r_b = 0.07$; 6, $r_b = 0.073$; 7, $r_b = 0.078$; 8, $r_b = 0.085$; 9, $r_b = 0.09$; 10, $r_b = 0.096$; 11, $r_b = 0.1$. D) lanes: 1 and 12, control, nonplatinated DNA; 2, $r_b = 0.052$; 3, $r_b = 0.06$; 4, $r_b = 0.07$; 5, $r_b = 0.074$; 6, $r_b = 0.08$; 7, $r_b = 0.085$; 8, $r_b = 0.093$; 9, $r_b = 0.1$; 10, $r_b = 0.11$; 11, $r_b = 0.12$. E) lanes: 1 and 12, control, nonplatinated DNA; 2, $r_b = 0.04$; 3, $r_b = 0.05$; 4, $r_b = 0.058$; 5, $r_b = 0.065$; 6, $r_b = 0.075$; 7, $r_b = 0.08$; 8, $r_b = 0.087$; 9, $r_b = 0.091$; 10, $r_b = 0.1$; 11, $r_b = 0.11$. F) lanes: 1 and 12, control, nonplatinated DNA; 2, $r_b = 0.045$; 3, $r_b = 0.052$; 4, $r_b = 0.054$; 5, $r_b = 0.06$; 6, $r_b = 0.065$; 7, $r_b = 0.07$; 8, $r_b = 0.079$; 9, $r_b = 0.085$; 10, $r_b = 0.1$; 11, $r_b = 0.11$.

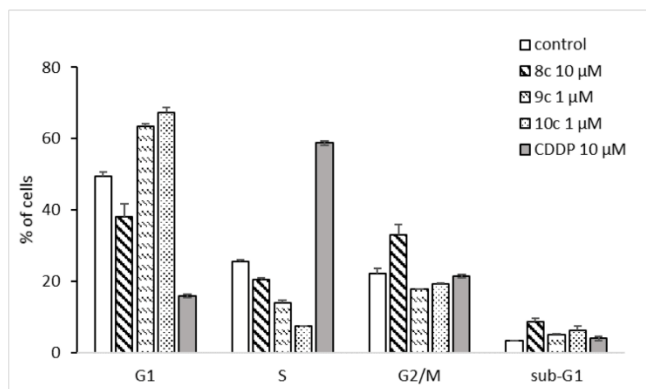


Fig. S 44: Effects of **8c** (10 μ M), **9c** (1 μ M), **10c** (1 μ M), **CDDP** (10 μ M) on the progression of the cell cycle of HCT116 p53^{-/-} colon carcinoma cells after 24 h of treatment in comparison to untreated cells (vehicle control). The bars represent the percentages of cells in each phase of the cell cycle (G1, S and G2/M) and dead cells (sub-G1). Analysis was done via propidium iodide staining and flow cytometry, values represent means \pm SDs of three experiments.

References

- [1] R. Rubbiani, I. Ott *et al.*, *J. Med. Chem.*, 2010, **53**, 8608–8618, DOI: 10.1021/jm100801e.
- [2] H. Valdés, M. Poyatos, G. Ujaque, E. Peris, *Chem. Eur. J.*, 2015, **21**, 1578 – 1588, DOI: 10.1002/chem.201404618.
- [3] H. Lu and R. L. Brutchey, *Chem. Mater.*, 2017, **29**, 1396–1403, DOI: 10.1021/acs.chemmater.6b05293.

5.5 Publikation IV

Synthesis, structures and cytotoxic effects in vitro of *cis*- and *trans*-
[Pt^{IV}(Cl₄(NHC)₂] complexes and their Pt^{II} precursors

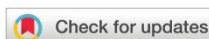
*Tobias Rehm,^a Matthias Rothmund,^a Thomas Dietel,^b Rhett Kempe,^b und Rainer Schobert^{*a}*

^aDepartment of Chemistry, University Bayreuth, Universitaetsstr. 30, 95440 Bayreuth, Germany

^bLehrstuhl fuer Anorganische Chemie II, University Bayreuth, Universitaetstr. 30, 95440 Bayreuth, Germany

*e-mail: Rainer.Schobert@uni-bayreuth.de; jana@ibp.cz

Dalton Trans. 2019, 48, 16358 – 16365.



Cite this: *Dalton Trans.*, 2019, **48**, 16358

Synthesis, structures and cytotoxic effects *in vitro* of *cis*- and *trans*-[Pt^{IV}Cl₄(NHC)₂] complexes and their Pt^{II} precursors†

Tobias Rehm,^a Matthias Rothemund,^a Thomas Dietel,^b Rhett Kempe^b and Rainer Schobert  ^{*a}

Four new bis(*N,N*-dialkylbenzimidazol-2-ylidene)dichlorido platinum(II) complexes **2** featuring *N*-alkyl substituents of increasing size (**a**: Me, **b**: Et, **c**: *n*-butyl, **d**: *n*-octyl) were synthesised and oxidised with PhICl₂ to give the corresponding [Pt^{IV}Cl₄(*N,N*-dialkylbenzimidazol-2-ylidene)₂] complexes **4** as potential anticancer prodrugs. The known bis(*N,N*-dibenzylimidazol-2-ylidene)dichlorido platinum(II) complex **1** was likewise oxidised to [Pt^{IV}Cl₄(*N,N*-dibenzylimidazol-2-ylidene)₂] **3**. In contrast, oxidation of complexes **1** and **2** with H₂O₂ or hypochlorites, or exchange of chlorido for hydroxo ligands in tetrachlorido complexes **4** failed to give isolable complexes of type [Pt^{IV}Cl_{4-n}(OH)_n(NHC)₂]. In MTT assays the [Pt^{II}Cl₂(NHC)₂]/[Pt^{IV}Cl₄(NHC)₂] complex couples **1/3**, **2c/4c**, and *trans*-**2c/trans-4c**, bearing either *N*-benzyl or *N*-butyl substituents, each showed similar single-digit micromolar IC₅₀ values against at least three out of five human cancer cell lines, presumably due to an intracellular reduction of the Pt^{IV} complexes to their active Pt^{II} congeners. Unlike cisplatin, whose anticancer effect requires functional p53, each of them was active both in wildtype and in p53-negative HCT116 colon carcinoma cells. In ethidium bromide saturation assays with isolated DNA, *cis*-(bis-NHC)Pt^{II} complexes such as **1** caused morphological DNA changes more pronounced than those initiated by cisplatin, while the corresponding *cis*-(bis-NHC)Pt^{IV} complexes such as **3** interacted with DNA in a less structure-modifying way.

Received 8th June 2019,
Accepted 14th October 2019
DOI: 10.1039/c9dt02438g
rsc.li/dalton

Introduction

After the discovery of the biological effects of cisplatin by Barnett Rosenberg in the late 1960s, the FDA eventually approved it as the first platinum chemotherapeutic in 1978.¹ To this day it remains a mainstay drug for the treatment of certain tumour entities, *e.g.* testicular cancer.² Its severe side effects and often observed induction of resistance led to an ongoing search for better tolerated and more tumour specific Pt^{II} drugs such as carboplatin and oxaliplatin, that are being clinically applied worldwide (Fig. 1). A more recent line of platinum drug refinement was the development of Pt^{IV} complexes which are thought to act as prodrugs, being themselves less toxic than Pt^{II} complexes, more resistant to substitution, and pharmacologically more adjustable by attaching further axial ligands to the metal centre. Since cancer cells are more

hypoxic than nonmalignant cells, Pt^{IV} prodrugs are believed to be reduced and so activated predominantly in cancerous tissues thus minimising unwanted side effects. Upon reduction of the Pt^{IV} prodrug to give the active Pt^{II} drug proper, any axial ligands with additional anticancer effects are released and so enhance the overall impact.³

So far only a few Pt^{IV} complexes made it into clinical trials and none of them exhibited significantly greater activity than

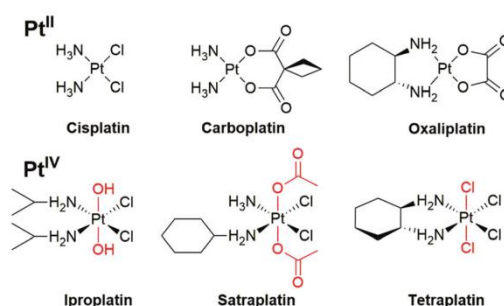


Fig. 1 Structures of approved platinum(II) anticancer drugs and investigational Pt^{IV} prodrugs that entered clinical trials.

^aOrganic Chemistry Laboratory, University Bayreuth, Universitätsstrasse 30, 95440 Bayreuth, Germany. E-mail: Rainer.Schobert@uni-bayreuth.de

^bLehrstuhl fuer Anorganische Chemie II, University Bayreuth, Universitätsstrasse 30, 95440 Bayreuth, Germany

† Electronic supplementary information (ESI) available: NMR spectra; X-ray structural data. CCDC 1912954 and 1912955. For ESI and crystallographic data in CIF or other electronic format see DOI: 10.1039/c9dt02438g

cisplatin.⁴ The first-generation Pt^{IV} prodrugs iproplatin, satraplatin, and tetraplatin consist of cisplatin-analogous square planar *cis*-dichlorido-diamino platinum fragments carrying two biologically innocent axial ligands such as chlorido, hydroxo or acetato, respectively. In recent years more diversified Pt^{IV} complexes have been developed by attaching ancillary drugs or cancer-targeting units as axial ligands to the original Pt^{II} complex fragment.^{5–7}

Pt^{IV} complexes with N-heterocyclic carbene (NHC) ligands were investigated for their medicinal potential only recently,⁸ despite a rich literature on the synthesis and structures of such complexes with mono-NHC,^{9a} *trans*-bis(NHC),^{9b} chelating^{9a,c,d} and non-chelating^{9e} *cis*-bis(NHC), or even tris(NHC)^{9a} ligand spheres.

In the past, our group has synthesised bioactive Pt^{II} complexes with (benz)imidazol-2-ylidene ligands in combination with DMSO or phosphine ligands and we also developed a protocol that allows the successive introduction of two different NHC ligands to afford *cis*-[Pt^{II}Cl₂(NHC)¹(NHC)²] complexes.¹⁰ In continuation of this work, we now report on the synthesis, structures and anticancer effects of four new benzimidazol-2-ylidene complexes *cis*-[Pt^{II}Cl₂(NHC)₂] **2a–d** as well as the *trans*-isomer *trans*-**2c**, and on their oxidation products, including six new complexes [Pt^{IV}Cl₄(NHC)₂] **3**, **4a–d** and *trans*-**4c** (Fig. 2).

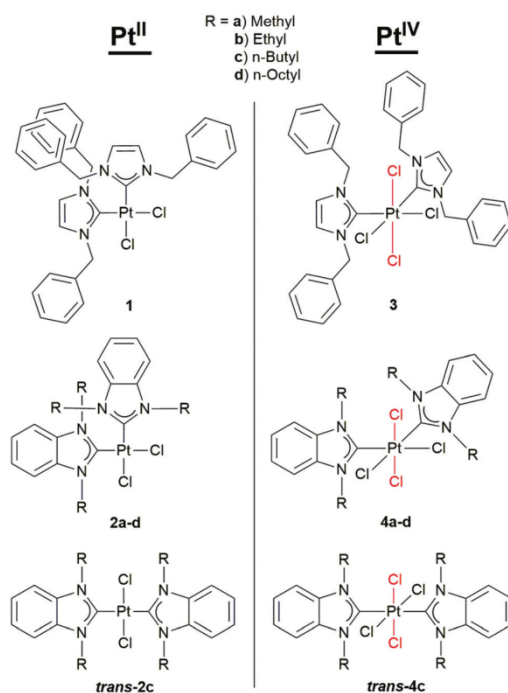


Fig. 2 Structures of **1** and the eleven newly synthesised complexes **2a–d**, *trans*-**2c**, **3**, **4a–d** and *trans*-**4c**.

Results and discussion

Synthesis and characterisation

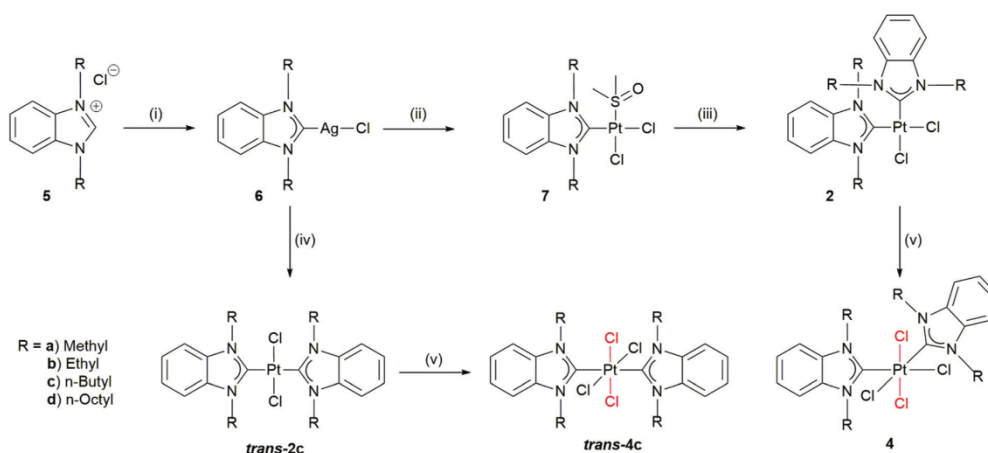
Following established protocols^{10b,c,11} the known benzimidazolium chlorides **5** (**a**: Me, **b**: Et, **c**: *n*-butyl, **d**: *n*-octyl) were treated with silver(i) oxide to afford the corresponding silver carbene complexes **6** which in turn were transmetalated with K₂PtCl₄ in DMSO to leave the *cis*-[Pt^{II}Cl₂(DMSO)(NHC)] complexes **7**.^{10c} Substitution of their DMSO by a second NHC ligand, prepared *in situ* from the same benzimidazolium chloride **5** and KOtBu, gave the new biscarbene complexes **2a–d**. The Pt^{II} complex *trans*-**2c** was obtained by treating silver complex **6c** with only half an equivalent of K₂PtCl₄ in dichloromethane.¹¹ While in DMSO the complex *cis*-[Pt^{II}Cl₂(DMSO)₂] is formed as an intermediate leading to *cis* complexes **7**, in CH₂Cl₂ the *trans* effect of the first NHC at the Pt^{II} centre directs the second NHC into *trans* configuration.

Oxidation of Pt^{II} to Pt^{IV} complexes is customarily performed by means of hydrogen peroxide, bromine or chlorine.¹² Also frequently used and better manageable than chlorine is iodobenzene dichloride (PhICl₂), obtained from iodobenzene, NaOCl and HCl.^{8,13} By stirring with 10 equivalents of PhICl₂ in CH₂Cl₂ for several hours Pt^{II} complexes **1**, **2** and *trans*-**2c** were converted to their respective [Pt^{IV}Cl₄(NHC)₂] complexes **3**, **4** and *trans*-**4c** with retained stereochemistry (Scheme 1).

The new Pt^{II} and Pt^{IV} complexes were characterised by ¹H, ¹³C and ¹⁹⁵Pt NMR spectroscopy, mass spectrometry, and elemental analysis. Crystal structure analyses were carried out for complexes **2c** and **3**. The *N*-methyl substituted Pt^{IV} complex **4a** turned out to be insufficiently soluble in all tested solvents suitable for NMR analysis and was therefore characterised only by elemental analysis and mass spectrometry.

The ¹H NMR spectra of complexes **2b–d** show an inequivalence of the two geminal protons of the CH₂ groups – one proton facing the neighbouring chlorido ligand, the other facing the neighbouring NHC ligand – resulting in two split signals. This effect is strongest for the N-CH₂ groups and peters out along the chain for **2c** and **2d**. While the N-CH₂-CH₃ protons in **2b** show two doublets of quartets (dq), complexes **2c** and **2d** show two ddd's for their N-CH₂ protons corroborating the *cis* configuration of the NHC ligands as well as a perpendicular orientation of the benzimidazole ligands relative to the plane spanned by the PtCl₂ fragment. Complex *trans*-**2c**, in contrast, exhibits no split signals since the geminal N-CH₂ protons possess identical environments.^{10a}

The ¹H NMR spectra of the Pt^{IV} complexes **3** and **4** show even more complex coupling patterns. In comparison to the Pt^{II} complexes the N-CH₂ protons lead to four dq or td, respectively, instead of just two signals, indicating that the NHC ligands, after addition of the axial chlorido ligands, rotate away from a perpendicular orientation into the space between the axial and equatorial ligands, as confirmed by crystallography (Fig. 3). Thus, one alkyl residue of each NHC faces two chlorido ligands, while the second alkyl residue leans towards one chlorido and the neighbouring NHC ligand giving



Scheme 1 Synthesis of complexes **2a–d**, **trans-2c**, **4a–d** and **trans-4c**. Reagents and conditions: (i) Ag_2O , CH_2Cl_2 , rt; (ii) K_2PtCl_4 , DMSO, 60 °C; (iii) 5, KO^tBu , dry CH_2Cl_2 , Ar atmosphere, rt; (iv) 0.5 eq. K_2PtCl_4 , CH_2Cl_2 , rt; (v) PhI_2 , CH_2Cl_2 , rt.

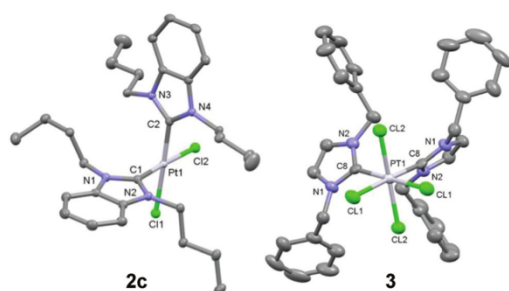


Fig. 3 Molecular structures of complexes **2c** and **3** as thermal ellipsoid representations at the 50% probability level (H atoms omitted). Selected bond lengths [Å], angles [°] and torsion angles [°]: **2c**: Pt1–C1 2.3582(10), Pt1–Cl2 2.3571(8), Pt1–C1 1.972(2), Pt1–C2 1.972(2), Cl1–Pt1–Cl2 90.657(17), Cl1–Pt1–C1 86.55(6), Cl2–Pt1–C2 88.50(5), C1–Pt1–C2 94.32(8), N1–C1–N2 106.27(16), N3–C2–N4 106.52(16), Cl1–Pt1–C1–N1 89.3(1), Cl1–Pt1–C1–N2 85.7(8), Cl2–Pt1–C2–N3 85.9(5), Cl2–Pt1–C2–N4 92.9(5); **3**: Pt1–C1 2.379(2), Pt1–Cl2 2.330(2), Pt1–C8 2.050(9), Cl1–Pt1–C1 85.50(13), Cl1–Pt1–Cl2 85.83(8), Cl1–Pt1–C8 90.61(8), Cl2–Pt1–Cl2 175.12(11), Cl1–Pt1–C8 91.7(3), Cl1–Pt1–C8 177.8(2), Cl2–Pt1–C8 87.9(2), Cl2–Pt1–C8 95.5(2), C8–Pt1–C8 90.0(5), N1–C8–N2 106.5(8), Cl2–Pt1–C8–N1 46.8(4), Cl2–Pt1–C8–N2 49.1(6), Cl1–Pt1–C8–N1 43.9(4), C8–Pt1–C8–N2 46.3(6).

a distinct signal splitting (*cf.* Fig. S19, ESI†). Again, the spectra of complex **trans-4c** showed no such proton inequivalence.

In the ^{13}C NMR spectra the carbene signals, which are highly diagnostic, agree with these results.¹⁰ The N–C–N signals of complexes **2a–d** lay at 158.8–159.5 ppm while, typical of *trans* configured Pt^{II} complexes, **trans-2c** showed a downfield signal at 178.0 ppm.^{10a,14} When oxidised to $[\text{Pt}^{\text{IV}}\text{Cl}_4(\text{NHC})_2]$ complexes the carbene signals appeared upfield at 136.0–136.8 ppm for the *cis* complexes and at 147.5 ppm for **trans-4c**.

With –3622 to –3660 ppm (*cis*) and –3245 ppm (*trans*) the ^{195}Pt NMR signals of all Pt^{II} compounds were in the expected range. Pt^{IV} complexes showed downfield signals at –1427 to –1430 ppm for **4b–d**, at –1250 ppm for complex **3**, and at –1051 ppm in the case of **trans-4c**.

For an estimate of the stability of the new Pt^{IV} complexes under biological conditions, a DMSO/water solution of **4b** was monitored over 16 h by ESI-MS. It showed, aside of other minor platinum species, a continuously increasing peak cluster with main peak at $m/z = 579$ and an isotopic pattern typical of a $[\text{Pt}^{\text{IV}}\text{Cl}(\text{NHC})_2]^+$ species. In keeping with that, the UV/vis spectrum of **4b** in DMSO/water showed a steadily decreasing absorption and a change of the band shapes between 230 and 730 nm (*cf.* ESI, Fig. S37–39†).

As Pt^{IV} hydroxo complexes with NHC ligands have not been published yet, we also investigated the oxidation of complexes **1** and **2** with H_2O_2 or hypochlorites¹⁵ as well as an exchange of chlorido for hydroxo ligands in **4** to give $[\text{Pt}^{\text{IV}}\text{Cl}_{4-n}(\text{OH})_n(\text{NHC})_2]$ complexes. However, these were not accessible in this way, although we had some indication of a transient species of this type in the hypochlorite oxidation of complex **2b** (*cf.* ESI†).

Crystallography

Crystals suitable for X-ray diffraction analyses were grown by slow infusion of hexane or diethyl ether into saturated solutions of **2c** in CH_2Cl_2 or **3** in CHCl_3 kept at 4 °C. Fig. 3 shows their molecular structures. The Pt–C bond lengths were 1.972 Å for **2c** and 2.050 Å for **3**. The latter is 0.082 Å longer than the corresponding bond in the previously published Pt^{II} complex **1**.^{10b} The Pt–Cl^{axial} distances of **3** are 2.330 Å and so slightly shorter than the Pt–Cl^{equat} bonds of **2c** (2.357–2.358 Å) and **1** (2.379 Å). The X-ray diffraction analysis of **3** revealed the NHC ligand rotation away from a perpendicular orientation of its plane relative to the plane spanned by the $\text{PtCl}_2^{\text{equat}}$ frag-

ment as in Pt^{II} complex **1**.^{10b} The torsion angle between these two planes lies between 43.94° and 49.16° for octahedral complex **3** (Fig. 3) and is about 90° for square-planar Pt^{II} complexes **2c** and **1**.

Cytotoxicity

The antiproliferative effect and tumour specificity of the new Pt^{II} and Pt^{IV} complexes were evaluated by means of MTT (3-(4,5-dimethylthiazol-2-yl)-2,5-diphenyltetrazolium bromide) assays on a panel of three human colon carcinoma and a melanoma cell lines, chosen because platinum drugs are part of the most used standard chemotherapy regimens for the treatment of advanced colorectal carcinoma (FOLFOX) and melanoma (TMZ-CDDP), as well as on nonmalignant dermal fibroblasts. For wildtype and p53 knock-out mutant HCT116 colon carcinoma cells we also calculated r^{p53} ($= (IC_{50}^{wt}/IC_{50}^{-/-}) - 1$) as a measure for the dependency of the complex cytotoxicity on the integrity of the proapoptotic p53-gene which is frequently mutated in cancers. The IC₅₀ values of the complexes and their r^{p53} values are listed in Table 1. Of the four *cis*-[(1,3-dialkylbenzimidazol-2-ylidene)₂Cl₂]Pt^{II} complexes **2a–d** only the *N*-butyl substituted complex **2c** showed a significant cytotoxicity, with low single-digit IC₅₀ values against three of the five tested cancer cell lines. This resembles the structure-activity pattern of the *cis*-[(1,3-dialkylbenzimidazol-2-ylidene)(PPh₃)Cl₂]Pt^{II} complexes on which we had reported earlier.^{10c} Their derivative with *N*-alkyl = methyl was, like **2a**, inactive against the same cell lines, while that bearing an *N*-butyl residue was, like **2c**, distinctly more active than the *N*-octyl derivative. However, unlike the inactive complex **2b**, the *cis*-[(1,3-diethylbenzimidazol-2-ylidene)(PPh₃)Cl₂]Pt^{II} complex was highly cytotoxic. The reasons for these structure-activity relations are yet unknown, but are unlikely to be correlated to different intracellular complex concentrations as we know from previous uptake studies with the mono-NHC complexes.

Complexes **4a** and **4d** were poorly soluble in aqueous media and so not tested. While Pt^{II} complex **2b** showed no significant cytotoxic activity, its corresponding Pt^{IV} complex **4b** was moderately active with IC₅₀ values in the double-digit, or even single-digit micromolar range in the case of DLD-1 colon carcinoma cells. This discrepancy might be due to a higher uptake,

to a diminished deactivation/efflux, or to additional modes of action of Pt^{IV} complex **4b**.¹⁵ It showed no antiproliferative effect on the nonmalignant fibroblasts. The butyl substituted complexes **2c** (Pt^{II}) and **4c** (Pt^{IV}) showed a strikingly similar activity pattern with low single-digit micromolar IC₅₀ values against 518A2 melanoma, HT-29 and DLD-1 colon carcinoma cells.

To investigate the effect the *cis*-/*trans*-orientation of the NHC ligands has on the cytotoxic activity, complexes *trans*-**2c** and *trans*-**4c** with opposite dibutyl substituted NHC ligands were synthesised and investigated for their cytotoxic activities. Somewhat reminiscent of the butyl-NHC couple **2c**/**4c** both *trans* complexes showed similar and high antiproliferative activities against all cancer cell lines but the 518A2 melanoma. All active complexes **2** and **4** were also more active against the p53 knock out mutant than the wildtype HCT116 cells ($r^{p53} > 0$). For comparison, the IC₅₀ values of imidazol-2-ylidene complex **1**, whose biological activity we had reported previously, were added.^{10b} Pt^{II} complex **1** and its corresponding Pt^{IV} complex **3** showed a similar antiproliferative effect in most of the cell lines with low single-digit micromolar IC₅₀ values, except for the nonmalignant HDfa cells where the Pt^{IV} complex **3** was only a fifth as toxic as the Pt^{II} complex **1**.

DNA interaction

To confirm the general assumption that Pt^{IV} complexes are biologically more inert than Pt^{II} complexes, the DNA interaction of the best soluble Pt^{II} and Pt^{IV} congeners **1** and **3** was investigated by means of ethidium bromide (EtdBr) saturation assays with linear salmon sperm DNA (Fig. 4). The Pt^{II} complex **1** led to a pronounced concentration-dependent attenuation of the EtdBr fluorescence indicating a strong interaction of **1** with the DNA, which exceeded that of cisplatin by far. This is in keeping with the results obtained previously for similar (bis-NHC)Pt^{II} complexes.¹⁰ Unlike complex **1** and cisplatin, the Pt^{IV} complex **3** caused only a slight reduction of the EtdBr fluorescence. Whether this weak effect is due to a real platination of, *i.e.* coordination to, the DNA bases or merely to

Table 1 Means ± SD of IC₅₀ (72 h) values [μM] of complexes **1**, **2a–d**, **3**, **4b–c**, *trans*-**2c** and *trans*-**4c** in MTT assays against human cancer cell lines^a and nonmalignant dermal fibroblasts HDfa as calculated from four independent measurements

Compounds	IC ₅₀ (72 h) [μM]									
	1 ^{10b}	3	2a	2b	4b	2c	4c	2d	<i>trans</i> - 2c	<i>trans</i> - 4c
518A2 ^a	6.2 ± 0.4	3.7 ± 0.1	>100	>50	18.1 ± 1.7	1.3 ± 0.1	1.7 ± 0.2	>50	9.6 ± 0.9	17.8 ± 0.5
HT29 ^a	14.6 ± 1.4	22.0 ± 0.3	>100	n.d.	35.4 ± 1.7	3.4 ± 0.1	5.7 ± 1.2	>50	2.7 ± 0.3	2.9 ± 0.7
DLD-1 ^a	4.7 ± 1.4	2.0 ± 0.3	n.d.	>50	7.9 ± 1.9	3.3 ± 0.1	4.2 ± 0.9	>100	2.0 ± 0.5	3.0 ± 0.2
HCT116 ^{wt a}	2.3 ± 0.8	4.6 ± 1.0	>50	>100	32.8 ± 3.3	18.3 ± 1.1	32.8 ± 3.3	>50	3.8 ± 0.5	3.0 ± 0.5
HCT116 ^{-/- a}	2.2 ± 0.6	9.0 ± 0.5	n.d.	>50	17.5 ± 2.3	12.5 ± 0.7	11.4 ± 0.8	>50	1.7 ± 0.1	1.6 ± 0.6
HDfa	3.8 ± 0.1	17.5 ± 0.6	>100	n.d.	>50	20.7 ± 3.3	8.1 ± 0.6	>50	6.0 ± 0.3	13.2 ± 0.5
$r^{p53 b}$	0.05	-0.49	—	—	0.87	0.46	4.76	—	1.24	0.88

^a 518A2 – melanoma, HT-29 – colon adenocarcinoma, DLD-1 – Dukes type C colorectal adenocarcinoma, HCT116^{wt} – colon carcinoma (wildtype); HCT116^{-/-} – colon carcinoma (p53 knock-out mutant). ^b p53 dependency of IC₅₀ values in HCT116 colon carcinoma cells, indicated by $r^{p53} = (IC_{50}^{wt}/IC_{50}^{-/-}) - 1$.

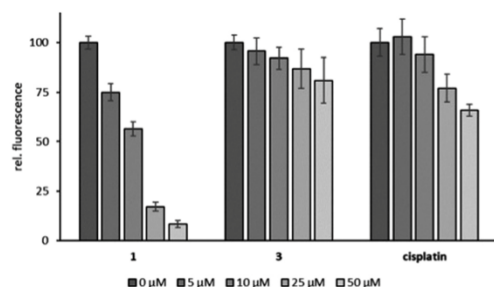


Fig. 4 Relative fluorescence intensities of ethidium bromide after intercalation into salmon sperm DNA treated with **1**, **3** or cisplatin for 2 h.

an electrostatic interaction, or to an intercalation of the planar NHC ligands into the DNA helix, remains to be clarified. It seems, however, obvious that bis-NHC complexes of Pt^{II} show a higher affinity for DNA than their Pt^{IV} analogues. Attempts to “switch on” the DNA affinity of complex **3** *in situ* by adding ascorbic acid as a reductant failed (data not shown). This is in line with findings of Gibson *et al.*, who reported that Pt^{IV} complexes are reduced in cells by high molecular weight, membrane-associated molecules (>3000 Da) rather than small ones such as GSH or ascorbic acid.¹⁶ This would also go a long way towards explaining the similar antiproliferative effects of some $\text{Pt}^{\text{II}}/\text{Pt}^{\text{IV}}$ complex couples in our MTT cell tests.

Conclusions

The oxidation of complexes **2** and of the known bis(*N,N*-dibenzylimidazol-2-ylidene)dichlorido platinum(II) complex **1** with PhICl_2 afforded the new stable $[\text{Pt}^{\text{IV}}\text{Cl}_4(\text{NHC})_2]$ complexes **3** and **4** in excellent yields. In contrast, hydroxo complexes of type $[\text{Pt}^{\text{IV}}\text{Cl}_{4-n}(\text{OH})_n(\text{NHC})_2]$ were generally not accessible by oxidation of **1** or **2** with H_2O_2 or hypochlorites, or by exchange of chlorido for hydroxo ligands in tetrachlorido complexes **4**, presumably due to their inherent instability. For future approaches to hydroxo-ligated (bis-NHC) Pt^{IV} complexes, it might be advisable to employ electron-withdrawing residues on the NHC ligands to attenuate their strong donor effect.

The IC_{50} values of the $[\text{Pt}^{\text{II}}\text{Cl}_2(\text{NHC})_2]/[\text{Pt}^{\text{IV}}\text{Cl}_4(\text{NHC})_2]$ complex couples **1/3**, **2c/4c**, and *trans*-**2c/trans-4c** against the five selected tumour cell lines were each quite similar and in a clinically meaningful range for most cell lines. This may be rationalised by assuming an intracellular reduction of the Pt^{IV} complexes to their active Pt^{II} congeners. What needs to be done now, is to determine the speed and extent of the cellular uptake of corresponding $\text{Pt}^{\text{II}}/\text{Pt}^{\text{IV}}$ complex couples. Under a clinical aspect it is also worthy of note that each of these complexes was of similar activity both in wildtype and in p53-negative HCT116 colon carcinoma cells, in stark contrast to the mentioned $[(1,3\text{-dialkylbenzimidazol-2-ylidene})\text{Cl}_2\text{L}]\text{Pt}^{\text{II}}$ complexes and to the mainstay drug cisplatin which rely on functional p53.

Our EtdBr saturation experiments with DNA in a cell-free context suggest that *cis*-(bis-NHC) Pt^{II} complexes such as **1** cause morphological changes to DNA more pronounced than those initiated by cisplatin, while the corresponding *cis*-(bis-NHC) Pt^{IV} complexes such as **3** interact with DNA in a different, less structure-modifying way. This also corroborates the assumption of an intracellular reduction of the latter so as to achieve the antiproliferative effects against cancer cells similar in magnitude to those of the respective Pt^{II} congener. The fact that the *trans* complexes are on average as active as their *cis* analogues hints at a mode of action not involving DNA metalation. Further studies into the uptake, intracellular distribution and details of the modes of action of the new (bis-NHC) Pt^{IV} complexes are now indicated. Their prodrug character and their unique positive features when compared with the established platinum drugs make them interesting candidates for further development.

Experimental

Materials and methods

All chemicals and reagents were purchased from Sigma Aldrich, Alfa Aesar, ChemPur or ABCR and were used without further purification. Melting points are uncorrected; NMR spectra were run on a 500 MHz spectrometer; chemical shifts are given in ppm (δ) and referenced relative to the internal solvent signal; ^{195}Pt NMR shifts are quoted relative to $\Xi(^{195}\text{Pt}) = 21.496784$ MHz; K_2PtCl_4 was used as external standard ($\delta = -1612.81$); mass spectra: direct inlet, EI, 70 eV; elemental analyses: Vario EL III elemental analyser; X-Ray diffractometer: STOE-IPDS II. All biotested compounds were >95% pure by elemental analysis. Synthesis of **1** and precursors **5**, **6c** and **7** was performed as described in the literature.^{10b,c} Abbreviations used for NMR signal attribution: Ar = aromatic; BI = Benzimidazole; Cq = quaternary Carbon; Imi = Imidazole.

Syntheses and characterisation

General synthesis of *cis*- $[\text{Pt}^{\text{II}}\text{Cl}_2(\text{NHC})_2]$ complexes **2.** The *cis*- $[\text{Pt}^{\text{II}}\text{Cl}_2(\text{DMSO})(\text{NHC})]$ complexes **7** (1 eq.) and the respective benzimidazolium chlorides **5** (1.2 eq.) in dry CH_2Cl_2 were treated with KO^tBu (1.5 eq.) under an argon atmosphere and stirred for 72 h at ambient temperature. After filtration the solvent was reduced *in vacuo* and the product was precipitated by addition of diethyl ether at 4 °C. Lipophilic complex **2d** could not be precipitated and was purified by column chromatography.

***cis*-Dichlorido-bis(1,3-dimethylbenzimidazol-2-ylidene) platinum(II) (**2a**).** **7a** (200 mg, 408 μmol), **5a** (75 mg, 408 μmol , 1 eq.), KO^tBu (63 mg, 612 μmol , 1.5 eq.), CH_2Cl_2 (25 mL). Yield: 82 mg (146 μmol , 36%); colourless solid of m.p. >400 °C; elemental analysis (%): calc. for $\text{C}_{18}\text{H}_{20}\text{N}_4\text{Cl}_2\text{Pt}$ (558.37): C, 38.72; H, 3.61; N, 10.03. Found: C, 38.05; H, 4.048; N, 9.921. ^1H NMR (500 MHz, $\text{DMSO}-d_6$): δ 4.10 (12 H, s, CH_3), 7.34 (4 H, dd, $J = 6.1, 3.1$ Hz, BI), 7.63 (4 H, dd, $J = 6.1, 3.1$ Hz, BI); ^{13}C NMR (125 MHz, $\text{DMSO}-d_6$): δ 34.7 (CH_3), 110.3 (BI),

123.8 (BI), 134.3 (BI-Cq), 159.5 (NHC); ^{195}Pt NMR (108 MHz, DMSO- d_6): δ –3660 ppm; m/z (EI): 558, 522, 485, 353, 339, 244, 209, 145.

cis-Dichlorido-bis(1,3-diethylbenzimidazol-2-ylidene) platinum(II) (2b). 7b (500 mg, 837 μmol), 5b (211 mg, 1.00 mmol, 1.2 eq.), KO^tBu (141 mg, 1.26 mmol, 1.5 eq.), CH₂Cl₂ (100 mL). Yield: 399 mg (649 μmol , 78%); colourless solid of m.p. 353 °C (decomp.); elemental analysis (%): calc. for C₂₂H₂₈N₄Cl₂Pt (614.47): C, 43.00; H, 4.59; N, 9.12. Found: C, 42.04; H, 4.661; N, 8.955. ^1H NMR (500 MHz, CDCl₃): δ 1.46 (12 H, t, J = 7.0 Hz, CH₃), 4.66 (4 H, dq, J = 14, 7.0 Hz, CH₂), 5.07 (4 H, dq, J = 14, 7.0 Hz, CH₂), 7.25–7.31 (4 H, m, BI), 7.39 (4 H, dd, J = 6.0, 3.2 Hz, BI); ^{13}C NMR (125 MHz, CDCl₃): δ 14.3 (CH₃), 43.6 (CH₂), 111.0 (BI), 123.5 (BI), 133.5 (BI-Cq), 158.7 (NHC); ^{195}Pt NMR (108 MHz, CDCl₃): δ –3632 ppm; m/z (EI): 726, 690, 653, 420, 231, 203, 119, 44.

cis-Dichlorido-bis(1,3-dibutylbenzimidazol-2-ylidene) platinum(II) (2c). 7c (965 mg, 1.68 mmol), 5c (574 mg, 2.02 mmol, 1.2 eq.), KO^tBu (283 mg, 2.52 mmol, 1.5 eq.), CH₂Cl₂ (105 mL). Yield: 875 mg (1.20 mmol, 72%); colourless solid of m.p. 210 °C; elemental analysis (%): calc. for C₃₀H₄₄N₄Cl₂Pt (726.69): C, 49.58; H, 6.10; N, 7.71. Found: C, 49.01; H, 6.022; N, 7.832. ^1H NMR (500 MHz, CDCl₃): δ 0.96 (12 H, t, J = 7.3 Hz, CH₃), 1.42–1.51 (4 H, m, CH₂–CH₃), 1.53–1.69 (8 H, m, CH₂–CH₃, NCH₂–CH₂), 2.13–2.26 (4 H, m, NCH₂–CH₂), 4.32 (4 H, ddd, J = 13, 11, 5.0 Hz, N–CH₂), 4.98 (4 H, ddd, J = 13, 11, 5.0 Hz, N–CH₂), 7.25–7.29 (4 H, d, J = 3.2 Hz, BI), 7.32–7.38 (4 H, m, BI); ^{13}C NMR (125 MHz, CDCl₃): δ 13.8 (CH₃), 20.4 (CH₂–CH₃), 31.1 (NCH₂–CH₂), 48.7 (N–CH₂), 111.0 (BI), 123.3 (BI), 133.7 (BI-Cq), 158.8 (NHC); ^{195}Pt NMR (108 MHz, CDCl₃): δ –3622 ppm; m/z (EI): 726, 690, 653, 420, 231, 203, 119, 44. Crystal data: C₃₀H₄₄Cl₂N₄Pt·CHCl₃, M = 846.07, triclinic, space group $P\bar{1}$, a = 8.6162(17) Å, b = 12.200(2) Å, c = 17.892(4) Å, α = 104.49(3)°, β = 95.13(3)°, γ = 104.88(3)°, V = 1736.1(7) Å³, Z = 2, λ = 0.71073 Å, μ = 4.45 mm^{–1}, T = 133 K; 20 838 reflections measured, 8234 unique; $R[F_2 > 2\sigma(F_2)]$ = 0.0175 and R_w = 0.0382, GOF = 1.040. CCDC 1912955.†

cis-Dichlorido-bis(1,3-dioctylbenzimidazol-2-ylidene) platinum(II) (2d). 7d (75 mg, 109 μmol), 5d (50 mg, 164 μmol , 1.5 eq.), KO^tBu (36 mg, 328 μmol , 3 eq.), CH₂Cl₂ (10 mL), SiO₂ hexane: ethyl acetate 6 : 1 → 2 : 1. Yield: 57 mg (60 μmol , 55%); colourless solid of m.p. 146 °C; elemental analysis (%): calc. for C₄₅H₇₆N₄Cl₂Pt (951.11): C, 58.09; H, 8.05; N, 5.89. Found: C, 57.94; H, 7.451; N, 5.305. ^1H NMR (500 MHz, CDCl₃): δ 0.90 (12 H, t, J = 6.9 Hz, CH₃), 1.25–1.33 (32 H, m, CH₂), 1.38–1.44 (4 H, m, NC₂H₄–CH₂), 1.48–1.55 (4 H, m, NC₂H₄–CH₂), 1.59–1.68 (4 H, m, NCH₂–CH₂), 2.15–2.26 (4 H, m, NCH₂–CH₂), 4.28–4.39 (4 H, ddd, J = 13, 12, 5.0 Hz, N–CH₂), 4.95 (4 H, ddd, J = 13, 12, 5.0 Hz, N–CH₂), 7.26 (4 H, d, J = 3.1 Hz, BI), 7.34 (4 H, dd, J = 6.1, 3.2 Hz, BI); ^{13}C NMR (125 MHz, CDCl₃): δ 14.1 (CH₃), 22.6 (CH₂), 27.3 (CH₂), 29.2 (CH₂), 29.3 (CH₂), 29.3 (CH₂), 31.8 (CH₂), 48.9 (N–CH₂), 111.0 (BI), 123.3 (BI), 133.7 (BI-Cq), 158.8 (NHC); ^{195}Pt NMR (108 MHz, CDCl₃): δ –3622; m/z (EI): 950, 914, 877, 843, 532, 341, 285, 119.

General synthesis of cis-[Pt^{IV}Cl₂(NHC)₂] complexes 3 and 4. The cis-[Pt^{IV}Cl₂(NHC)₂] complexes 1 and 2 (1 eq.) in CH₂Cl₂

were treated with iodobenzene dichloride (PhICl₂, 10 eq.) and stirred at ambient temperature for 4 h to 16 h. The product was precipitated at 4 °C by adding diethyl ether or hexane, respectively, after reducing the solvent *in vacuo*.

cis-Tetrachlorido-bis(1,3-dibenzylimidazol-2-ylidene) platinum(IV) (3). 1 (50 mg, 66 μmol), PhICl₂ (180 mg, 655 μmol , 10 eq.), CH₂Cl₂ (20 mL), 4 h. Yield: 49 mg (59 μmol , 90%); pale yellow solid of m.p. 252 °C (decomp.); elemental analysis (%): calc. for C₃₄H₃₂N₄Cl₄Pt (833.54): C, 48.99; H, 3.87; N, 6.72. Found: C, 48.25; H, 3.876; N, 6.574. ^1H NMR (500 MHz, DMSO- d_6): δ 4.45 (2 H, d, J = 13.9 Hz, CH₂), 5.34 (2 H, d, J = 13.9 Hz, CH₂), 6.10 (2 H, d, J = 15.0 Hz, CH₂), 6.30 (2 H, d, J = 15.0 Hz, CH₂), 7.08 (2 H, d, J = 2.1 Hz, Imi), 7.18 (2 H, d, J = 2.1 Hz, Imi), 7.23–7.30 (10 H, m, Ar), 7.31–7.39 (6 H, m, Ar), 7.42 (4 H, t, J = 7.4 Hz, Ar); ^{13}C NMR (125 MHz, DMSO- d_6): δ 51.7 (CH₂), 55.3 (CH₂), 122.4 (Imi), 124.9 (Imi), 125.5 (Imi), 127.9 (Ar), 128.1 (Ar), 128.2 (Ar), 128.3 (Ar), 128.6 (Ar), 128.7 (Ar), 135.5 (Ar–C_q), 136.0 (NHC), 137.1 (Ar–C_q); ^{195}Pt NMR (108 MHz, DMSO- d_6): δ –1250 ppm; m/z (EI): 833, 797, 760, 724, 687, 440, 247, 157, 91. Crystal data: C₃₄H₃₂Cl₄N₄Pt·2(CH₂Cl₂), M = 983.87, monoclinic, space group $C2/c$, a = 24.684(5) Å, b = 8.277(5) Å, c = 22.505(5) Å, α = β = γ = 121.662(5)°, V = 3914(3) Å³, Z = 4, λ = 0.71069 Å, μ = 3.808 mm^{–1}, T = 133 K; 10 695 reflections measured, 3414 unique; $R[F_2 > 2\sigma(F_2)]$ = 0.0554 and R_w = 0.1630, GOF = 0.987. CCDC 1912954.†

cis-Tetrachlorido-bis(1,3-dimethylbenzimidazol-2-ylidene) platinum(IV) (4a). 2a (30 mg, 54 μmol), PhICl₂ (148 mg, 537 μmol , 10 eq.), CH₂Cl₂ (12 mL), 4 h. Yield: 33 mg (52 μmol , 98%); pale yellow solid of m.p. 330 °C (decomp.); elemental analysis (%): calc. for C₁₈H₂₀N₄Cl₄Pt (629.27): C, 34.36; H, 3.20; N, 8.90. Found: C, 34.88; H, 3.647; N, 9.051; m/z (EI): 630, 603, 559, 523, 486, 340, 147, 44, 36.

cis-Tetrachlorido-bis(1,3-diethylbenzimidazol-2-ylidene) platinum(IV) (4b). 2b (100 mg, 163 μmol), PhICl₂ (47 mg, 1.63 mmol, 10 eq.), CH₂Cl₂ (50 mL), 4 h. Yield: 111 mg (162 μmol , 100%); yellow solid of m.p. 326 °C (decomp.); elemental analysis (%): calc. for C₂₂H₂₈N₄Cl₄Pt (685.38): C, 38.55; H, 4.12; N, 8.17. Found: C, 38.98; H, 4.846; N, 8.230. ^1H NMR (500 MHz, CDCl₃): δ 1.36 (6 H, t, J = 6.94 Hz, CH₃), 1.74 (6 H, t, J = 7.02 Hz, CH₃), 3.47 (2 H, dq, J = 14, 7.0 Hz, CH₂), 3.87 (2 H, dq, J = 14, 7.0 Hz, CH₂), 5.36 (2 H, dq, J = 14, 7.1 Hz, CH₂), 5.72 (2 H, dq, J = 14, 7.1 Hz, CH₂), 7.41–7.46 (4 H, m, Ar), 7.51 (2 H, ddd, J = 8.3, 5.4, 2.8 Hz, Ar), 7.72 (2 H, d, J = 8.3 Hz, Ar); ^{13}C NMR (125 MHz, CDCl₃): δ 14.9 (CH₃), 15.9 (CH₃), 44.2 (CH₂), 46.3 (CH₂), 112.3 (BI), 113.4 (BI), 125.4 (BI), 125.4 (BI), 133.4 (BI-Cq), 134.4 (BI-Cq), 136.8 (NHC); ^{195}Pt NMR: δ –1430 ppm; m/z (EI): 684, 648, 615, 576, 542, 368, 339, 176, 36.

cis-Tetrachlorido-bis(1,3-dibutylbenzimidazol-2-ylidene) platinum(IV) (4c). 2c (100 mg, 138 μmol), PhICl₂ (378 mg, 1.38 mmol, 10 eq.), CH₂Cl₂ (50 mL), 4 h. Yield: 96 mg (120 μmol , 88%); yellow solid of m.p. 222 °C; elemental analysis (%): calc. for C₃₀H₄₄N₄Cl₄Pt (797.59): C, 45.18; H, 5.56; N, 7.02. Found: C, 44.69; H, 6.607; N, 7.502. ^1H NMR (500 MHz, CDCl₃): δ 0.64 (6 H, t, J = 7.3 Hz, CH₃), 0.76–0.87 (2 H, m, CH₃–CH₂), 1.03–1.16 (8 H, m, CH₃–CH₂, CH₃), 1.42–1.52 (2 H,

m, CH₂), 1.59–1.71 (4 H, m, CH₂), 1.98–2.11 (4 H, m, CH₂), 2.18–2.29 (2 H, m, CH₂), 3.33 (2 H, td, *J* = 13, 4.3 Hz, N–CH₂), 3.75 (2 H, td, *J* = 13, 4.3 Hz, N–CH₂), 5.30–5.45 (4 H, m, N–CH₂), 7.38 (2 H, d, *J* = 8.2 Hz, BI), 7.42 (2 H, t, *J* = 7.6 Hz, BI), 7.49 (2 H, t, *J* = 7.6 Hz, BI), 7.67 (2 H, d, *J* = 8.2 Hz, BI); ¹³C NMR (125 MHz, CDCl₃): δ 13.2 (CH₃), 13.9 (CH₃), 19.9 (CH₃–CH₂), 19.9 (CH₃–CH₂), 31.0 (NCH₂–CH₂), 32.4 (NCH₂–CH₂), 49.4 (N–CH₂), 51.1 (N–CH₂), 112.4 (BI), 113.4 (BI), 125.3 (BI), 125.4 (BI), 133.6 (BI–C_q), 134.7 (BI–C_q), 136.4 (NHC); ¹⁹⁵Pt NMR: δ –1427 ppm; *m/z* (EI): 797, 762, 728, 655, 421, 365, 266, 230, 120, 36.

cis-Tetrachlorido-bis(1,3-dioctylbenzimidazol-2-ylidene) platinum(IV) (4d). 2d (25 mg, 26 μmol), PhICl₂ (72 mg, 263 μmol, 10 eq.), CH₂Cl₂ (10 mL), 16 h. Yield: 25 mg (25 μmol, 93%); yellow solid of m.p. 202 °C; elemental analysis (%): calc. for C₄₆H₇₆N₄Cl₄Pt (1022.02): C, 54.06; H, 7.50; N, 5.48. Found: C, 54.29; H, 7.103; N, 5.051. ¹H NMR (500 MHz, CDCl₃): δ 0.71–0.79 (2 H, m, CH₃–CH₂), 0.83–0.92 (14 H, m, CH₃, CH₂), 1.00–1.14 (10 H, m, CH₂), 1.18–1.24 (4 H, m, CH₂), 1.27–1.38 (14 H, m, CH₂), 1.39–1.48 (6 H, m, CH₂), 1.61 (4 H, dt, *J* = 14, 7.2 Hz, CH₂), 2.07 (4 H, s, CH₂), 2.23 (2 H, dd, *J* = 12, 7.3 Hz, CH₂), 3.35 (2 H, td, *J* = 13, 3.7 Hz, N–CH₂), 3.74 (2 H, td, *J* = 13, 3.7 Hz), 5.23 (2 H, td, *J* = 13, 3.7 Hz, N–CH₂), 5.41–5.56 (2 H, td, *J* = 13, 3.7 Hz, N–CH₂), 7.36 (2 H, d, *J* = 8.2 Hz, BI), 7.42 (2 H, t, *J* = 7.6 Hz, BI), 7.48 (2 H, t, *J* = 7.6 Hz, BI), 7.65 (2 H, d, *J* = 8.2 Hz, BI); ¹³C NMR (125 MHz, CDCl₃): δ 14.0 (CH₃), 14.1 (CH₃), 22.5 (CH₂), 22.7 (CH₂), 26.6 (CH₂), 26.7 (CH₂), 28.8 (CH₂), 29.0 (CH₂), 29.0 (CH₂), 29.3 (CH₂), 29.3 (CH₂), 30.4 (CH₂), 31.6 (CH₂), 31.7 (CH₂), 49.7 (N–CH₂), 51.3 (N–CH₂), 112.4 (BI), 113.3 (BI), 125.2 (BI), 125.3 (BI), 133.6 (BI–C_q), 134.7 (BI–C_q), 136.3 (NHC); ¹⁹⁵Pt NMR: δ –1429 ppm; *m/z* (EI): 1020, 984, 950, 912, 877, 513, 339, 119, 36.

Synthesis of *trans* complexes *trans-2c* and *trans-4c*

***trans*-Dichlorido-bis(1,3-dibutylbenzimidazol-2-ylidene) platinum(II) (*trans-2c*).** 6c (100 mg, 267 μmol, 2 eq.) in CH₂Cl₂ (20 mL) was treated with K₂PtCl₄ (55 mg, 133 μmol, 1 eq.) and stirred at ambient temperature for 4 days. After filtration the solution was concentrated *in vacuo* and addition of hexane precipitated the product at 4 °C. Yield: 49 mg (67 μmol, 51%); colourless solid of m.p. 272 °C; elemental analysis (%): calc. for C₃₀H₄₄N₄Cl₂Pt (726.69): C, 49.58; H, 6.10; N, 7.71. Found: C, 49.98; H, 6.295; N, 7.392. ¹H NMR (500 MHz, CDCl₃): δ 1.06 (12 H, t, *J* = 7.3 Hz, CH₃), 1.54–1.63 (8 H, m, CH₃–CH₂), 2.21 (8 H, quin, *J* = 7.8 Hz, NCH₂–CH₂), 4.84–4.95 (8 H, t, *J* = 7.8 Hz, N–CH₂), 7.26–7.31 (4 H, m, BI), 7.42 (4 H, dd, *J* = 6.0, 3.1 Hz, BI); ¹³C NMR (125 MHz, CDCl₃): δ 14.0 (CH₃), 20.6 (CH₃–CH₂), 32.0 (NCH₂–CH₂), 47.5 (N–CH₂), 110.5 (BI), 122.7 (BI), 134.3 (BI–C_q), 178.0 (NHC); ¹⁹⁵Pt NMR: δ –3245 ppm; *m/z* (EI): 726, 653, 420, 365, 229, 119.

***trans*-Tetrachlorido-bis(1,3-dibutylbenzimidazol-2-ylidene) platinum(IV) (*trans-4c*).** *trans-2c* (41 mg, 56 μmol) and PhICl₂ (47 mg, 169 μmol, 10 eq.) in CH₂Cl₂ (5 mL) was stirred at ambient temperature for 3 days. To the concentrated solution was added hexane to precipitate the product at 4 °C. Yield: 40 mg (50 μmol, 89%); yellow solid of m.p. 253 °C; elemental

analysis (%): calc. for C₃₀H₄₄N₄Cl₄Pt (797.59): C, 45.18; H, 5.56; N, 7.02. Found: C, 45.04; H, 5.522; N, 7.392. ¹H NMR (500 MHz, CDCl₃): δ 1.08 (12 H, t, *J* = 7.4 Hz, CH₃), 1.60 (8 H, sxt, *J* = 7.4 Hz, CH₃–CH₂), 2.13 (8 H, quin, *J* = 7.8 Hz, NCH₂–CH₂), 5.05–5.17 (8 H, m, N–CH₂), 7.39 (4 H, dd, *J* = 6.2, 3.1 Hz, BI), 7.57 (4 H, dd, *J* = 6.2, 3.1 Hz, BI); ¹³C NMR (125 MHz, CDCl₃): δ 13.9 (CH₃), 20.3 (CH₃–CH₂), 32.0 (NCH₂–CH₂), 49.9 (N–CH₂), 112.5 (BI), 124.0 (BI), 134.5 (BI–C_q), 147.5 (NHC); ¹⁹⁵Pt NMR: δ –1051 ppm; *m/z* (EI): 798, 762, 728, 691, 655, 421, 266, 230, 176, 120.

X-ray data collection and structural determination

Diffractionmeter used: STOE-IPDS II; data collection by: X-Area-Stoe; cell refinement by: X-Area-Stoe. The single crystal samples were measured with Mo-Kα and reflexes collected at 133 K. The structures were solved by direct methods using SIR97 and refined by full matrix least-squares on *F*² for all data using SHELXL2014. All hydrogen atoms were added at calculated positions and refined using a riding model. Anisotropic thermal displacement parameters were used for all non-hydrogen atoms. Further details about the data collection and reliability factors are listed together with the analytical data and in the ESI† Supplementary crystallographic data were deposited with The Cambridge Crystallographic Data Centre CCDC under no. 1912955 (2c), 1912954 (3).†

MTT based anti-proliferation assay¹⁷

The cell titer was adjusted to 0.05 × 10⁶ cpm (cells per mL) or 0.1 × 10⁶ cpm (DLD1, Hdfa) and the cells were seeded into the wells (100 μL per well) of 96 well plates. After an incubation period of 24 h at 37 °C, 5% CO₂ and 95% humidity appropriate dilutions of 2, 3, 4b, 4c, *trans-2c* or *trans-4c* or DMSO in ddH₂O (final concentrations 100 μM–25 nM) were added into the wells and the plates were incubated for a further 72 h at 37 °C. The plates were centrifuged (5 min, 300 g, 4 °C) and the supernatant was removed. 50 μL of a 0.05% MTT solution (PBS) was added into each well and the plates were further incubated at 37 °C for 2 h. The plates were centrifuged as before and the MTT solution was discarded again. The cells and the formed formazan were dissolved in DMSO (10% SDS, 0.6% AcOH) for 1 h at 37 °C. The absorption of the violet formazan was measured at 570 nm, respectively of the background at 630 nm. Values for the DMSO carrier were set to 100% viability and the percentage of living cells inside the wells treated with the platinum complexes was calculated accordingly. The IC₅₀ values were determined using GraphPad Prism. Means ± SDs were calculated from four independent experiments.

Ethidiumbromide saturation assay

All solutions were sterile filtered before use. A 96 black well plate was prepared with wells containing 100 μL of TE-buffer (10 mM Tris/HCl, 1 mM EDTA, pH 8.0) with 10 μg mL^{−1} salmon sperm DNA. 11.1 μL of appropriate dilutions of 1 and 3 in H₂O were added into each well to reach final concentrations of 5, 10, 25 and 50 μM. As negative control wells treated with DMSO analogously to the highest concentration

were prepared. Treatment of the DNA was conducted in triplicates. To remove possible background fluorescence, one well containing 100 μL TE buffer without DNA was prepared for each concentration and compound. After 2 h of incubation at 37 $^{\circ}\text{C}$ 100 μL of a 10 $\mu\text{g mL}^{-1}$ EtdBr solution in TE-buffer was added into each well. After another 5 minutes of incubation in the dark (RT), the fluorescence of the intercalated ethidium-bromide was measured at $\lambda_{\text{ex}} = 535$ and $\lambda_{\text{em}} = 595$. The fluorescence values were corrected for their respective background fluorescence and a possible fluorescence decrease was calculated relative to the fluorescence in the control wells which was adjusted to 100%.

Conflicts of interest

There are no conflicts to declare.

Acknowledgements

We thank the Deutsche Forschungsgemeinschaft (grant Scho 402/12-2) and the COST Action CM1105 'Functional metal complexes that bind to biomolecules' for financial support.

We are indebted to Dr Ulrike Lacher (Central Analytical Services) for ESI-MS studies and Sofia Bär for additional MTT-assays.

Notes and references

- (a) B. Rosenberg, L. VanCamp, J. E. Trosko and V. H. Mansour, *Nature*, 1969, **222**, 385–386, DOI: 10.1038/222385a0; (b) M. Rozenzweig, D. D. Von Hoff, M. Slavik and F. M. Muggia, *Ann. Intern. Med.*, 1977, **86**, 803–812, DOI: 10.7326/0003-4819-86-6-803.
- P. J. O'Dwyer, J. P. Stevenson and S. W. Johnson, *Clinical Status of Cisplatin, Carboplatin, and Other Platinum-Based Antitumor Drugs, in Cisplatin*, ed. B. Lippert, Verlag Helvetica Chimica Acta, Zürich, Switzerland, 1999.
- D. Gibson, *Dalton Trans.*, 2016, **45**, 12983–12991, DOI: 10.1039/c6dt01414c.
- N. J. Wheate, S. Walker, G. E. Craig and R. Oun, *Dalton Trans.*, 2010, **39**, 8113–8127, DOI: 10.1039/c0dt00292e.
- (a) T. C. Johnstone, K. Suntharalingam and S. J. Lippard, *Chem. Rev.*, 2016, **116**, 3436–3486, DOI: 10.1021/acs.chemrev.5b00597; (b) H. P. Varbanov, M. A. Jakupc, A. Roller, F. Jensen, M. Galanski and B. K. Keppler, *J. Med. Chem.*, 2013, **56**, 330–344, DOI: 10.1021/jm3016427; (c) X. Wang, X. Wang and Z. Guo, *Acc. Chem. Res.*, 2015, **48**, 92622–92631, DOI: 10.1021/acs.accounts.5b00203.
- (a) X. Huang, R. Huang, S. Gou, Z. Wang, Z. Liao and H. Wang, *Bioconjugate Chem.*, 2016, **27**, 2132–2148, DOI: 10.1021/acs.bioconjchem.6b00353; (b) E. Petruzzella, R. Sirota, I. Solazzo, V. Gandin and D. Gibson, *Chem. Sci.*, 2018, **9**, 4299–4307, DOI: 10.1039/c8sc00428e; (c) L. Gaviglio, A. Gross, N. Metzler-Nolte and M. Ravera, *Metallomics*, 2012, **4**, 260–266, DOI: 10.1039/C2MT00171C.
- (a) V. Brabec, O. Hrabina and J. Kasparkova, *Coord. Chem. Rev.*, 2017, **351**, 2–31, DOI: 10.1016/j.ccr.2017.04.013; (b) R. G. Kenny and C. J. Marmion, *Chem. Rev.*, 2019, **119**, 1085–1137, DOI: 10.1021/acs.chemrev.8b00271; (c) X. Wang and Z. Guo, *Chem. Soc. Rev.*, 2013, **42**, 202–224, DOI: 10.1039/c2cs35259a.
- (a) M. Bouché, A. Bonnefont, T. Achard and S. Bellemin-Laponnaz, *Dalton Trans.*, 2018, **47**, 11491–11502, DOI: 10.1039/c8dt02113a; (b) M. Bouché, G. Dahm, M. Wantz, S. Fournel, T. Achard and S. Bellemin-Laponnaz, *Dalton Trans.*, 2016, **45**, 11362–11368, DOI: 10.1039/c6dt01846g.
- (a) R. Lindner, C. Wagner and D. Steinborn, *J. Am. Chem. Soc.*, 2009, **131**, 8861–8874, DOI: 10.1021/ja901264t; (b) V. N. Demidov, Y. N. Kukushkin, L. N. Vedeneeva and A. N. Belyaev, *Zh. Obshch. Khim.*, 1988, **58**, 738; (c) V. Khlebnikov, M. Heckenroth, H. Müller-Bunz and M. Albrecht, *Dalton Trans.*, 2013, **42**, 4197–4207, DOI: 10.1039/c3dt32423g; (d) D. Meyer, S. Ahrens and T. Strassner, *Organometallics*, 2010, **29**, 3392–3396, DOI: 10.1021/om100488s; (e) W. Weigand, U. Nagel and W. Beck, *Z. Naturforsch., B: Chem. Sci.*, 1988, **43**, 328–338.
- (a) J. Muenzner, T. Rehm, B. Biersack, A. Casini, I. de Graaf, P. Worawutputtpong, A. Noor, R. Kempe, V. Brabec, J. Kasparkova and R. Schobert, *J. Med. Chem.*, 2015, **58**, 6283–6292, DOI: 10.1021/acs.jmedchem.5b00896; (b) T. Rehm, M. Rothemund, J. K. Muenzner, A. Noor, R. Kempe and R. Schobert, *Dalton Trans.*, 2016, **45**, 15390–15398, DOI: 10.1039/c6dt02350a; (c) T. Rehm, M. Rothemund, A. Bär, T. Dietel, R. Kempe, H. Kostrhunova, V. Brabec, J. Kasparkova and R. Schobert, *Dalton Trans.*, 2018, **47**, 17367–17381, DOI: 10.1039/c8dt03360a.
- C. P. Newman, R. J. Deeth, G. J. Clarkson and J. P. Rourke, *Organometallics*, 2007, **26**, 6225–6233, DOI: 10.1021/om700671y.
- J. J. Wilson and S. J. Lippard, *Chem. Rev.*, 2014, **114**, 4470–4495, DOI: 10.1021/cr4004314.
- X.-F. Zhao and C. Zhang, *Synthesis*, 2007, 551–557, DOI: 10.1055/s-2007-965889.
- A. G. Tennyson, V. M. Lynch and C. W. Bielawski, *J. Am. Chem. Soc.*, 2010, **132**, 9420–9429, DOI: 10.1021/ja102686u.
- (a) L. Ma, R. Ma, Y. Wang, X. Zhu, J. Zhang, H. C. Chan, X. Chen, W. Zhang, S.-K. Chiu and G. Zhu, *Chem. Commun.*, 2015, **51**, 6301–6304, DOI: 10.1039/c4cc10409a; (b) R. Haputhanthri, R. Ojha, E. I. Izgorodina, S. X. Guo, G. B. Deacon, D. McNaughton and B. R. Wood, *Vib. Spectrosc.*, 2017, **92**, 82–95, DOI: 10.1016/j.vibspec.2017.02.006; (c) E. G. Talman, Y. Kidani, L. Mohrmann and J. Reedijk, *Inorg. Chim. Acta*, 1998, **283**, 251–255.
- A. Nemirovski, Y. Kasherman, Y. Tzaraf and D. Gibson, *J. Med. Chem.*, 2007, **50**, 5554–5556, DOI: 10.1021/jm070740j.
- (a) T. Mosmann, *J. Immunol. Methods*, 1983, **65**, 55–63, DOI: 10.1016/0022-1759(83)90303-4; (b) R. B. Badisa, S. F. Darling-Reed, P. Joseph, J. S. Cooperwood, L. M. Latinwo and C. B. Goodman, *Anticancer Res.*, 2009, **29**, 2993–2996.

Electronic Supplementary Material (ESI) for Dalton Transactions.
This journal is © The Royal Society of Chemistry 2019

Electronic Supporting Information

Synthesis, structures and cytotoxic effects *in vitro* of *cis*- and *trans*-[Pt^{IV}Cl₄(NHC)₂] complexes and their Pt^{II} precursors

Tobias Rehm,^a Matthias Rothemund,^a Thomas Dietel,^b Rhett Kempe^b and Rainer Schobert^a

^aOrganic Chemistry Laboratory, University Bayreuth, Universitaetsstrasse 30, 95440 Bayreuth, Germany. E-mail: Rainer.Schobert@uni-bayreuth.de

^bLehrstuhl fuer Anorganische Chemie II, University Bayreuth, Universitaetsstrasse 30, 95440 Bayreuth, Germany.

Table of content

Single crystal X-ray diffraction data of complexes 2c and 3 (Table S1)	S2
NMR spectra of complexes 2a-d , <i>trans</i> - 2c , 3 , 4a-d and <i>trans</i> - 4c (Fig. S1-S30)	S3–S17
Oxidation of complex 2b with NaOCl	S18–S21
Stability of complex 4b in DMSO / water	S22–S24
Confirmative MTT-assays with 2c / 2d (Table S2)	S25

Table S 1: Single crystal X-ray diffraction data of platinum carbene complexes **2c** and **3**.

Crystal data	2c	3
Chemical formula	C ₃₀ H ₄₄ Cl ₂ N ₄ Pt·CHCl ₃	C ₂₄ H ₃₂ Cl ₄ N ₄ Pt·2(CH ₂ Cl ₂)
<i>M_r</i>	846.07	983.87
Crystal system, space group	Triclinic, P	Monoclinic, C2/c
Temperature (K)	133	133
<i>a</i> , <i>b</i> , <i>c</i> (Å)	8.6162 (17), 12.200 (2), 17.892 (4)	24.684 (5), 8.277 (5), 22.505 (5)
α , β , γ (°)	104.49 (3), 95.13 (3), 104.88 (3)	121.662 (5)
<i>V</i> (Å ³)	1736.1 (7)	3914 (3)
<i>Z</i>	2	4
<i>F</i> (000)	842.5	1945
<i>D_x</i> (Mg m ⁻³)	1.618	1.670
Radiation type	Mo K α	Mo K α
No. of reflections for cell measurement	1222	8743
θ range (°) for cell measurement	5.7–25.8	1.9–28.3
μ (mm ⁻¹)	4.45	3.81
Crystal shape	Block	Block
Colour	Clear colourless	Colourless
Crystal size (mm)	0.07 × 0.01 × 0.004	0.21 × 0.12 × 0.09
Data collection		
Diffractometer	STOE-STADIVARI	STOE-STADIVARI
Scan method	ω scans	ω scan
Absorption correction	Numerical	Numerical
		STOE-X-RED32
<i>T_{min}</i> , <i>T_{max}</i>	0.613, 0.733	0.841, 0.912
No. of measured, independent and observed [<i>I</i> > 2 σ (<i>I</i>)] reflections	20838, 8234, 7605	10695, 3414, 2307
<i>R_{int}</i>	0.015	0.077
θ values (°)	θ_{\max} = 28.5, θ_{\min} = 1.8	θ_{\max} = 25.0, θ_{\min} = 2.0
($\sin \theta/\lambda$) _{max} (Å ⁻¹)	0.671	0.595
Range of <i>h</i> , <i>k</i> , <i>l</i>	<i>h</i> = -11 → 7 <i>k</i> = -16 → 16 <i>l</i> = -23 → 22	<i>h</i> = -29 → 29 <i>k</i> = -5 → 9 <i>l</i> = -26 → 22
Refinement		
Refinement on	<i>F</i> ²	<i>F</i> ²
<i>R</i> [<i>F</i> ² > 2 σ (<i>F</i> ²)], <i>wR</i> [<i>F</i> ²], <i>S</i>	0.018, 0.038, 1.04	0.055, 0.163, 0.99
No. of reflections	8234	3414
No. of parameters	374	223
No. of restraints	0	18
H-atom treatment	H-atom parameters constrained	H-atom parameters constrained
Weighting scheme	$w = 1/[\sigma^2(F_o^2) + (0.0198P)^2 + 0.8853P]$ where $P = (Fo^2 + 2Fc^2)/3$	$w = 1/[\sigma^2(F_o^2) + (0.1072P)^2]$ where $P = (Fo^2 + 2Fc^2)/3$
(Δ/σ) _{max}	< 0.001	< 0.001
$\Delta\rho_{\max}$, $\Delta\rho_{\min}$ (e Å ⁻³)	0.62, -0.54	2.14, -2.78

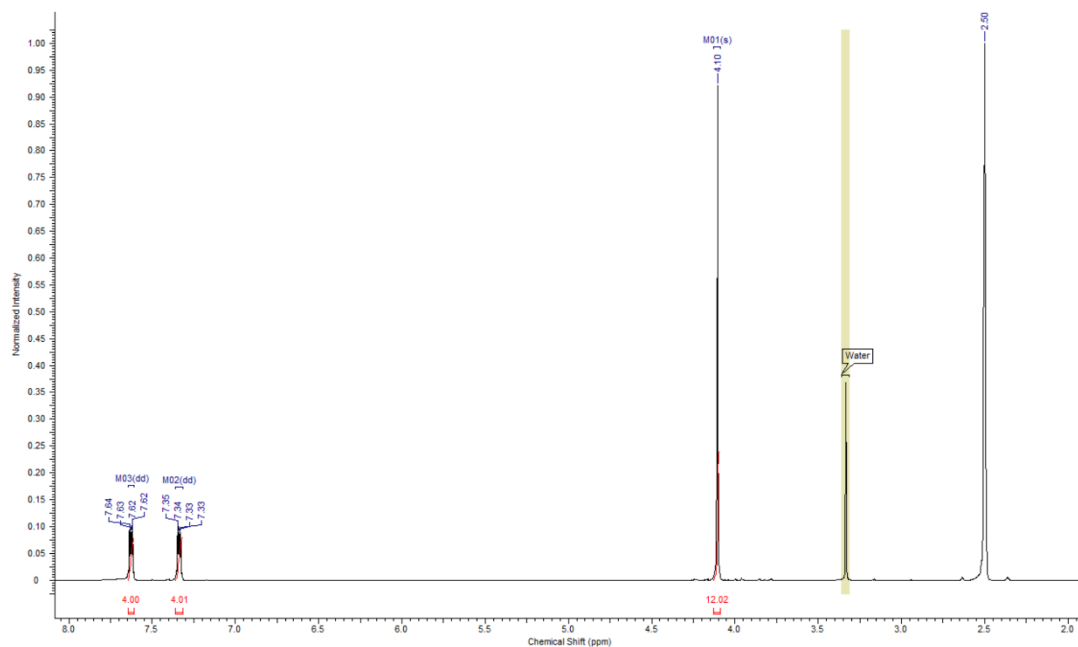


Fig. S 1: ^1H -NMR spectrum (500 MHz, $\text{DMSO}-d_6$) of complex 2a.

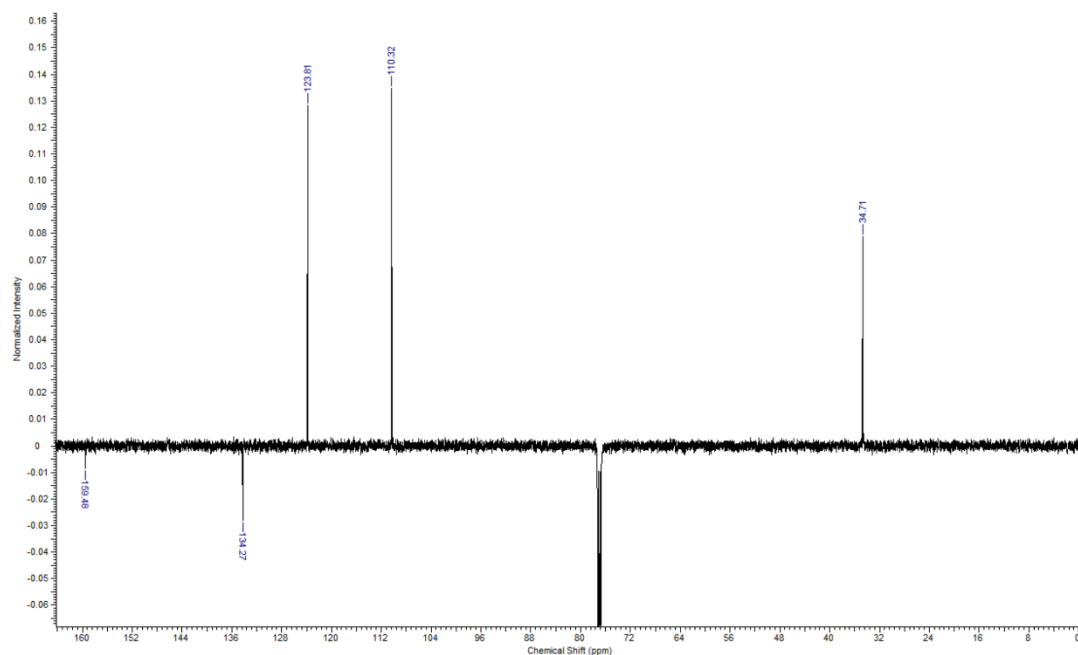


Fig. S 2: ^{13}C -NMR spectrum (126 MHz, CDCl_3) of complex 2a.

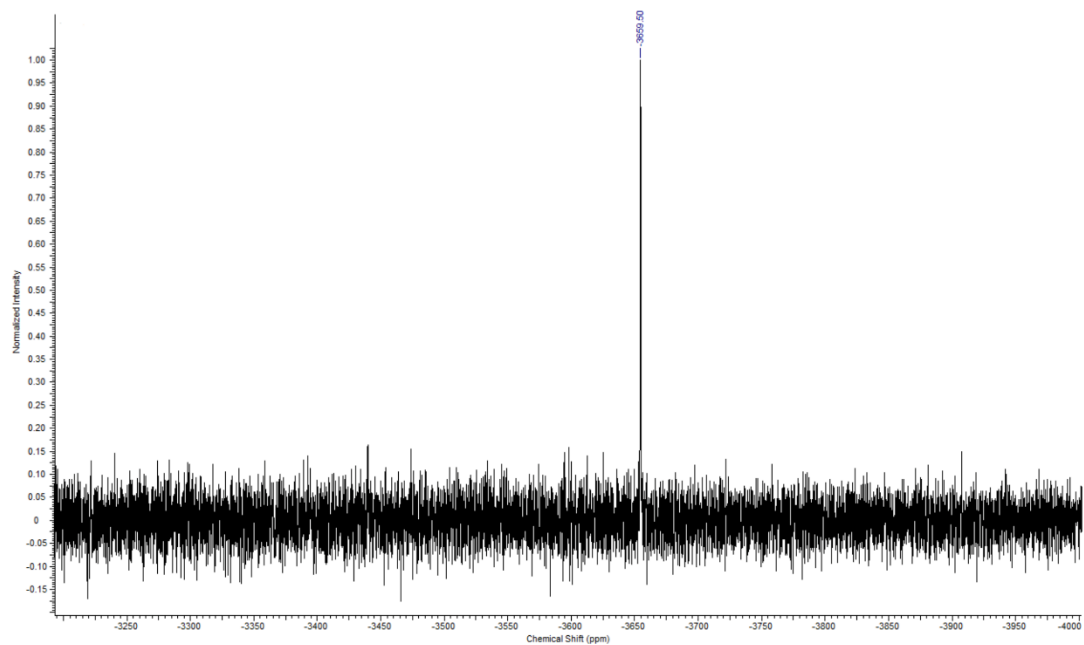


Fig. S 3: ^{195}Pt -NMR spectrum (108 MHz, CDCl_3) of complex **2a**.

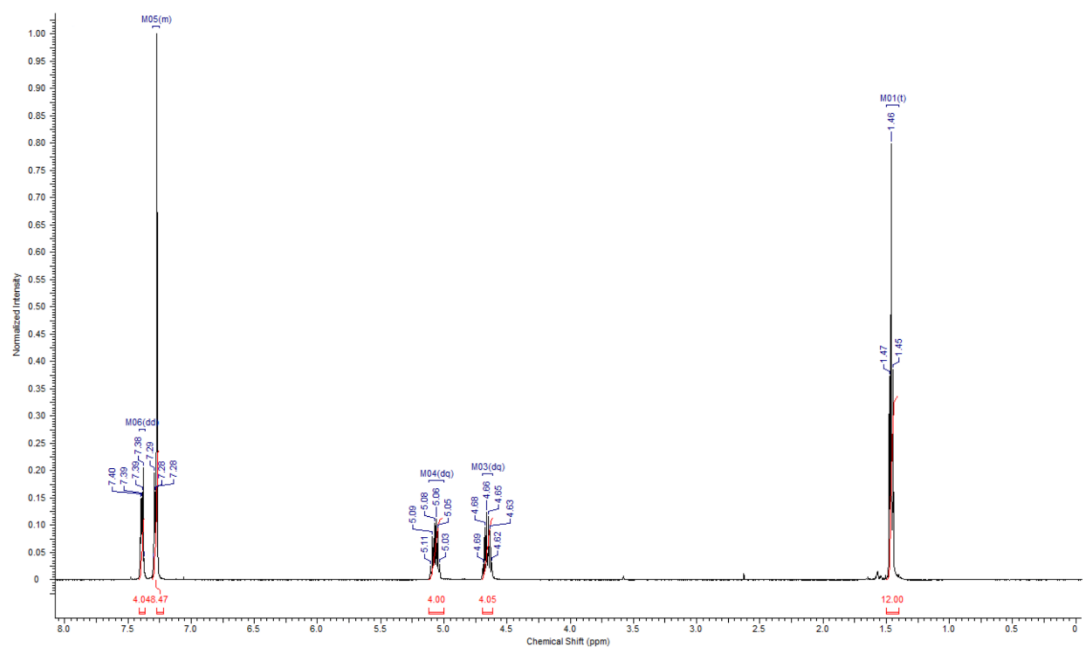


Fig. S 4: ^1H -NMR spectrum (500 MHz, CDCl_3) of complex **2b**.

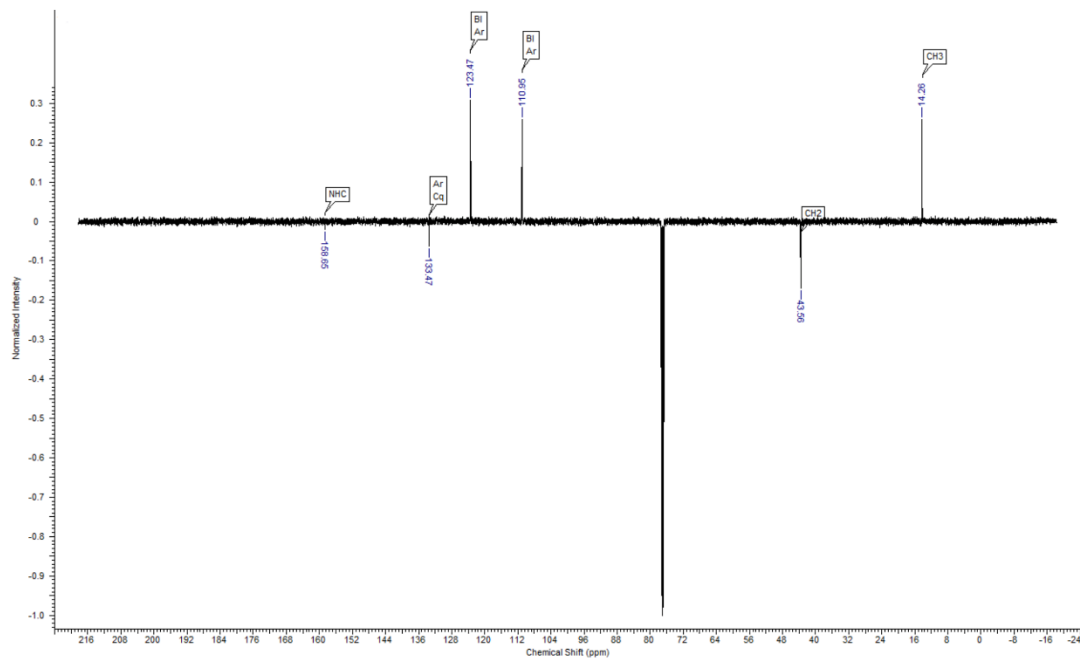


Fig. S 5: ¹³C-NMR spectrum (126 MHz, CDCl₃) of complex **2b**.

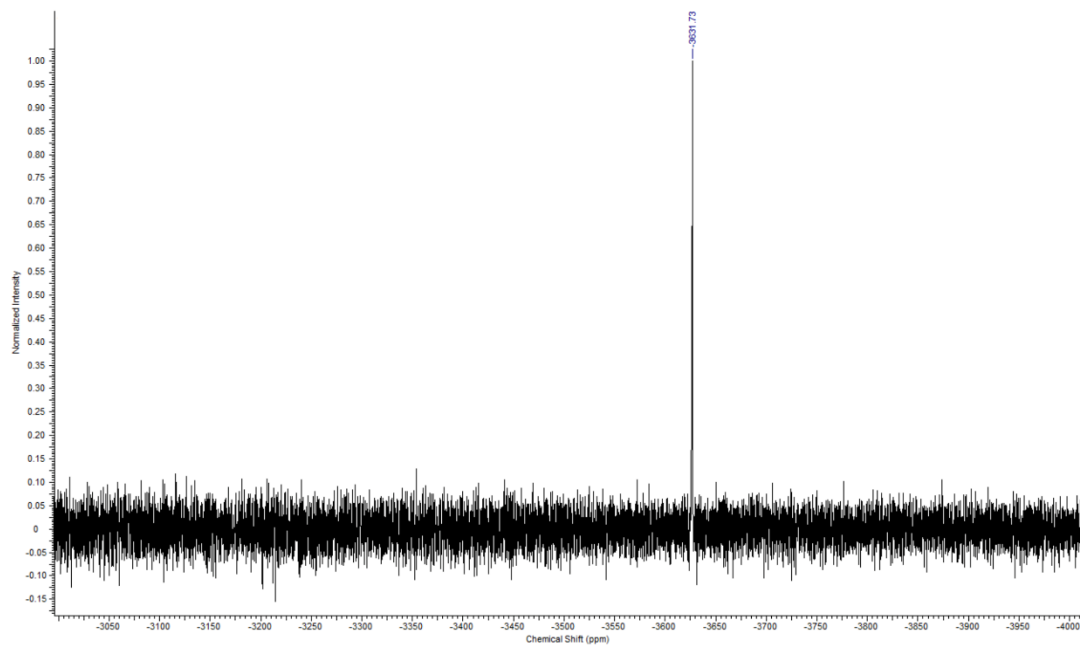


Fig. S 6: ¹⁹⁵Pt-NMR spectrum (108 MHz, CDCl₃) of complex **2b**.

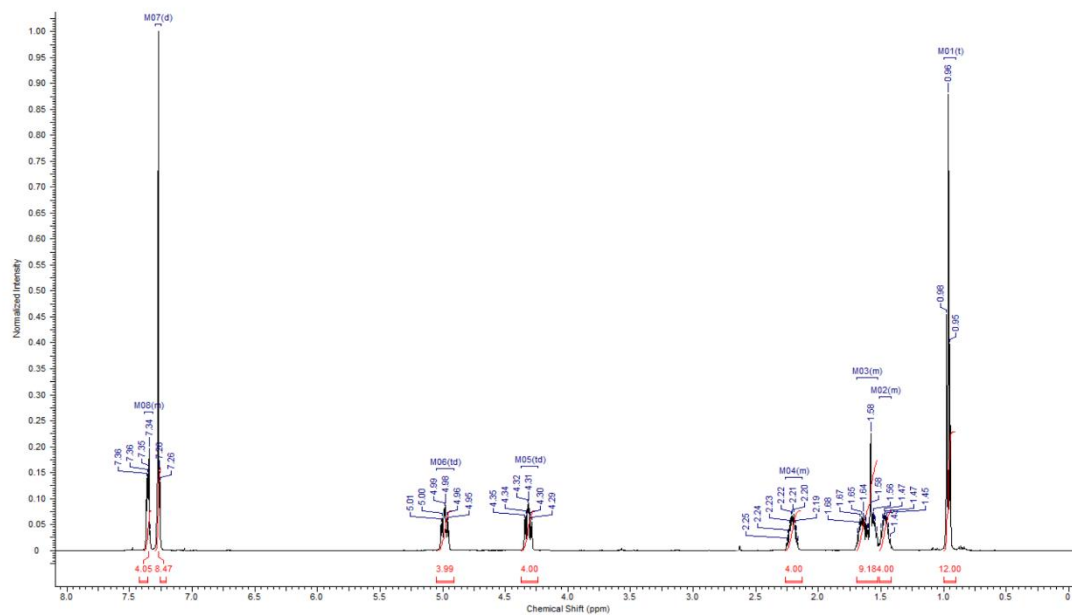


Fig. S 7: ^1H -NMR spectrum (500 MHz, CDCl_3) of complex **2c**.

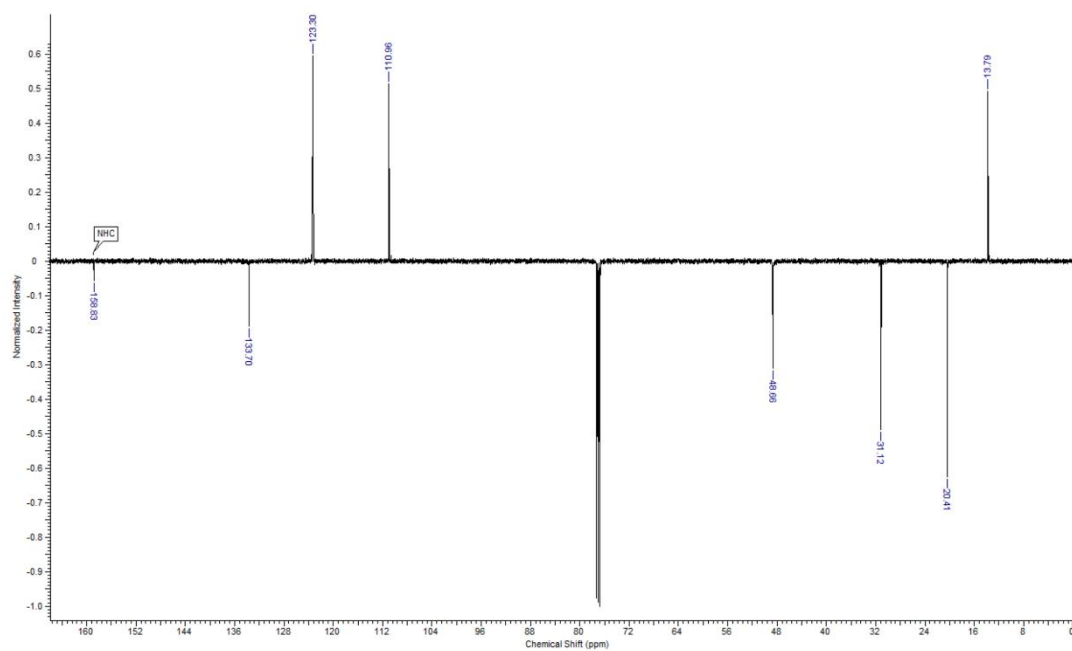


Fig. S 8: ^{13}C -NMR spectrum (126 MHz, CDCl_3) of complex **2c**.

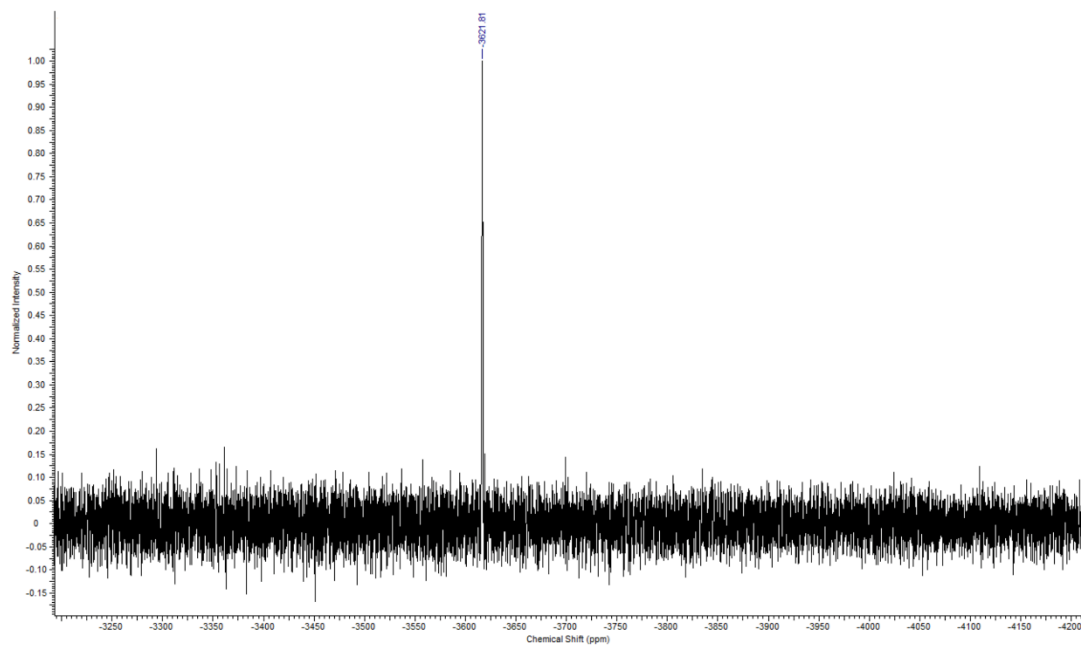


Fig. S 9: ^{195}Pt -NMR spectrum (108 MHz, CDCl_3) of complex **2c**.

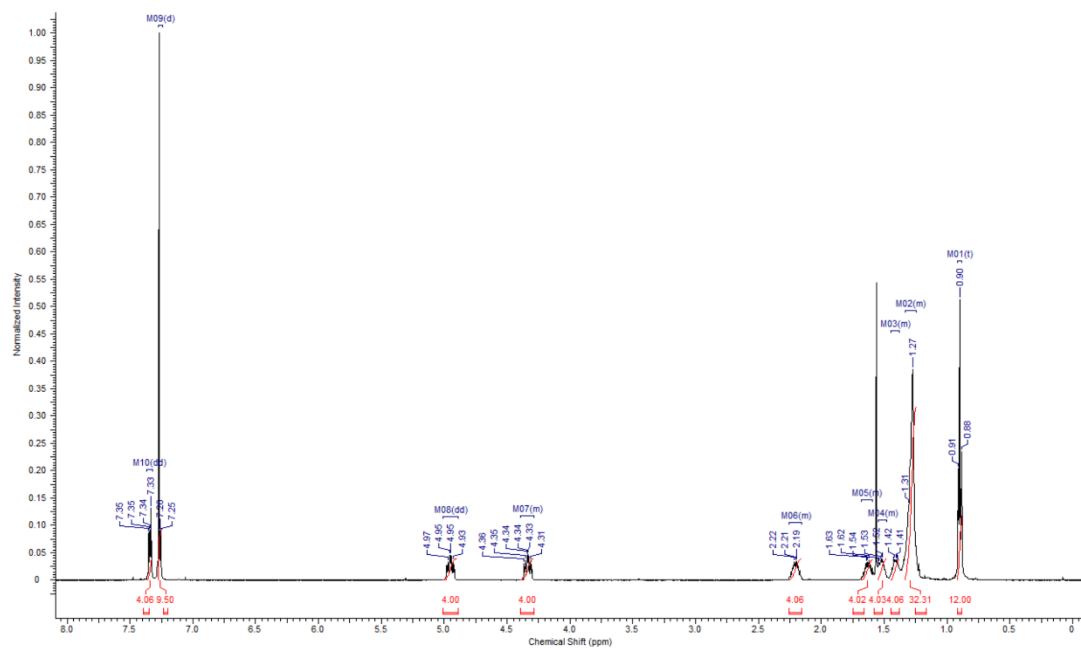


Fig. S 10: ^1H -NMR spectrum (500 MHz, CDCl_3) of complex **2d**.

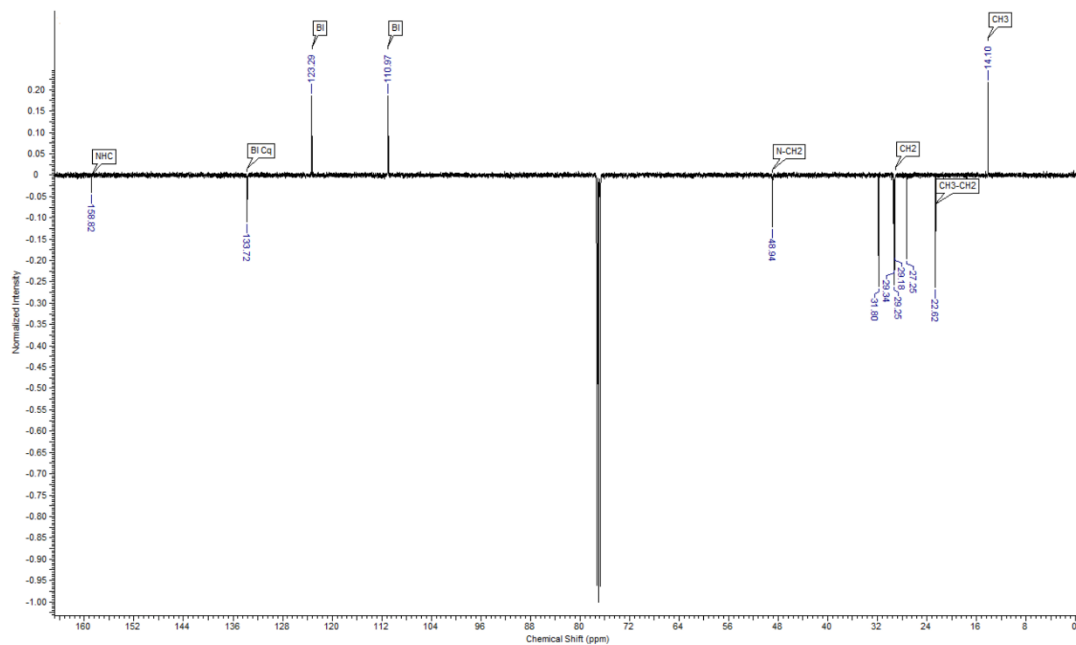


Fig. S 11: ^{13}C -NMR spectrum (126 MHz, CDCl_3) of complex **2d**.

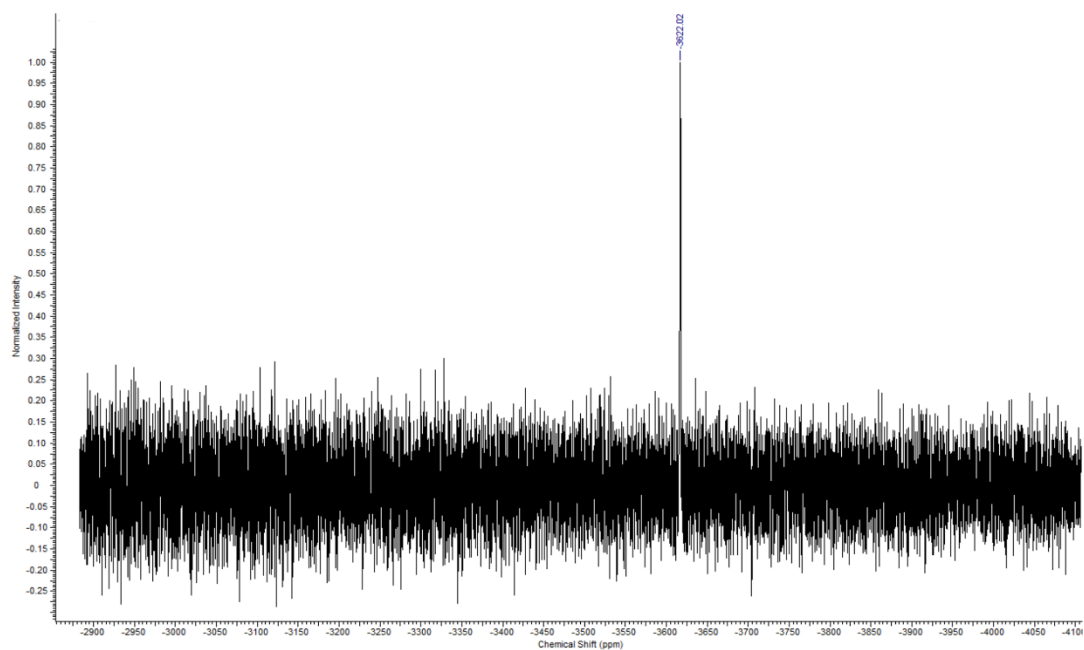


Fig. S 12: ^{195}Pt -NMR spectrum (108 MHz, CDCl_3) of complex **2d**.

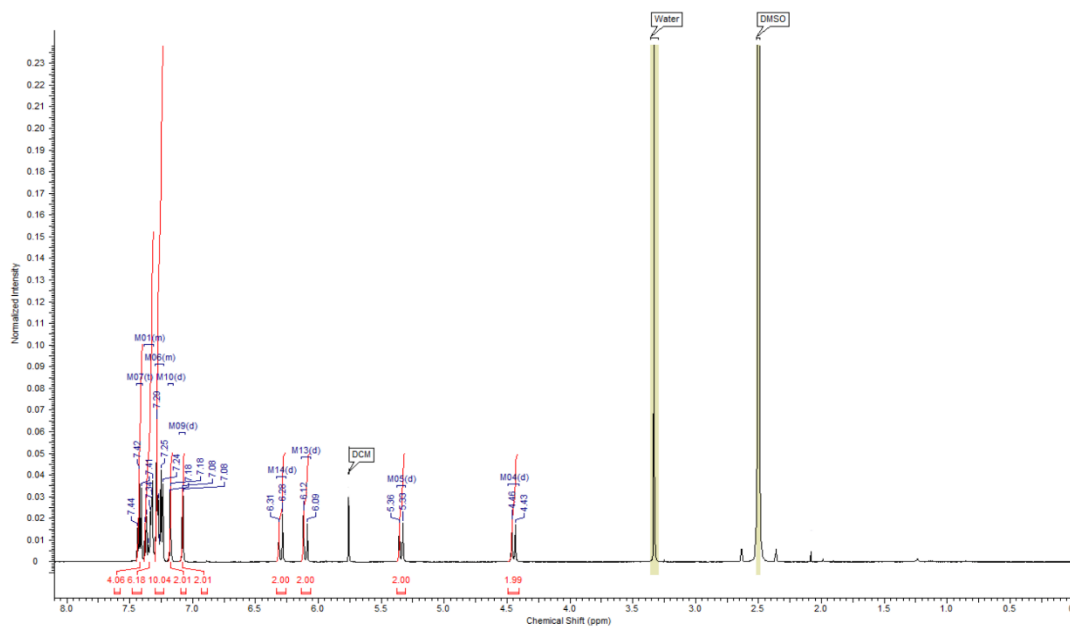


Fig. S 13: ^1H -NMR spectrum (500 MHz, $\text{DMSO}-d_6$) of complex **3**.

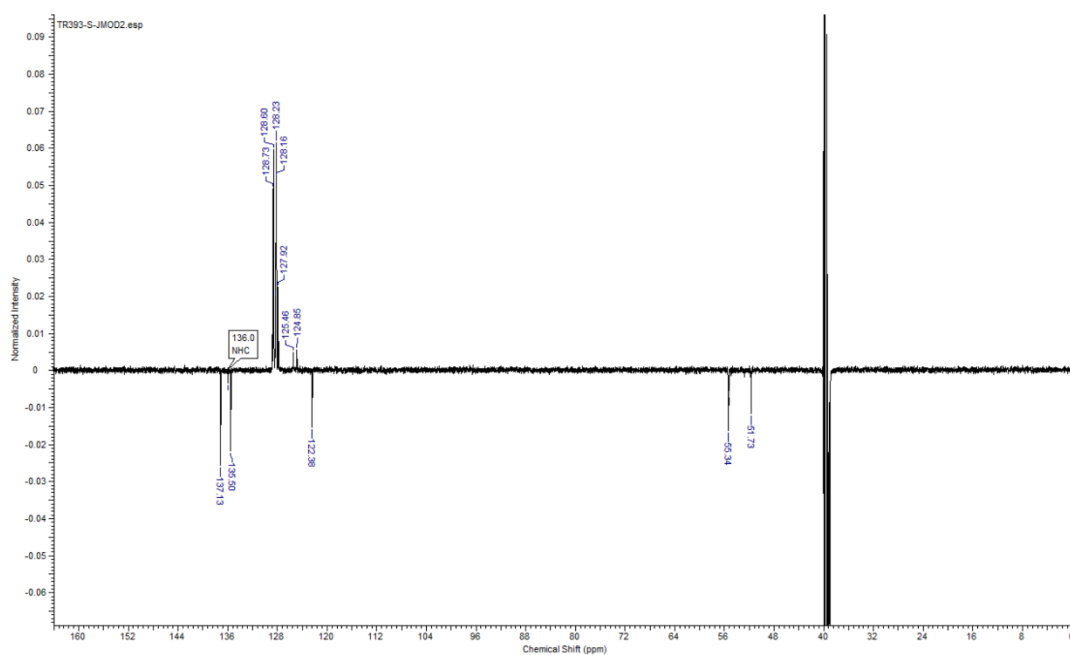


Fig. S 14: ^{13}C -NMR spectrum (126 MHz, $\text{DMSO}-d_6$) of complex **3**.

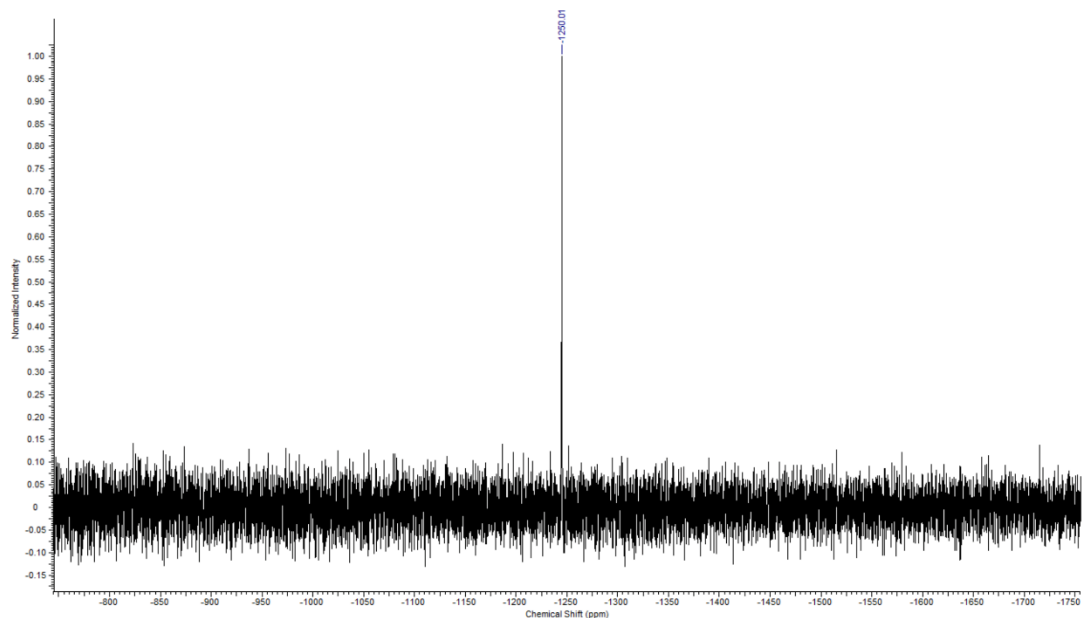


Fig. S 15: ^{195}Pt -NMR spectrum (108 MHz, $\text{DMSO}-d_6$) of complex 3.

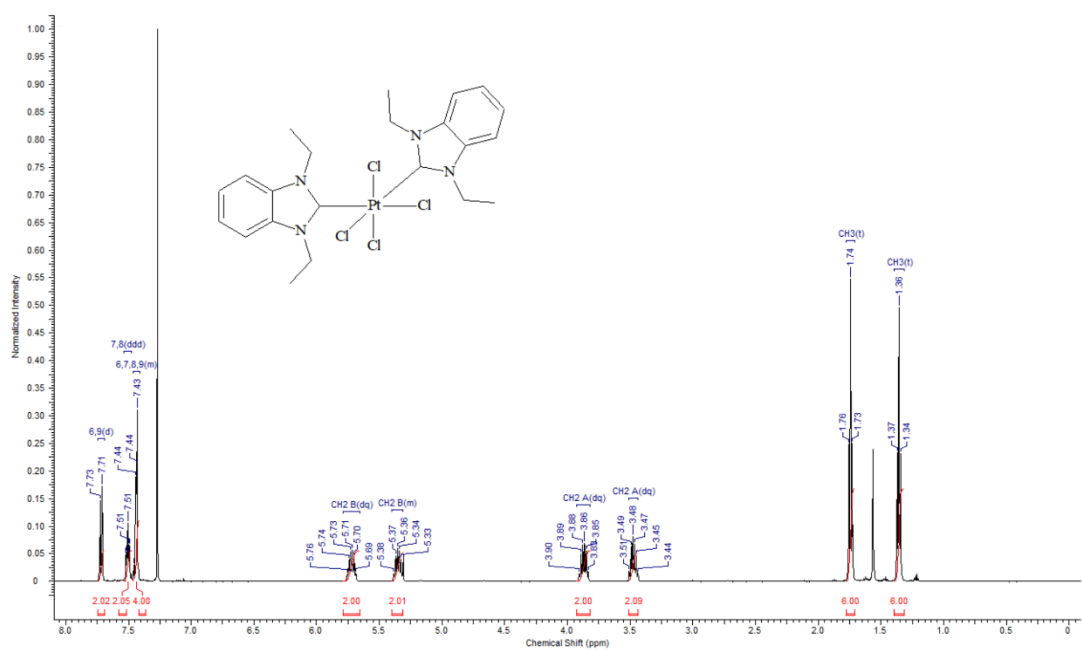


Fig. S 16: ^1H -NMR spectrum (500 MHz, CDCl_3) of complex 4b.

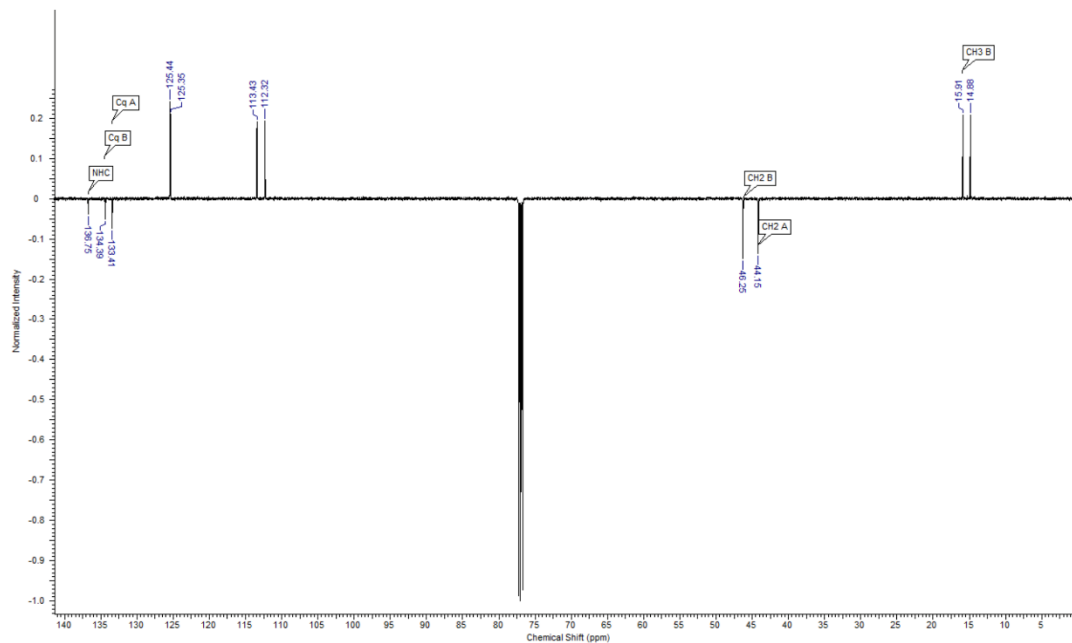


Fig. S 17: ^{13}C -NMR spectrum (126 MHz, CDCl_3) of complex **4b**.

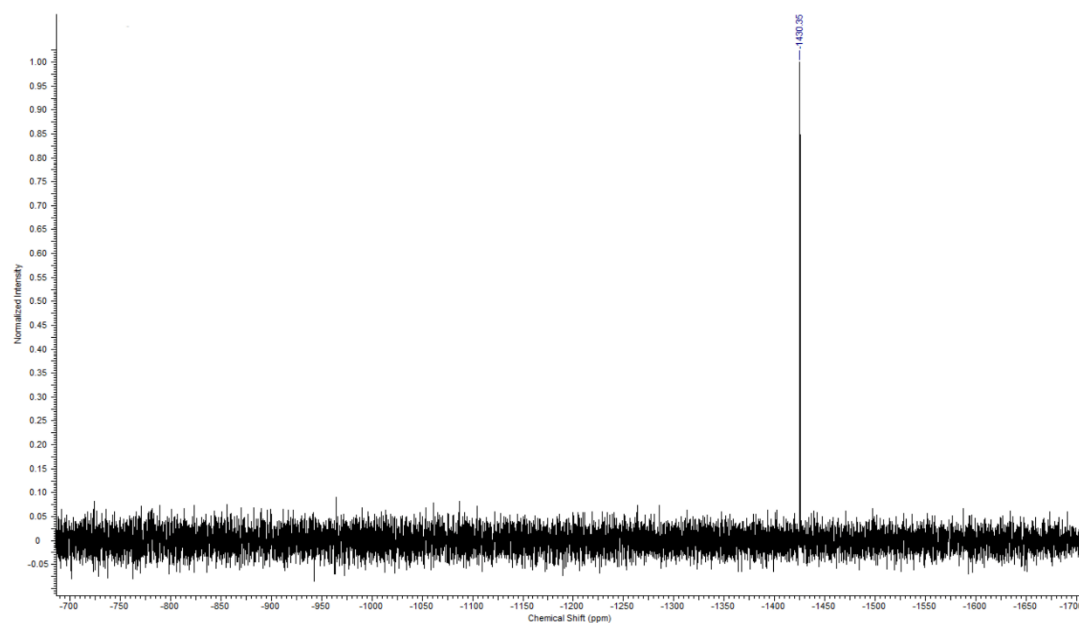


Fig. S 18: ^{195}Pt -NMR spectrum (108 MHz, CDCl_3) of complex **4b**.

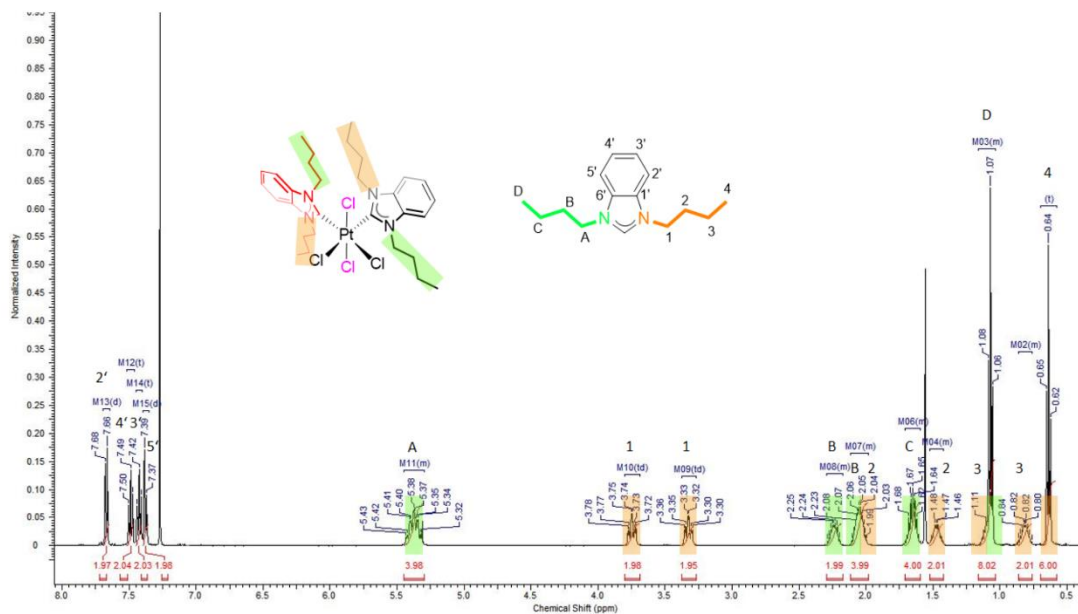


Fig. S 19: ^1H -NMR spectrum (500 MHz, CDCl_3) of complex **4c**.

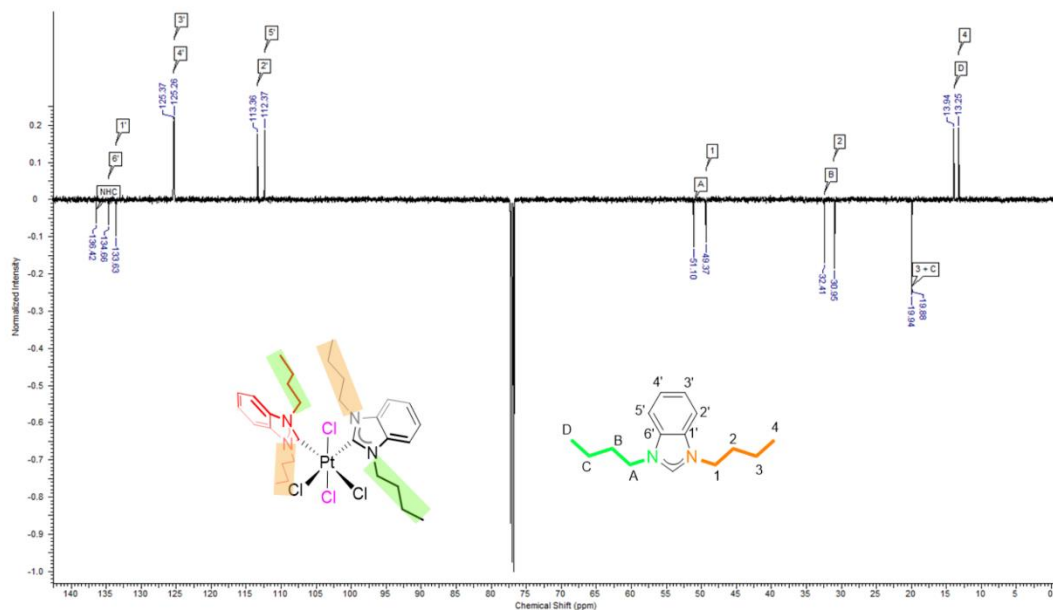


Fig. S 20: ^{13}C -NMR spectrum (126 MHz, CDCl_3) of complex **4c**.

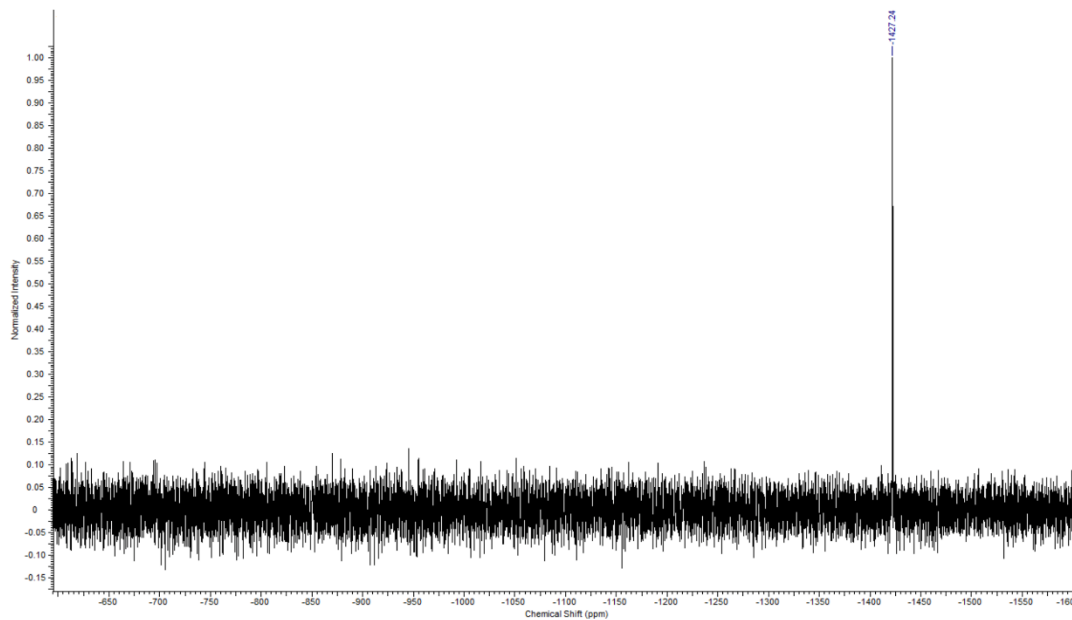


Fig. S 21: ^{195}Pt -NMR spectrum (108 MHz, CDCl_3) of complex 4c.

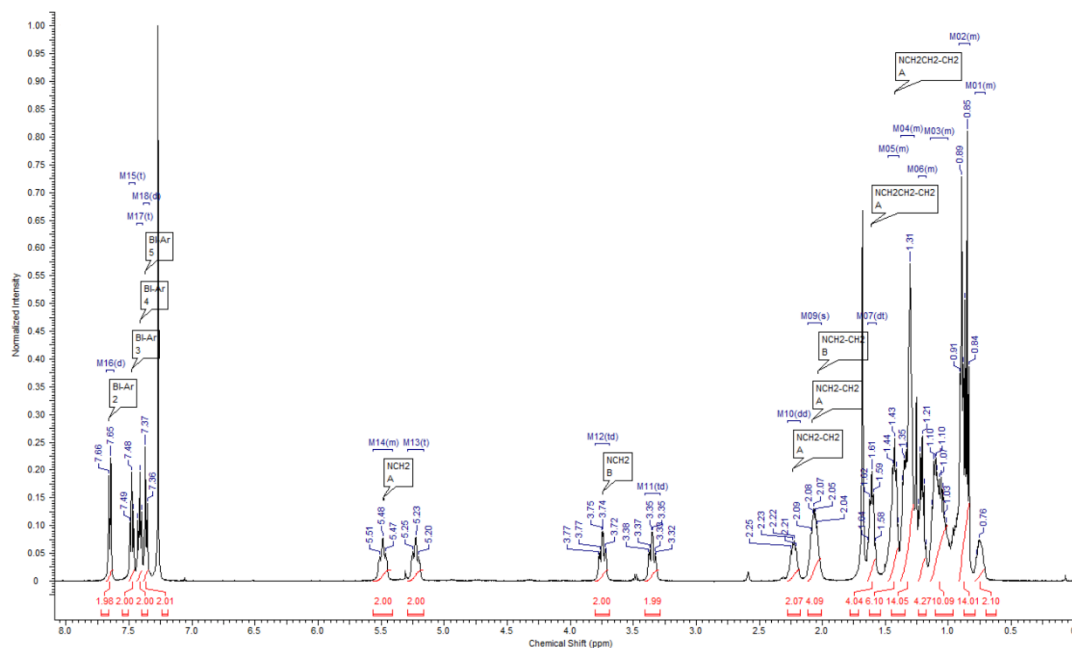


Fig. S 22: ^1H -NMR spectrum (500 MHz, CDCl_3) of complex 4d.

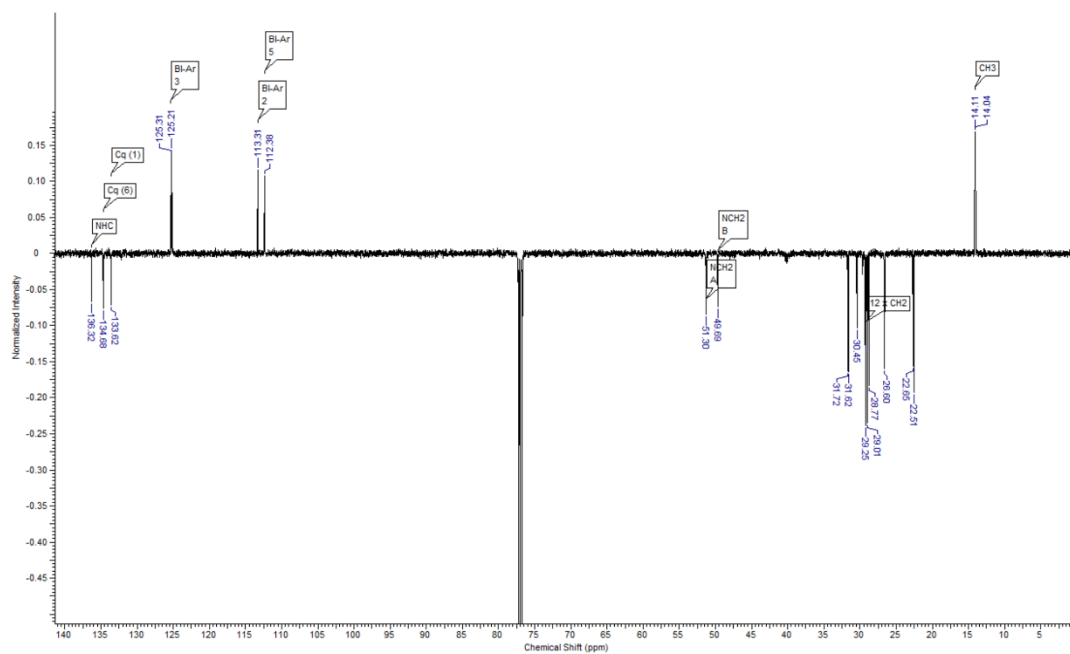


Fig. S 23: ¹³C-NMR spectrum (126 MHz, CDCl₃) of complex 4d.

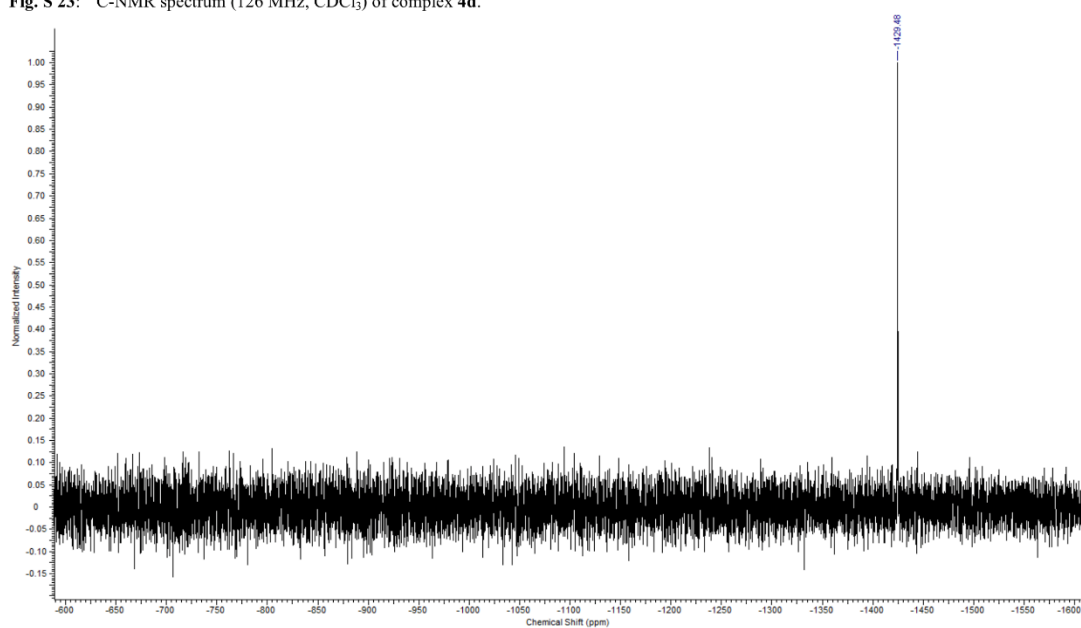


Fig. S 24: ¹⁹⁵Pt-NMR spectrum (108 MHz, CDCl₃) of complex 4d.

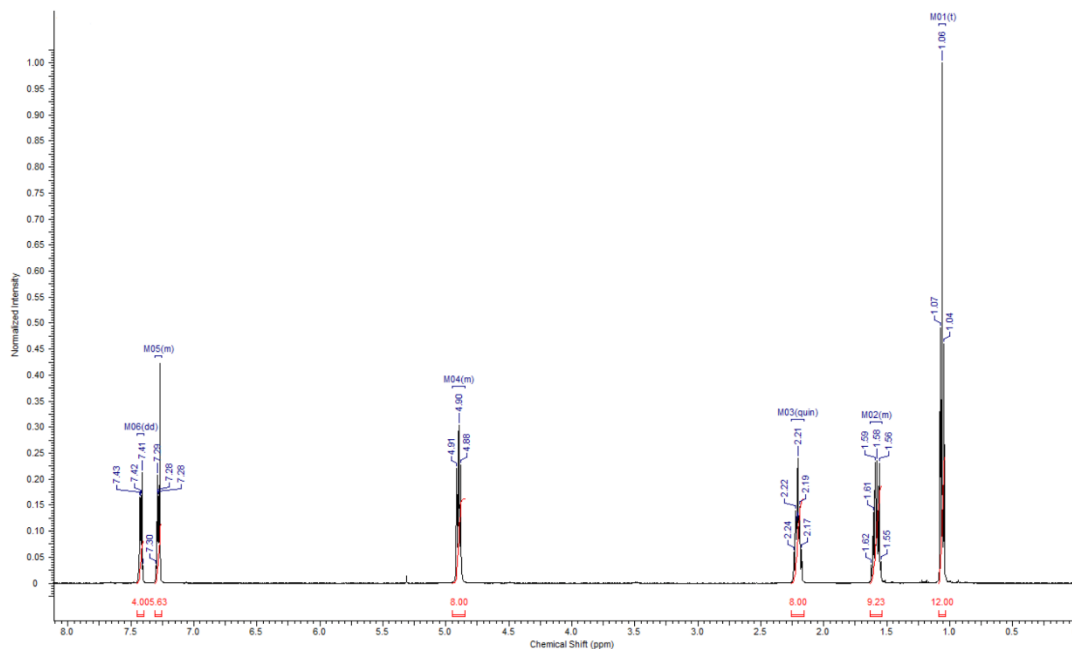


Fig. S 25: ^1H -NMR spectrum (500 MHz, CDCl_3) of complex *trans*-2c.

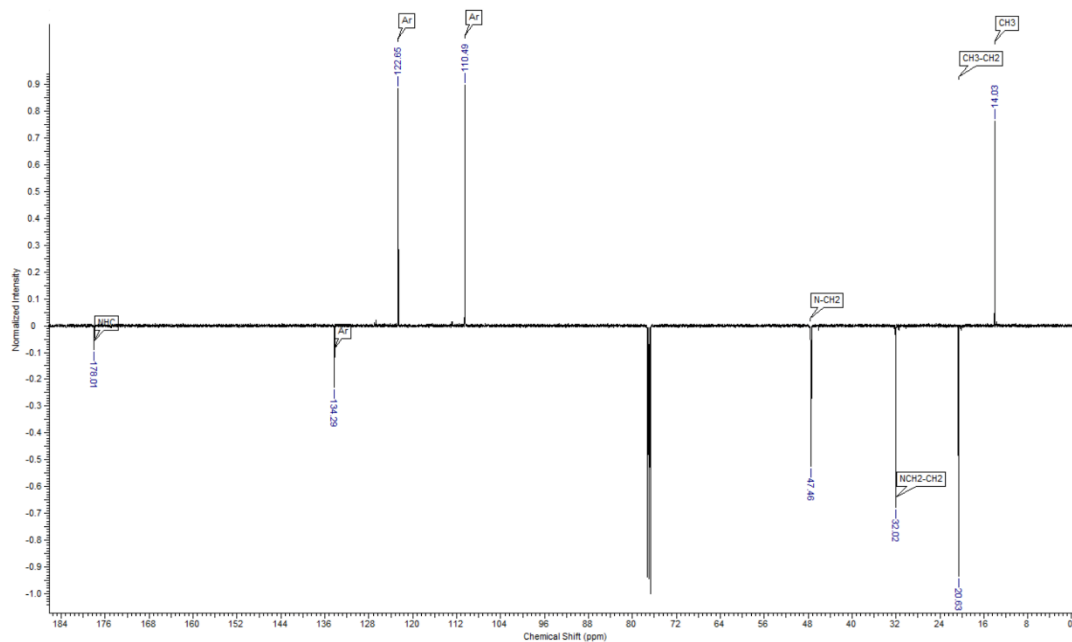


Fig. S 26: ^{13}C -NMR spectrum (126 MHz, CDCl_3) of complex *trans*-2c.

S15

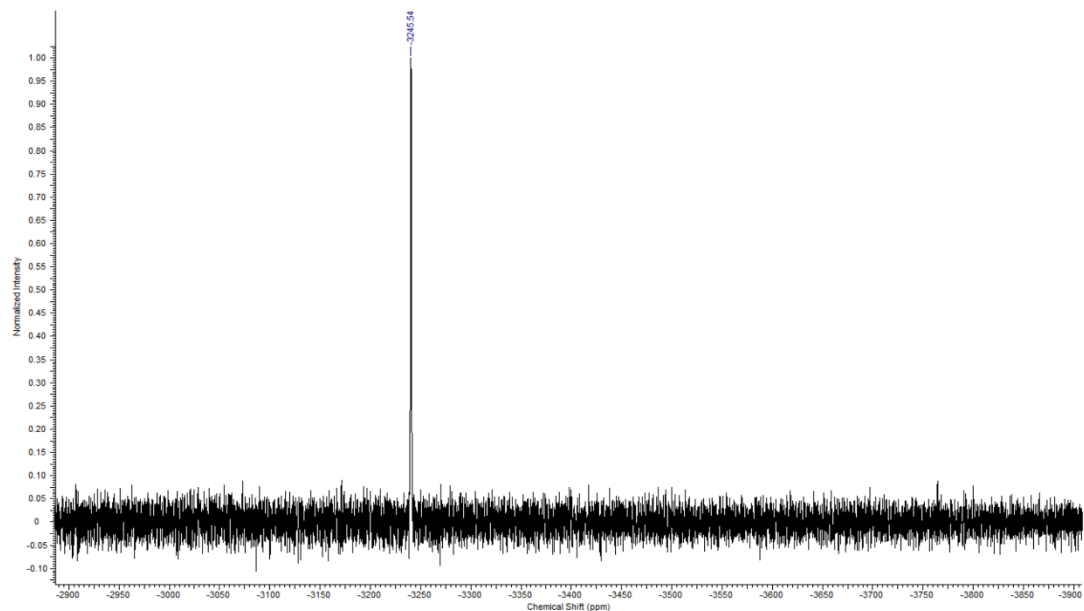


Fig. S 27: ^{195}Pt -NMR spectrum (108 MHz, CDCl_3) of complex *trans*-2c.

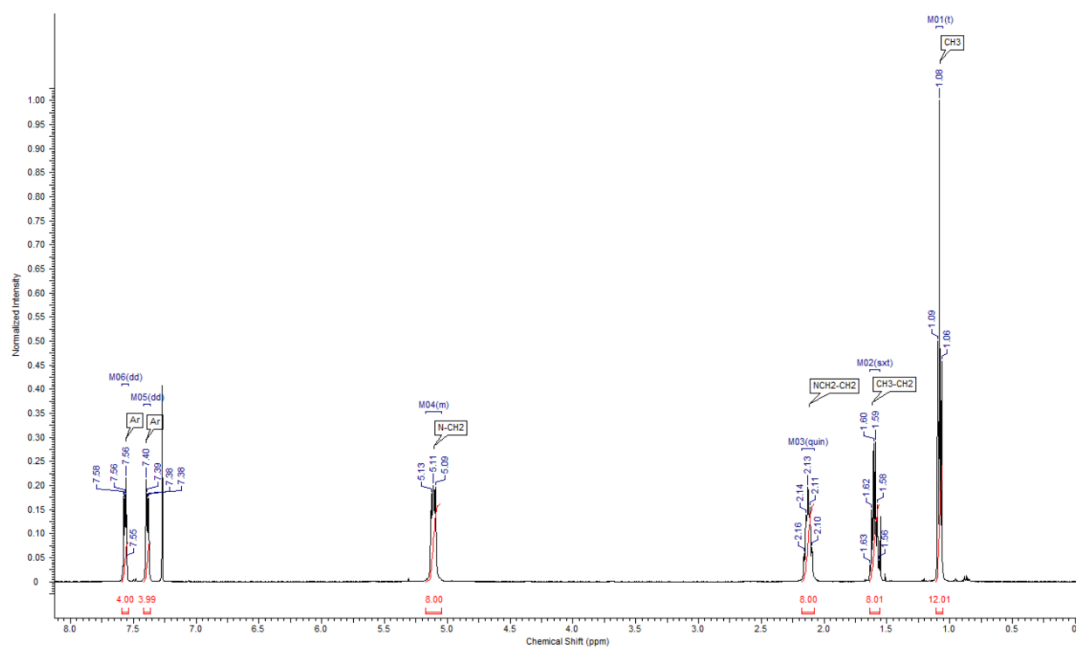


Fig. S 28: ^1H -NMR spectrum (500 MHz, CDCl_3) of complex *trans*-4c.

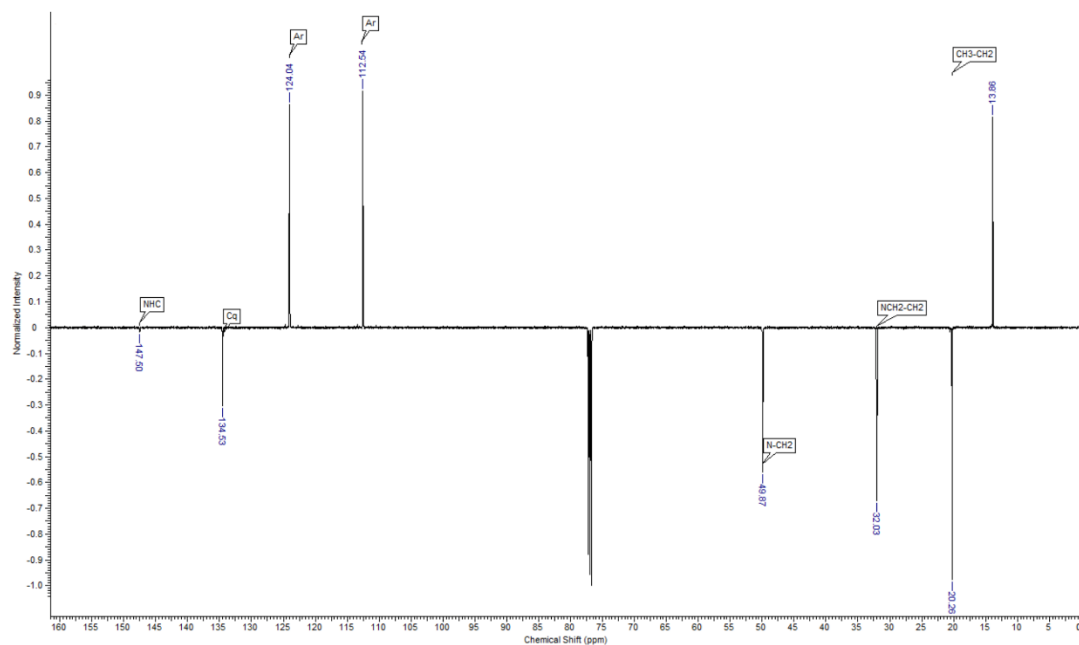


Fig. S 29: ^{13}C -NMR spectrum (126 MHz, CDCl_3) of complex *trans*-4c.

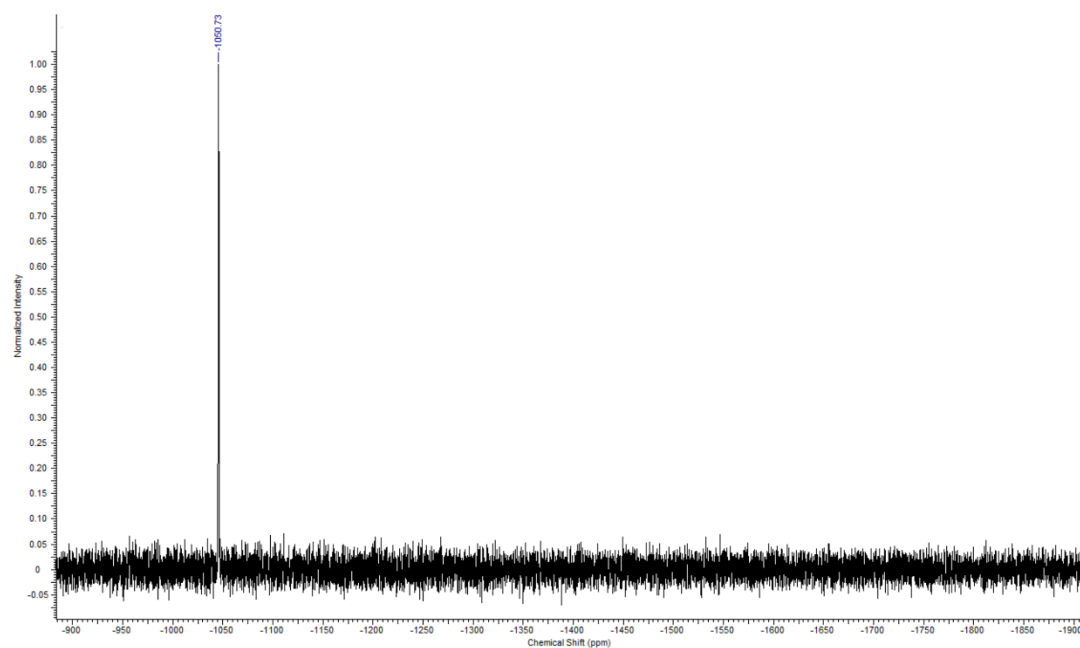


Fig. S 30: ^{195}Pt -NMR spectrum (108 MHz, CDCl_3) of complex *trans*-4c.

Oxidation of complex **2b** with NaOCl

Pt^{IV} hydroxo complexes with NHC ligands have not been published yet.

Upon treating benzylated complex **1** with H₂O₂, a new ¹⁹⁵Pt NMR signal around -855 ppm (CDCl₃) arose but the reaction was never completed and at the same time accompanied by decomposition due to cleavage of the benzyl group forming benzoic acid.

H₂O₂ oxidation of the *N*-alkylated benzimidazole-2-ylidene complexes **2** afforded only starting material even with a vast excess of peroxide (H₂O₂ or ^tBuOOH) at elevated temperatures.

By treating **2b** with NaOCl in water/acetonitrile a new compound with a ¹⁹⁵Pt NMR signal at about -905 ppm (CDCl₃) appeared, but like before, neither did the reaction go to completion nor was it possible to separate any products from residual starting materials.

In one such run, crystals of a reaction product precipitated from CDCl₃ in the NMR tube. NMR spectra of freshly prepared solutions of these crystals in DMSO-*d*₆ were in agreement with the tentative structure **8** although alternative structures cannot be excluded with certainty. The same sample five days later showed only signals of pure starting Pt^{II} complex **2b**.

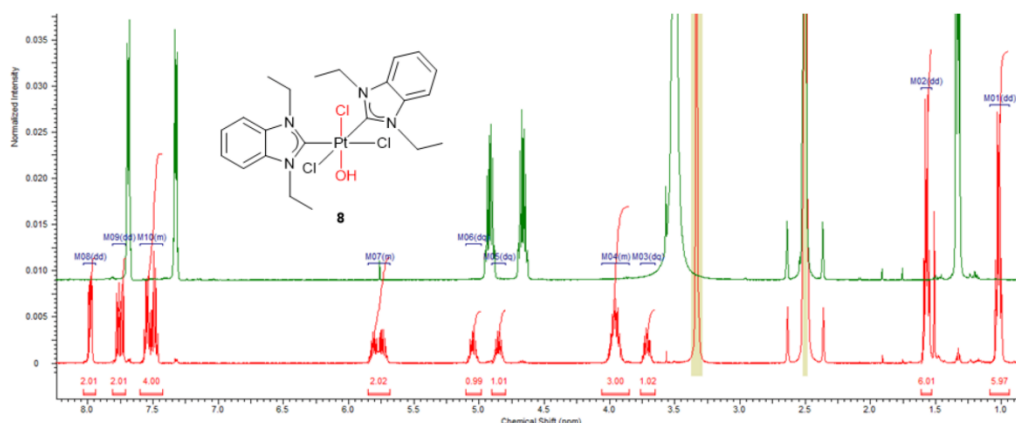


Fig. S 31 red: ¹H NMR (DMSO-*d*₆) of purported Pt^{IV} hydroxo complex **8** with characteristic signals of individual N-CH₂ protons between 3.5 and 6.0 ppm caused by inequivalent axial ligands;
green: same sample five days later shows spectrum of starting Pt^{II} complex **2b**.

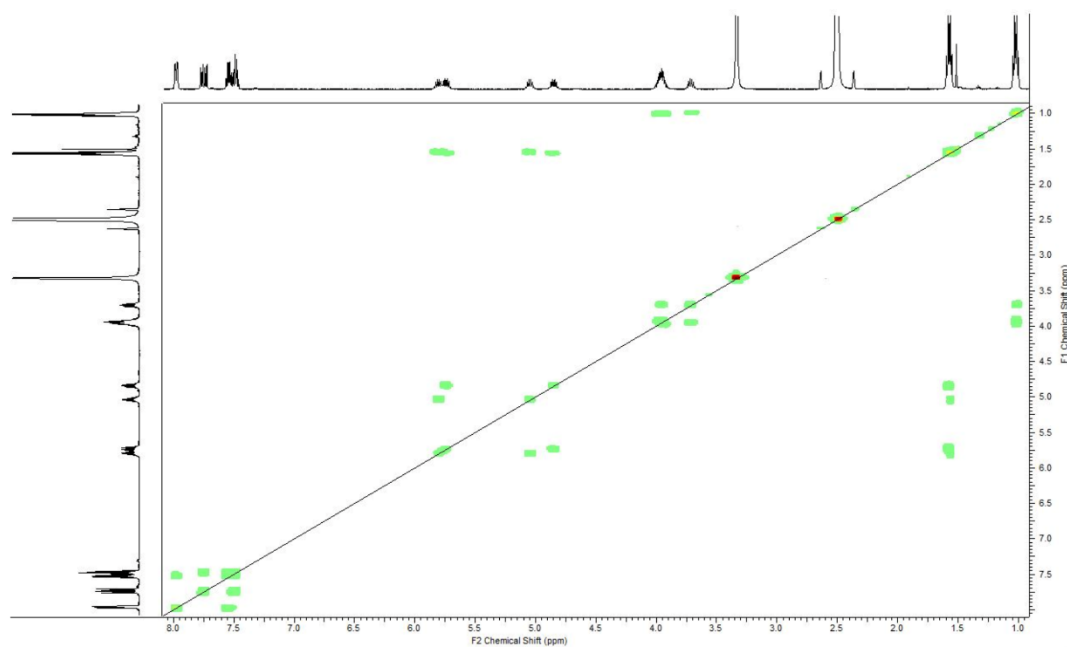


Fig. S 32 COSY-Spectrum of compound **8** in DMSO- d_6

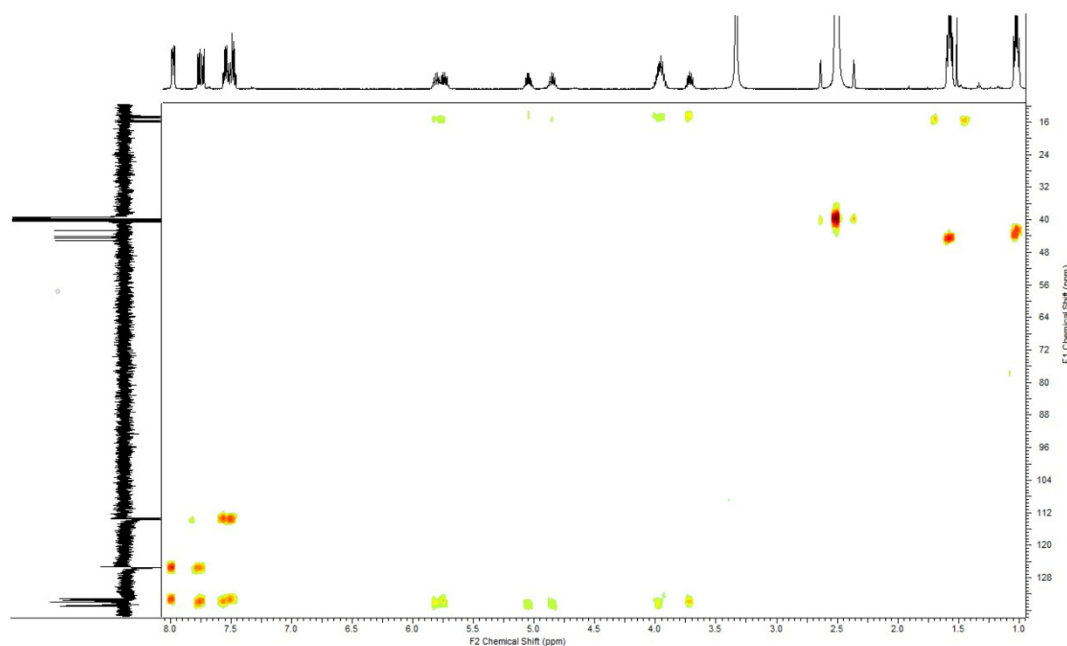
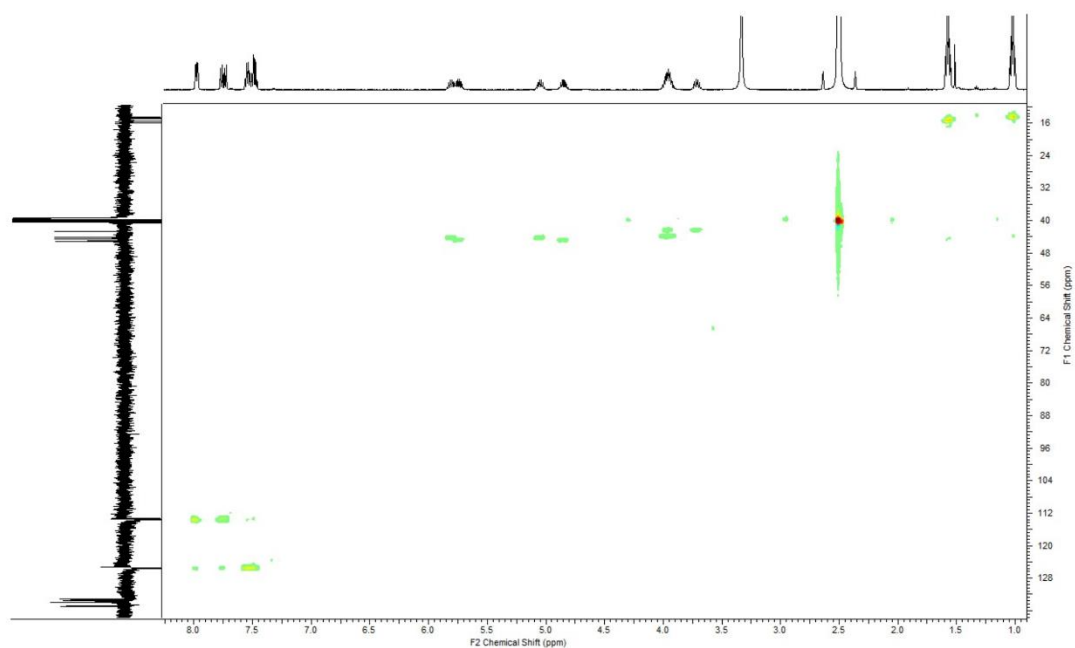
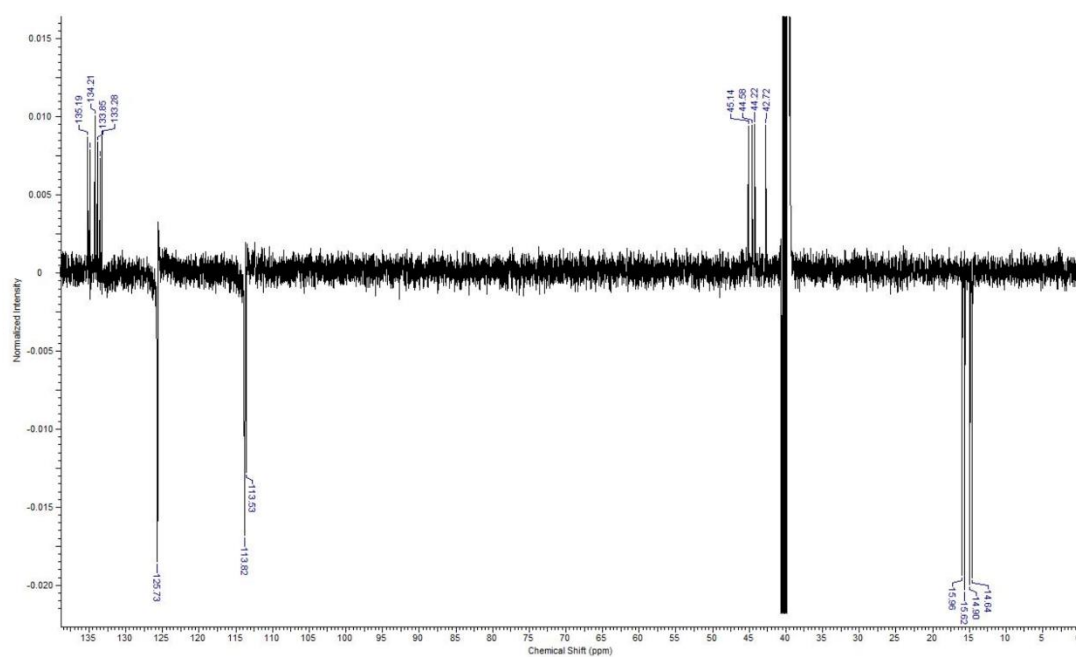


Fig. S 33 HMBC-Spectrum of compound **8** in DMSO- d_6

S19

Fig. S 34 HSQC-Spectrum of compound **8** in DMSO- d_6 Fig. S 35 JMOD-Spectrum of compound **8** in DMSO- d_6

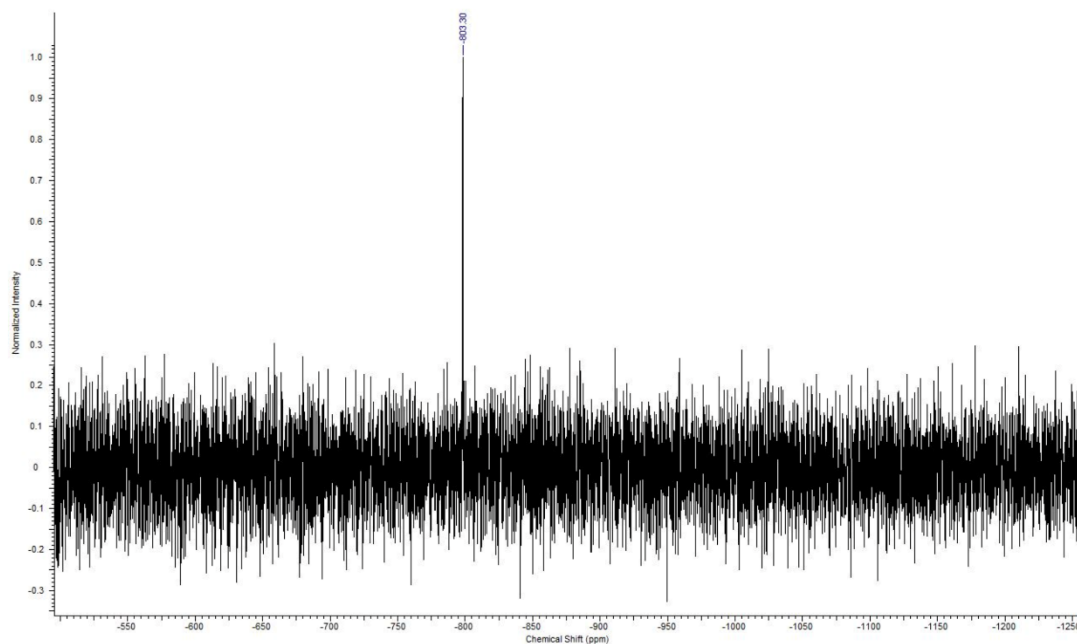
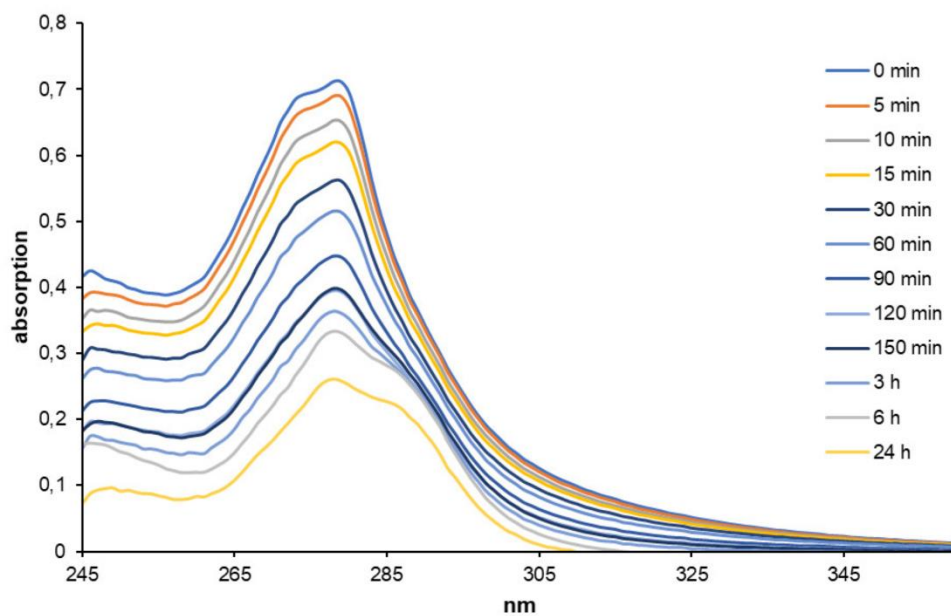


Fig. S 36 ^{195}Pt -Spectrum of compound **8** in $\text{DMSO-}d_6$

Stability of complex 4b in DMSO / water

UV/vis spectra (Fig. S 37): were recorded of 2 mL of a 25 μ M solution of complex **4b** (from a 5 mM stock solution in DMSO) in water/DMSO (4:1) over a period of 24 h (every 5 min for the first 3 h) by means of a Cary 60 UV-Vis Spectrometer (Agilent Technologies). Absorptions are relative to a baseline set to 0 at 400 nm.



S22

HPLC–ESI mass spectra: were recorded on a Varian 1200 Quadrupole MS/MS spectrometer of diluted NMR solutions of complex **4b** in water / DMSO- d_6 (30:70) after 0 min, 5 min, 10 min, 15 min, 30 min, 1 h, 2 h, and 16 h. The area of the total ion current (TIC) filtered for the main decomposition species with $m/z = 579$ was calculated for each of these points in time.

Exemplary MS after 10 min:

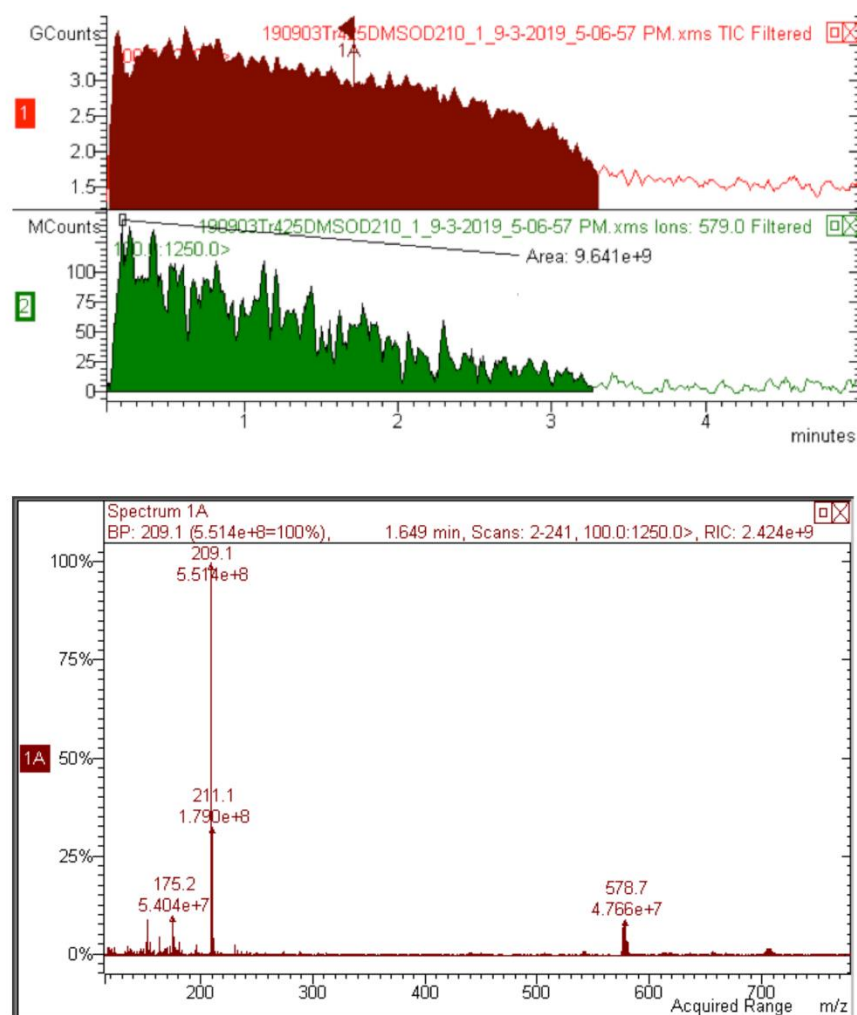


Fig. S 38:

1. Top in red: TIC = Total Ion Current from 0-3.2 min;
2. Middle in green: peak $m/z = 579$ integrated from 0-3.2 min to give an area of 9.641×10^9
3. Bottom: spectrum 1A, pertinent to TIC from 0-3.2 min.

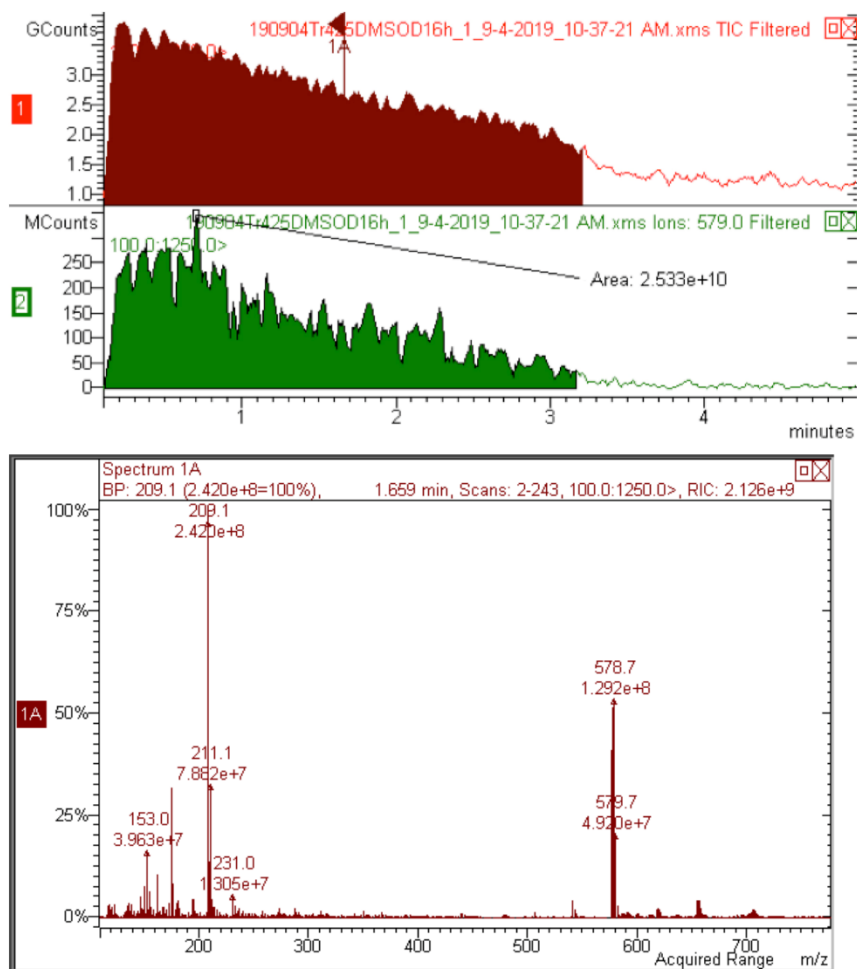
Exemplary MS after 16 h:

Fig. S 39: 1. Top in red: TIC = Total Ion Current from 0-3.2 min;
 2. Middle in green: peak $m/z = 579$ integrated from 0-3.2 min to give an area of 2.533×10^{10}
 3. Bottom: spectrum 1A, pertinent to TIC from 0-3.2 min.

Integration of peak $m/z = 579$ in spectra from 0-3.2 min recorded over time:

Time	Area
0 min	5.35×10^9
5 min	8.6×10^9
10 min	9.64×10^9
15 min	1.08×10^{10}
30 min	1.26×10^{10}
1 h	1.42×10^{10}
2 h	1.8×10^{10}
16 h	2.53×10^{10}

Confirmative MTT-assays with compounds 2c and 2d: were carried out with cells of the same lines yet of *distinctly different* passage numbers:

Table S 2: Means \pm SD of IC₅₀ (72 h) values [μ M] of complexes **2c** and **2d** in MTT assays against human cancer cell lines^a as calculated from four independent measurements

compounds	IC ₅₀ (72h) [μ M]	
	2c ^{10b}	2d
^a 518A2	2.1 \pm 0.3	> 50
^a HT29	10.8 \pm 1.0	> 50
^a DLD-1	17.4 \pm 1.0	> 50
^a HCT116 ^{wt}	7.0 \pm 0.8	> 50
^a HCT116 ^{-/-}	5.3 \pm 0.2	> 50

^a518A2 – melanoma, HT-29 – colon adenocarcinoma, DLD-1 – Dukes type C colorectal adenocarcinoma, HCT116^{wt} – colon carcinoma (wildtype); HCT116^{-/-} – colon carcinoma (p53 knock-out mutant).

6 Aufstellung weiterer Publikationen

1. Ferrocene-substituted 3,3'-diindolylmethanes with improved anticancer activity

Julienne K. Muenzner, Aamir Ahmad, Matthias Rothmund, Sebastian Schrüfer, Subhash Padhye, Fazlul H. Sarkar, Rainer Schobert, und Bernhard Biersack

Appl. Organometal. Chem. 2016, 30(6), 441-445.

2. Exploring the Influence of the Aromaticity on the Anticancer and Antivascular Activities of Organoplatinum(II) Complexes

Anna Zamora, Sergio A. Pérez, Matthias Rothmund, Venancio Rodríguez, Rainer Schobert, Christoph Janiak, und José Ruiz

Chem. Eur. J. 2017, 23(23), 5614 – 5625.

3. Synthesis and anticancer activity of the proposed structure of caldoramide, an N-peptidyltetramate from the cyanobacterium Caldora penicillate

Anja Wunder, Matthias Rothmund, Rainer Schobert

Tetrahedron 2018, 74(38), 5138 – 5142.

4. Synthesis and Cytotoxicity Studies of Novel NHC*-Gold(I) Complexes Derived from Lepidiline A

Danielle Curran, Oyinlola Dada, Helge Müller-Bunz, Matthias Rothmund, Goar Sánchez-Sanz, Rainer Schobert, Xiangming Zhu, und Matthias Tacke

Molecules 2018, 23(8), 2031 – 2048.

5. A new C,N-cyclometalated osmium(II) arene anticancer scaffold with a handle for functionalization and antioxidative properties

Enrique Ortega, Jyoti G. Yellol, Matthias Rothmund, Francisco J. Ballester, Venancio Rodríguez, Gorakh Yellol, Christoph Janiak, Rainer Schobert, und José Ruiz
Chem. Commun. 2018, 54(79), 11120 – 11123.

6. New Naphthopyran Analogues of LY290181 as Potential Tumor Vascular disrupting Agents

Florian Schmitt, Madeleine Gold, Matthias Rothmund, Ion C. Andronache, Bernhard Biersack, Rainer Schobert, Thomas Mueller
Eur. J. Med. Chem. 2019, 163, 160 – 168.

7. Oxazole-Bridged Combretastatin A-4 Derivatives with Tethered Hydroxamic Acids: Structure-Activity Relations of New Inhibitors of HDAC and/or Tubulin Function

Florian Schmitt, Lisa Chiara Gosch, Alexandra Dittmer, Matthias Rothmund, Thomas Mueller, Rainer Schobert, Bernhard Biersack, Andrea Volkamer, und Michael Höpfner
Int. J. Mol. Sci. 2019, 20(2), 383 – 409.

8. Luminescent Gold(I) Complexes of 1-Pyridyl-3-anthracenylchalcone Inducing Apoptosis in Colon Carcinoma Cells and Antivascular Effects

Juan Jesús González, Enrique Ortega, Matthias Rothmund, Madeleine Gold, Consuelo Vicente, Concepción de Haro, Delia Bautista, Rainer Schobert, José Ruiz
Inorg. Chem. 2019, 58, 12954 – 12963.

9. Copper(II) complexes with tridentate Schiff base-like ligands: solid state and solution structures and anticancer activity

Katja Dankhoff, Madeleine Gold, Luisa Kober, Florian Schmitt, Lena Pfeifer, Andreas Dürrmann, Hana Kostrhunova, Matthias Rothmund, Viktor Brabec, Rainer Schobert, Birgit Weber

Dalton Trans. 2019, 48, 15220-15230.

10. *N*-Metallocenoylsphingosines as targeted ceramidase inhibitors: Syntheses and antitumoral effects

Matthias Rothmund, Alexander Bär, Felix Klatt, Sascha Weidler, Leonhard Köhler, Carlo Unverzagt, Claus-D. Kuhn, Rainer Schobert

Bioorg. Chem. 2020, 97, 103703

7 Posterbeiträge und Konferenzen

1. Antitumoral activity of novel *cis*-platinum(II) NHC complexes: Cytotoxicity and alternative modes of DNA interaction

Matthias Rothemund, Tobias Rehm, Julienne Münzner, and Rainer Schobert

Gordons research conference “Metals in medicine”, Andover, NH USA 2016.

2. Structure-activity study of *cis*-platinum(II) *N*-heterocyclic carbene complexes

Matthias Rothemund, Tobias Rehm, and Rainer Schobert

12th International symposium on platinum coordination compounds in cancer chemotherapy, Sydney, NSW AUS 2017.

8 Danksagung

Mein besonderer Dank gilt Prof. Dr. Rainer Schobert für die interessante Themenstellung, die wissenschaftlichen Diskussionen und interessanten Gespräche. Weiter möchte ich mich für die Unterstützung und die Freiheit bedanken, die Prof. Dr. Schobert mir bei der Durchführung meiner Promotion überlassen hat. Ebenso dankbar bin ich, dass er mir die Gelegenheit gab, mich auf internationalen Konferenzen in den USA und Australien fortbilden zu können.

Mein Dank gilt weiter den Chemikern, die die Substanzen synthetisierten, die ich im Laufe meiner Promotion getestet habe, insbesondere Dr. Tobias Rehm ohne den diese Arbeit so nicht möglich gewesen wäre.

Ebenso möchte ich mich bei Madeleine Gold, Sofia Bär und Leonhard Köhler für die angenehme Zeit im Labor und die Unterstützung in der letzten Zeit meiner Promotion bedanken. Weiter gilt mein Dank meinen ehemaligen Laborkollegen Dr. Julienne Münzner, Dr. Florian Schmitt und Dr. Katharina Mahal mit denen ich einen Großteil meiner Zeit am Lehrstuhl ein Labor geteilt habe und die mir stets eine große Unterstützung waren. Meinen Praktikanten und Bacheloranten danke ich für die Unterstützung durch ihre wissenschaftlichen Arbeiten im Labor.

Ich möchte mich auch bei Prof. Dr. Stemmann, Prof. Dr. Unverzagt, Prof. Dr. Kuhn, Prof. Dr. Weber, sowie den Mitgliedern ihrer Lehrstühle für die tatkräftige Unterstützung, Nutzung der Geräte und die Hilfsbereitschaft bei Problemen bedanken. Insbesondere möchte ich hier Sascha Weidler und Felix Klatt für ihre Mitarbeit beim „Ceramidase-Paper“ danken. Allen weiteren Kooperationspartnern, mit denen ich zusammenarbeiten durfte danke ich für die gute Zusammenarbeit und ihre wissenschaftliche Arbeit.

Mein Dank gilt auch allen noch nicht erwähnten ehemaligen und aktuellen Mitgliedern des Lehrstuhls für die großartige Zeit während meiner Promotion. Dr. Thomas Schmalz gilt mein Dank für die häufigen wissenschaftlichen Diskussionen, die Unterstützung und die guten Ratschläge während meiner Zeit am Lehrstuhl

Meiner Familie und meinen Freunden bin ich ebenfalls für ihre Unterstützung und die super Zeit in Bayreuth dankbar.

9 Eidesstattliche Versicherung und Erklärung des Verfassers

(§ 8 Satz 2 Nr. 3 PromO Fakultät)

Hiermit versichere ich eidesstattlich, dass ich die Arbeit selbstständig verfasst und keine anderen als die von mir angegebenen Quellen und Hilfsmittel benutzt habe (vgl. Art. 64 Abs. 1 Satz 6 BayHSchG).

(§ 8 Satz 2 Nr. 3 PromO Fakultät)

Hiermit erkläre ich, dass ich die Dissertation nicht bereits zur Erlangung eines akademischen Grades eingereicht habe und dass ich nicht bereits diese oder eine gleichartige Doktorprüfung endgültig nicht bestanden habe.

(§ 8 Satz 2 Nr. 4 PromO Fakultät)

Hiermit erkläre ich, dass ich Hilfe von gewerblichen Promotionsberatern bzw. –vermittlern oder ähnlichen Dienstleistern weder bisher in Anspruch genommen habe noch künftig in Anspruch nehmen werde.

(§ 8 Satz 2 Nr. 7 PromO Fakultät)

Hiermit erkläre ich mein Einverständnis, dass die elektronische Fassung der Dissertation unter Wahrung meiner Urheberrechte und des Datenschutzes einer gesonderten Überprüfung unterzogen werden kann.

(§ 8 Satz 2 Nr. 8 PromO Fakultät)

Hiermit erkläre ich mein Einverständnis, dass bei Verdacht wissenschaftlichen Fehlverhaltens Ermittlungen durch universitätsinterne Organe der wissenschaftlichen Selbstkontrolle stattfinden können.

.....

Ort, Datum

Rothemund Matthias